North Sea Energy Island

Technical Report - Birds

Energinet Eltransmission A/S

Date: 20 August 2024

Rev. no.	Date	Description	Done by	Peer reviewed by	Quality assured by
3	20.08.2024	North Sea Energy Island Birds	Ib Krag Petersen (DCE) Heidi Maria Thomsen (DCE) Lindesay Scott-Hayward (CREEM) Saana Isojuuno (CREEM) Monique Mac Kenzie (CREEM) Claus Lunde Pedersen (DCE) Rasmus Bisschop-Larsen (NIRAS) Troels Eske Ortvad (DCE) Rasmus Due Nielsen (DCE) Jacob Sterup (DCE)	Antony David Fox (DCE) Rasmus Bisschop-Larsen (NIRAS) Rune Sø Nergaard (NIRAS)	Annette Lützen Møller (NIRAS)

Contents

List of key terms

A list of terms (in English and Danish) and their explanations.

Table 0.1 Terminology including Danish and English terms as well as explanations.

English (abbreviation)	Danish	Explanation
Pre-investigation area	Forundersøgelsesområde	The area covered by the survey permit for North Sea Energy Island and the geographical scope of the technical baseline reports.
Phase 1 area of the proposed plan for the programme North Sea Energy Island	Fase 1-område af Plan for Program Energiø Nordsøen	The phase 1 area defines the area of the proposed plan for the programme North Sea Energy Island where bird surveys were undertaken.
NSEI	Nordsø Energi-ø området	The area for the Plan for Programme North Sea Energy Island
Extended bird survey area	Udvidet undersøgelsesområde for fugle	An area defined by a 20 km buffer zone around the phase 1 area. This area was surveyed for birds by use of aerial surveys. The phase 1 area' is used in the text as a short form for the area.
Distance sampling	Distance sampling	A method to record observations with distance to an observer to estimate density and total abundance for a species.
Detection function	Detektionsfunktion	Modelling the declining probability of detection of an individual or cluster of individuals with increased distance from the observer to the object.
Spatial modelling	Rumlig modellering	A method to produce distribution maps, and associated uncertainty, from sampled data.

Report preface

This report This report was commissioned by the Danish Energy Agency to the corsortium of NIRAS and Aarhus University. It constitutes a description of the obtained results from the birds survey in connection with the planned construction of an Energy Island in the North Sea.

The report builds upon existing knowledge on birds and data on birds in the North Sea area, as well as new data collected and analyses conducted during this programme. It consists of six main chapters and an initial report summary. Chapter 1 introduces the report and explains the aim of the birds study. Chapter 2 gives an overview of existing available data on birds in the North Sea area. Chapter 3 describes the methods for field surveys and data analysis, and Chapter 4 describes the results of the study. Chapters 5 and 6 contains the discussion and the conclusion, respectively, of the report, and a list of references is provided in Chapter 7. Appendix 1 describes details the principles for estimating species abundance based on visual-areal observations.

The work was carried out by Aarhus University (DCE) in collaboration with the University of St. Andrews and NIRAS A/S.

Aarhus University (DCE) designed and conducted the data collection for this project. DCE collected and analysed the data for all parts of the work. The University of St. Andrews conducted the distance sampling analyses and the spatial models for selected bird species in chapter 3.4.1 and chapter 3.4.2. NIRAS oversaw report structure and design. NIRAS staff also assisted with data collection.

Energinet helped write the introductory section of Chapter 1.

Summary

From 2021 to 2023, a comprehensive birds survey were conducted for the North Sea Energy Island site in the northern central part of the Danish North Sea. In combination with the somewhat limited existing data on birds in the area, this survey aimed to gather thorough background data for future environmental impact assessments of upcoming wind farm projects. The investigation area in the North Sea consists of tidal, exposed, saline waters 22 – 60 m deep and is among the most oceanic of the Danish waters. It covered a total area of 4,814 km^2. The investigation area is referred to as 'the extended bird survey area' and included the phase 1 area with a buffer of 20 m around it. The originally designated pre-investigation area is contained within the extended bird survey area, see Figure 1.1.

Twelve aerial bird surveys were conducted from March 2022 to November 2023 to quantify the abundance, distribution and trends of relevant birds at sea. Each survey was conducted by a single aircraft over a single day. The surveys employed the distance sampling survey method. This approach allowed for modelling selected bird species' total abundances and distributions. Based on these modelled estimates, persistency maps for the surveys area were created, highlighting areas of high or low importance for specific species or species groups across all surveys. Data from each of the twelve surveys were used to derive information for the following species/species groups: northern fulmar, northern gannet, black-legged kittiwake, and razorbill/common guillemot. The maximum estimated numbers per survey were 2,364 northern fulmars, 3,797 northern gannets, 4,967 black-legged kittiwakes, and 27,245 razorbills/common guillemots. The aerial survey revealed that the avifauna within the extended bird survey area was dominated by offshore bird species, with northern fulmar, northern gannet, black-legged kittiwake, razorbill and common guillemot being the most numerous. Other gull species than black-legged kittiwake, such as European herring gull, lesser black-backed gull and great black-backed gull were also frequently recorded in the area. Terns were recorded in low numbers. Arctic tern was most abundant, while common tern occurred in lower numbers. Terns are migratory species and not present in Danish waters over the winter.

Eleven ship-based observations of birds were conducted from November 2021 to November 2023 with special focus on species flight altitudes and flight patterns.

Nearly all individuals of some species groups, such as alcids, terns and skuas, were recorded flying very low over the sea surface (0-25 m). In contrast, waders and gulls tended to fly at higher altitudes. For example, European herring gull and great black-backed gull were recorded flying up to 214 m and 184 m above the sea surface, respectively. Observations from these surveys also provided valuable insights into species composition for birds that are challenging to identify from aerial surveys. For example, divers were exclusively red-throated divers, while alcids comprised 16% razorbills and 84% common guillemots, with notable seasonal variations in their composition.

There was from the onset of this project scheduled for recording of bird flight information from a radar system on a platform to the west of survey area with the purpose with the aim of gathering data on a) altitude distribution of birds in the area day and night and b) relative volume/movement intensity of flying birds in the vertical plane. This proved to be impractical, and the ship-based platform using rangefinder was chosen for the purpose. The flight altitudes of birds investigated from ship-based surveys represent daylight observations only and might differ from nocturnal flight patterns, which could not be measured.

An overview of existing bird data from the Danish North Sea is presented, including data from a three day aerial survey in April/May 2019, covering the entire Danish North Sea. These data were used to estimate abundances and distributions for selected species/species groups. For that data set, the following species could be used: red-throated/black-throated diver, northern fulmar, northern gannet, black-legged kittiwake and razorbill/common guillemot. These species' estimated abundances for the entire Danish North Sea in April/May 2019 were 22,648 divers,

46,437 northern fulmars, 31,723 northern gannets, 4,472 black-legged kittiwakes and 89,681 razorbills/common guillemots.

1. Introduction

With the Climate Agreement for Energy and Industry of the 22nd of June 2020, the majority of the Danish Parliament agreed to establish an energy island in the Danish part of the North Sea, the 'North Sea Energy Island' (hereafter, NSEI), as an energy hub with a connection to Jutland as well as interconnectors to neighbouring countries. To establish an environmental baseline for the later environmental permitting processes for the specific projects, a series of environmental pre-investigations have been carried out. This report concerns baseline data and information on birds.

1.1 Aim

The birds survey aims to generate new data and compile existing data and information for the pre-investigation area of the North Sea Energy Island to be handed over to the future concessionaires as environmental baseline information for the concessionaires' environmental permitting processes (Danish Energy Agency, 2022). This technical report aims to collate bird data to facilitate future evaluations of avian impact assessments related to the proposed NSEI and associated offshore wind farms.

The specific objective of the birds survey is to provide specific information on three-dimensional bird distribution and abundance in time and space throughout the annual cycle within the phase 1 area. In addition of compilation of existing data and information, the programme comprised two main elements, namely:

1. Mapping avian species abundance and distribution at sea throughout the annual cycle.
2. Describing the density of bird flight volume in three dimensions, including flight altitude.

Avian abundance was primarily assessed based on distance sampling line transect surveys undertaken from high-winged aircraft, based on twelve surveys conducted from March 2022 to November 2023. Information on avian flight volume and altitude was gathered from eleven ship-based surveys conducted between November 2021 and March 2023. The ship-based surveys focused on providing essential information to support future avian collision risk assessments. The ship-based surveys also provided information on the composition of species that were difficult to identify from aerial surveys.

1.2 Survey area

In this report, three area definitions are used, as shown in Figure 1.1. These were defined in the original scoping report for the survey and follow a somewhat different layout than was later determined. The areas are: *'the phase 1 area of the proposed plan for the program North Sea Energy Island'* (hereinafter referred to as *'the phase 1 area'*), *'the pre-investigation area'* and the *'extended bird survey area'*. The first was used to design the environmental survey programmes as per the scoping report. *'The extended bird survey area'* is equal to the *'phase 1 area'* plus a 20 km buffer surrounding it. The *'pre-investigation area'* is the trapeze-shaped area.

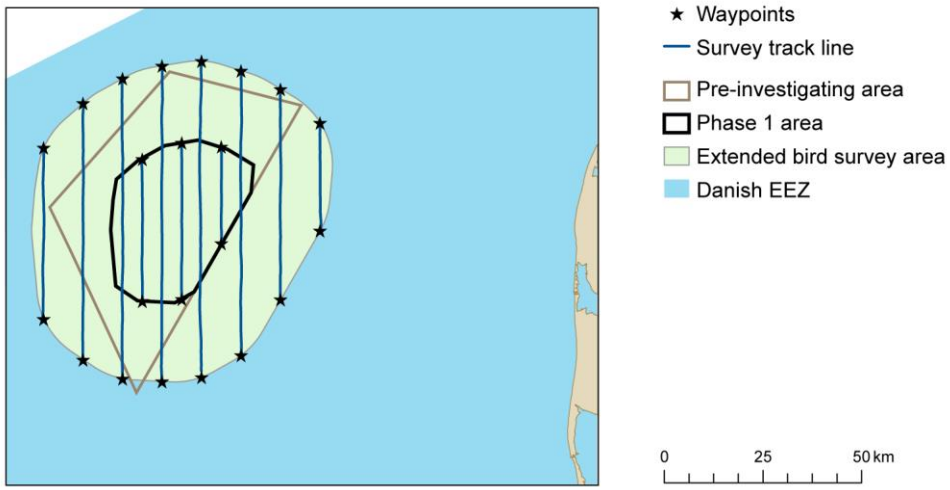

Figure 1.1 The North Sea Energy Island investigation area. The phase 1 area, pre-investigation area, extended bird survey area, and pre-defined transect lines and waypoints for the aerial bird surveys are shown.

2. Existing data

2.1 Overview of existing bird data from the Danish part of the North Sea

While the inner Danish waters have been surveyed for birds for many years, the available data on bird distributions in the North Sea is scarce. The Danish part of the North Sea was surveyed for birds by ship-based surveys in the 1970s and 1980s (Skov, Durinck, Leopold, & Tasker, 1995; Stone, et al., 1995; Tasker, Webb, Hall, Pienkowski, & Langslow, 1987) and aerial surveys in the 1980s (Laursen, et al., 1997). Since then, relatively few surveys of birds have been conducted in the North Sea. The most notable activity was a series of aerial line transect bird surveys concerning the Horns Rev area wind farms. These started in 1999 and continued until 2012, compiling around 50 surveys spread across the annual cycle but covering a relatively small geographical area.

The southern part of the Danish North Sea has been surveyed irregularly since 2002. These surveys mainly focused on the presence of red-throated and black-throated divers as part of the designation of a Birds Directive area designated for those two bird species (Petersen, Nielsen, & Clausen, 2016; Petersen, Nielsen, & Clausen, 2019).

The central eastern parts of the Danish North Sea have been irregularly surveyed for birds by aerial surveys from 2015. This encompasses an area from Blåvand in the south to Thyborøn in the north, extending approximately 70 km to sea. Most of these surveys were conducted in late spring, focusing on the red-throated diver and its relation to the Marine Strategic Framework Directive. In 2019, five surveys were conducted in this area, commissioned by the Energy Agency in relation to a strategic environmental assessment of the wind farm developments (Petersen & Sterup, 2019).

In the northern parts of the North Sea, aerial surveys for birds were undertaken with a special focus on marine birds along the southern flank of the Norwegian Trench. These were requested by the Environmental Agency for a plan for the designation of a Birds Directive Special Protection Area for seabirds such as the northern fulmar (Petersen, Nielsen, & Clausen, 2016).

In 2012 and 2013, five aerial surveys of birds in a geographically restricted area in Jammerbugten were conducted (Nielsen & Petersen, 2014). The surveys were commissioned by Vattenfall to plan offshore wind farms in that area.

The only recent survey with total bird survey coverage in the Danish North Sea was conducted in April/May 2019. These surveys were conducted over three days (Petersen, Nielsen, & Clausen, 2019). Spatial models for selected species from this survey were carried out as part of the North Sea Energy Island project and presented in chapter 4.2.

Between November 2013 and April 2014, six aerial bird surveys were conducted around the Vesterhav Syd offshore wind farm. The surveys were conducted along 18 east-west oriented transect lines from the coast to 25 to 30 km from the coast and from Nymindegab in the south to Øby in the north (NIRAS, 2015).

Between February and April 2014, six aerial bird surveys were conducted around the Vesterhav Nord offshore wind farm. The surveys were conducted along 20 east-west oriented transect lines from the coast to 25 to 30 km from the coast and from north of Thorsminde in the south to north of Thyborøn in the north (NIRAS, 2015).

The area of Horns Rev has been intensively monitored since 2000. A total of 56 aerial surveys of that area have been conducted up until 2024. Due to water depth and distance to the coast, that area has a different species composition from the North Sea Energy Island survey area. At Horns Rev, common scoters were abundantly present across most of the annual cycle, excluding summer. Also, red-throated divers appeared in that area in higher numbers than in the North Sea Energy Island survey area (Petersen, Nielsen, & Mackenzie, 2014).

2.2 Overview of birds in the extended bird survey area

The bird species composition of the extended bird survey area (Figure 1.1) is dominated by marine birds that acquire food either from the sea surface (surface feeders) or from pursuing fish or zooplankton in the pelagic zone (pelagic feeders). The area is generally too deep for benthos feeders acquiring food from the seabed. The distribution of pelagic food items is clumped and dynamic over time at a fine geographical scale. The prey distribution is likely to be driven by oceanographic and topographic features.

The distribution of the foraging birds can quickly adjust to the local and temporal distribution of prey. Therefore, using information on prey distribution would be beneficial predictor variables for modelling bird abundances at a fine geographical scale. Data on prey distributions at geographical and temporal scales relevant to the bird distributions are unavailable, and such variables have not been used here.

In this report, we model the spatial abundance and distribution of selected bird species using aerial surveys. While the distribution of bird species can often be very clumped for individual surveys, the data reveals little clustering when distributions are evaluated over multiple surveys in persistency analyses (chapter 3.4.2.5). We assume this relates to the rather uniform topographic and oceanographic nature of the extended bird survey area, where features that determine the bird distributions vary considerably between surveys.

The bird community in the extended bird survey area is dominated by staging birds and, to a smaller degree, by actively migrating species. The extended bird survey area is 60 to 140 km west of Jutland's west coast, which means there are no major migration corridors throughout the area. The area could have nocturnal migration of terrestrial birds, especially in the autumn. Such data was not collected under this project.

Northern fulmars, northern gannets, black-legged kittiwakes, razorbills and common guillemots are prominent bird species in the survey area. These species are described below.

2.2.1 Northern fulmar

The northern fulmar is a circumpolar species with a population in the northern Pacific and the northern Atlantic, utilising marine arctic to temperate areas all year. Northern fulmars are surface feeders collecting food from the sea surface. They breed on cliff ledges.

The northern fulmar is a long-lived species. They mature at approximately nine years and have an average life span of 18 years (Tasker, Webb, Hall, Pienkowski, & Langslow, 1987). Laying clutches of only one egg per year, the reproduction rate of the species is very low.

The global northern fulmar population is estimated at 10,000,000 to 12,000,000 individuals (Mallory, Hatch, & Nettleship, 2020). The European population is estimated at 3,380,000 to 3,500,000 breeding pairs, corresponding to 6,760,000 to 7,000,000 mature individuals (BirdLife International, 2024). The total European population, including immature birds, is thus larger. It should be noted that the estimates listed above are associated with considerable uncertainties. The northern fulmar is listed as Least Concern (LC) on the Global Red List (BirdLife International, 2018) but as Vulnerable (VU) on the latest European Red List (BirdLife International, 2021b).

There are no recent estimations of northern fulmar abundances in the North Sea.

2.2.2 Northern gannet

The northern gannet is an Atlantic seabird species. It breeds in coastal colonies in the temperate zone. It is migratory, utilising the Atlantic Ocean southwards to ca. 20°N and, to a lesser extent, the Mediterranean Sea. The northern gannet diet comprises fish, and birds plunge dive to moderate depth for schooling fish species (Mowbray, 2020).

The migration pattern of twelve northern gannets from Helgoland showed that three of the twelve birds wintered off the west African coast, while the rest wintered in Western Europe. One bird wintered in the Baltic, and over the last 18 years, northern gannets have occurred in Skagerrak and Kattegat in markedly higher numbers than was previously the case (Garthe, et al., 2024).

The northern gannet is a long-lived species. They mature at three to five years, and birds are known to have reached 25 years (Mowbray, 2020). Laying clutches of only one egg per year, the reproduction rate of the species is very low.

The global population, all within the northern Atlantic Ocean, comprise 950,000 to 1,200,000 individuals. The largest part of the population breeds in colonies in the United Kingdom (BirdLife International, 2024). The northern gannet is listed as Least Concern (LC) both under the Global Red List (BirdLife International, 2024) and the European Red List (BirdLife International, 2021a).

No recent estimates of total northern gannet abundance in the North Sea exist.

The East Atlantic northern gannet population was influenced by a severe, Highly Pathogenic Avian Influenza (HPAI) outbreak in the summer of 2022. As a result of this event, the breeding population in the United Kingdom decreased by 25% between the breeding seasons of 2021 and 2023 (Tremlett, Morley, & Wilson, 2024).

2.2.3 Black-legged kittiwake

The black-legged kittiwake is a medium-sized gull species. It breeds in the temperate and arctic zones, with a non-breeding distribution primarily in the temperate zone. Black-legged kittiwakes are surface feeders, and their diet comprises small fish species and larger zooplankton (Hatch, Robertson, & Baird, 2020).

Black-legged kittiwakes breed at three to five years of age. They typically lay clutches of three eggs. Survival rates for northeast European birds showed annual survival rates of 79% to 88% (Hatch, Robertson, & Baird, 2020). The species is migratory.

The global population of black-legged kittiwakes is estimated at 14,600,000 to 15,700,000 birds. The European population is estimated at 1,730,000 to 2,200,000 pairs, which equates to 3,460,000 to 4,410,000 mature individuals (BirdLife International, 2024). The species is listed as Vulnerable (VU) under both (BirdLife International, 2021a) the (BirdLife International, 2024) and the European Red List (BirdLife International, 2021a).

2.2.4 Razorbill

The razorbill has an arctic, subarctic and temperate breeding distribution in the Atlantic Ocean, including the Baltic Sea. During the non-breeding season, the birds are found in temperate parts of the same area. The species breeds in rocky coastal areas and has an entirely marine distribution over the non-breeding season (Lavers, Hipfner, & Chapdelaine, 2020).

Razorbills are long-lived and reach maturity at four to seven years old, and the clutch size is always one egg. The estimated annual survival rate is 89% to 92%, with geographical variation (Lavers, Hipfner, & Chapdelaine, 2020).

Razorbills mainly feed on small schooling fish but also crustaceans and polychaete species. They acquire their food by pursuit diving.

The razorbill has a global population of 1,250,000 to 2,480,000 individuals (Wetlands International, 2022). This species has two subspecies, *Alca torda torda* (*A. t. torda*) and *Alca torda islandica* (*A. t. islandica*), and the former subspecies is divided into two subpopulations, a west Atlantic and an east Atlantic. The subspecies *A. t. torda* breeds in eastern North America, Greenland, Bear Island, Norway, Murmansk, White Sea and the Baltic Sea. The western population is

estimated at 130,000 individuals, while the eastern part is estimated at 290,000 to 350,000 individuals. The *A. t. islandica* subspecies breeds in Iceland, the Faroes, the United Kingdom, Helgoland and northwest France. It has an estimated population size of 830,000 to 2,000,000 individuals (AEWA, 2022).

The origin of razorbills found in the Danish part of the North Sea is poorly known. It is estimated that 33% originates from the United Kingdom's population, 59% from the Norwegian population and 8% from the Baltic population (Lyngs & Kampp, 1996). The Baltic razorbills are considered residents of the Baltic or are moving into Kattegat. Razorbills in the Danish North Sea thus comprise the UK and Norwegian populations.

The species is listed as Least Concern (LC) under the Global Red List (BirdLife International, 2024) and the European Red List (BirdLife International, 2021a).

2.2.5 Common guillemot

The common guillemot has an arctic, subarctic and temperate distribution in the Atlantic and the Pacific Oceans. The species breeds in coastal cliffs and has an entirely marine distribution over the non-breeding season.

The common guillemot is a long-lived species. It reaches maturity at two to seven years old, and the clutch size is always one egg. The annual adult survival rate is high, from 78% to 97.4% in Atlantic colonies (Ainley, Nettleship, & Storey, 2021).

Common guillemots feed on small schooling fish, larger zooplankton and squids by pursuit diving.

The common guillemot has an estimated global population of 8,300,000 breeding pairs. 3,300,000 of those pairs breed in the Atlantic Ocean (Ainley, Nettleship, & Storey, 2021). In the northeastern Atlantic area, three subspecies of common guillemot are recognised, *Uria aalge aalge (U. a. aalge)*, *Uria aalge albionis (U. a. albionis)* and *Uria aalge hyperborea (U. a. hyperborea)*. The subspecies *U. a. aalge* is divided into two sub-populations, an east Atlantic and a Baltic subpopulation. The east Atlantic subpopulation is numerically the largest, estimated to count 4,600,000 to 5,700,000 individuals, while the Baltic subpopulation is estimated at 77,000 to 100,000 individuals. The population size of *U. a. albionis* is estimated at 500,000 individuals, while *U. a. hyperborea* is estimated at 600,000 to 640,000 individuals (Wetlands International, 2022).

The Atlantic *U. a. aalge* population breeds in the northern United Kingdom, Faroes, Iceland and west Norway, while the Baltic population of the same subspecies breeds in the Baltic Sea. *U. a. hyperborea* breeds in northern Norway and Svalbard, while *U. a. albionis* breeds in the southern parts of the United Kingdom, Ireland, France, the Iberian Peninsula and Helgoland, Germany.

The origin of common guillemots found in the Danish part of the North Sea is poorly known. From ringing recoveries, it was estimated that 85% of the common guillemots in Danish waters derive from the United Kingdom breeding population. In comparison, another 5% was estimated to derive from the Faroese breeding population and the remaining 10% from the *U. a. albionis* population. The Baltic part of the *U. a. aalge* population was estimated to comprise 7% of non-breeding common guillemots in the Danish waters, all of which are considered to stay in the Baltic or Kattegat area. The *U. a. hyperborea* subspecies is considered to spend the non-breeding season north of Danish waters (Lyngs & Kampp, 1996).

The east Atlantic population is listed as Least Concern (LC) under the Global (BirdLife International, 2024) and the European Red List (BirdLife International, 2021a). The Norwegian breeding population was classified as critically endangered under the Norwegian Red List, based on an 85% to 90% decline since the 1960s (Stokke, et al., 2021).

2.3 EU Special Protection areas for birds in the North Sea

In the Danish part of the North Sea, three EU Special Protection Areas have been designated. The closest area is the EU SPA number 126, Skagerrak, approximately 50 km north of the North Sea Energy Island phase 1 area. The second closest area is the Southern North Sea, EU SPA number 113, approximately 80 km southeast of the North Sea Energy Island phase 1 area (Figure 2.1). The third area, EU SPA number 57, has a marine part in the western part of it but has mainly been designated for coastal or Waddenzee bird species.

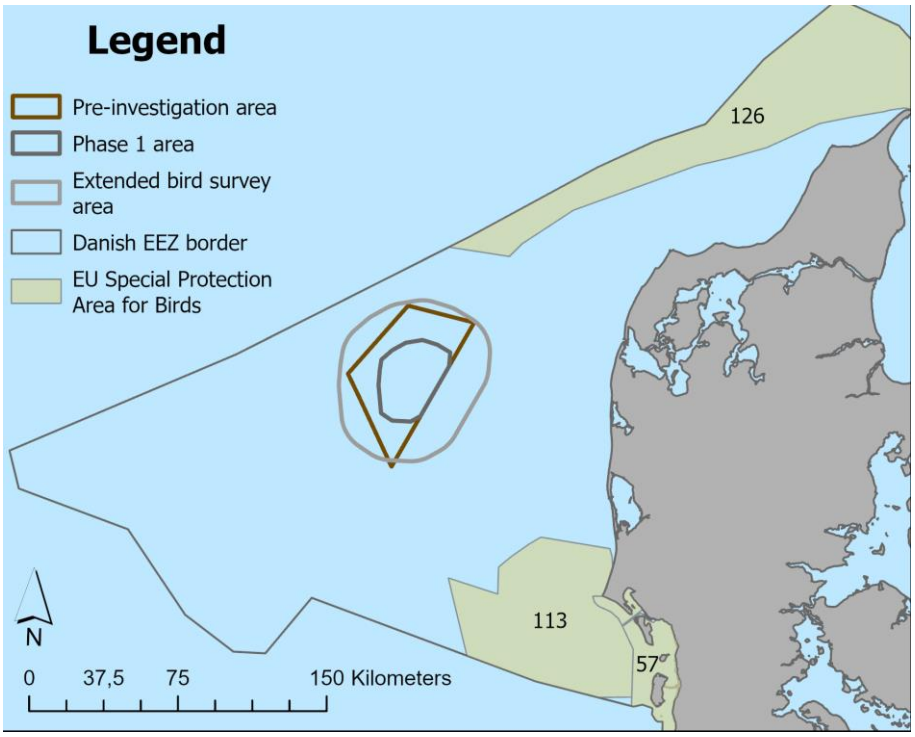

Figure 2.1 The marine EU Special Protection Areas of the Danish part of the North Sea. The position of the North Sea Energy Island phase 1 area, the pre-investigation area and the extended bird survey area is indicated, as is the Danish EEZ border.

EU SPA number 126 was designated in 2021, with northern fulmar and great skua on the list of designated bird species. EU SPA number 113 was designated in 2023, with red-throated diver, black-throated diver, common scoter and little gull on the list of designated species.

3. Methods and surveys

This chapter outlines the data collection methods and analytical approaches employed to investigate the occurrence of birds within and around the phase 1 area of the North Sea Energy Island.

The objective of the bird survey program was to collect site-specific data on the spatial and temporal distribution of staging and migrating birds in and around the phase 1 area. Twelve aerial and eleven ship-based surveys were conducted to study this, as described below.

3.1 Survey area

The extended NSEI bird survey area covers an area of 4,814 km^2 (hereafter, 'extended bird survey area'), covering the phase 1 area and a buffer zone of 20 km around that. The extended bird survey area thus stretches from approximately 60 to 140 km west of the west coast of Jutland (Figure 1.1).

The extended bird survey area's water depth ranges between 22 and 60 m, with a mean of 38.7 m. The seabed is relatively uniform, with water depths between 30 and 48 m over almost 90% of the area.

3.2 Aerial surveys

Data on bird abundance and distribution were collected using standard methods; human observers visually gathered data during aerial surveys while flying transects between designated GPS waypoints at regular speed and altitude (Figure 1.1). Observations are recorded within distance bands out from the aircraft to allow for the modelling of differential detectability at increasing distances from the observers, following standard distance sampling line transect survey methods (Buckland et al. 2001, 2015). For further details on this method, please refer to chapter 3.4.

For the surveys, twin-engine high-winged aircraft were used. The aircraft types were Cessna 337, Partenavia P-68, and Tecnam P2006T.

The data collection was performed from a flight altitude of 76 m. Two observers record birds on either side of the aircraft. The bird species or species group was noted for each record, along with information on flock size, behaviour, perpendicular distance from the survey track and time. The perpendicular distance was classified in predefined distance bands with increasing distance from the survey track line to 1.5 km on either side of the aircraft (Error! Reference source not found.).

A GPS device recorded the time and position of the aircraft every six seconds. The data for this assessment comes from twelve surveys undertaken between March 2022 and November 2023, all completed in a single day (Table 3.1).

Table 3.1 Timing of the 12 aerial surveys covered in this analysis. The length of the transects covered for each survey is given.

Date	Total length of transect lines (km)	Aircraft type
2 March 2022	596	Cessna 337
1 April 2022	596	Cessna 337
27 April 2022	597	Tecnam P2006T
30 July 2022	596	Cessna 337
11 September 2022	600	Cessna 337
23 December 2022	596	Cessna 337
21 January 2023	596	Cessna 337
2 March 2023	590	Partenavia P-68 V
3 April 2023	596	Cessna 337
8 July 2023	592	Partenavia P-68 V
27 September 2023	596	Cessna 337
10 November 2023	593	Cessna 337

The species distribution maps in chapter 4.1 present the precise survey track lines flown during each survey.

3.3 Ship-based surveys

Data on bird species composition, flight magnitude and flight altitudes were collected from ship-based surveys within the phase 1 area. In total, eleven ship-based surveys were conducted between November 2021 and March 2023 (Table 3.2). Each survey comprised 2.3 (± 0.2) observation days and 21.2 (± 2.2) observation hours on average, comprising 25 observation days and 233 observation hours across all surveys.

Table 3.2 Overview of the eleven ship-based surveys conducted in the NSEI survey area. The table shows the survey start and end dates and the number of observation days (N = 25) and hours (N = 233).

Survey ID	Start date	End date	Observation days	Observation hours
S1	15 November 2021	16 November 2021	2	16
S2	14 February 2022	15 February 2022	2	16
S3	12 April 2022	12 April 2022	1	13
S4	22 April 2022	25 April 2022	3	22
S5	30 April 2022	02 May 2022	3	26
S6	20 May 2022	21 May 2022	2	26
S7	24 August 2022	26 August 2022	3	36
S8	22 October 2022	22 October 2022	1	10
S9	13 November 2022	14 November 2022	2	18
S10	14 February 2023	16 February 2023	3	26
S11	28 March 2023	30 March 2023	3	24

A single observer would record flight altitudes and bird counts simultaneously or separately during each survey. Four different observers conducted the surveys in total. Each observer conducted an average of 2.8 (± 1.4) surveys, with one observer responsible for most of the surveys (63.6%), observation days (56%), and observation hours (57.1%). As the ship-based bird surveys were conducted from ship surveys with other primary purposes, there were no fixed observation positions or transect lines.

3.3.1 Bird flight altitude records

Flight altitude measurements were conducted in all directions around the ship during both active sailing (918 observations) and stationary periods (703 observations). Observers attempted to limit the measurements as much as possible to birds seemingly little or unaffected by the ship. Consequently, measurements were obtained as far away from the ship as possible.

A laser rangefinder was used to measure the flight altitude. However, in some cases, obtaining measurements with a rangefinder was impossible, e.g., due to sea state. In these cases, the observer would estimate the flight altitude. In total, observers made 1883 measurements and estimates of bird flight altitude (hereafter, 'altitude records'). Of these, 1021 were measurements (54.2%), whereas 862 were estimates (45.8%). Observers would continuously measure and estimate bird flight altitudes to improve their estimations. This proved successful as no significant difference (Wilcoxon signed rank test: v = 173015, p = 0.1) was found between measured and estimated bird flight altitudes for observations where both were recorded.

Flight altitude was measured on birds flying alone and in flocks, for which flock size was recorded. Whenever possible (especially during undulating flight), observers would measure the altitude of the same individual/flock multiple times to capture the range and variation in flight altitude. Repeated measures of the same individual/ flock were recorded with the same observation ID.

3.3.2 Transect bird counts

Transect counts were conducted while the ship actively sailed along a straight line between two points. Some observers continued counting when the ship was stationary to assess species composition. Each transect covered an area of 300 m perpendicular to the ship's course, on either one or both sides of the ship, depending on the observer, number of birds present and light conditions. Thus, the total transect span was either 300 m or 600 m.

The perpendicular distance to birds was measured using a laser rangefinder, or it was estimated when using a rangefinder was impossible. Each observation was assigned to one of four distance bands: 0-50 m, 50-100 m, 100-200 m, 200-300 m, and one of three behaviour categories: 'flying', 'on water', and 'following ship'. Flock size was always recorded. Birds observed outside 300 m were coded as 'outside transect'.

During transect counts, some observers noted all birds observed, regardless of behaviour, while others focused on birds categorised as 'on water'. In the latter case, so-called 'snapshot' observations were used to obtain information on the number of flying birds. During snapshots, all flying birds within an area of 300 x 1000 m in front of the vessel were instantaneously counted and recorded, undertaken routinely at 15-minute intervals. This report obtained density estimates from aerial survey data (chapter 3.4.1). The transect counts from the ship were exclusively used for calculating the species composition of birds that were difficult to identify during aerial surveys (chapter 3.5.2).

3.4 Data analysis

The first aim of this part of the work was to generate an 'instantaneous' avian density surface across the phase 1 area based on data collected from each survey and by different observers along transects under differing environmental conditions. The first objective was to estimate the total abundance and overall density of all suitable species, correcting for the effects of observer and prevailing conditions on detectability with increasing distance from the aircraft during the survey, described in the distance sampling analysis section. A second process is to generate a spatial model of abundance, generating a density map for each species from each survey based on key environmental parameters. This process is described in the spatial analysis framework section below. Finally, based on the combined outputs from the spatial models created for each species across the multiple surveys, the persistence of each species in its occurrence across the extended bird survey area can be mapped, quantifying areas of high or low persistence in its presence across more surveys. This is described in the persistence estimation section below.

3.4.1 Estimation of abundances and distribution from aerial surveys

3.4.1.1 Distance sampling analysis

The bird distribution data was collected using the distance sampling methods. Data was collected so that the declining probability of detecting a bird or a group of birds with increased distance from the survey track line could be modelled. Distance bins or bands to all observations enable the modelling of a detection function as described below.

Distance sampling analyses were conducted for each of the species/species groups by pooling the information from each survey.

When fitting detection functions, the effects of covariates, other than perpendicular distance, are incorporated into the detection function model directly (Multiple Covariate Distance Sampling, MCDS) (Marques & Buckland, 2004; Marques, Thomas, Fancy, & Buckland, 2007; Buckland, et al., 2001). Such covariates could be ´sun intensity´ (a factor indicating sun intensity in four categories) or ´sea state' (a measure for the wave activity). In these cases, the probability of detection becomes a multivariate function, representing the probability of detection at perpendicular distance and covariates, where Q is the number of covariates). In this study, using a half-normal detection function $e^{-\left(\frac{y^2}{\sigma^2}\right)}$ the covariates were incorporated via the scale term, σ, where for sighting j, σ has the form:

$$\sigma_j = \exp\left(\beta_0 + \sum_{q=1}^{Q}(\beta_q v_{jq})\right)$$

where β_0 and β_q $(q = 1, \dots, Q)$ are parameters to be estimated (Buckland et al. 2001). Both half-normal and hazard rate detection functions were fitted, and BIC was used to choose between the two models. The candidate variables trialled were bird group size, behaviour, observer, glare, and sea state (Table 3.3). There were too few observations for

some observers, so in those cases, the observers' observations were combined with the next smallest. Observations with a sea state of four or greater were removed.

Table 3.3 Table detailing the covariates used in the detection function fitting.

Covariates	Values
Behaviour	S (sitting or diving) and F (flying or flushing)
Observer	7 Observers
Glare	1 (full sun), 2, 3 (cloudy), 9 (changeable)
Sea State	0, 0.5, 1, 1.5, 2, 2.5, 3, 3.5 (calm to rough)

3.4.1.2 Mitigating the effects of glare

Detection of sea birds from aerial surveys can be influenced by conditions, such as sun glare and sea state. Data to describe sighting conditions is usually collected in situ; however, alternative methods are required to identify (and adjust for) heterogeneity in the detection probability when this is absent. Accounting for such heterogeneity is particularly important for distance sampling, where near-perfect detection at the track line is an often-required assumption.

We used detection information from band A for the left-hand and right-hand sides of the aircraft (Error! Reference source not found.) to identify transect lines with likely poor sighting conditions. For all species except flying northern gannets and black-legged kittiwakes, which are much easier to see even when glare is present, the identified transects removed observations from the affected side, and the coverage was reduced to one side (i.e., returning a one-sided transect).

The effects of glare and any mitigations, as a result, were approached using a dedicated analysis. The analysis was designed to quantify the extent to which directional sun glare can lead to left/right-hand side bias in counts within a single transect line with the same direction of travel. Specifically, we assumed that the proportion of left or right sightings in band A should be 0.5 and follow a Binomial distribution. We compared the proportions for each transect to a critical value calculated as the quantile of the Binomial $(n, p = 0.5)$ distribution at three standard errors greater than the mean and where n equals the number of observations on the transect. Three standard errors are common in extreme value theory (Leys, Ley, Klein, Bernard, & Licata, 2013). Any transects with values greater than the critical value had the observations from the smaller side removed and the coverage reduced to a single side.

3.4.2 Spatial analysis framework

The following sections describe the modelling methods employed for this analysis and the following outputs. This spatial modelling step estimates bird density and distribution on a fine geographical scale (1 x 1 km grid cells) using the above distance sampling analysis results. For a high-level executive summary of the spatial analysis framework methods, see Appendix 1.

3.4.2.1 Model framework

The response variable for the spatial models under analysis here are bird counts in a small area (segment) corrected for detectability. This response was modelled using a Tweedie framework, which includes an estimated dispersion parameter (ϕ) and Poisson-Gamma mixing parameter (ξ) to return an appropriate mean-variance relationship in each case. The mixing parameter takes on values from 1 (equivalent to quasi-Poisson) and 2 (equivalent to Gamma). If the estimated parameter was close to one, the models were considered quasi-Poisson. A set of candidate explanatory variables were associated with each segment to model the signal, and in this study, each of the 12 surveys was analysed separately, including covariate selection. The candidate environmental covariate was water depth (bathymetry, Figure 3.1). Distance from the coast (Figure 3.2), as a one-dimensional term, was also considered in each model in the unlikely case that there was compelling evidence for consistent spatial patterns with distance from the coast, which

were the same in all directions. Additionally, a spatial surface was fitted to each model to account for more realistic (and localised) surface patterns (due to potential unmeasured covariates). Specifically, a two-dimensional CReSS-based (Complex Region Spatial Smoother) surface using a Gaussian radial basis function was included in the model (Scott-Hayward, Mackenzie, Donovan, Walker, & Ashe, 2014).

As an illustration, the following equation represents an example of a Tweedie model with a log link function and fitted with a one-dimensional smooth term (e.g., bathymetry) alongside a two-dimensional spatial smooth:

$$y_{ij} \sim Tw(\mu_{ij}, \phi, \xi)$$

$$\mu_{ij} = e^{\left(\beta_0 + s_1\left(\text{Bathymetry}_{ij}\right) + s_2\left(\text{XPos}_{ij}, \text{YPos}_{ij}\right)\right)}$$

where y_{ij} is the estimated count for transect i segment j and s_1 represents either a quadratic B-spline or natural cubic spline smooth of depth. Here, s_2 is a two-dimensional smooth space (with coordinates XPos and YPos in UTMs). Implicit in this model are also coefficients for the intercept (β_0) and any spline-based coefficients associated with the smooth terms. The effort associated with each observation varied depending on the associated segment area, so the segment area was included as an offset term (on the log scale).

A globally applicable depth or distance to coast term and a more flexible spatial term were trialled for inclusion in each model to indicate how best to model spatial patterns in each case. This quantifies if any spatial patterns are sufficiently described by the one-dimensional covariates (which apply the same across the surface) or if a more considered approach to spatial patterns was required for each survey. For example, suppose the depth was selected, and a two-dimensional spatial element was not deemed necessary (as determined by the model selection procedure governed by objective fit criteria). In that case, this signals that any spatial patterns are primarily a function of the depth, regardless of the geographical location of this depth in the survey area.

If the two-dimensional spatial term was selected for inclusion in a model, then the spatial density patterns (over and above any environment-related terms) were accommodated using a spatially adaptive term which permits different amounts of flexibility across the surface in a targeted and yet parsimonious way (hence, relatively complex spatial patterns can be accommodated with very few parameters).

Selection between competing models was undertaken using a 5-fold cross-validation metric, which preserved any within-transect correlation via the appropriate blocking structures.

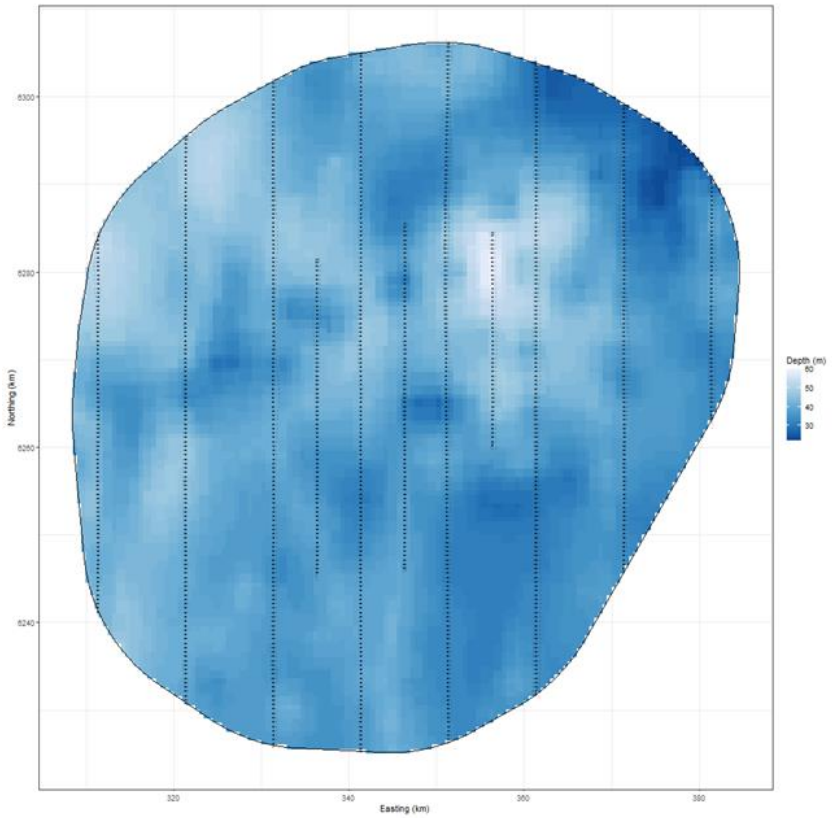

Figure 3.1 Visual representation of bathymetry (water depth). The black dots represent the pre-defined survey track lines. The black dots represent the centroid of each 500 m long segment used for analysis and show survey coverage.

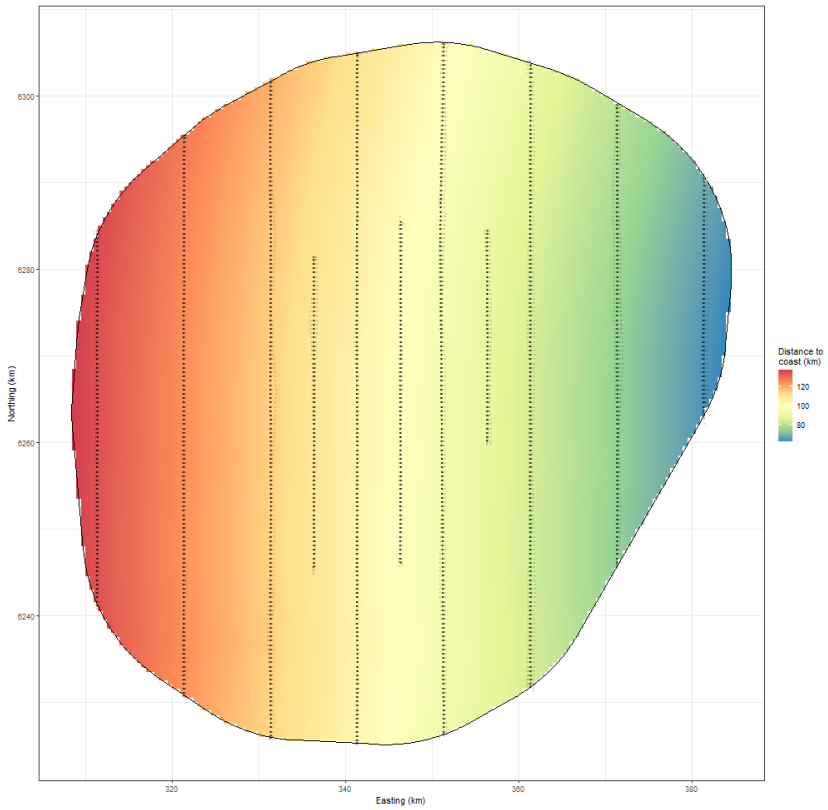

Figure 3.2 Visual representation of distance to the coast. The black dots represent the centroid of each 500 m long segment used for analysis and show survey coverage.

3.4.2.2 Model specification, selection and fitting

Spatially adaptive generalised additive models, with targeted flexibility, were fitted to data from each survey to allow for non-linear relationships between the one-dimensional and two-dimensional covariates and the response (Scott-Hayward, Mackenzie, Donovan, Walker, & Ashe, 2014; Scott-Hayward, Mackenzie, & Walker, 2023; Walker, Mackenzie, Donovan, & O'Sullivan, 2010).

All covariates were permitted to have a linear or nonlinear relationship with the response, and when a smooth term was included in a model, it was specified to be either a quadratic (degree 2) B-spline (df = 3, 4, 5) or a natural cubic spline (df = 2, 3, 4). However, in cases where these degrees of freedom boundaries were reached, a broader range of parameters was trialled instead. The degrees of freedom for these terms determine the flexibility of these smooth (and nonlinear) relationships - the more degrees of freedom, the more flexible the relationship can be.

The location of this flexibility (along the x-axis) in these terms (e.g., depth) was also determined as part of the model selection process. This permitted the relationship in some areas of the covariate range to be relatively complex (e.g., in shallow waters) and in other areas (e.g., in deep waters) to be relatively simple. Both smooth types permitted a maximum of three internal knots and a spline-specific number of boundary knots. The number and location of knots were determined by an objective fit criterion.

The spatial patterns in each analysis were based on a two-dimensional spatial term (of variable complexity). The flexibility of the spatial element constituted part of the model selection procedure, and for each survey, it was determined using a Spatially Adaptive Local Smoothing Algorithm (SALSA). While this model selection element technically occurred between limits (df = [2,100]), the flexibility chosen in each case was not bounded in practice by those values since the selection procedure occurred well within the bounds of the specified range.

The ***MRSea*** ***R*** package (R Core Team), designed to fit both CReSS and SALSA type models, was used for model fitting, and a 5-fold cross-validation (CV) procedure was used to govern all model selection elements (Scott-Hayward, Mackenzie, & Walker, 2023). The CV procedure attempts to balance the fit to data unseen by the model while minimising the number of parameters (parsimony). It was used here to select terms and the extent of their flexibility in each model. Note that this cross-validation was predicated on preserving correlated blocks of survey data (transect lines) so that any residual autocorrelation present was not disrupted when choosing folds. This was considered necessary to ensure independent sampling units under the scheme.

3.4.2.3 Parameter inference

The response data were collected along survey lines in sequence, so consecutive observations are likely to be correlated in space and time (i.e., points close together in space and/or time are likely to be more similar than points distance in time and/or space). Further, the covariates included in the model are unlikely to fully explain these patterns, so some elements of these patterns will likely remain in model residuals. These patterns violate residual independence (which underpin traditional model approaches such as Generalized Additive Models); thus, robust standard errors were routinely used as part of the ***MRSea*** modelling framework to account for residual autocorrelation.

Uncertainty about model parameter estimates proceeded via robust standard errors due to the nature of the survey procedure. These essentially work by inflating the standard errors (normally obtained under traditional approaches) concerning the positive correlation observed within pre-specified blocks of residuals. In cases where this residual correlation is minimal, the adjustments are small, and when the correlation is more extreme, the inflation is larger.

A transect-based blocking structure was used to reflect potential correlation within blocks while independence (i.e., no correlation) between blocks was assumed. To ensure that the model assumptions were realistic, we assessed the decay of any residual correlation to zero (i.e., independence) with the distance between points (within blocks along transects) visually. Specifically, transects in each survey were used as the blocking structure, and an Auto Correlation Function (ACF) plot was used to check the suitability of this blocking structure via a 'decay to zero' trend within blocks.

3.4.2.4 Modelling diagnostics

Several diagnostic measures were used to assess the adequacy of the model fit in each case.

The assumed mean-variance relationship under the model was assessed visually using plots of the model's fitted values against the residuals' variance. In this analysis, Tweedie models were employed, which assume a nonlinear mean-variance relationship:

$$Var(y) = V(\mu)\phi = \mu^{\xi}\phi$$

ϕ is the dispersion parameter. The dispersion parameter was estimated for each model, which was used in the visual assessment of this mean-variance relationship assumed to hold under the model. ξ is the power parameter estimated before model fitting using a maximum likelihood profile approach. Based on the nature of the response data, the values of ξ were permitted between 1 (Quasi-Poisson) and 2 (Gamma).

QQ plots and residuals against predicted values plots were assessed to ascertain the level of agreement between the data and the model. These plots were created using the ***DHARMa*** ***R*** package and using simulated residuals. (Figure 3.3; Figure 4.27) shows an example output for a model showing good agreement between the data model.

Regarding interpretation, the left panel is a uniform QQ plot, and the right panel shows residuals against predicted values, with outliers highlighted in red. Given these outputs, we would expect that a correctly specified model shows:

a) A straight 1-1 line and no compelling evidence against the null hypothesis of a correct overall residual distribution, as indicated by the *p*-values for the associated tests in the QQ plot.

b) Visual homogeneity of residuals in both the vertical and horizontal directions, in the residuals against the predictor plot.

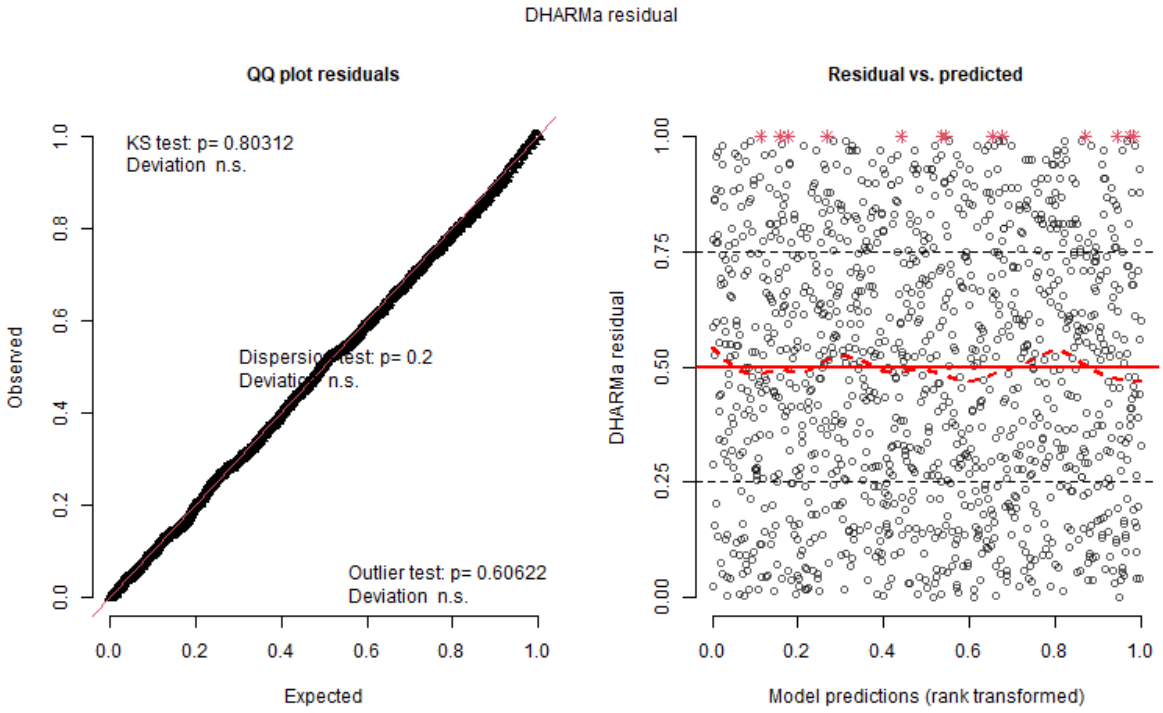

Figure 3.3 DHARMa diagnostics. Example QQ plot (left) and residuals against predicted values (right). The red stars are outliers, and the red line is a smooth spline around the mean of the residuals.

Pearson residuals for each model were also spatially visualised to ensure no areas of consistent bias across the survey area. Clusters of negative or positive residuals in spatially similar locations would indicate this.

Residual independence was not assumed to hold under the model; instead, model inference proceeded under robust standard errors. As described, Auto Correlation Function (ACF) plots were used to check the suitability of this blocking structure via a 'decay to zero' trend within blocks.

3.4.2.5 Model predictions and estimates of uncertainty

Based on each selected model, predictions of counts were made to a grid of points (each point representing a 1 km² grid cell) across the study region. Additionally, abundances within the survey-based prediction region were obtained by summing the grid cell counts across the relevant areas.

The uncertainty in the detection function was reflected using a parametric bootstrap ($n = 500$) of the fitted distance sampling model. This generated new estimated counts for each segment. The selected spatial model was then re-fitted to each of the new datasets to obtain a new set of parameter estimates for the model. The final output of this process was a parametric bootstrap procedure using the robust variance-covariance matrix from each parametric bootstrap model. These were used to calculate 500 sets of model predictions, which generated 95% percentile-based intervals and allowed a Coefficient of Variation (CoV) for each grid cell to be calculated. The CoV is defined as the ratio of the standard deviation to the mean, and this is calculated for each grid cell using the 500 bootstrap predictions. CoV < 1 are considered low-variance, whilst CoV > 1 are considered high-variance. The CoV is very sensitive to small mean values, which may lead to artificially large CoV values, so we present CoV plots with and without cells whose mean abundance is less than 0.01.

A calculation of 'persistence' was also undertaken across the two data types using the geo-referenced estimates of density (abundance/associated area) across the survey area. Persistence scores were calculated for every grid cell in the following way: Each bootstrap replicate was allocated a binary value based on whether the estimate in each location was above the mean estimated density (1) throughout the survey area or below this means estimated density (0). This was performed for all 500 sets of plausible predictions in each grid cell (based on the bootstrap replicates), and the proportion of these bootstrap predictions more than the mean (indicated by the value of 1) was calculated for each grid cell to give a persistence score for that location. A persistence score of 1 indicates that the density in that grid cell was estimated to be above average in every bootstrap replicate in every survey (so uniformly above the mean; high persistence), while a value of 0.1 indicates that just 10% of the estimates were above the estimated mean, and thus indicates low persistence in that location.

3.5 Data for future collision risk assessment

This element of the work is to provide data to support a future estimation of collision risk between turbines and birds and to provide data on species ratios for species groups that are difficult to identify to species from the aerial surveys.

Bird flight altitude information is an essential component of the collision risk assessment. The proportion of birds flying will be a component of the estimation of flight volume in the area, another important component of collision estimation. These analyses were conducted based on diurnal observations from ship-based surveys. During these surveys, no nocturnal data was collected.

Describing season-specific species ratios between species groups that are difficult to identify species from the aircraft will facilitate species-specific abundance estimates.

3.5.1 Bird flight altitude from ship-based surveys

For the analyses of flight altitude, measurements objectively obtained by rangefinder were preferred over estimates of flight altitude made by observers. However, flight altitude estimates were used for those observations where a measurement was not recorded or when the rangefinder produced a negative value (e.g. if the birds flew between the waves). Sometimes, observers did not report a precise altitude estimate but noted a maximum possible altitude, e.g. <10 m. In these cases, the maximum value was used. The maximum value used in this way was '<60 m'. Classes '<10 m' and '<15 m' comprised 71% of this type of altitude estimation.

Flight altitudes were divided into 25 m interval bands from 0 to 225 m, and the number of altitude recordings and individuals occurring in each interval was analysed. These analyses were done for each species individually, but in some cases, related species were grouped because they were hard to distinguish between in the field or to increase the sample size for species with few observations, e.g. species of passerines. Furthermore, the analyses were limited to species or groups with 10 or more flight altitude recordings.

Since flight altitude was measured multiple times on some individuals and flocks, these repeated measurements cannot be considered independent. The best way to account for this would have been to use mixed-effects models with observation ID as random effects. This was attempted, but models failed to produce meaningful results. Another possibility would have been to average the flight altitude for each observation ID and analyse the means. However, to retain the variation in flight altitude of individuals and flocks, we analysed all altitude recordings as if they were independent. This was done as we judged the pseudo-replication to be minimal. Flight altitude was recorded only once for 85.5 % of all individuals and flocks, whereas 12% had their flight altitude recorded twice and 2.5% had their flight altitude recorded between three and five times.

3.5.1.1 *The proportion of birds flying from aerial surveys*

As an estimation of the probability that a bird would be in flight (as opposed to sitting on the water), we calculated the proportion of birds recorded with the behaviour 'flying' out of the total number of birds observed during the aerial transect surveys in the North Sea. Birds recorded as 'flushed' or 'diving' were grouped with birds observed 'sitting on the water surface'. This was done to analyse the birds in their original, undisturbed behaviour, avoiding inflating the probability of flight by including birds potentially flushed or forced to dive by the aircraft. We then expressed the numbers of birds assigned to the 'flying' behavioural category (i.e. birds likely first encountered in flight from the aircraft as continuing that behaviour) as a proportion of the total number of encounters (i.e. those flying plus those sitting on the water, diving or flushing) to calculate the proportion of birds in flight. As for the analyses of flight altitude, we calculated the proportion on an observational and individual level separately for each species. We limited the analyses to species or species groups with a minimum of 10 observations (Table 3.4).

3.5.2 Species composition from ship-based surveys

We calculated the species composition based on ship-based data to generate species-specific density estimates for some species that were difficult to identify to species during aerial surveys. These species included divers, gulls (excluding black-headed gulls and black-legged kittiwakes), terns and alcids (razorbill/common guillemots). We calculated the composition for each of the eleven surveys based on the number of individuals. We included all types of observations (i.e., transect counts and snapshots) and birds seen both within and outside the 300 m wide transect band to calculate the composition. We, furthermore, included birds in all behavioural categories (i.e. 'flying', 'on water', 'following ship'). Birds observed following a ship were included since we judged that there would be little differences between the related species in their attraction to ships. Below is a complete list of species observed during ship surveys (Table 3.4).

Table 3.4 List of species that were grouped during the ship-based and aerial survey analyses. Unidentified species from a species group are abbreviated with 'sp.' in the species name.

Species group	Taxonomic relation	Species	
		Ship surveys	Aerial surveys
Divers	Genus (*Gavia*)	Red-throated diver	Red-throated diver Diver sp.
Sea ducks	Tribe (Mergini)	Common merganser Common scoter Red-breasted merganser	Too few observations from aerial surveys
Waders	Order (Charadriiformes; excluding gulls, terns, skuas and auks)	Common ringed plover European golden plover Common snipe Dunlin Eurasian curlew Eurasian oystercatcher Eurasian woodcock Ruddy turnstone Wader sp.	Too few observations from the aerial surveys
Skuas	Genus (*Stercorarius*)	Arctic skua Great skua	Too few observations
Terns	Subfamily (Sterninae)	Sandwich tern Common tern Arctic tern	Sandwich tern Common/arctic tern Tern sp.

		Common/arctic tern	
Alcids	Family (Alcidae)	Common guillemot Razorbill Common guillemot/razorbill	Common guillemot Razorbill Common guillemot/razorbill
Passerines	Order (Passeriformes)	Brambling Common blackbird Common chiffchaff Common starling Eurasian skylark European robin Fieldfare Meadow pipit Northern wheatear Redwing Song thrush Western yellow wagtail	Too few observations

4. Results of surveys

The available data on bird abundances and distributions in the phase 1 area was scarce before this project. For that reason, data on birds was collected between November 2021 and November 2023 to support future environmental assessments of offshore wind farms planned in that area. The surveys were conducted from aerial surveys and ship-based surveys. To describe bird abundances and distributions in the area, we conducted aerial surveys (chapter 4.1) using distance sampling and spatial modelling methods (Buckland, Rexstad, Marques, & Oedekoven, 2015).

To supplement the information on bird abundances and distributions, we analysed the results from aerial surveys in April and May 2019 for the Danish North Sea, deriving spatial models of bird distributions from selected bird species or species groups (chapter 4.2).

Since data from the aerial surveys derives information on bird distributions at one point and doesn't reveal information on bird flight altitudes, these surveys were completed with ship-based surveys. The ship-based approach aimed to derive data on flight altitudes, magnitudes, and bird species composition in the phase 1 area (chapter 4.3).

4.1 Aerial surveys in the NSEI extended bird survey area

The description of bird abundances and distributions was based on data from twelve aerial surveys spread over the project period from March 2022 to November 2023. The surveys covered the extended bird survey area. The data revealed that the area's avifauna consisted primarily of true marine bird species, most prominently northern fulmars, northern gannets, black-legged kittiwakes and razorbills/common guillemots (chapter 2.2).

The twelve aerial surveys showed relatively few bird species in the area. During the surveys performed from March to December 2022, 18 bird species and 7 species groups were recorded (Table 4.1). Similarly, between January and November 2023, 15 bird species and three species groups were recorded (Table 4.2). Overall, northern fulmars, northern gannets, black-legged kittiwakes and razorbills/common guillemots were the most frequently observed birds in the extended bird survey area during the 2022 and 2023 surveys.

Some species utilise the area for resting and foraging, whereas others only occur there during the time of migration. Divers, northern fulmars, shearwaters, and northern gannets are true seabirds and utilise the extended bird survey area for resting and foraging. This is also the case for several skua, gull and tern species. Finally, alcid species (razorbill and common guillemot) were found in relatively high numbers in the extended bird survey area (Table 4.1 and Table 4.2).

Table 4.1 The bird species or bird species groups recorded from aerial surveys in the extended bird survey area during six surveys between March and December 2022. The number of observed individuals per species or species group is indicated and not estimations of total abundance. Empty cells indicate that no individuals of the species/species group was observed during that survey. Abbreviation "sp." In species names indicate that the observed individuals belong to a species group, but could not be identified to species.

Species name	Sum	2 MAR 2022	1 APR 2022	27 APR 2022	30 JUL 2022	11 SEP 2022	23 DEC 2022
Diver sp.	17			17			
Red-throated diver	18	4		13			1
Northern fulmar	462	7	11	114	78	164	88
Manx shearwater	2					2	
Northern gannet	1,818	129	615	399	91	582	2
Great cormorant	2		2				
Common scoter	1			1			
Eurasian sparrowhawk	1					1	
European golden plover	9					9	
Wader sp.	6					6	
Great skua	3				1	2	
Skua sp.	1			1			
European herring gull	30	10		1			19
Lesser black-backed gull	12					12	
Great black-backed gull	36	21	8		1	3	3
Little gull	1			1			
Black-legged kittiwake	452	173	31	175			73
Gull sp.	44	9	5	22	6	1	1
Common/arctic tern	51			33	18		
Sandwich tern	3				3		
Tern sp.	19				19		
Razorbill	6	6					
Razorbill/common guillemot	1,855	220	822	137	145	212	319
Common guillemot	378	24	18	20	285	29	2
Atlantic puffin	9	6	3				

Species of diving ducks, birds of prey, and waders are all considered to be on migration passage through the extended bird survey area. Consequently, we identified four species/species groups of special interest as birds utilising the extended bird survey area for resting and foraging in significant numbers. Those were northern fulmars, northern

gannets, black-legged kittiwakes and razorbills/common guillemots. These species will be analysed in greater detail in this report. Other species, found in intermediate numbers, will be briefly described below.

Table 4.2 The bird species or bird species groups recorded from aerial surveys in the extended bird survey area during six surveys between January and November 2023. The number of observed individuals per species or species group is indicated and not estimations of total abundances. Empty cells indicate that no individuals of the species/species group was observed during that survey. Abbreviation "sp." In species names indicate that the observed individuals belong to a species group, but could not be identified to species.

Species Name	Sum	21 JAN 2023	02 MAR 2023	03 APR 2023	08 JUL 2023	27 SEP 2023	10 NOV 2023
Diver sp.	1	1					
Red-throated diver	4			4			
Yellow-billed diver	1		1				
Northern fulmar	504	14	20	4	113	131	222
Northern gannet	359	9	3	132	12	192	11
Great cormorant	1		1				
Eurasian wigeon	11			11			
Northern shoveler	10			10			
Common scoter	14			14			
Arctic skua	2					2	
Common gull	1			1			
European herring gull	303	7	39	217	26		14
Lesser black-backed gull	6				6		
Great black-backed gull	40	1	15	11	2		11
Black-legged kittiwake	846	160	183	427		28	48
Gull sp.	33	3	16	1	12		1
Razorbill	109		107	1			1
Razorbill/common guillemot	3,331	234	618	1,376	513	356	234
Common guillemot	1,147	16	4	117	908	23	79

4.1.1 Red-throated/black-throated diver

A total of 41 divers were observed during the twelve aerial surveys (Table 4.1 and Table 4.2). Of those, 35 birds were recorded in 2022, and another six were recorded in 2023. Of those, 22 birds were identified as red-throated divers, while 18 were recorded as unidentified (diver sp.). One yellow-billed diver was recorded during the survey in March 2023. Most divers (30) were recorded during the survey on 27 April 2022, while four were recorded in March 2022, one in December 2022, one in January 2023, one in March 2023 and four in April 2023.

Most of the observed divers were recorded in the eastern and central parts of the extended bird survey area on 27 April 2022 (Figure 4.1 and Figure 4.2). Divers were recorded as single birds or in small groups. The maximum flock size was four individuals, and the mean flock size was 1.37 birds.

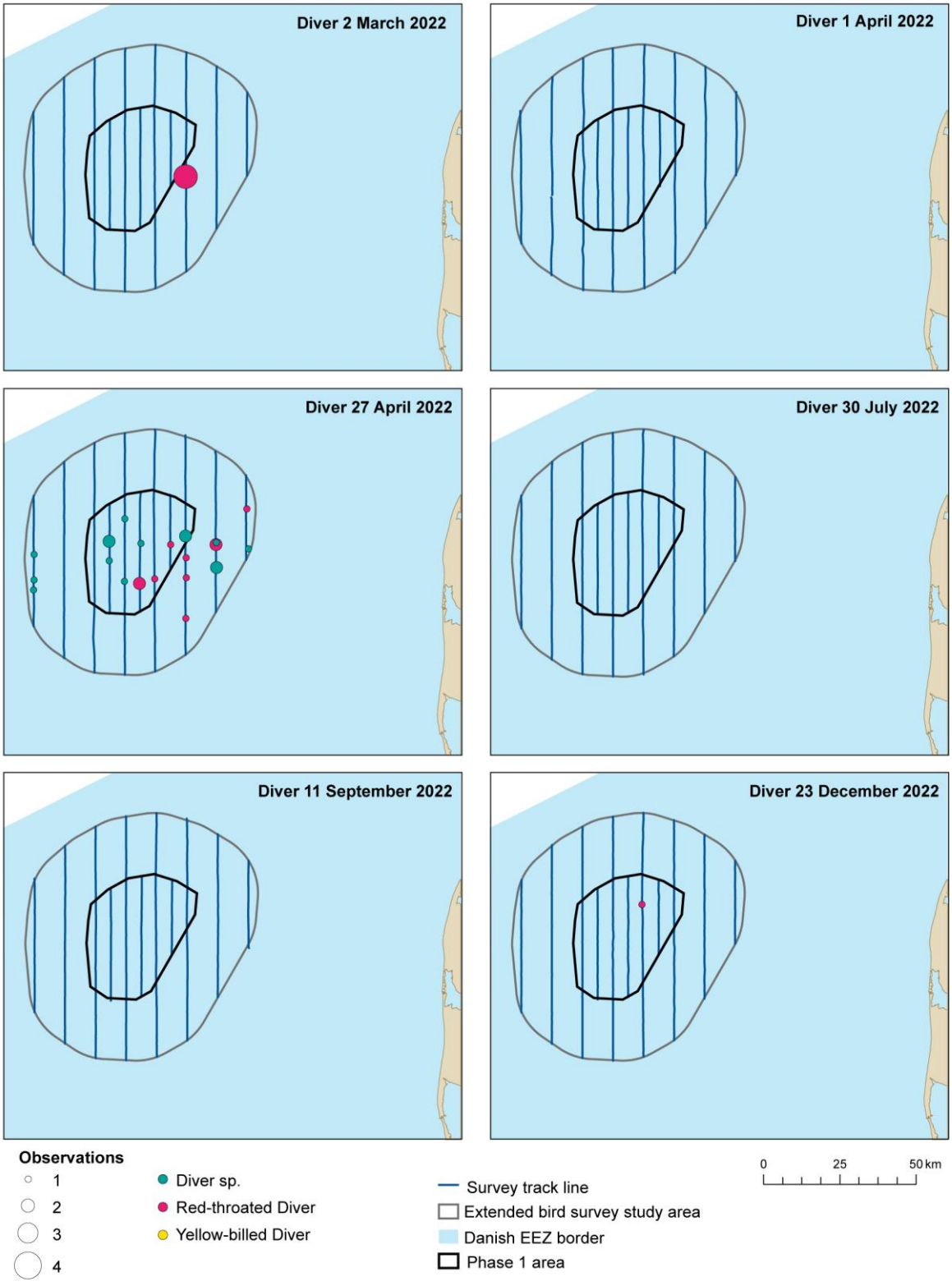

Figure 4.1 The distribution of 35 red-throated/black-throated divers in the North Sea Energy Island extended bird survey area for six surveys conducted between March and December 2022. The covered transect lines are indicated for each survey.

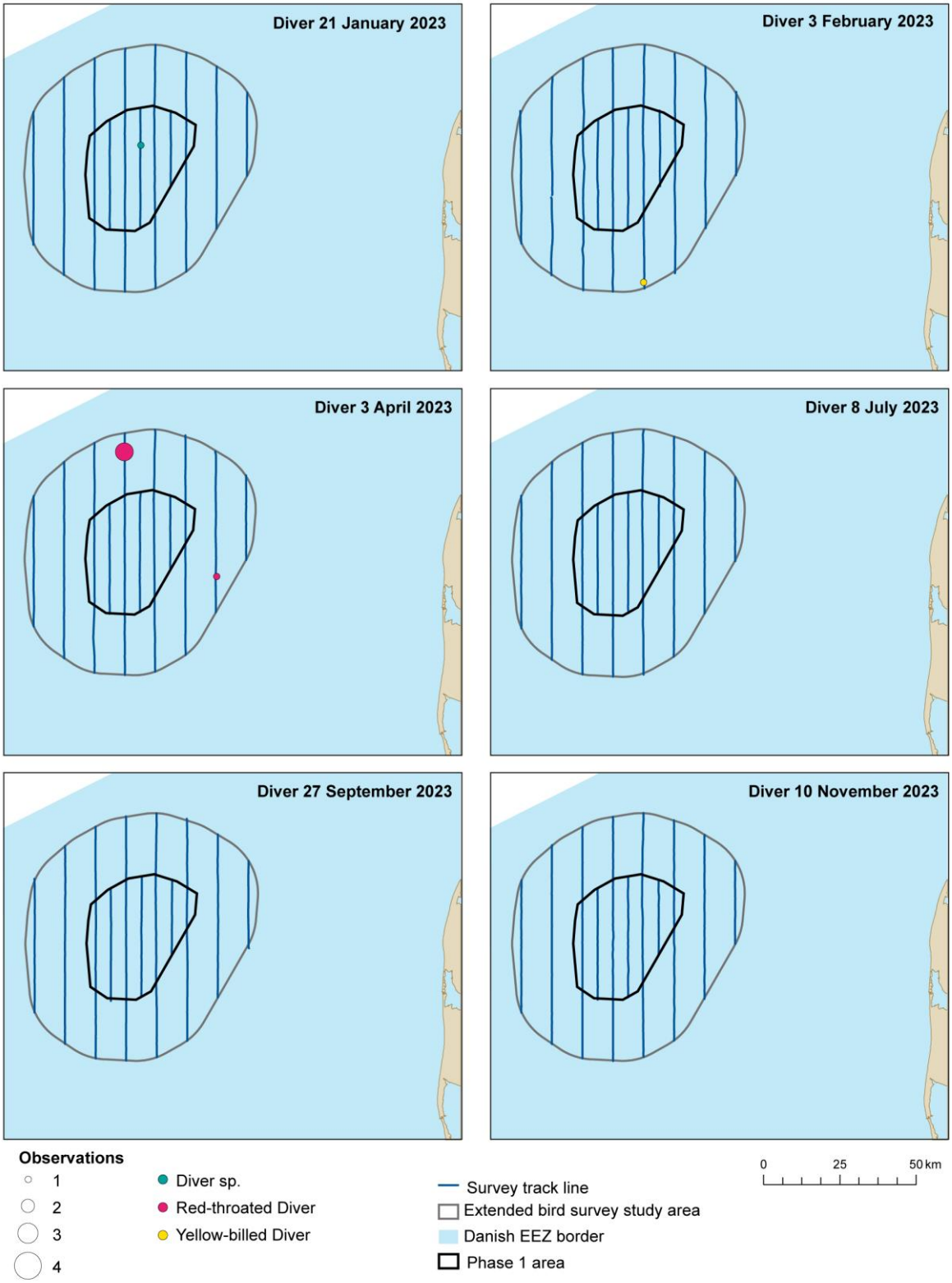

Figure 4.2 The distribution of 5 red-throated/black-throated divers and 1 yellow-billed diver in the North Sea Energy Island extended bird survey area for each of six surveys conducted between January and November 2023. The covered transect lines are indicated for each survey.

The number of observations of divers was insufficient to estimate total numbers and model spatial distribution.

4.1.2 Northern fulmar

A total of 462 northern fulmars was recorded during the twelve aerial surveys (Table 4.1 and Table 4.2). Most northern fulmars were recorded in September 2022 (164), on 27 April (114), and the fewest birds in March 2022.

Northern fulmars clumped within the extended bird survey area, with varying positioning of the occurrences between surveys. The distribution pattern changed between surveys (Figure 4.3 and Figure 4.4).

Northern fulmars were recorded as single birds or in moderate-sized groups. The maximum flock size, recorded by the observers, was 50 individuals, and the mean flock size was 1.62 birds.

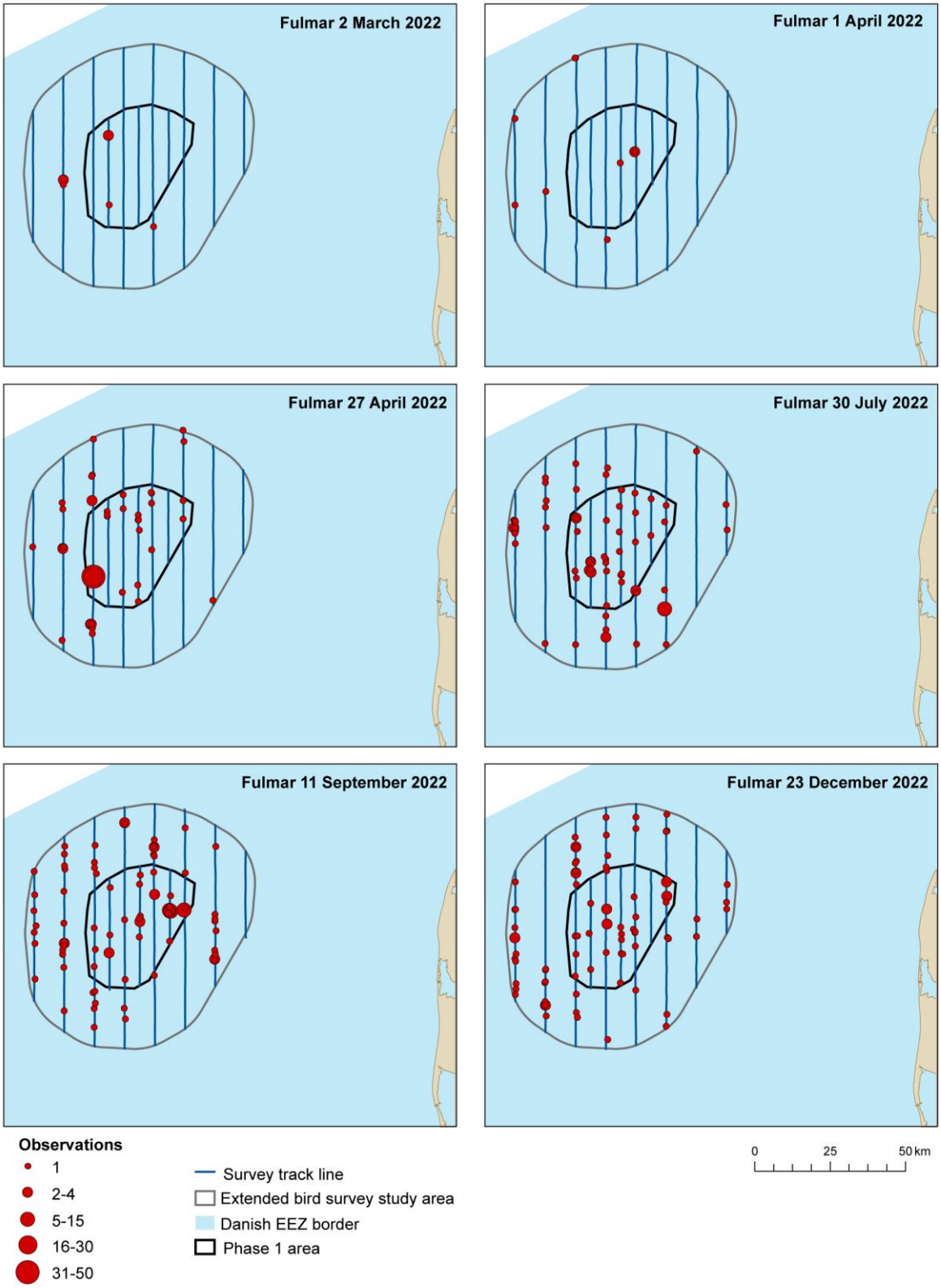

Figure 4.3 The number of observed northern fulmars (462 individuals) and their distribution in the North Sea Energy Island extended bird survey area for each of six surveys conducted between March and December 2022. The covered transect lines are indicated for each survey.

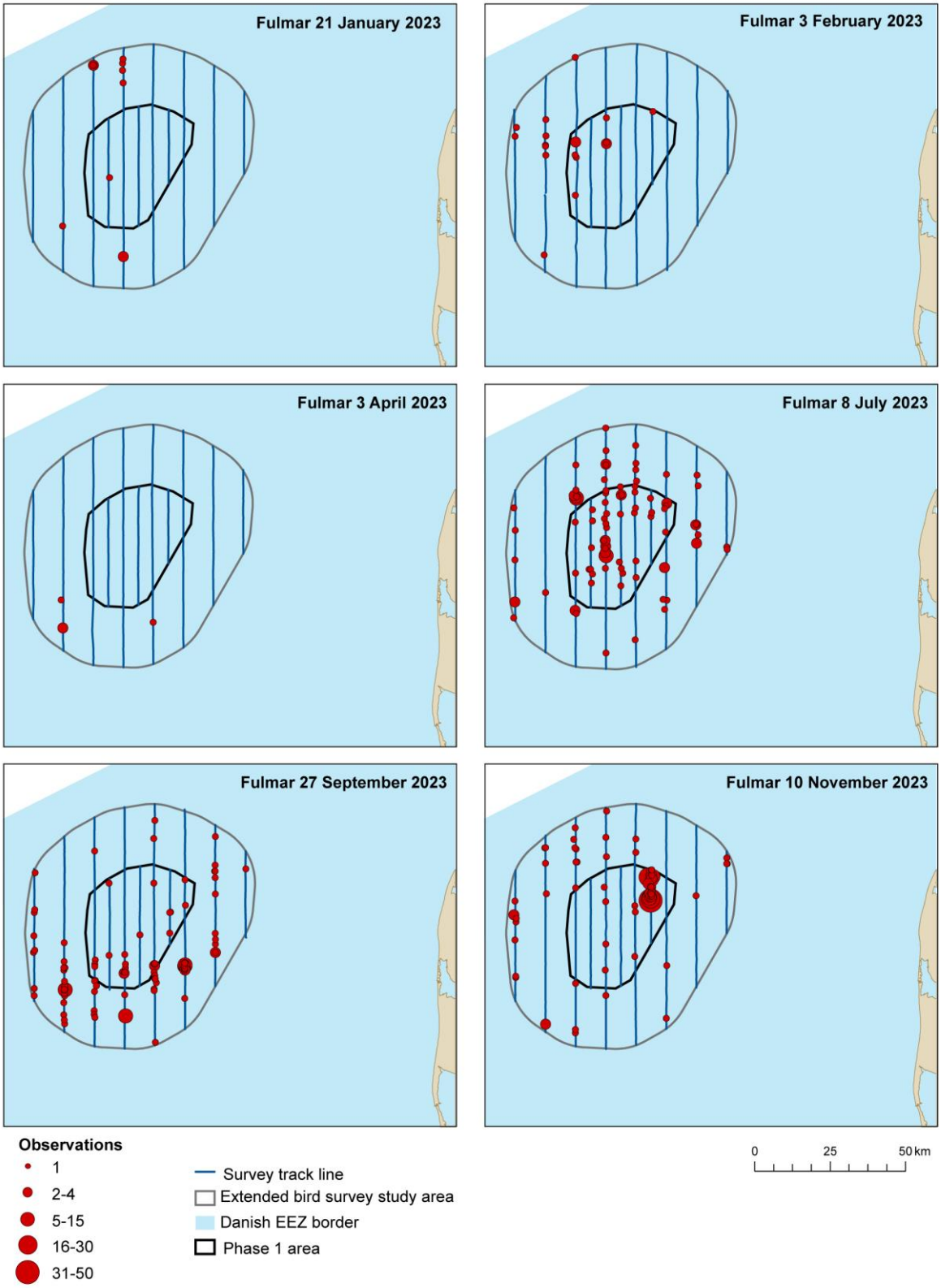

Figure 4.4 The number of observed northern fulmars (504 individuals) and their distribution in the North Sea Energy Island extended bird survey area for each of six surveys conducted between January and November 2023. The covered transect lines are indicated for each survey.

4.1.2.1 *Distance analysis*

The average probability of detecting northern fulmars was estimated to be 0.26 (CoV = 0.06). This probability was estimated using a hazard rate detection function, and no covariates were selected (Figure 4.5).

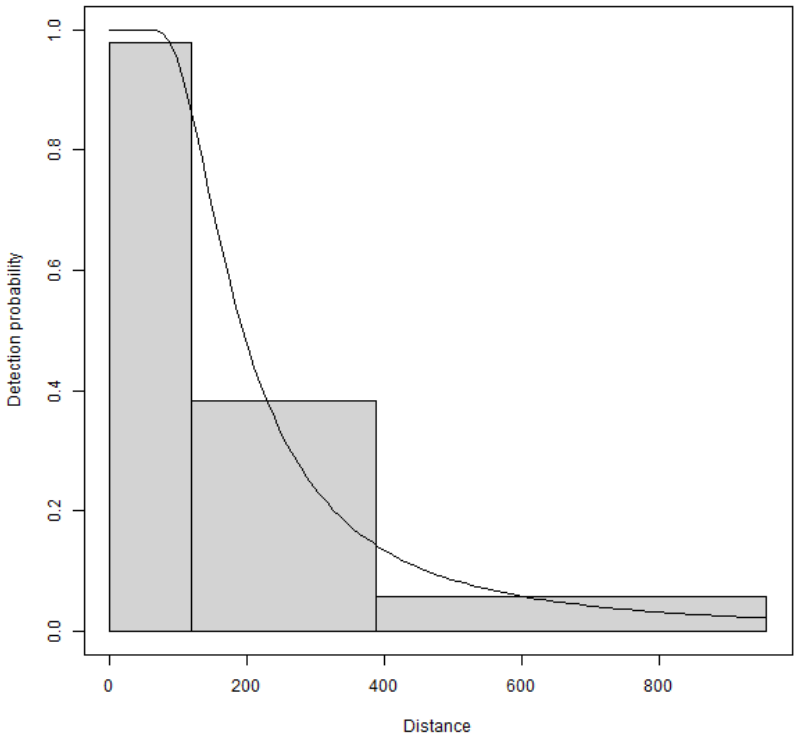

Figure 4.5 The estimated northern fulmar detection function. The histogram represents the distances of the observed sightings.

4.1.2.2 *Spatial analysis*

The data for the spatial analysis contained 14,387 segments overall, 3.3% of which contained fulmar sightings. Figure 4.6 shows the distribution of the distance corrected counts for each of the two months of surveys.

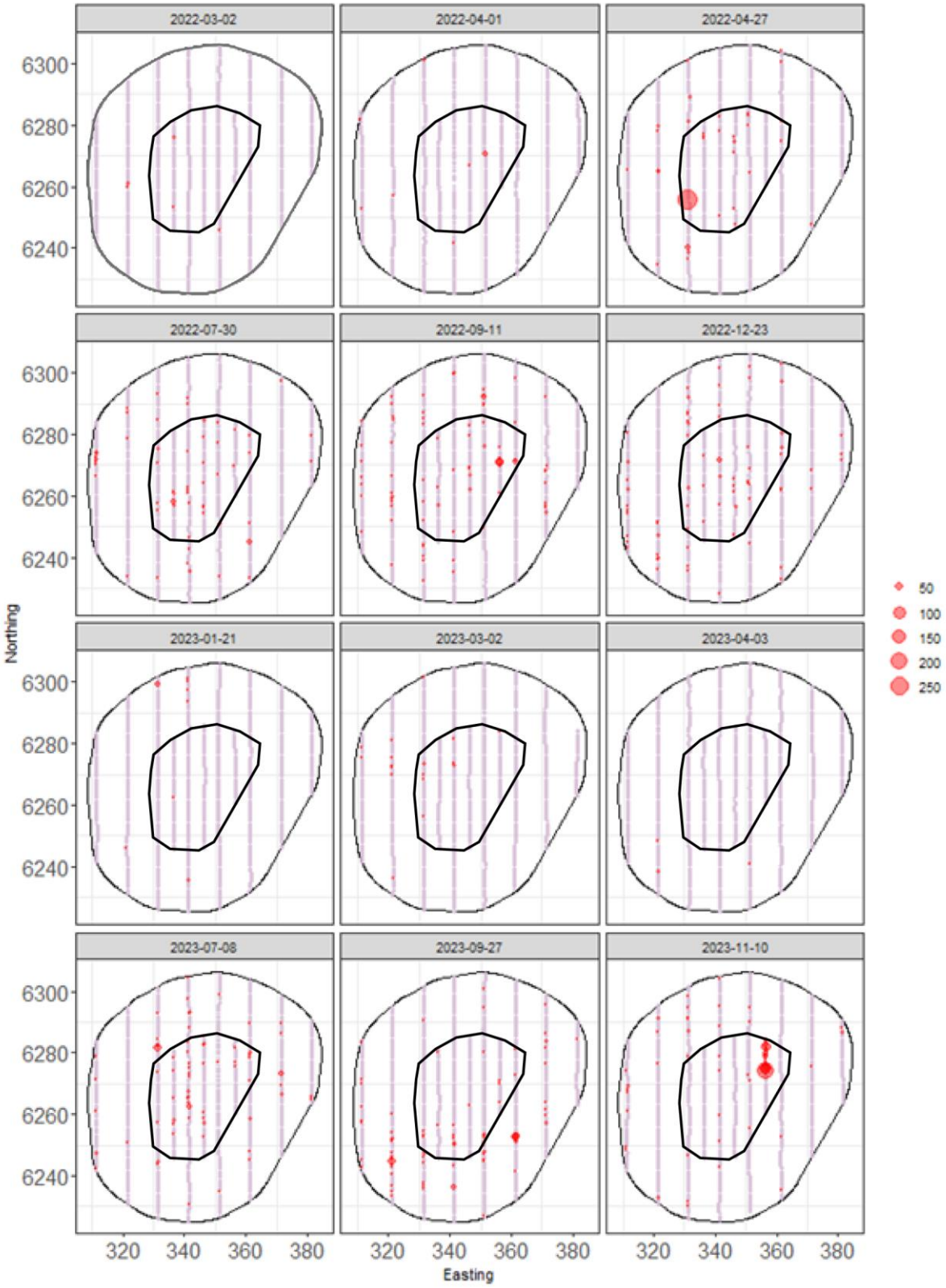

Figure 4.6 Distance-corrected counts for the northern fulmar species across the twelve surveys. The red circles indicate the distance-corrected counts along the transect lines. The pale purple dots are segments with a count of zero.

4.1.2.3 *Model selection*

The models selected for 7 of the 12 surveys included a spatial term (of varying complexity), while the depth covariate was selected as a linear term in two surveys. The distance-to-coast covariate was selected as a linear term for two models and a smooth term for one survey. This shows there was compelling evidence for non-uniform spatial patterns in most surveys, but given these spatial patterns, there was sporadic evidence of depth or distance-to-coast relationships. The spatial surfaces selected ranged from 2 to 10 parameters for the spatial term (Table 4.3).

Table 4.3 Model selection results for northern fulmar for each survey. The model column represents the terms in the model. The distribution column represents the type of distribution model used. The variable 1D column indicate which of the 1D variables has been included in the final model, while variable 2D refers to the spatial smooth. The number of degrees of freedom (df) for each term is given where applicable. "NA" indicates a non-applicable value. The dispersion and Tweedie parameters are as defined in chapter 3.4.2.1.

Name	Model	Distribution	Variable 1D	Variable 2D	Number of parameters	Dispersion parameter	Tweedie parameter
2 March 2022	Intercept only	quasipoisson	NA	NA	1	5.8	NA
1 April 2022	Intercept only	Tweedie	NA	NA	1	10.0	1.20
27 April 2022	2D Only	Tweedie	NA	s(x,y, df = 2)	3	46.9	1.58
30 July 2022	Best 1D2D	quasipoisson	DC, df = 1	s(x,y, df = 10)	12	5.0	NA
11 September 2022	2D Only	quasipoisson	NA	s(x,y, df = 5)	6	5.2	NA
23 December 2022	Best 1D2D	quasipoisson	DC, df = 1	s(x,y, df = 2)	4	6.1	NA
21 January 2023	2D Only	Tweedie	NA	s(x,y, df = 3)	4	9.2	1.26
2 March 2023	Distance to coast	quasipoisson	s(DC, df = 2)	NA	3	4.5	NA
3 April 2023	Intercept only	quasipoisson	NA	NA	1	5.6	NA
8 July 2023	Best 1D2D	quasipoisson	Depth, df = 1	s(x,y, df = 10)	12	5.2	NA
27 September 2023	2D Only	quasipoisson	NA	s(x,y, df = 10)	11	6.4	NA
10 November 2023	Depth	Tweedie	Depth, df = 1	NA	2	25.9	1.41

The estimated abundances and associated 95% percentile confidence intervals for each survey are given in Table 4.4 and Figure 4.7.

Table 4.4 Estimated survey abundance and density (N/km^2) of northern fulmar. The 95% CI are percentile-based confidence intervals.

Month	Area (km^2)	Estimated count	95% CI count	Estimated density	95% CI density
2 March 2022	4,812	114	(46, 307)	0.0	(0, 0.1)
1 April 2022	4,812	206	(103, 421)	0.0	(0, 0.1)
27 April 2022	4,812	1,250	(814, 2,081)	0.3	(0.2, 0.4)
30 July 2022	4,812	1,083	(757, 1,607)	0.2	(0.2, 0.3)
11 September 2022	4,812	1,511	(1,017, 2,407)	0.3	(0.2, 0.5)
23 December 2022	4,812	1,467	(976, 2,313)	0.3	(0.2, 0.5)

21 January 2023	4,812	264	(120, 734)	0.1	(0, 0.2)
2 March 2023	4,812	334	(216, 679)	0.1	(0, 0.1)
3 April 2023	4,812	64	(20, 222)	0.0	(0, 0)
8 July 2023	4,812	1,706	(1,141, 2,828)	0.4	(0.2, 0.6)
27 September 2023	4,812	2,364	(1,493, 4,302)	0.5	(0.3, 0.9)
10 November 2023	4,812	2,246	(976, 6,647)	0.5	(0.2, 1.4)

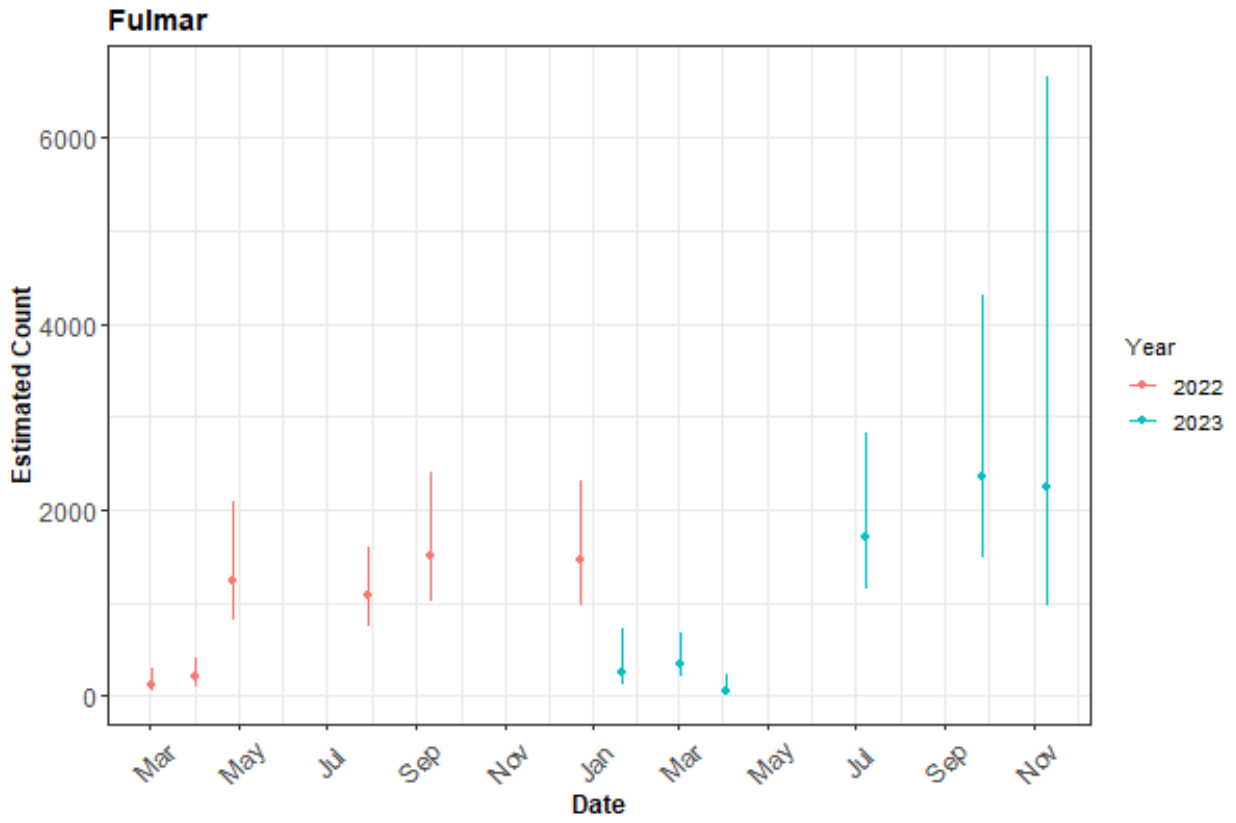

Figure 4.7 The estimated count of northern fulmar for each survey. The 95% CI are percentile-based confidence intervals are from a parametric bootstrap with 500 replicates.

4.1.2.4 Spatial results

Figure 4.8 shows the estimated counts of northern fulmar in each 1 km^2 grid cell for each month. Generally, the estimated abundances fitted well with the raw data, and there were no notable misalignments. In areas where the estimated counts were systematically higher, the abundances were also relatively high, and there were no areas with large, estimated abundances unsupported by the data.

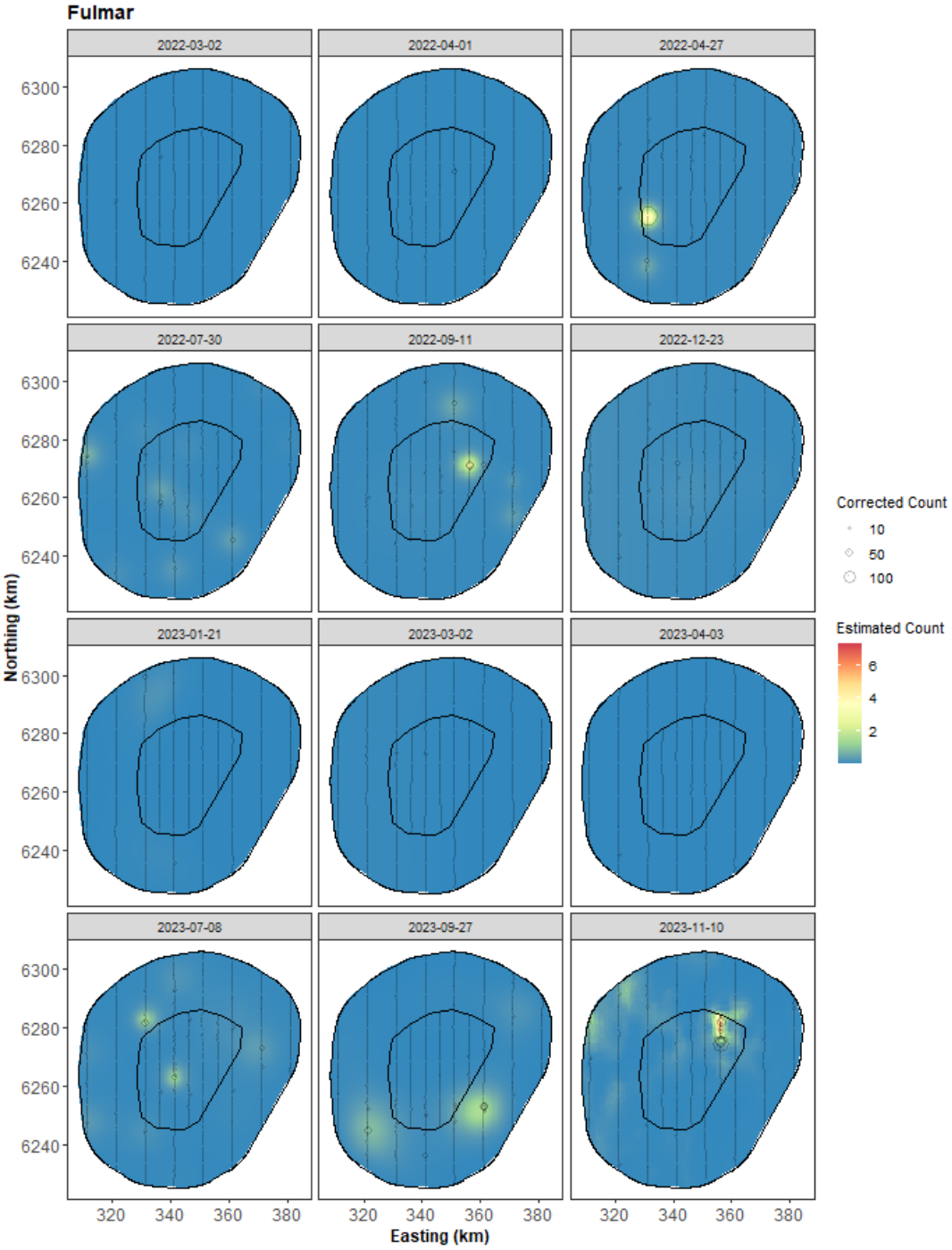

Figure 4.8 The estimated northern fulmar abundance across the study site for each survey. The estimated counts are per 1 km x 1 km grid cell. The open circles show the observed corrected count. The coloured graphics represent the predicted counts in each location.

4.1.2.5 Uncertainty in spatial predictions

Broadly, the highest coefficient of variation (CoV) scores were associated with the 'almost zero' predictions, and it is known that the CoV metric is highly sensitive to any uncertainty for very small predictions. There was one larger value on the eastern side for one of the surveys, but that was otherwise absent from the data. There was no material overlap between high values of the CoV metric and the transect lines/locations with non-zero counts, which results in no concerns in this case (Figure 4.9).

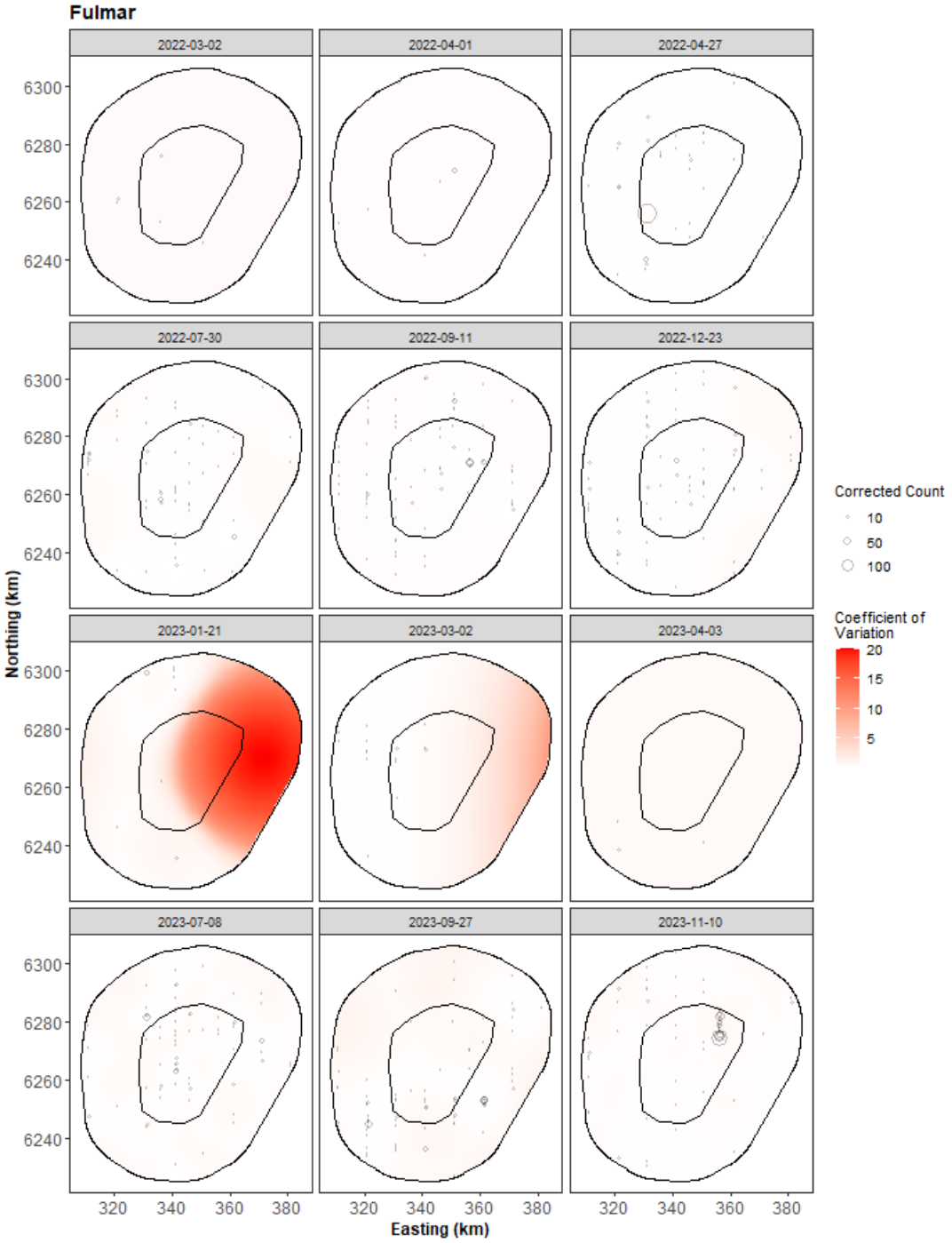

Figure 4.9 The Coefficient of Variation (CoV) across the study region for each survey. The open circles show the distance corrected counts of northern fulmars, where applicable, and the polygons represent the extended bird survey area (black line). The presence of dark red CoV scores in areas with virtually zero predictions is an artefact of the very small prediction rather than of any notable concern.

For the case when the very small, predicted values were excluded (Figure 4.10), the CoV for all surveys was <1.5 and so of no material concern.

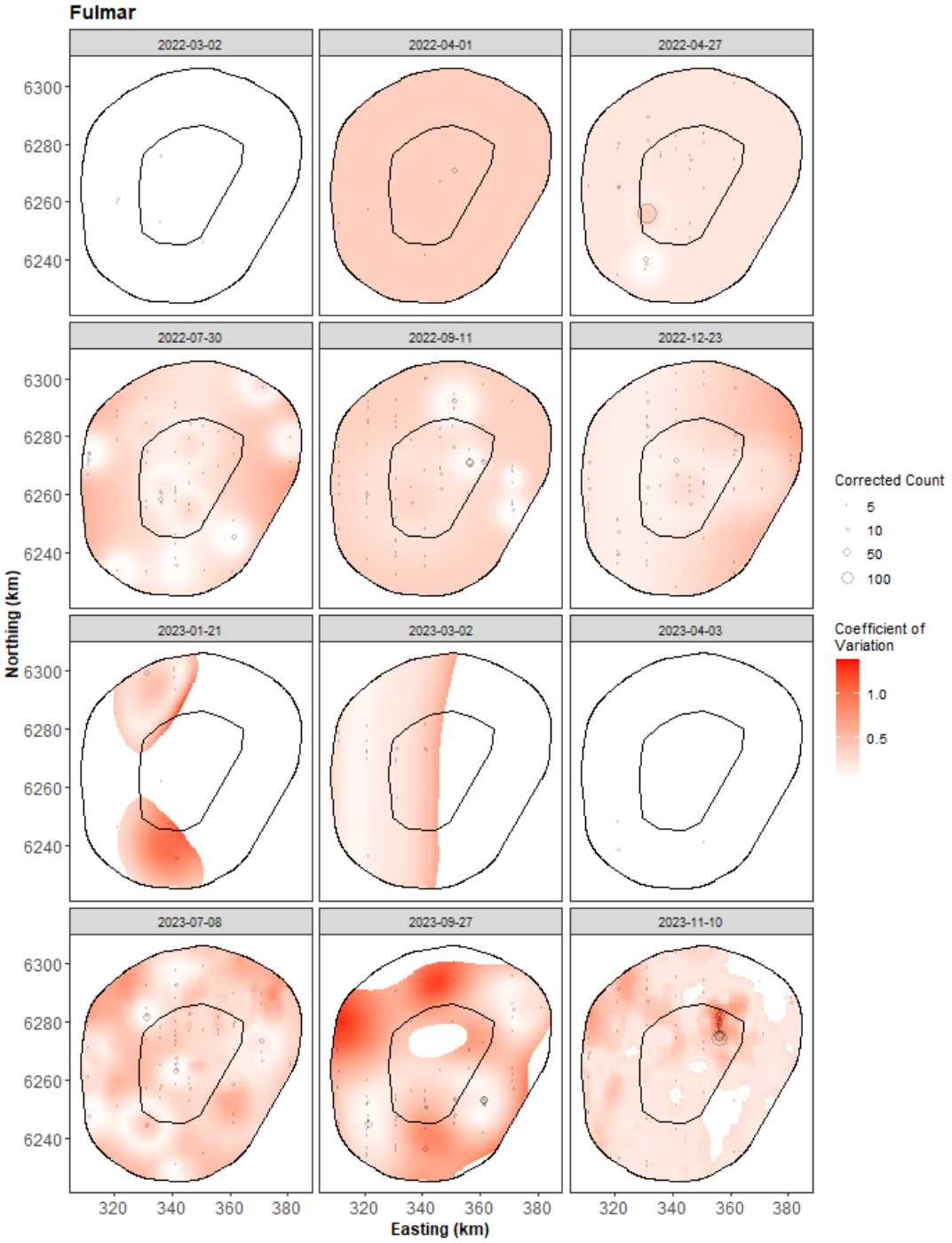

Figure 4.10 The Coefficient of Variation (CoV) for all cells whose mean abundance is > 0.01 birds. The open circles show the distance corrected counts of northern fulmars, where applicable, and the polygons represent the extended bird survey area (black line). The presence of dark red CoV scores in areas with virtually zero predictions is an artefact of the very small prediction rather than of any notable concern.

4.1.2.6 Model diagnostics

A blocking structure was used to account for potential residual non-independence for each model and a robust standard error approach was based on unique transects. In each model, we saw a reassuring decay to zero (indicated by the red and grey lines in Figure 4.11 implying that an appropriate blocking structure was used.

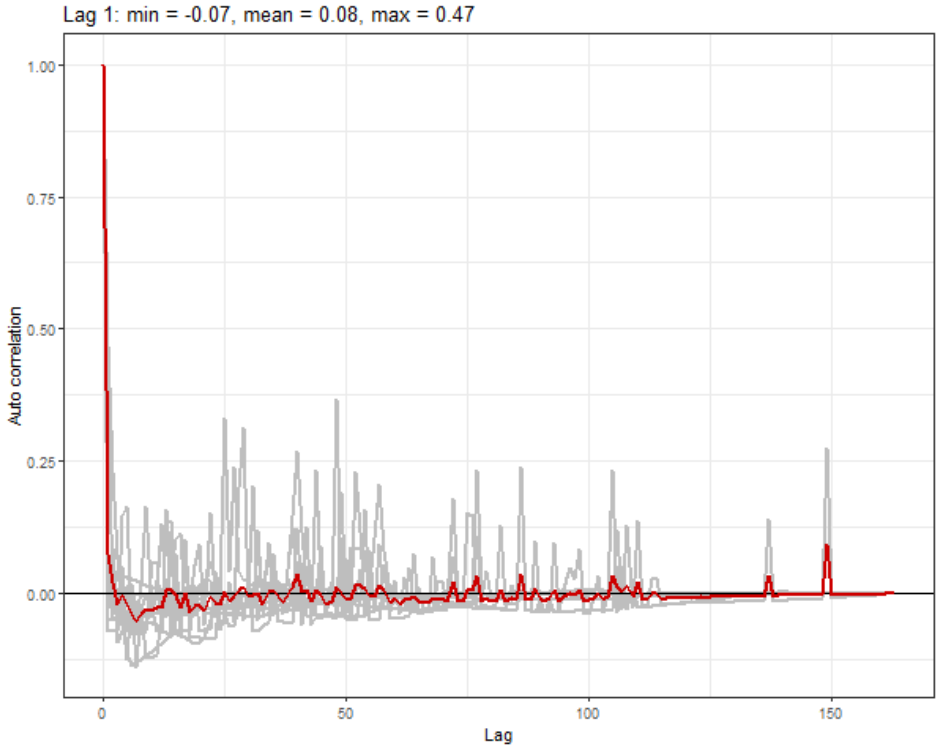

Figure 4.11 Example Auto Correlation Function (ACF) plot for northern fulmar. The grey lines represent the residual correlation observed in each transect, and the red line is the average of these values across transects.

The assumed mean-variance relationship was examined, and there was generally an agreement between the assumed (Quasi-Poisson or Tweedie) lines and the observed values. Figure 4.12 and Figure 4.13 show example relationships for a quasi-Poisson and a Tweedie model. The DHARMa diagnostics, shown for a northern fulmar model example in Figure 4.14, confirmed the nature of the mean-variance relationship was appropriate in all cases. In the example shown, the minor significance of the K-S test did not cause concern, and the residuals were considered homogeneous.

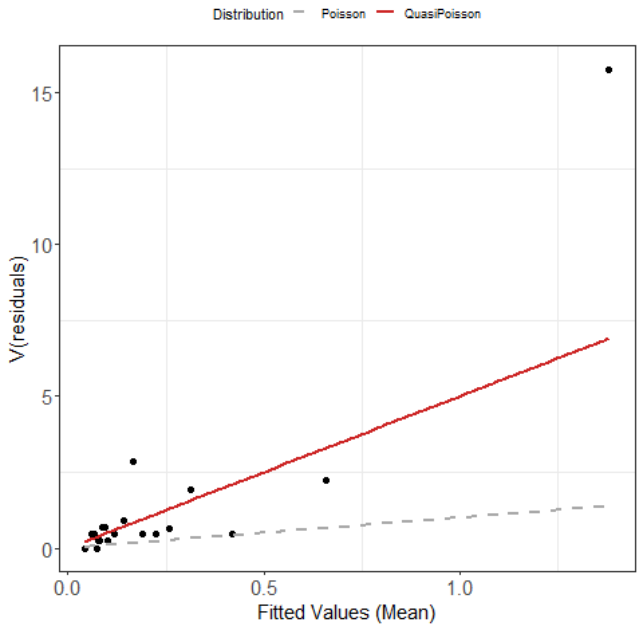

Figure 4.12 Example quasi-Poisson mean-variance relationship (red line) and actual (black dots) for northern fulmar. The black dots are based on 20 quantiles of the model residuals, and for reference, the grey dashed line shows the 1:1 relationship.

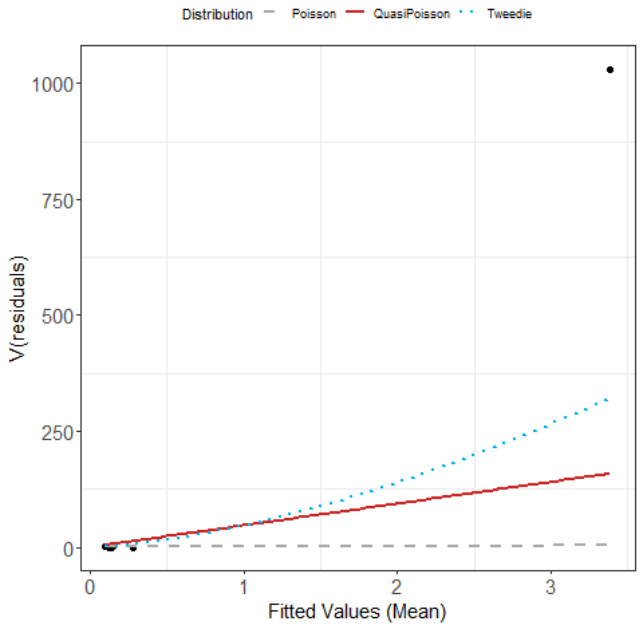

Figure 4.13 Example estimated Tweedie mean-variance relationship (blue dashed line) for northern fulmar. The red line shows the $V(\mu)=\phi\mu$ relationship, and the grey line shows the 1:1 relationship.

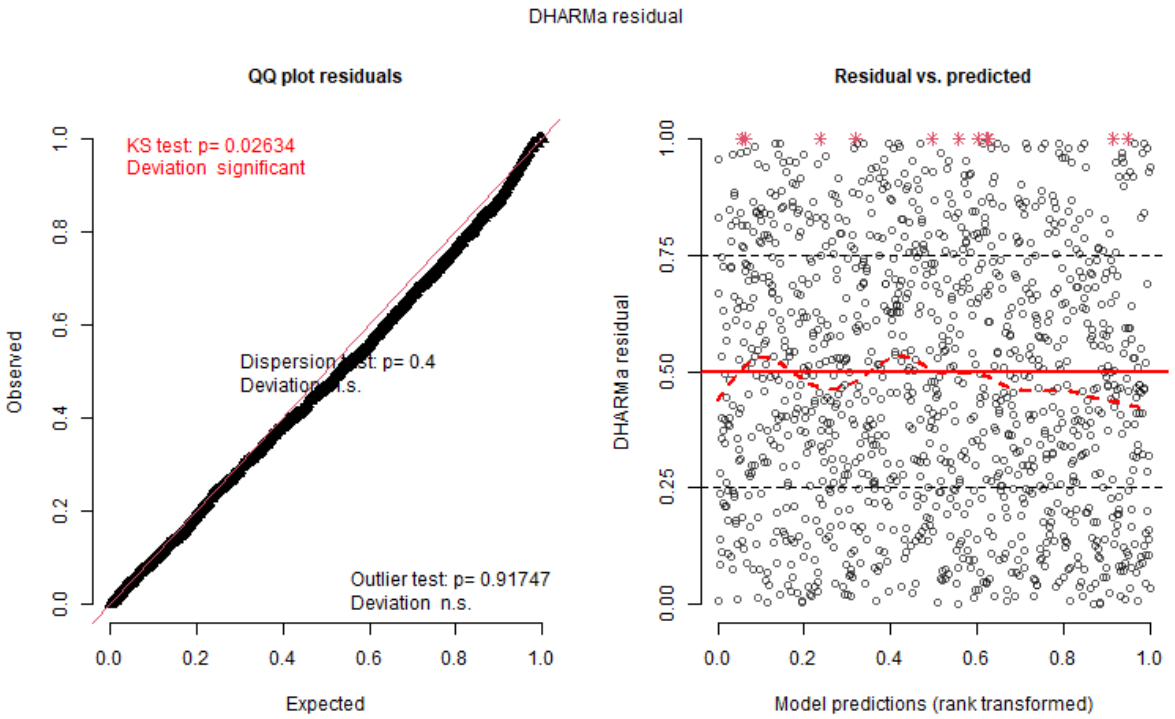

.

Figure 4.14 DHARMa diagnostics for northern fulmar. QQ plot (left) and residuals against predicted values (right). The red stars are outliers, and the red line is a smooth spline around the mean of the residuals.

4.1.2.7 *Areas of persistence*

There is moderate persistence across the 12 surveys (Figure 4.15). The highest persistence (~ 50%) was observed throughout most of the survey area, except the edges on the eastern side.

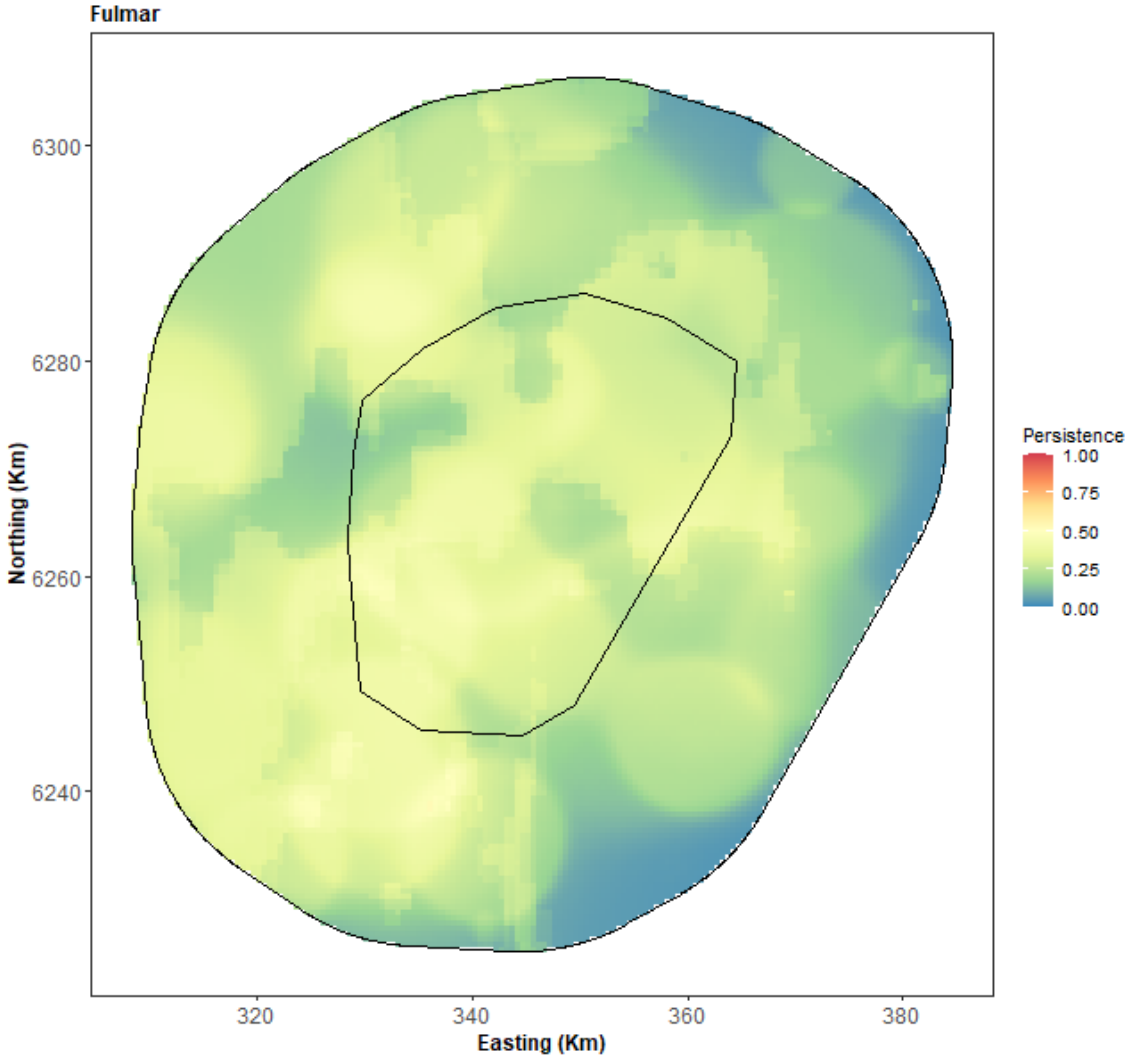

Figure 4.15 Northern fulmar persistence scores across the twelve surveys.

4.1.3 Northern gannet

A total of 2,177 northern gannets was recorded during the 12 aerial surveys (Table 4.1 and Table 4.2). Northern gannets were recorded during all twelve aerial surveys. Most birds were recorded on 1 April 2022 (615) and in September 2022 (582). In 2023, the observed numbers of northern gannets were considerably lower than during the 2022 surveys. This may be related to a severe avian influenza outbreak within this population in the summer of 2022 (Tremlett, Morley, & Wilson, 2024).

Northern gannets clumped over the survey area, with marked differences in distribution between surveys. On 1 and 27 April and September 2022, the central parts of the survey area had a high number of observations, while in March, the concentration was found in the western parts, and during the other surveys, birds were either very few or scattered across the area (Figure 4.16). In 2023, markedly fewer northern gannets were observed. During the April and September surveys, northern gannets were mainly recorded in the extended bird survey area's central and central/southern parts (Figure 4.17).

The North Sea northern gannet population was influenced by an avian influenza incidence in June 2022, with high mortality in a major breeding colony at Bath Rock, Scotland. This event resulted in a 25 % decline in breeding pairs in the United Kingdom between the summer of 2021 and 2023 (Tremlett, Morley, & Wilson, 2024) and may have influenced the fluctuations in northern gannet abundances in the extended bird survey area.

Northern gannets were recorded either as single birds or moderate-sized flocks. The maximum flock size was 30 individuals, and the mean flock size was 1.70 birds.

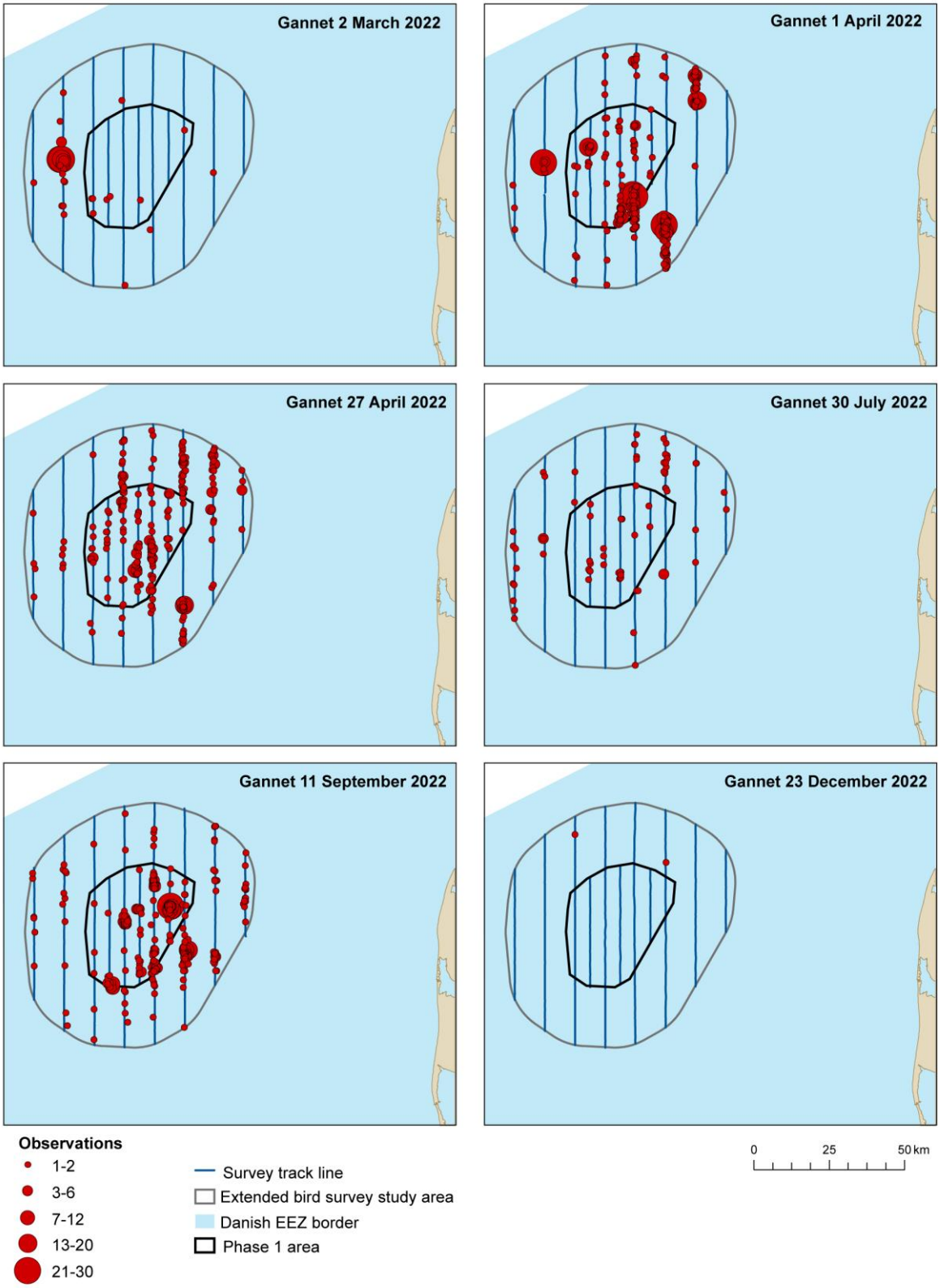

Figure 4.16 The number of observed northern gannets (1,018 individuals) and their distribution in the North Sea Energy Island extended bird survey area for each of six surveys conducted between March and December 2022. The covered transect lines are indicated for each survey.

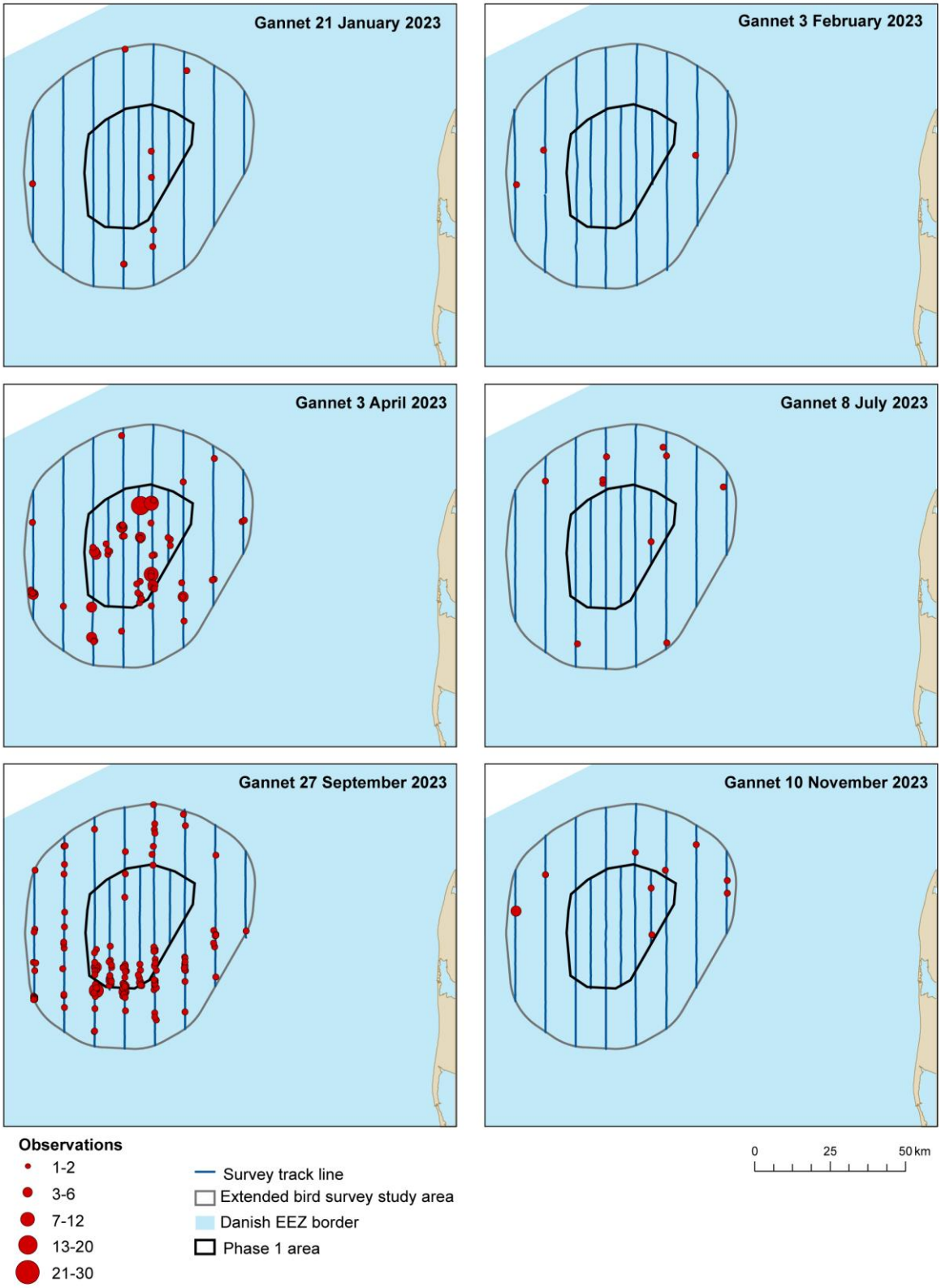

Figure 4.17 The number of observed northern gannets (359 individuals) and their distribution in the North Sea Energy Island extended bird survey area for six surveys conducted between January and December 2023. The covered transect lines are indicated for each survey.

4.1.3.1 *Distance analysis*

The average probability of sighting northern gannets was estimated to be 0.37 (CoV = 0.02). This probability was estimated using a half-normal detection function with flock size as a continuous covariate (Figure 4.18). The probability of detection of larger flocks (groups) is higher for all distance bins than the corresponding probability of detection of small groups because large flocks are more conspicuous to the observer than small flocks (groups).

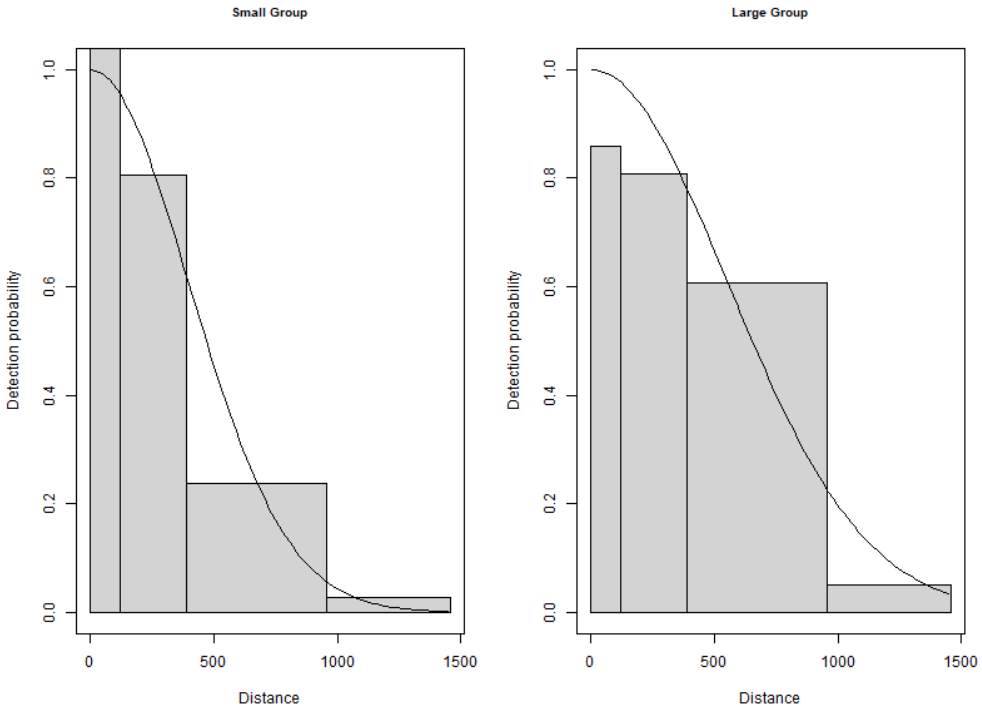

Figure 4.18 The estimated northern gannet detection function for small and large group sizes. The histogram represents the distances of the observed sightings. Large and small are defined by the 10th and 90th quantiles of the distribution of observed group sizes.

4.1.3.2 *Spatial analysis*

The spatial analysis data contained 14,453 segments, 5.4% of which contained northern gannet sightings. Figure 4.19 shows the distribution of the distance corrected counts for each of the twelve surveys.

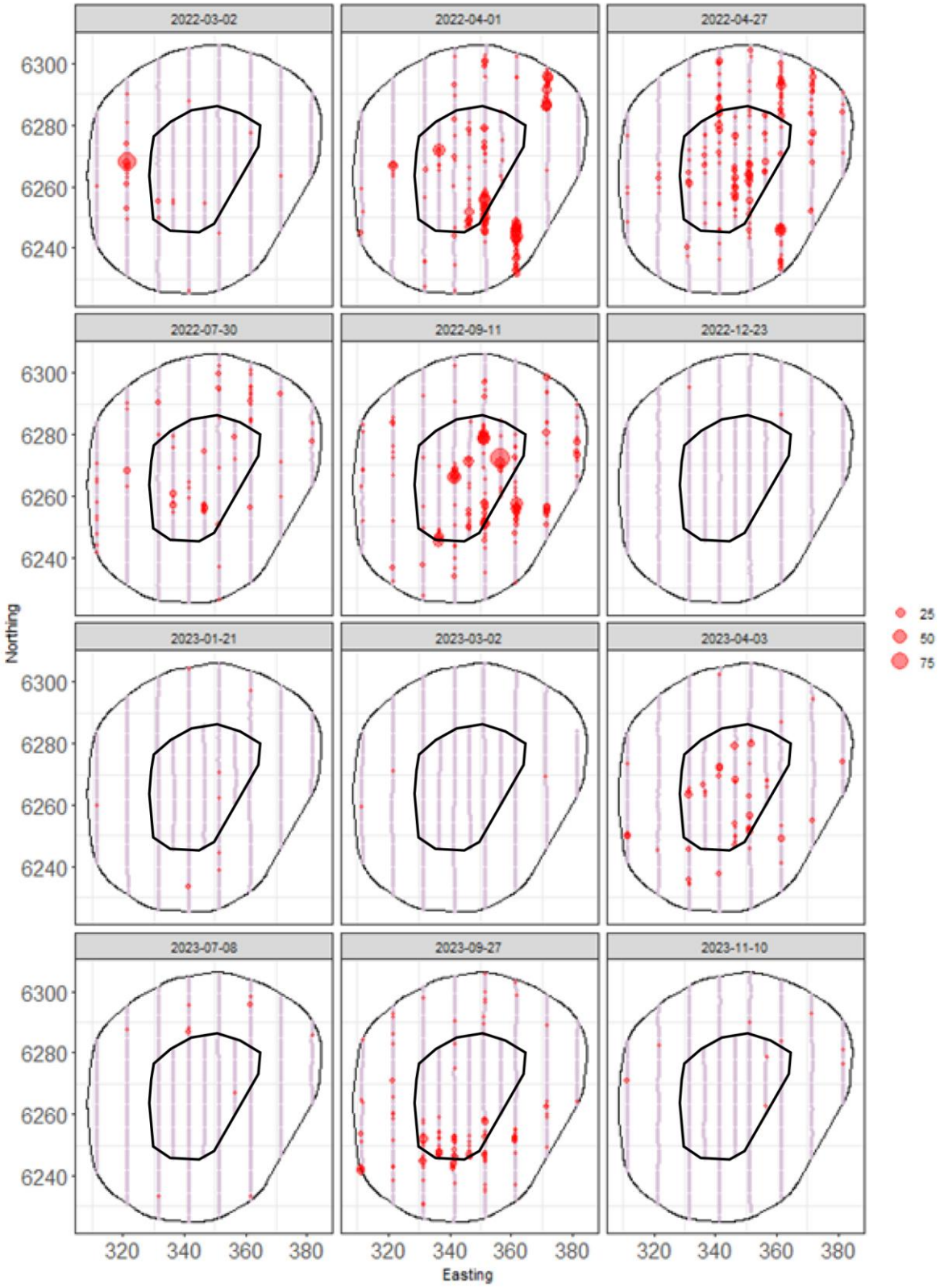

Figure 4.19 Distance-corrected counts for the northern gannet across the 12 surveys. The red circles indicate the distance-corrected counts along the transect lines. The pale purple dots are segments with a count of zero.

4.1.3.3 Model selection

For 8 of the 12 surveys, the models selected for each survey included a spatial term (of varying complexity), while the depth covariate (either as a linear or smooth term) was not selected for any surveys. The distance-to-coast covariate was selected as a smooth term for just one model. This shows compelling evidence for non-uniform spatial patterns in each survey, but given these spatial patterns, there was little evidence of depth or distance-to-coast relationships. The spatial surfaces selected ranged from 3 to 20 parameters for the spatial term (Table 4.5).

Table 4.5 Model selection results for northern gannet for each survey. The model column represents the terms in the model. The distribution column represents the type of distribution model used. The variable 1D column indicate which of the 1D variables has been included in the final model, while variable 2D refers to the spatial smooth. The number of degrees of freedom (df) for each term are given where applicable. "NA" indicates a non-applicable value. The dispersion and Tweedie parameters are as defined in section 3.4.2.1.

Name	Model	Distribution	Variable 1D	Variable 2D	Number of parameters	Dispersion parameter	Tweedie parameter
2 March 2022	2D Only	Tweedie	NA	s(x,y, df = 6)	7	11.7	1.35
1 April 2022	2D Only	quasipoisson	NA	s(x,y, df = 9)	10	15.1	1.34
27 April 2022	Best 1D2D	Tweedie	s(DC, df = 2)	s(x,y, df = 20)	23	5.2	1.18
30 July 2022	2D Only	quasipoisson	NA	s(x,y, df = 12)	13	4.7	NA
11 September 2022	2D Only	Tweedie	NA	s(x,y, df = 6)	7	14.6	1.40
23 December 2022	Intercept only	quasipoisson	NA	NA	1	2.9	NA
21 January 2023	Intercept only	quasipoisson	NA	NA	1	3.5	NA
2 March 2023	Intercept only	quasipoisson	NA	NA	1	2.9	NA
3 April 2023	2D Only	Tweedie	NA	s(x,y, df = 14)	15	8.9	1.22
8 July 2023	Intercept only	quasipoisson	NA	NA	1	3.6	NA
27 September 2023	2D Only	quasipoisson	NA	s(x,y, df = 9)	10	5.8	NA
10 November 2023	2D Only	quasipoisson	NA	s(x,y, df = 3)	4	2.9	NA

The estimated abundances and associated 95% percentile confidence intervals for each survey are given in Table 4.6 and Figure 4.20.

Table 4.6 Estimated survey abundance and density (N/km^2) of northern gannet. The 95% CI are percentile-based confidence intervals.

Month	Area (km^2)	Estimated count	95% CI count	Estimated density	95% CI density
2 March 2022	4,812	537	(333, 932)	0.1	(0.1, 0.2)
1 April 2022	4,812	3,797	(2,228, 7,830)	0.8	(0.5, 1.6)
27 April 2022	4,812	2,465	(1,819, 3,662)	0.5	(0.4, 0.8)
30 July 2022	4,812	664	(421, 1,173)	0.1	(0.1, 0.2)
11 September 2022	4,812	3,112	(1,918, 5,182)	0.6	(0.4, 1.1)
23 December 2022	4,812	16	(4, 54)	0.0	(0, 0)
21 January 2023	4,812	73	(33, 183)	0.0	(0, 0)

2 March 2023	4,812	24	(9, 73)	0.0	(0, 0)
3 April 2023	4,812	668	(421, 1,186)	0.1	(0.1, 0.2)
8 July 2023	4,812	95	(45, 211)	0.0	(0, 0)
27 September 2023	4,812	1,422	(902, 2,526)	0.3	(0.2, 0.5)
10 November 2023	4,812	81	(48, 170)	0.0	(0, 0)

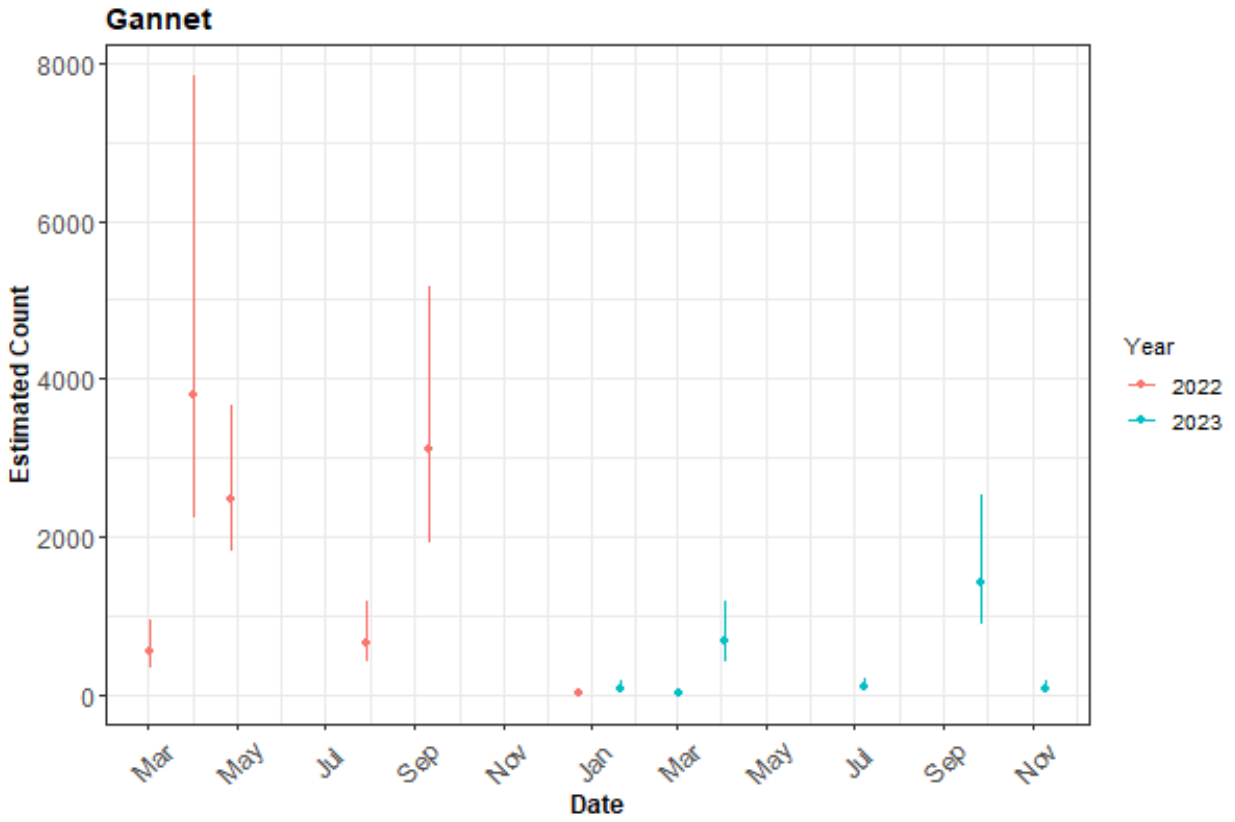

Figure 4.20 The estimated count of northern gannets for each survey. The 95% CI are percentile-based confidence intervals are from a parametric bootstrap with 500 replicates.

4.1.3.4 Spatial results

Figure 4.21 shows the estimated counts of northern gannets in each 1 km^2 grid cell for each month. Generally, the estimated abundances fitted well with the raw data, and there were no notable misalignments. In areas where the estimated counts were systematically higher, the abundances were also relatively high, and there were no areas with large, estimated abundances unsupported by the data.

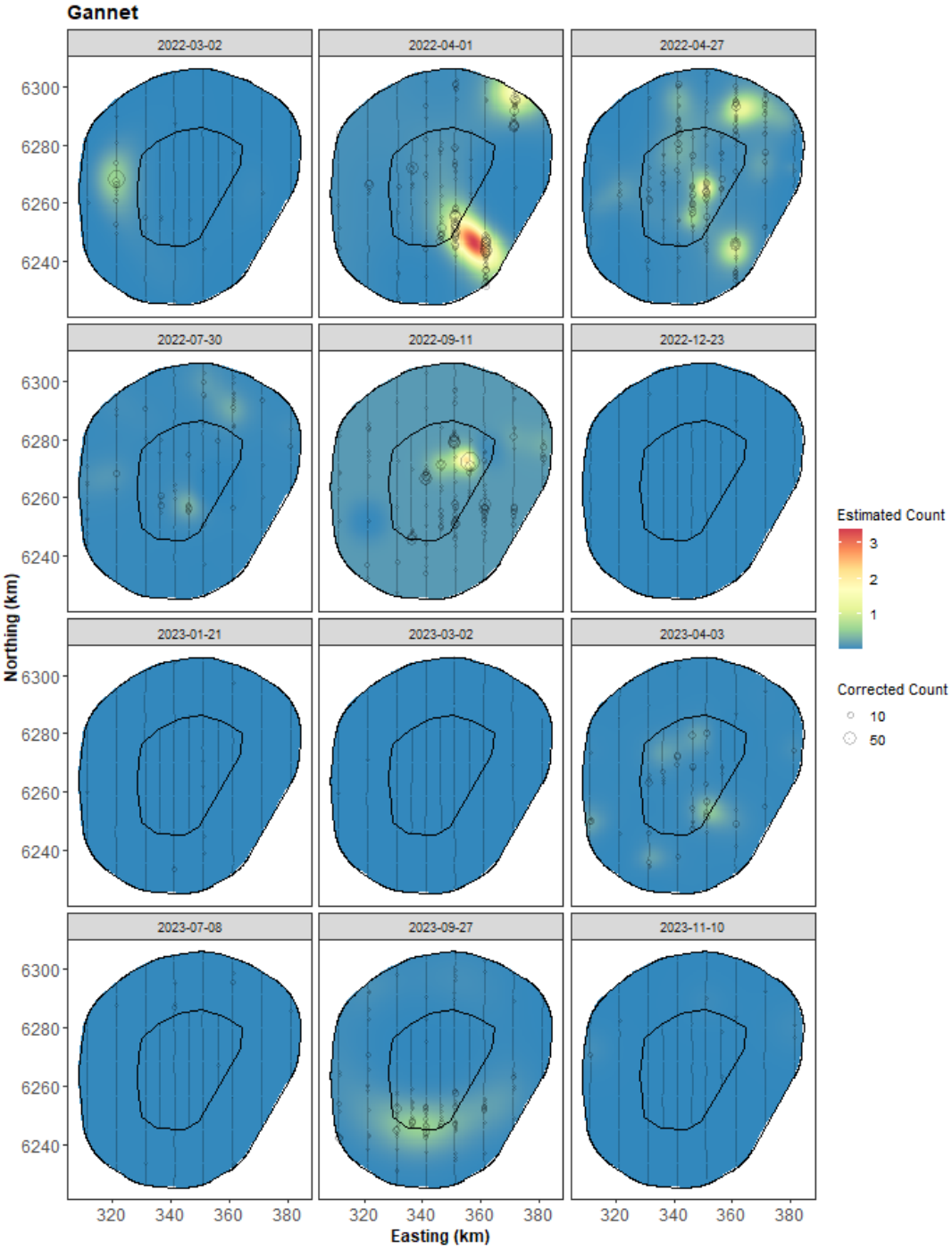

Figure 4.21 The estimated northern gannet abundance across the study site for each survey. The estimated counts are per 1 km x 1 km grid cell. The open circles show the observed corrected count. The coloured graphics represent the predicted counts in each location.

4.1.3.5 Uncertainty in spatial predictions

Broadly, the highest Coefficient of Variation (CoV) scores were associated with 'almost zero' predictions, and it is known that the CoV metric is highly sensitive to any uncertainty for very small predictions. There was one larger value in the centre of the survey area on 30 July 2022, but that was otherwise absent of data. There was no material overlap between high values of the CoV metric and the transect lines/locations with non-zero counts, resulting in no concerns in this case (Figure 4.22).

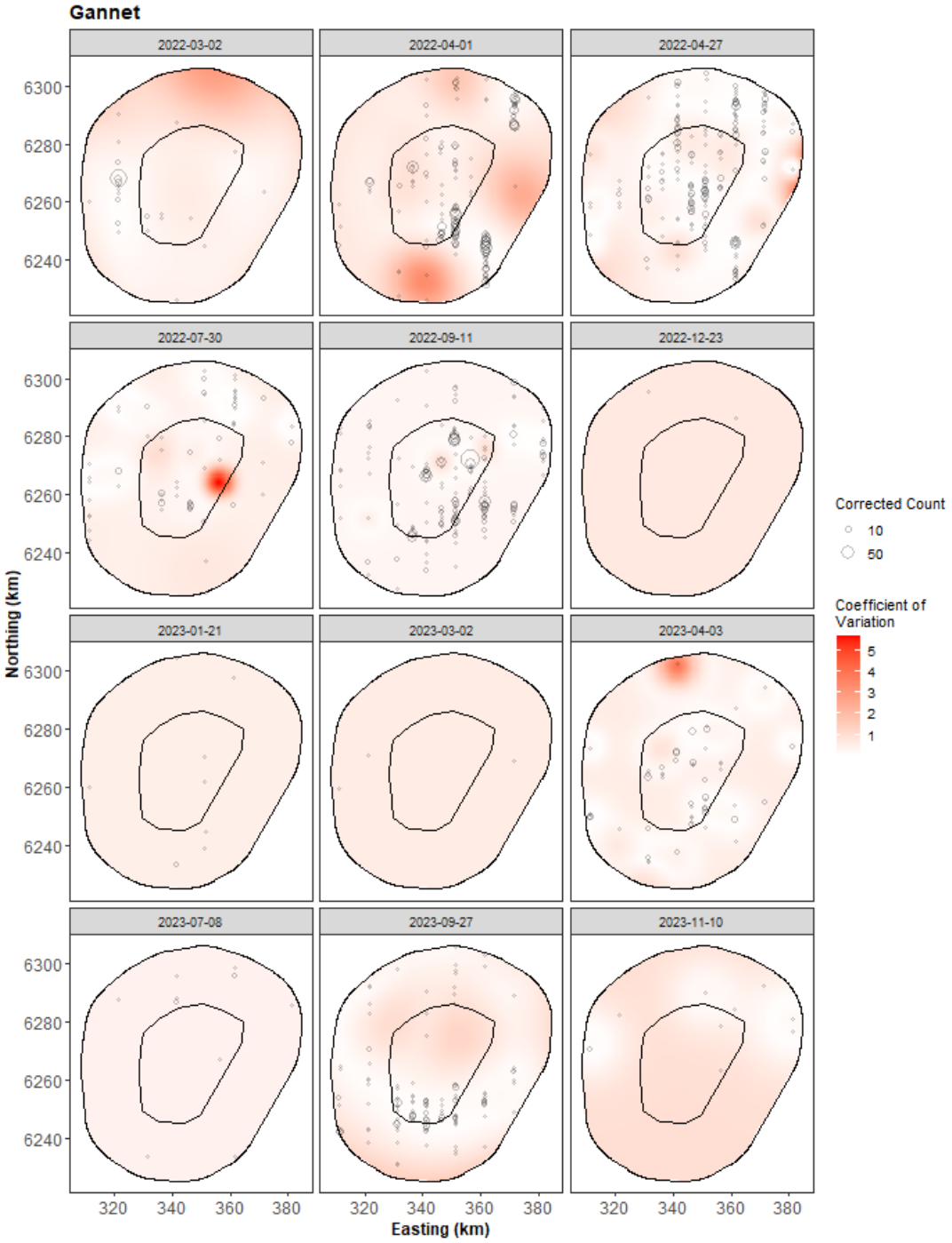

Figure 4.22 The Coefficient of Variation (CoV) across the study region for each survey. The open circles show the distance corrected northern gannet counts, where applicable, and the polygons represent the extended bird survey area (black line). The presence of dark red CoV scores in areas with virtually zero predictions is an artefact of the very small prediction rather than of any notable concern.

For the case when the very small, predicted values were excluded (Figure 4.23), the CoV for all surveys was <1 for most surveys, so it is of no material concern. There remains some high uncertainty for two surveys around very small values, which will play a role in the related confidence intervals for the abundances (Table 4.6 and Figure 4.20).

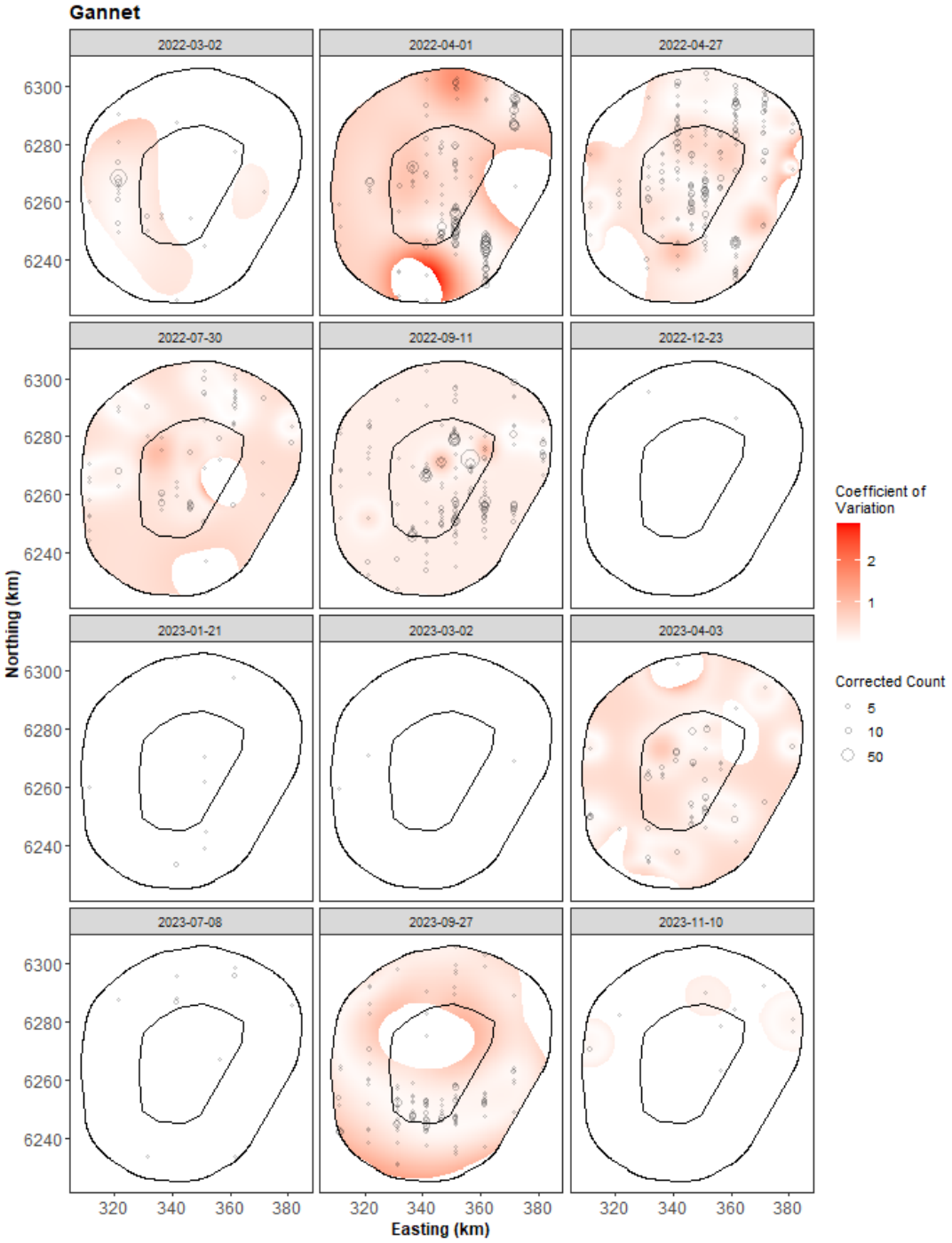

Figure 4.23 The Coefficient of Variation (CoV) for all cells whose mean abundance is > 0.01 birds. The open circles show the distance corrected northern gannet counts, where applicable, and the polygons represent the extended bird survey area (black line). The presence of dark red CoV scores in areas with virtually zero predictions is an artefact of the very small prediction rather than of any notable concern.

4.1.3.6 Model diagnostics

A blocking structure was used to account for potential residual non-independence for each model and a robust standard error approach was based on unique transects. In each model, we saw a reassuring decay to zero (indicated by the red and grey lines in Figure 4.24), implying that an appropriate blocking structure was used.

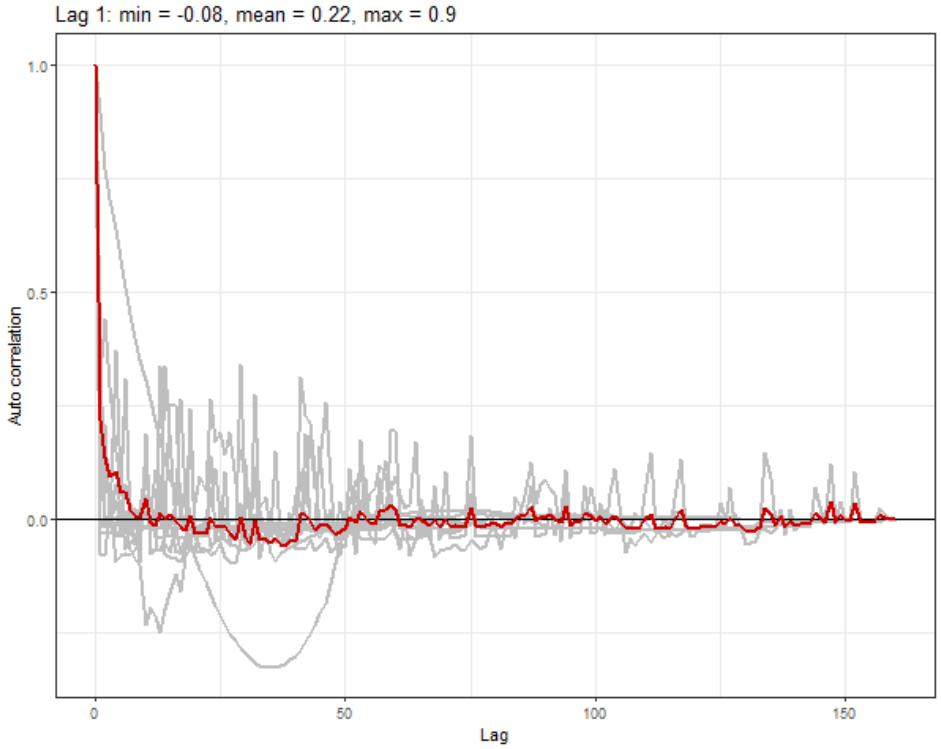

Figure 4.24 Example of northern gannet Auto Correlation Function (ACF) plot. The grey lines represent the residual correlation observed in each transect, and the red line is the average of these values across transects.

The assumed mean-variance relationship was examined, and there was generally an agreement between the assumed (Quasi-Poisson or Tweedie) lines and the observed values. Figure 4.25 and Figure 4.26 show example relationships for a quasi-Poisson and a Tweedie model. The DHARMa diagnostics, shown for a northern gannet model example in Figure 4.27, confirmed the nature of the mean-variance relationship was appropriate in all cases. In the example shown, there is no compelling evidence against the null hypothesis of a correct overall residual distribution, as indicated by the p-values for the associated tests, and the residuals were also considered homogeneous.

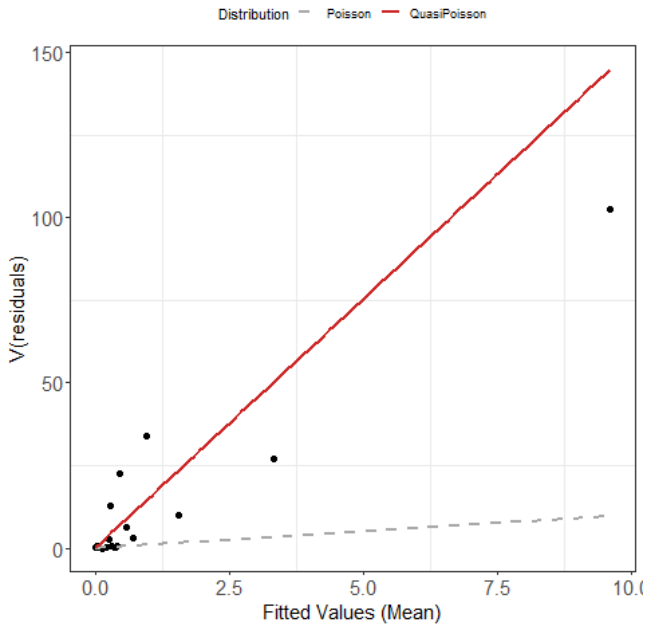

Figure 4.25 Example quasi-Poisson mean-variance relationship (red line) and actual (black dots) for northern gannet. The black dots are based on 20 quantiles of the model residuals, and for reference, the grey dashed line shows the 1:1 relationship.

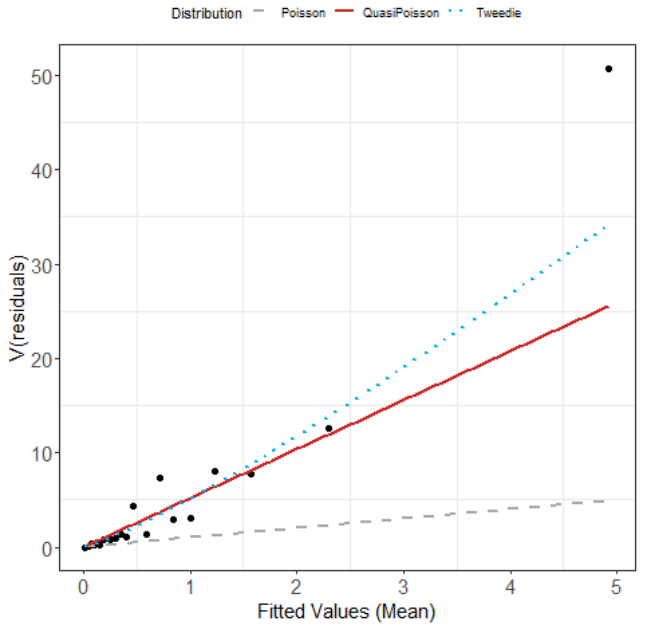

Figure 4.26 Example estimated Tweedie mean-variance relationship (blue dashed line) for northern gannet. The red line shows the $V(\mu)=\phi\mu$ relationship, and the grey line shows the 1:1 relationship.

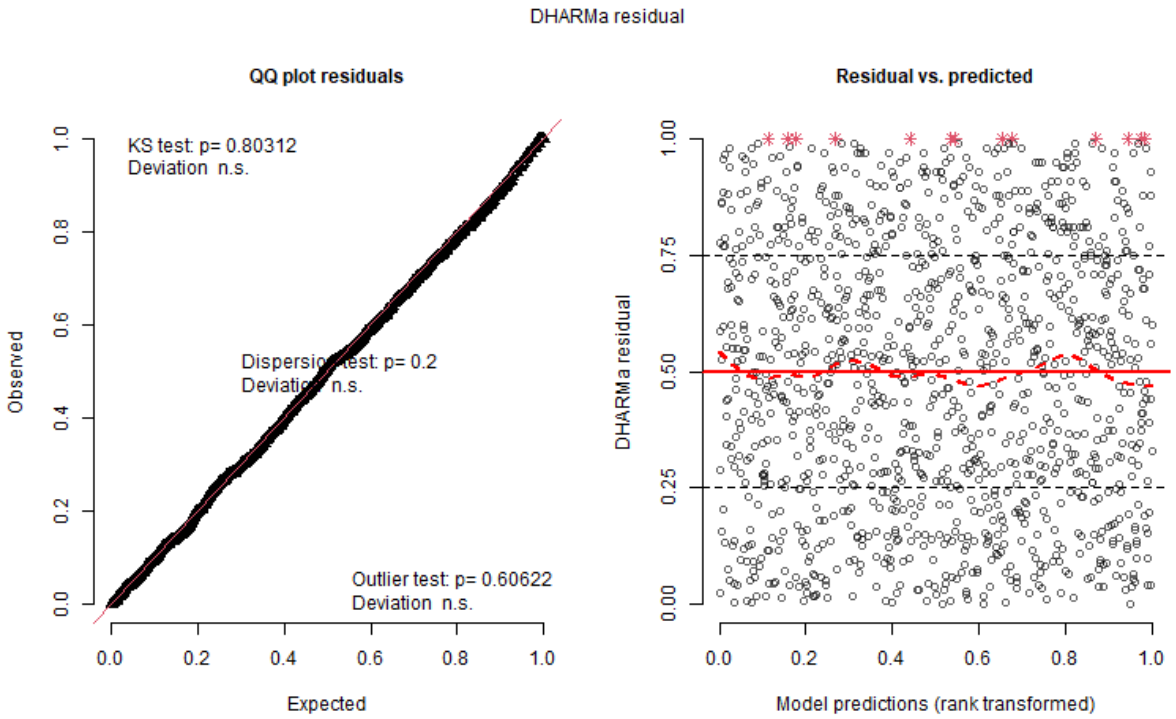

Figure 4.27 Northern gannet DHARMa diagnostics. Example QQ plot (left) and residuals against predicted values (right). The red stars are outliers, and the red line is a smooth spline around the mean of the residuals.

4.1.3.7 Areas of persistence

Across the 12 surveys, there is moderate to low persistence across the survey area (Figure 4.28). The persistency analysis indicates that, analysed over multiple surveys, the area has areas of constant high or low importance.

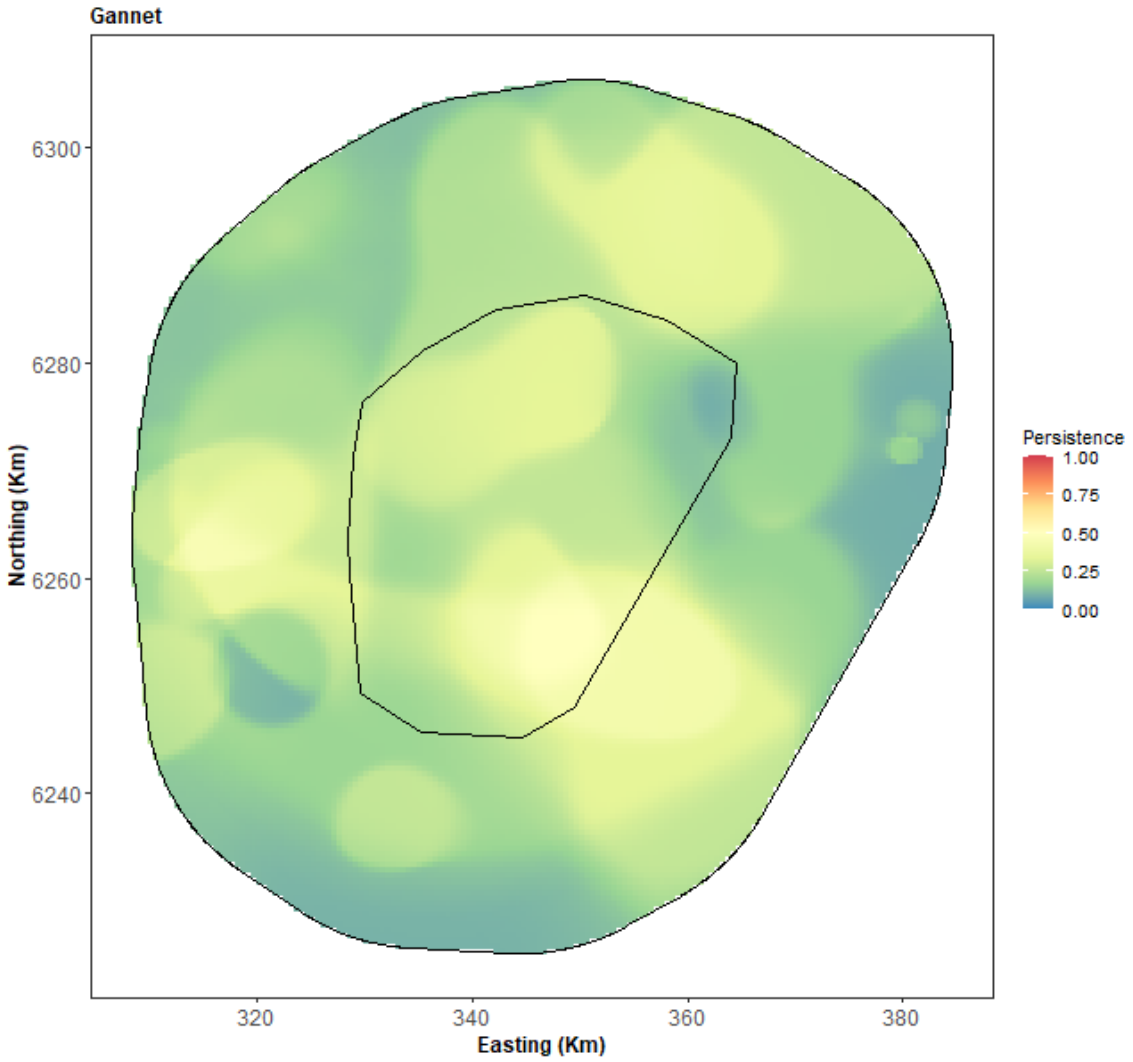

Figure 4.28 Northern gannet persistence scores across the twelve surveys.

4.1.4 Skuas

Very few skuas were recorded during the aerial surveys, namely four great skuas and one unidentified skua sp. (Table 4.1). The great skuas were recorded in July and September 2022, while the unidentified skua was recorded on 27 April 2022. In 2023, only two arctic skuas were observed during a survey on 27 September (Table 4.2)

4.1.5 Gulls

European herring gulls, great black-backed gulls, lesser black-backed gulls, black-headed gulls, little gulls, and unidentified gull sp. are grouped for treatment in this section, while the black-legged kittiwake (another gull species) is treated separately because of their higher abundance in the extended bird survey area.

The gull species display species-specific distribution patterns, which were very clumped. Therefore, no spatial model for this group of species was attempted.

In 2022, the great black-backed and European herring gull were the most numerous species in the survey area, with 36 and 30 birds recorded, respectively. Great black-backed gulls were most numerous in March 2022 (21), and European herring gulls were most numerous in December 2022 (19). Lesser black-backed gull was recorded with 22 individuals in September 2022. One little gull was observed on 27 April 2022 (Table 4.1). The number of gulls unidentified

to species amounted to 44 individuals out of 123 gulls recorded across the six aerial surveys. In 2023, European herring gull and great black-backed gull were the most numerous species, with 322 and 43 birds recorded for the two species. Most European herring gull sightings were recorded on 3 April 2023 (Table 4.2).

These gull species were sometimes spread across the survey area (Figure 4.29 and Figure 4.30), while sometimes also very clumped, particularly when fishing vessels operate in the area. No geographical hotspot areas can be identified.

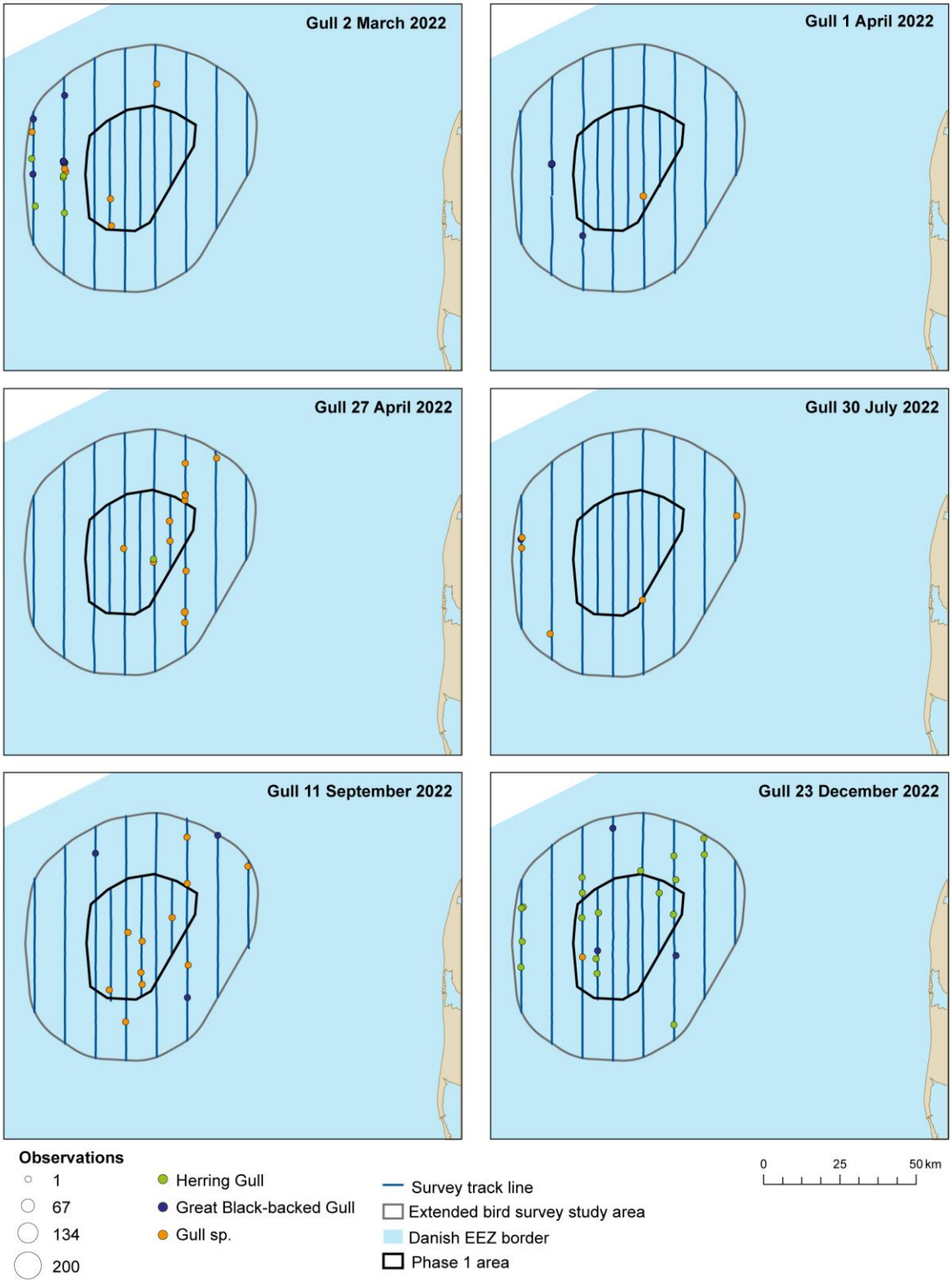

Figure 4.29 The number of observed gulls (30 herring gulls, 36 great black-backed gulls and 44 gull sp.) and their distribution in the North Sea Energy Island extended bird survey area for each of six surveys conducted between March and December 2022. Gull sp. indicates gull species that could not be identified as species of a higher level of species group. The covered transect lines are indicated for each survey.

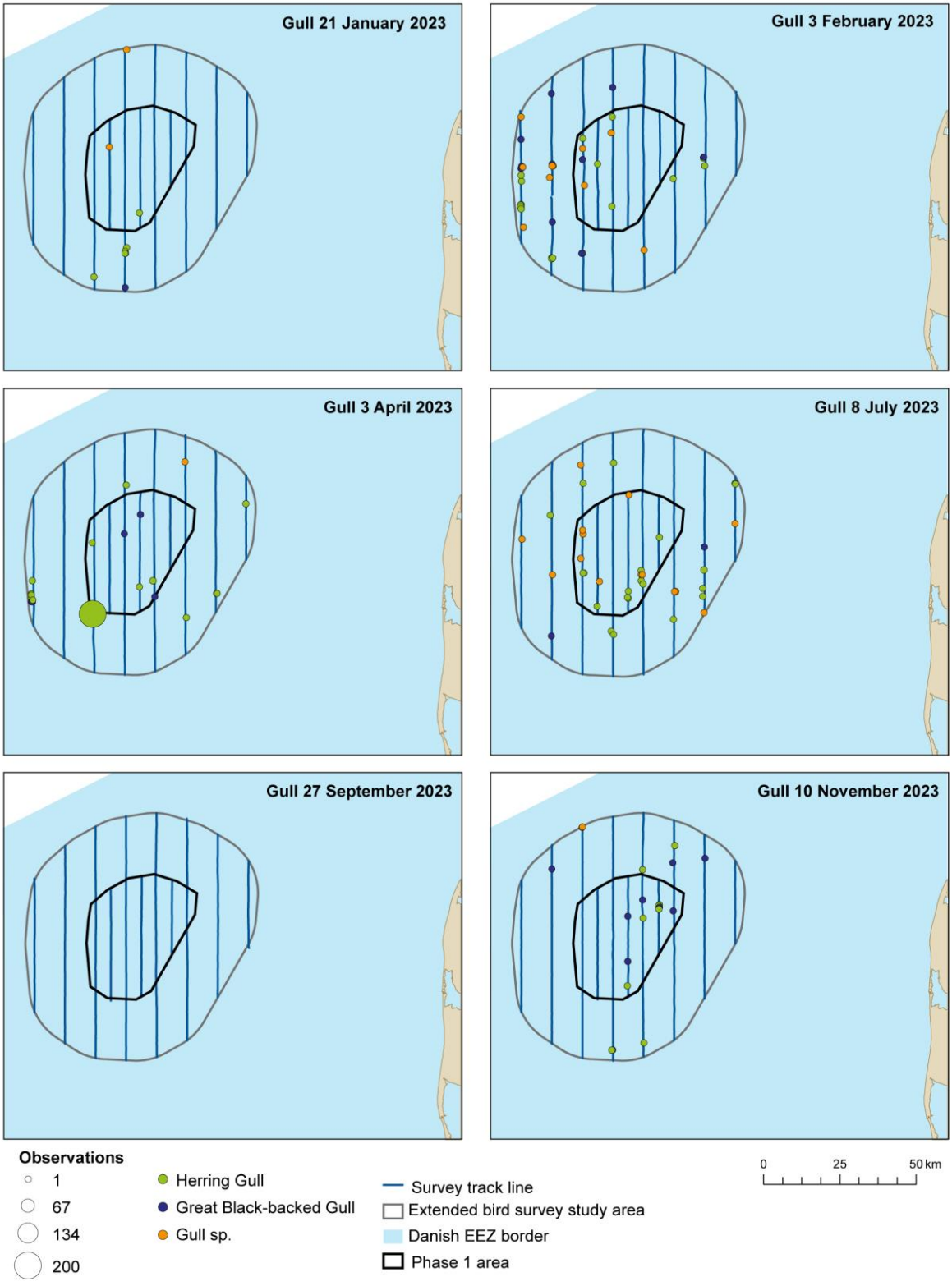

Figure 4.30 The number of observed gulls (303 herring gulls, 40 great black-backed gulls and 33 gull sp.) and their distribution in the North Sea Energy Island extended bird survey area for each of six surveys conducted between January and November 2023. The covered transect lines are indicated for each survey.

4.1.6 Black-legged kittiwake

Black-legged kittiwakes were the extended bird survey area's most abundant and most effectively-identified gull species (Table 4.1 and Table 4.2). A total of 1,298 black-legged kittiwakes were recorded. Most birds were recorded in March 2022 (173) and on 3 April 2023 (427), but also numbers above 100 on 2 March 2022 (173) and on 27 April 2022 (175), on 21 January 2023 (160) and on 2 March 2023 (183) while 73 individuals were seen in December 2022. No black-legged kittiwakes were observed in the extended bird survey area in July, September 2022 and July 2023.

Black-legged kittiwakes were recorded across the extended bird survey area, with a tendency for more birds in the western and central parts (Figure 4.31 and Figure 4.32).

Black-legged kittiwakes were seen either as single birds or small to medium groups. The maximum flock size was 40 birds, and the mean flock size was 1.82.

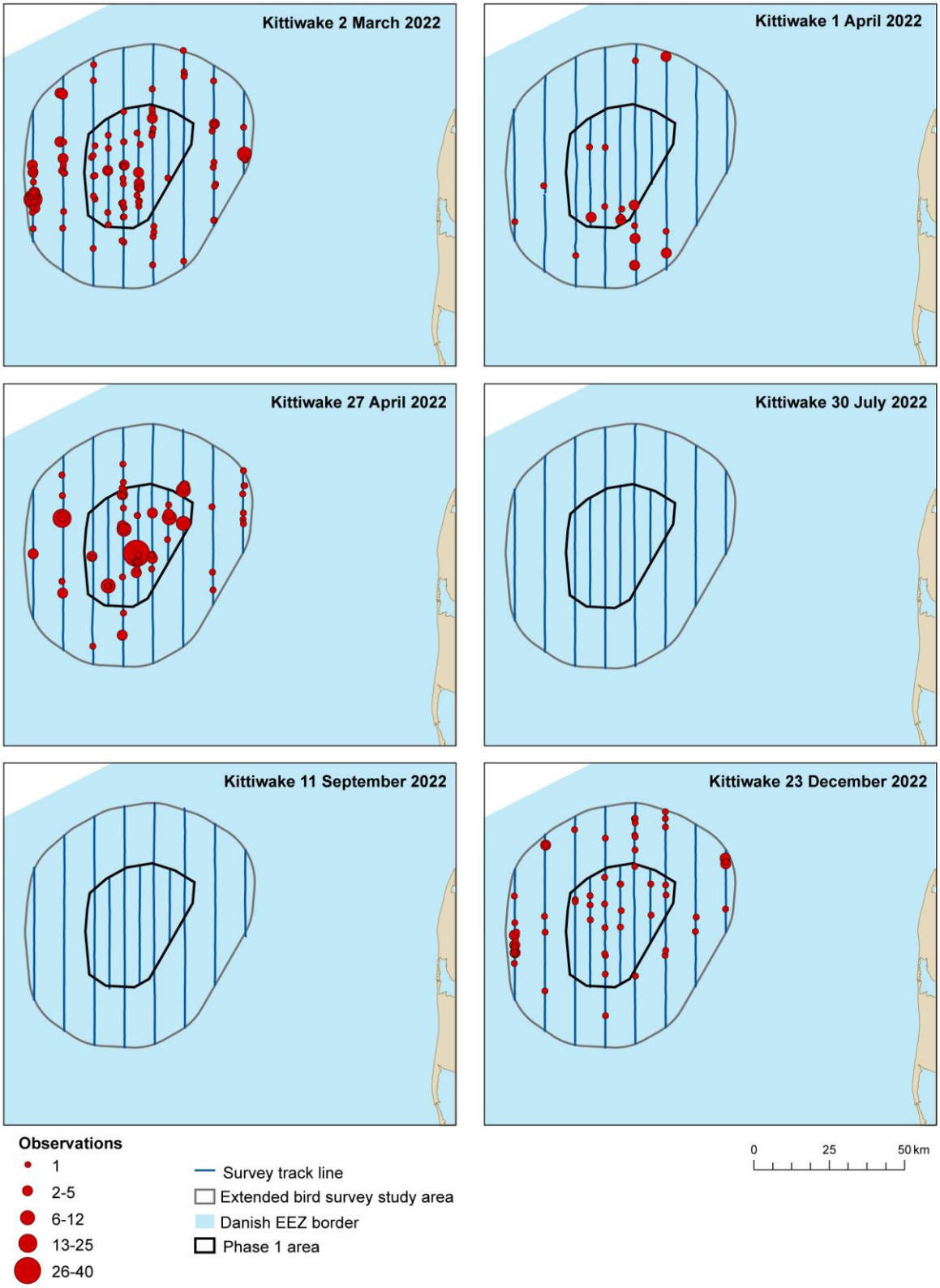

Figure 4.31 The number of observed black-legged kittiwakes (452 individuals) and their distribution in the North Sea Energy Island extended bird survey area for each of six surveys conducted between March and December 2022. The covered transect lines are indicated for each survey.

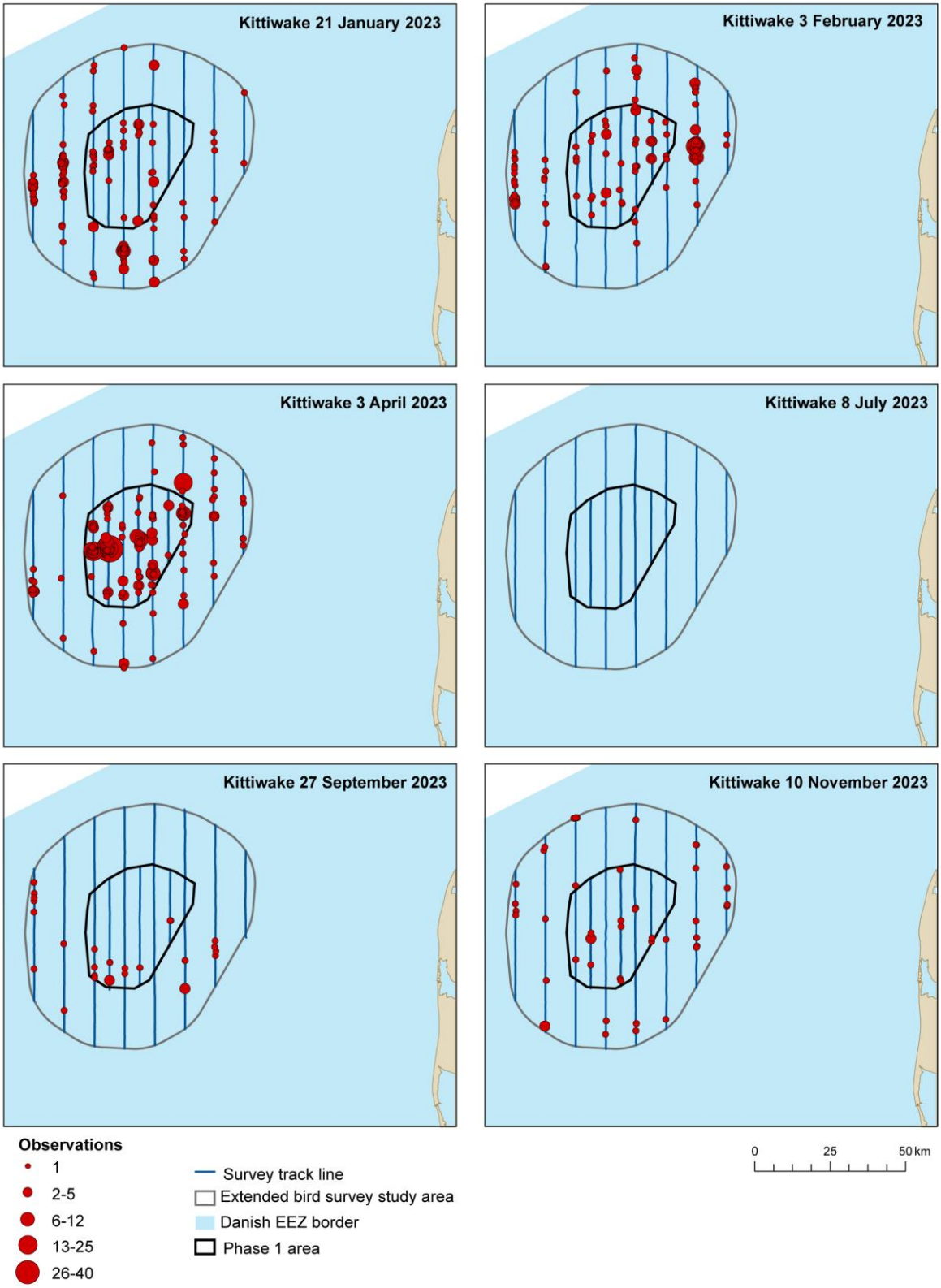

Figure 4.32 The number of observed black-legged kittiwakes (846 individuals) and their distribution in the North Sea Energy Island extended bird survey area for each of six surveys conducted between January and November 2023. The covered transect lines are indicated for each survey.

4.1.6.1 *Distance analysis*

The average probability of sighting black-legged kittiwakes was estimated to be 0.28 (CoV = 0.05). This probability was estimated using a hazard rate detection function, and no covariates were selected (Figure 4.33).

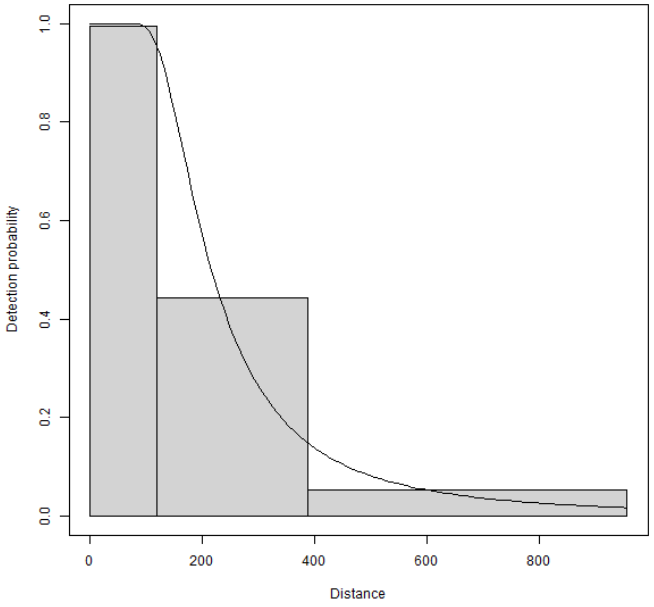

Figure 4.33 The estimated black-legged kittiwake detection function. The histogram represents the distances of the observed sightings.

4.1.6.2 *Spatial analysis*

The spatial analysis data contained 14,453 segments, 3.8% of which contained black-legged kittiwake sightings. Figure 4.34 shows the distribution of the distance-corrected counts for each of the twelve surveys.

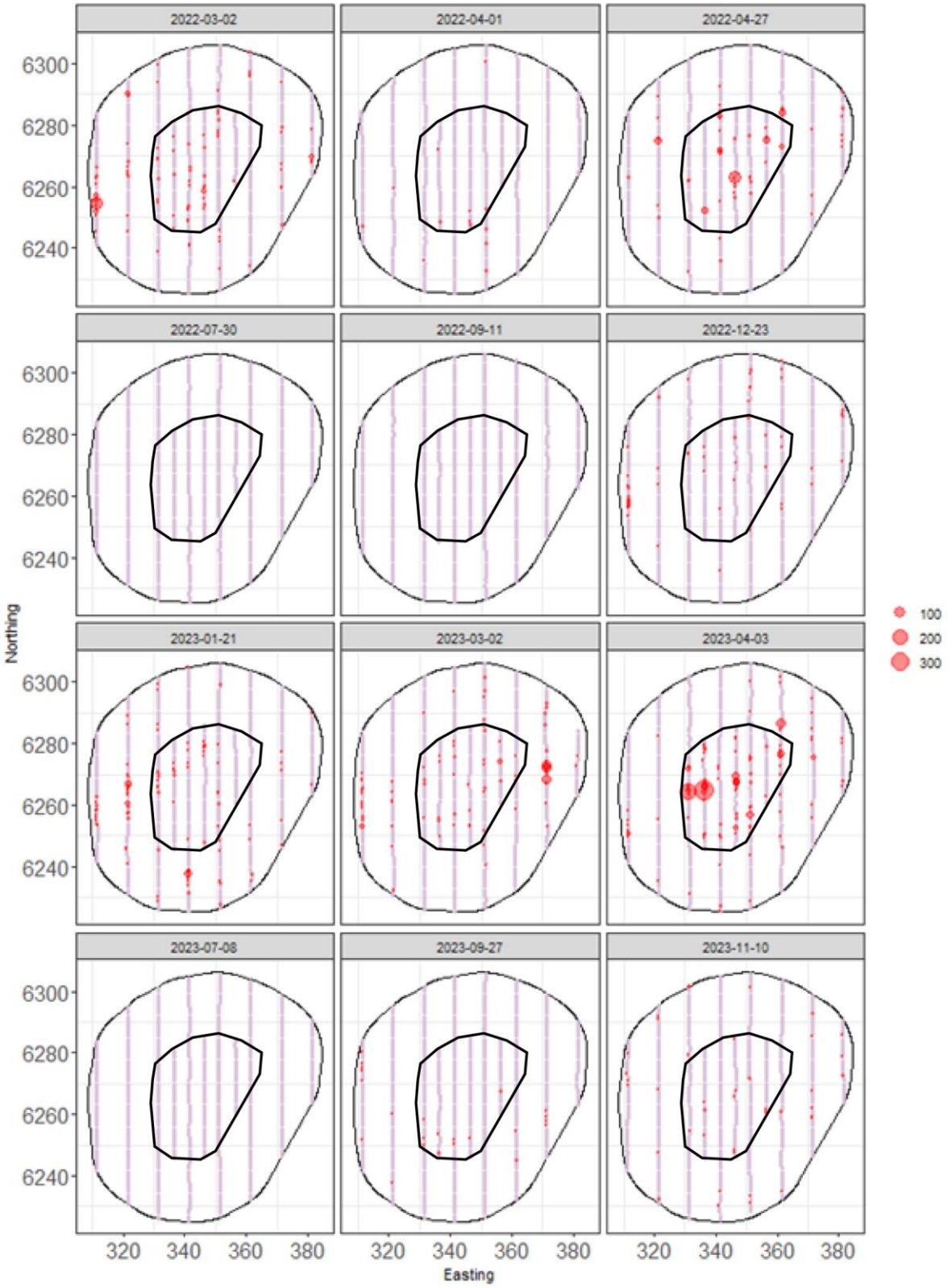

Figure 4.34 Distance-corrected counts for the black-legged kittiwake species across the 12 surveys. The red circles indicate the distance-corrected counts along the transect lines. The pale purple dots are segments with a count of zero.

4.1.6.3 Model selection

For all but 3 surveys, the models selected for each survey included a spatial term (of varying complexity), while the depth and distance from coast covariates (either as a linear or smooth term) were not selected for any surveys. This shows there was compelling evidence for non-uniform spatial patterns in each survey, but given these spatial patterns, there was no evidence for depth or distance-to-coast relationships. The spatial surfaces selected ranged from 2 to 10 parameters for the spatial term (Table 4.7).

Table 4.7 Model selection results for black-legged kittiwake for each survey. The model column represents the terms in the model. The distribution column represents the type of distribution model used. The variable 1D column indicate which of the 1D variables has been included in the final model, while variable 2D refers to the spatial smooth. The number of degrees of freedom (df) for each term are given where applicable. "NA" indicates a non-applicable value. The dispersion and Tweedie parameters are as defined in section 3.4.2.1.

Name	Model	Distribution	Variable 1D	Variable 2D	Number of parameters	Dispersion parameter	Tweedie parameter
2 March 2022	2D Only	Tweedie	NA	s(x,y, df = 5)	6	7.4	1.34
1 April 2022	2D Only	Tweedie	NA	s(x,y, df = 10)	11	6.0	1.15
27 April 2022	2D Only	Tweedie	NA	s(x,y, df = 10)	11	27.0	1.48
30 July 2022	No Model	NA	NA	NA	NA	NA	NA
11 September 2022	No Model	NA	NA	NA	NA	NA	NA
23 December 2022	2D Only	quasipoisson	NA	s(x,y, df = 9)	10	4.2	NA
21 January 2023	2D Only	quasipoisson	NA	s(x,y, df = 2)	3	146.6	NA
2 March 2023	2D Only	Tweedie	NA	s(x,y, df = 10)	11	9.3	1.40
3 April 2023	2D Only	Tweedie	NA	s(x,y, df = 9)	10	19.8	1.57
8 July 2023	No Model	NA	NA	NA	NA	NA	NA
27 September 2023	2D Only	quasipoisson	NA	s(x,y, df = 10)	11	3.2	NA
10 November 2023	2D Only	quasipoisson	NA	s(x,y, df = 7)	8	8.1	NA

The estimated abundances and associated 95% percentile confidence intervals for each survey are given in Table 4.8 and Figure 4.35.

Table 4.8 Estimated survey abundance and density (N/km^2) of black-legged kittiwake. The 95% CI are percentile-based confidence intervals.

Month	Area (Km^2)	Estimated count	95% CI count	Estimated density	95% CI density
2 March 2022	4,812	1,831	(1,420, 2,288)	0.4	(0.3, 0.5)
1 April 2022	4,812	219	(135, 489)	0.0	(0, 0.1)
27 April 2022	4,812	1,756	(1,108, 2,941)	0.4	(0.2, 0.6)
30 July 2022	4,812	0	(NA, NA)	0.0	(NA, NA)
11 September 2022	4,812	0	(NA, NA)	0.0	(NA, NA)
23 December 2022	4,812	1,049	(679, 1,798)	0.2	(0.1, 0.4)

21 January 2023	4,812	2,534	(1,750, 3,746)	0.5	(0.4, 0.8)
2 March 2023	4,812	2,822	(2,065, 3,996)	0.6	(0.4, 0.8)
3 April 2023	4,812	4,967	(2,914, 8,896)	1.0	(0.6, 1.8)
8 July 2023	4,812	0	(NA, NA)	0.0	(NA, NA)
27 September 2023	4,812	299	(213, 435)	0.1	(0, 0.1)
10 November 2023	4,812	754	(506, 1,152)	0.2	(0.1, 0.2)

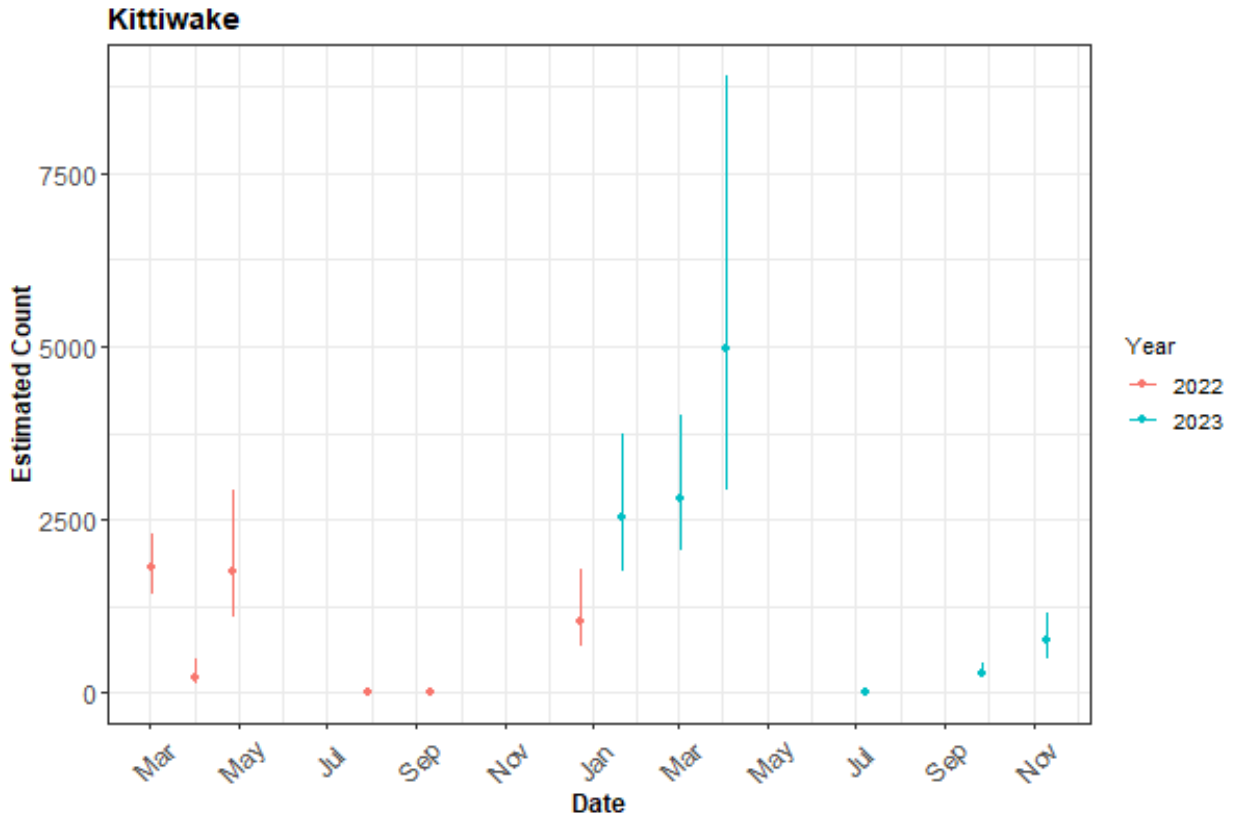

Figure 4.35 The estimated count of black-legged kittiwakes for each survey. The 95% CI are percentile-based confidence intervals are from a parametric bootstrap with 500 replicates.

4.1.6.4 Spatial results

Figure 4.36 shows the estimated counts of black-legged kittiwakes in each 1 km^2 grid cell for each month. Generally, the estimated abundances fitted well with the raw data, and there were no notable misalignments. In areas where the estimated counts were systematically higher, the abundances were also relatively high, and there were no areas with large, estimated abundances unsupported by the data.

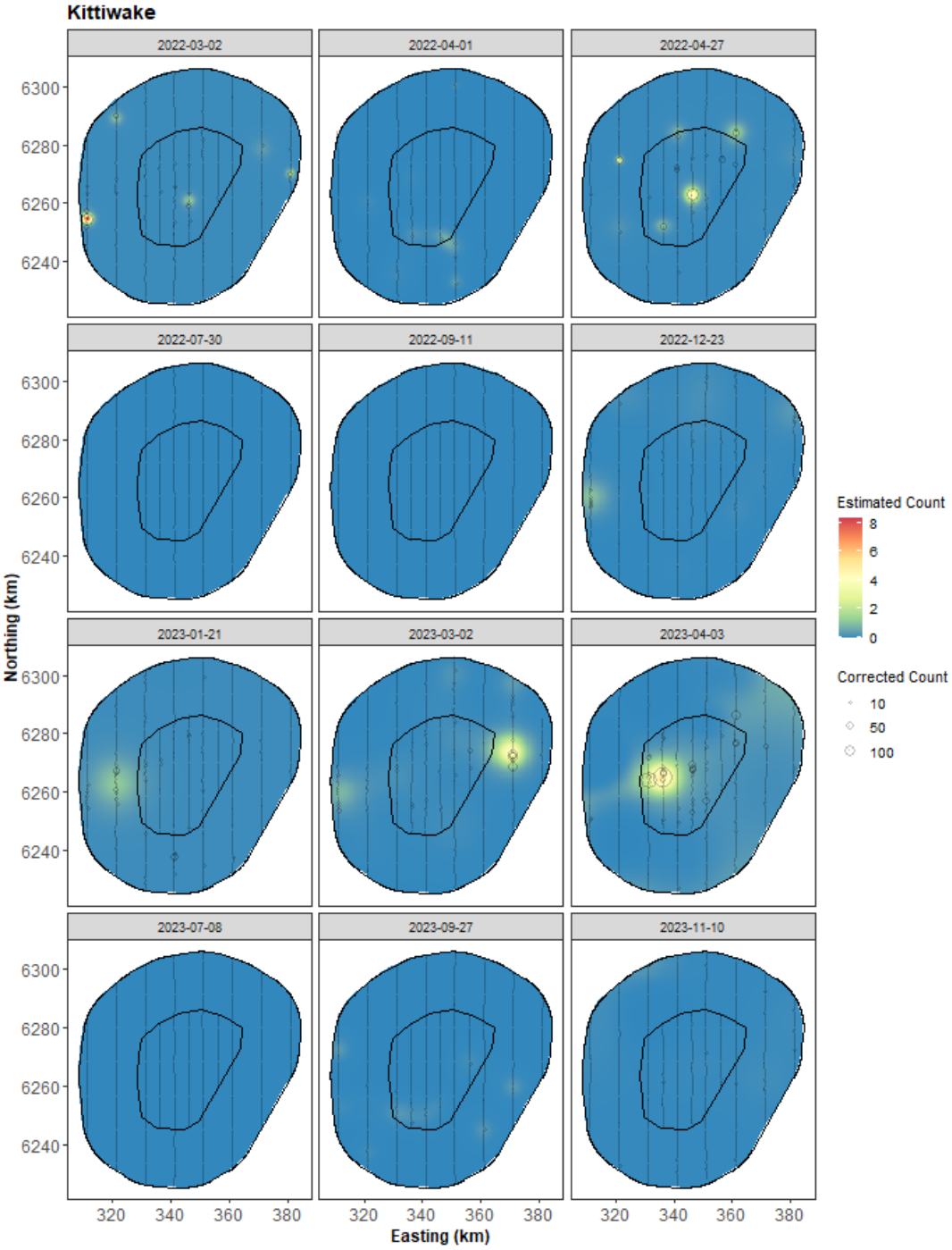

Figure 4.36 The estimated black-legged kittiwake abundance across the study site for each survey. The estimated counts are per 1 km x 1 km grid cell. The open circles show the observed corrected count. The coloured graphics represent the predicted counts in each location.

4.1.6.5 Uncertainty in spatial predictions

Broadly, the highest Coefficient of Variation (CoV) scores were associated with 'almost zero' predictions, and it is known that the CoV metric is highly sensitive to any uncertainty for very small predictions. One larger value was in the western edge of the survey area, otherwise absent from the data. There was no material overlap between high values of the CoV metric and the transect lines/locations with non-zero counts, resulting in no concerns in this case (Figure 4.37).

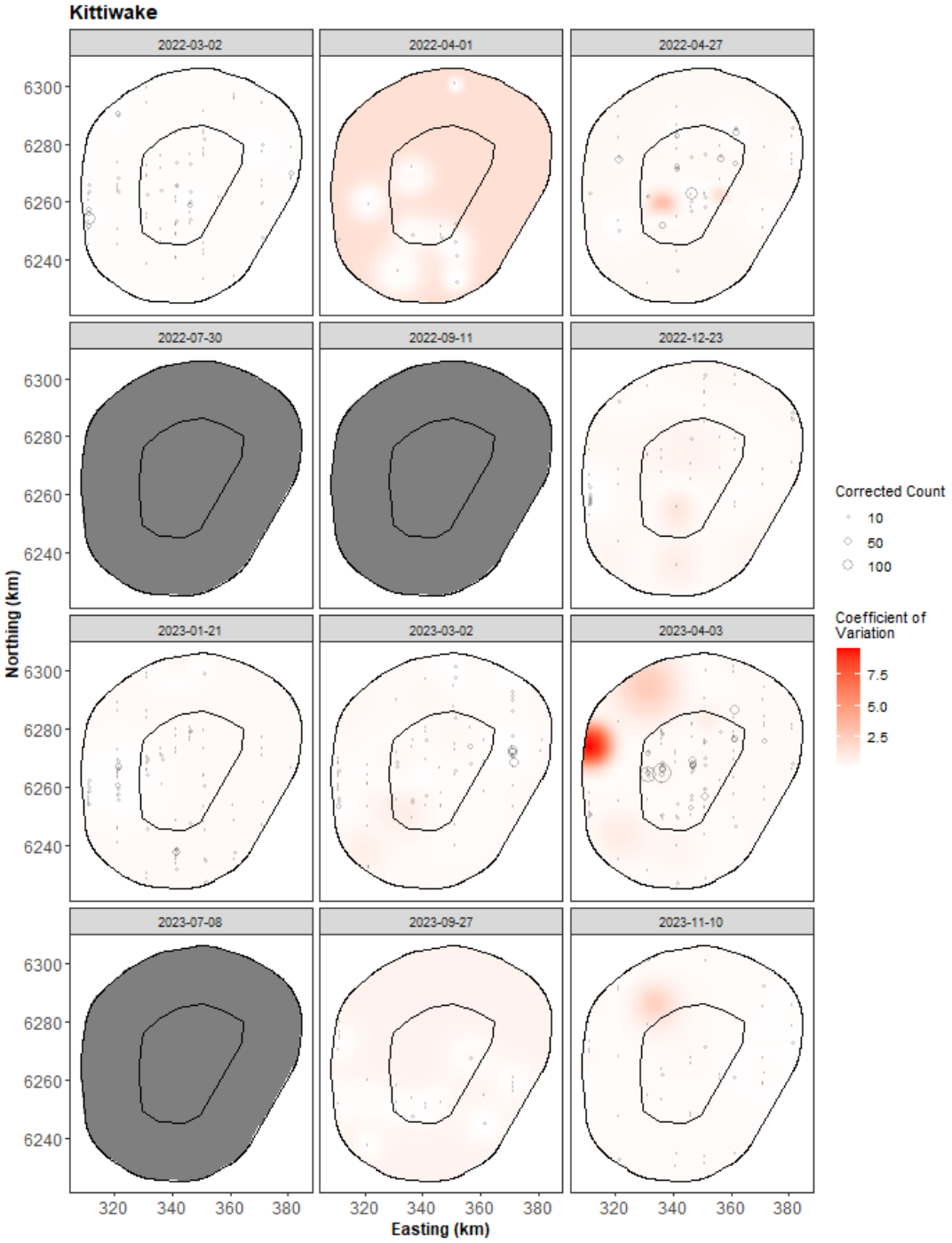

Figure 4.37 The Coefficient of Variation (CoV) across the study region for each survey. The open circles show the distance corrected black-legged kittiwake counts, where applicable, and the polygons represent the area of the extended bird survey area (black line). The presence of dark red CoV scores in areas with virtually zero predictions is an artefact of the very small prediction rather than any notable concern. The dark grey shading is for surveys where no spatial models were fitted.

For the case when the very small, predicted values were excluded (Figure 4.38), the CoV for all surveys was <1 for most surveys and so of no material concern. For example, one survey (3 March 2023) shows apparent high values for the CoV (~8), but once cells with very small, predicted values are excluded, the CoV is <1 across the surface. However, for one survey (27 April 2022), there remains some high uncertainty in the central area, and this is reflected in the wide 95% confidence interval for the abundance for this survey (Table 4.8 and Figure 4.35).

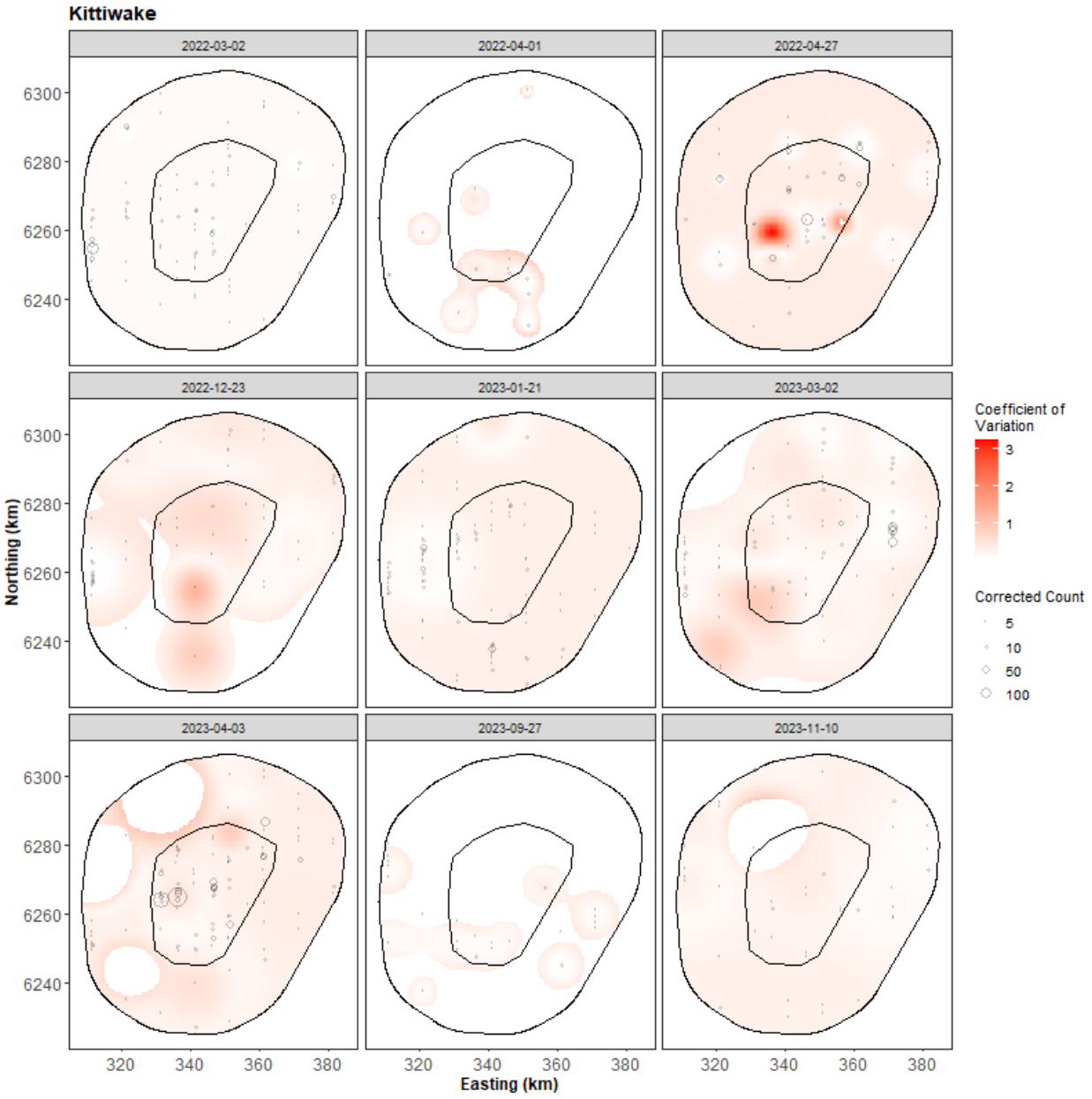

Figure 4.38 The Coefficient of Variation (CoV) for all cells whose mean abundance is > 0.01 birds. The open circles show the distance corrected black-legged kittiwake counts, where applicable, and the polygons represent the area of the extended bird survey area (black line). The presence of dark red CoV scores in areas with virtually zero predictions is an artefact of the very small prediction rather than any notable concern.

4.1.6.6 Model diagnostics

A blocking structure was used to account for potential residual non-independence for each model and a robust standard error approach was based on unique transects. In each model, we saw a reassuring decay to zero (indicated by the red and grey lines in Figure 4.39), implying that an appropriate blocking structure was used.

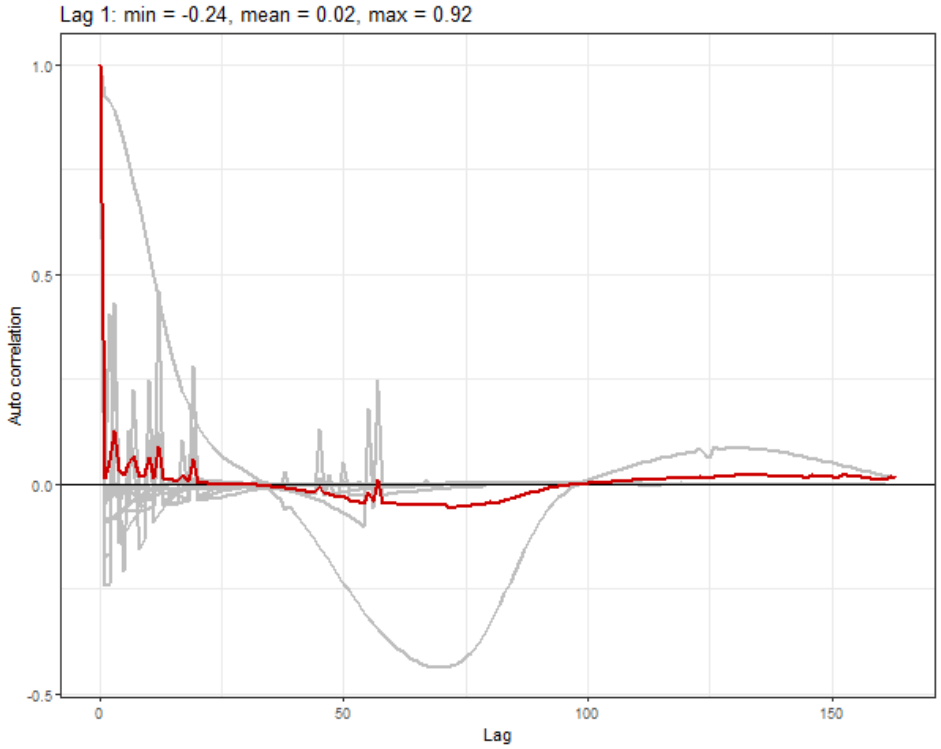

Figure 4.39. Example of black-legged kittiwake Auto Correlation Function (ACF) plot. The grey lines represent the residual correlation observed in each transect, and the red line is the average of these values across transects.

The assumed mean-variance relationship was examined, and an agreement was generally found between the assumed (Quasi-Poisson or Tweedie) lines and the observed values. Figure 4.40 and Figure 4.41 show example relationships for a quasi-Poisson and a Tweedie model. The DHARMa diagnostics, shown, for example, the black-legged kittiwake model in Figure 4.42, confirmed the nature of the mean-variance relationship was appropriate in all cases. In the example shown, there is no compelling evidence against the null hypothesis of a correct overall residual distribution, as indicated by the p-values for the associated tests, and the residuals were also considered homogeneous.

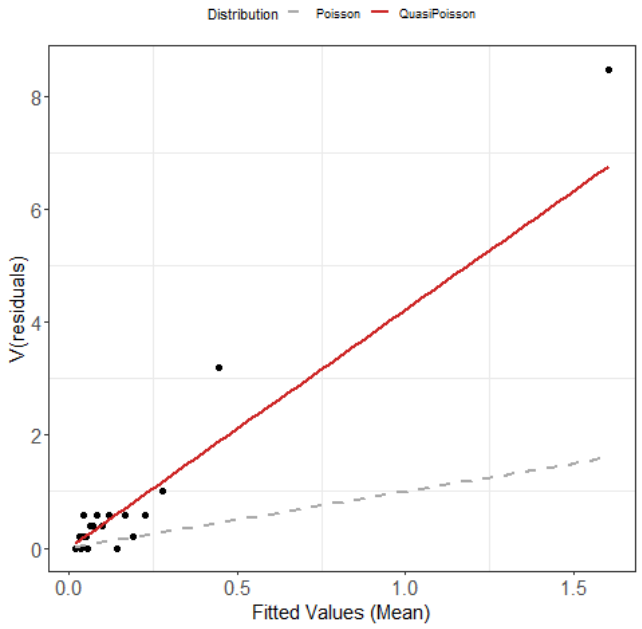

Figure 4.40 Example quasi-Poisson mean-variance relationship (red line) and actual (black dots) for black-legged kittiwake. The black dots are based on 20 quantiles of the model residuals, and for reference, the grey dashed line shows the 1:1 relationship.

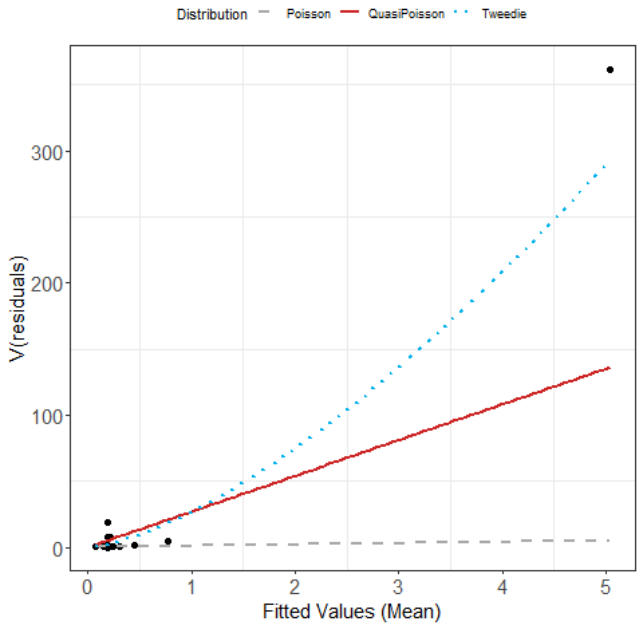

Figure 4.41 Example of estimated Tweedie mean-variance relationship (blue dashed line) for black-legged kittiwake. The red line shows the $V(\mu)=\phi\mu$ relationship, and the grey line shows the 1:1 relationship.

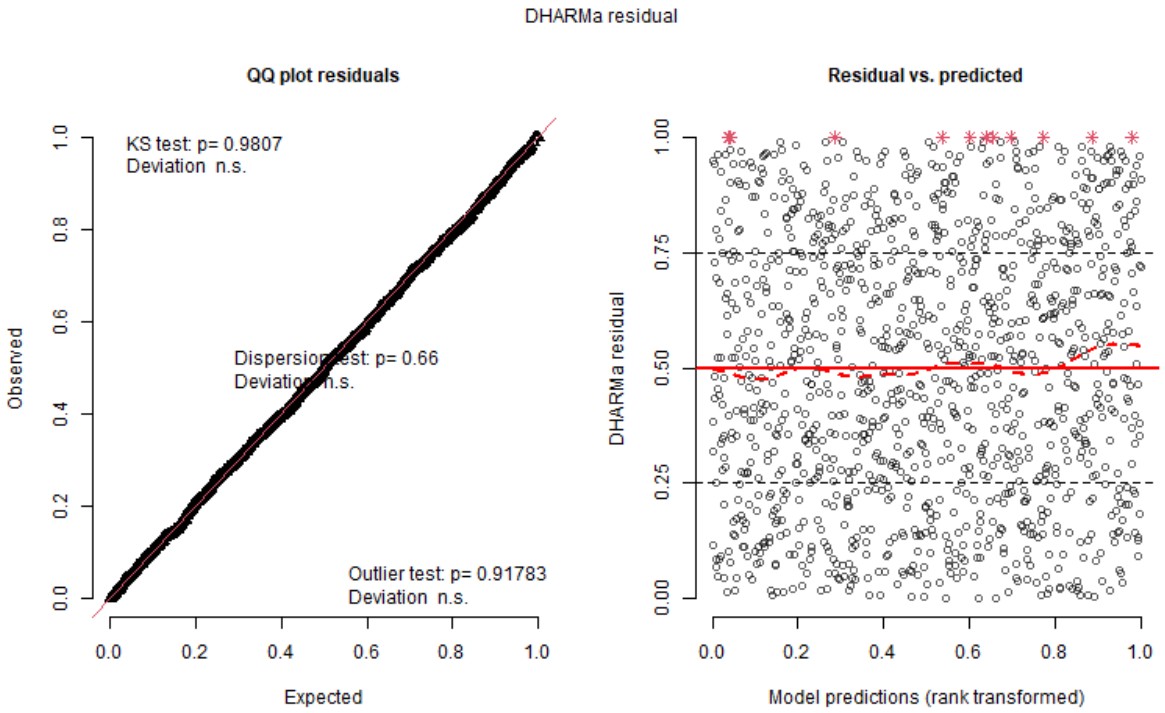

Figure 4.42 Black-legged kittiwake DHARMa diagnostics. Example QQ plot (left) and residuals against predicted values (right). The red stars are outliers, and the red line is a smooth spline around the mean of the residuals.

4.1.6.7 Areas of persistence

Across the 12 surveys, there was a rather uniform distribution of the species across the extended bird survey area (Figure 4.43). There was a slightly lower persistence on the southern edge of the survey area.

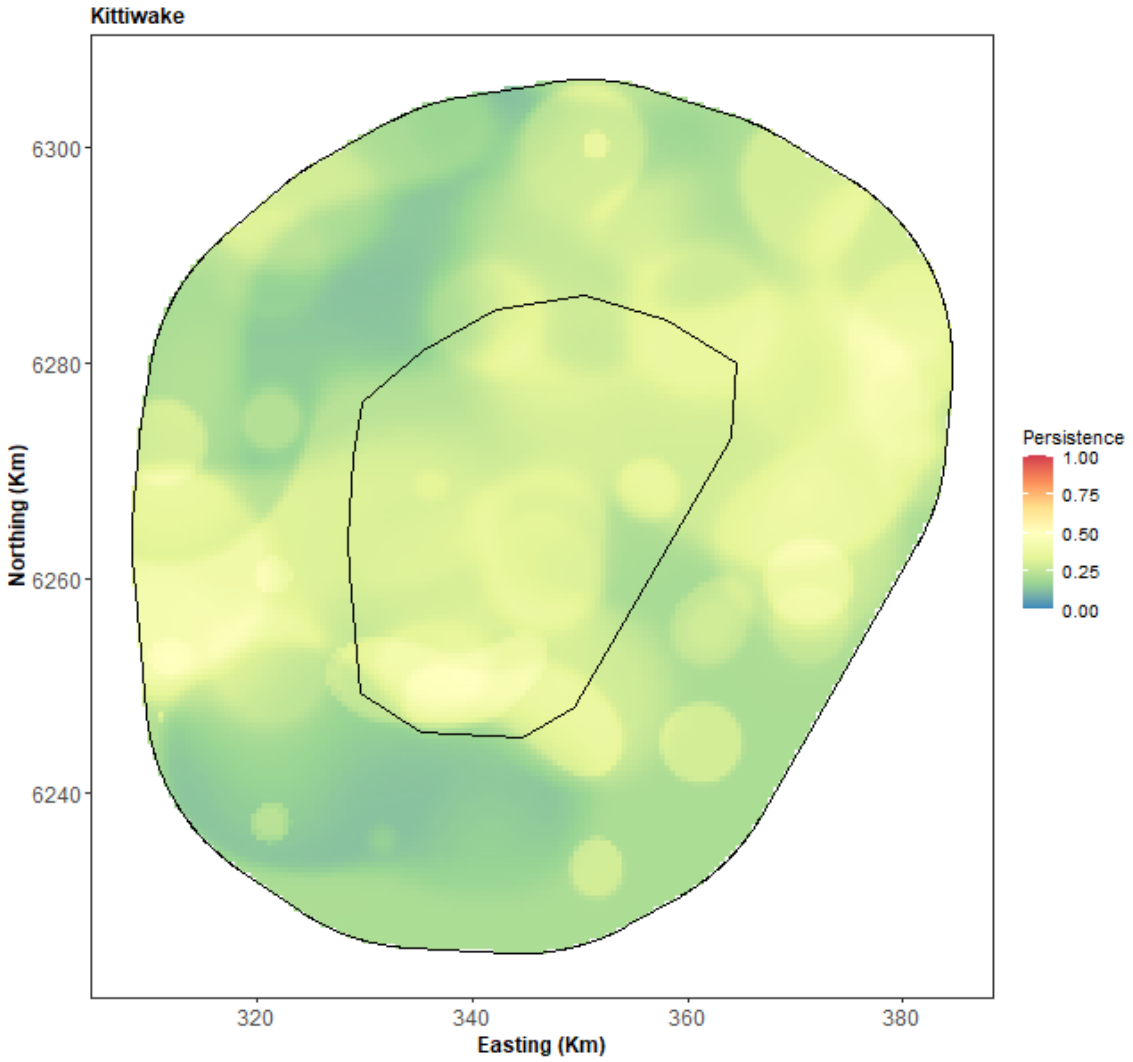

Figure 4.43 Black-legged kittiwake persistence scores across the twelve surveys.

4.1.7 Terns

The only tern identified as a species during the aerial survey was the sandwich tern. Two categories of unidentified terns were recorded: common/arctic tern and sp. (Table 4.1 and Table 4.2).

The common/arctic tern was the most numerously recorded group, with 51 individuals. These were recorded on 27 April (33) and September 2022 (18). In September, an additional 19 unidentified terns were recorded. No terns were recorded in the extended bird survey area during the six surveys performed in 2023.

The terns were mainly recorded in the western and central parts of the extended bird survey area (Figure 4.44 and Figure 4.45).

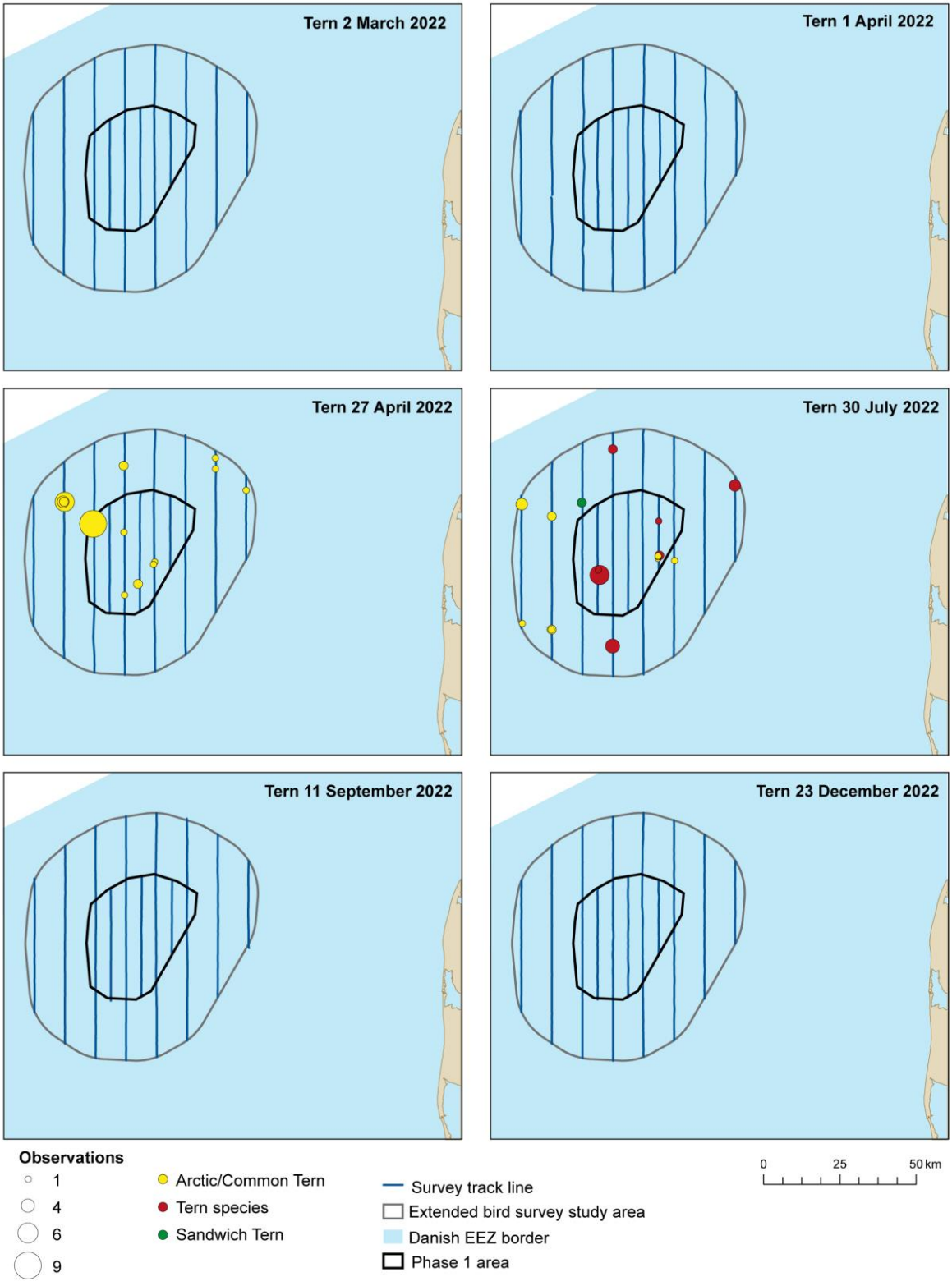

Figure 4.44 The distribution of 73 terns in the North Sea Energy Island extended bird survey area, combined for six surveys between March and December 2022. The predefined transect survey lines are indicated.

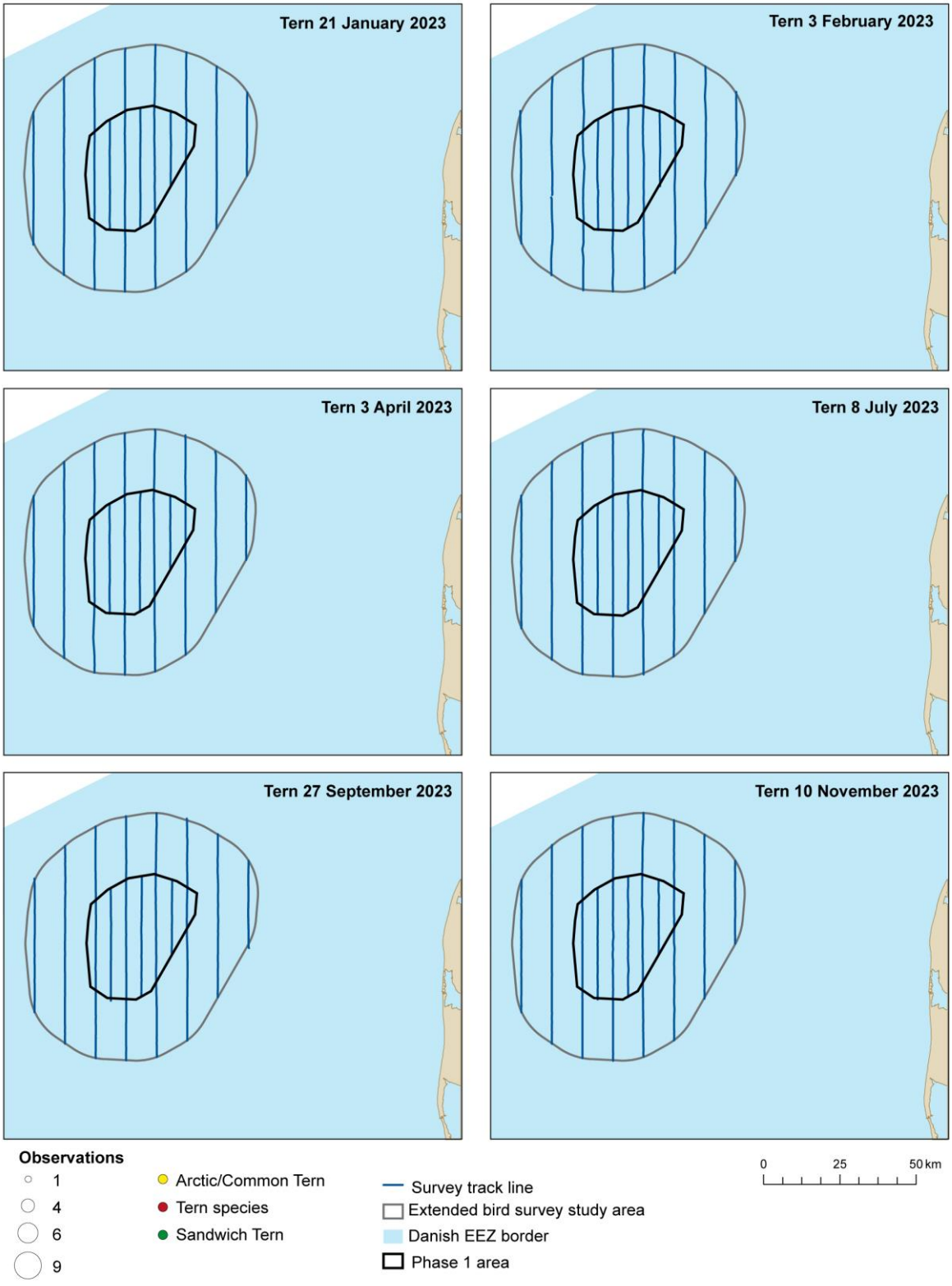

Figure 4.45 The distribution of terns (no sightings) in the North Sea Energy Island extended bird survey area, combined for six surveys between January and November 2023. The predefined transect survey lines are indicated.

4.1.8 Alcids (razorbill, common guillemot and Atlantic puffin)

The most numerous bird group recorded in the extended bird survey area was alcids (razorbills, common guillemots and Atlantic puffins). Most of these birds were recorded as unidentified razorbill/common guillemots (1,855 birds), while five razorbills and 378 common guillemots were recorded to species (Table 4.1 and Table 4.2).

Alcids were present in the extended bird survey area during all twelve aerial surveys, most of which were present on 3 April 2023 (1,494), 8 July 2023 (1,421), and 1 April 2022 (840). Nine Atlantic puffins were recorded, six in March and three on 1 April 2022. No Atlantic puffins were recorded in 2023. Atlantic puffin has, therefore, been omitted from the abundance and distribution analyses below. The lowest number of alcids was 157 birds in July 2022 (Table 4.1 and Table 4.2).

Razorbills/common guillemots were found across the extended bird survey area. In March and September 2022, most birds were recorded in the western and central parts of the area, while on 1 April, July and December, the birds were scattered across the area. On 27 April 2022, most birds were found in the central and eastern parts of the area, while on 27 September 2023, the birds were concentrated in the westernmost parts of the extended bird survey area (Figure 4.46 and Figure 4.47).

Razorbills and common guillemots were recorded as single individuals or small groups. The maximum flock size was 20 birds, with a mean flock size of 1.90.

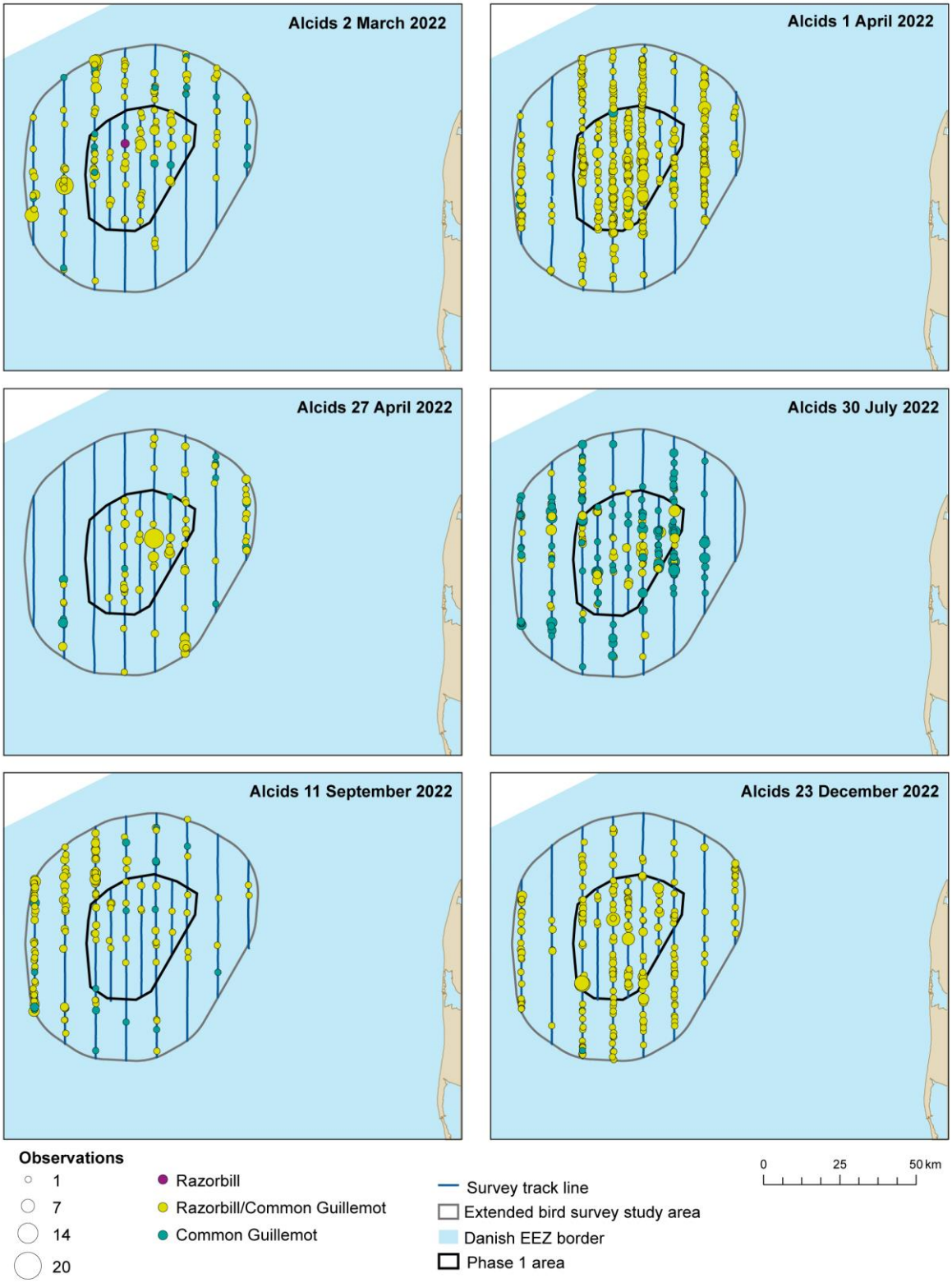

Figure 4.46 The number of observed razorbills or common guillemots (2,239 individuals) and their distribution in the North Sea Energy Island extended bird survey area for each of the six surveys conducted between March and December 2022. The covered transect lines are indicated for each survey.

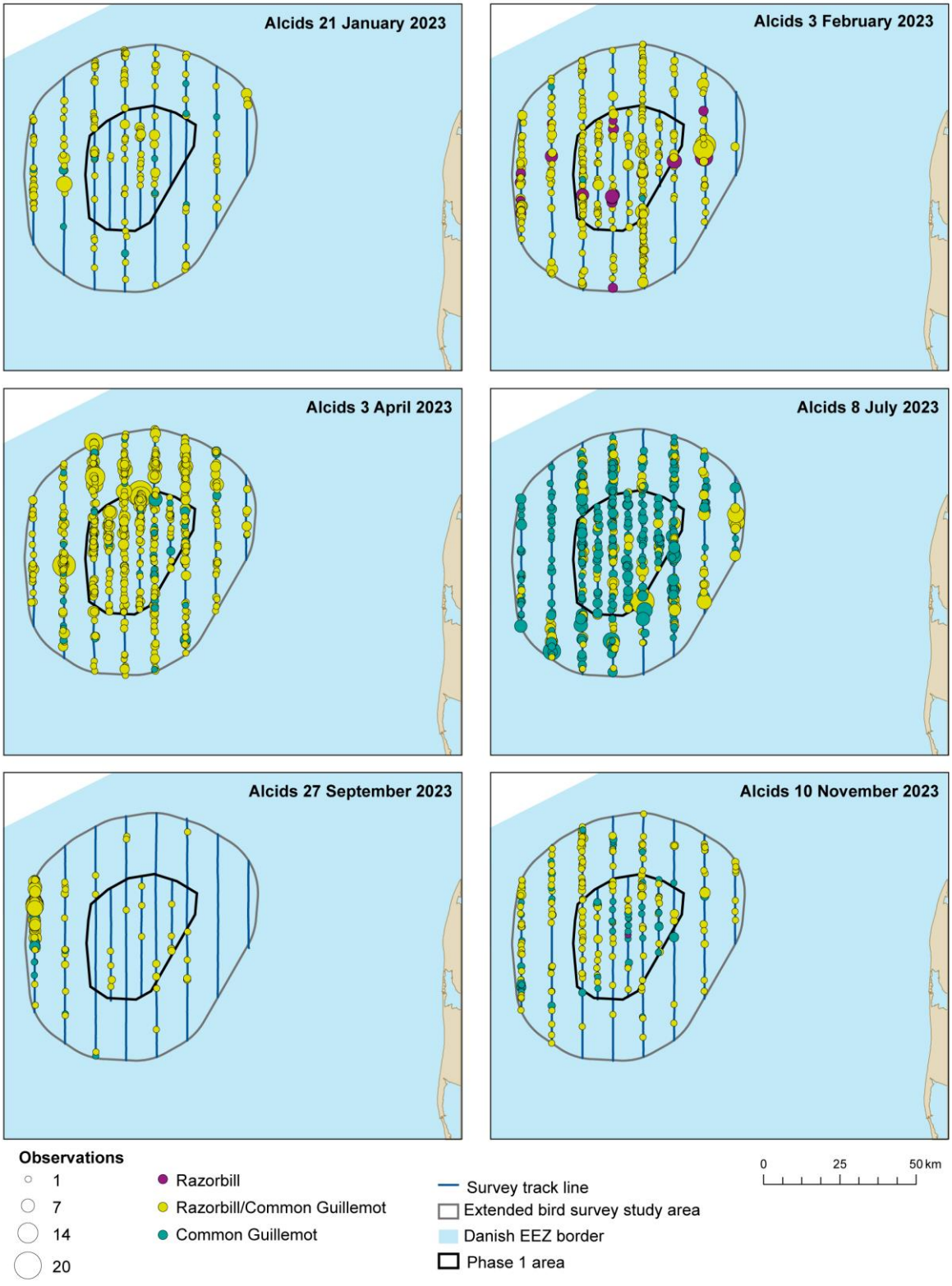

Figure 4.47 The number of observed razorbills or common guillemots (4,587 individuals) and their distribution in the North Sea Energy Island extended bird survey area for each of six surveys conducted between January and November 2023. The covered transect lines are indicated for each survey.

4.1.8.1 *Distance analysis*

The average probability of sighting alcids was estimated at 0.23 (CoV = 0.02). This probability was estimated using a hazard rate detection function and observer and glare as covariates (Figure 4.48 and Figure 4.49).

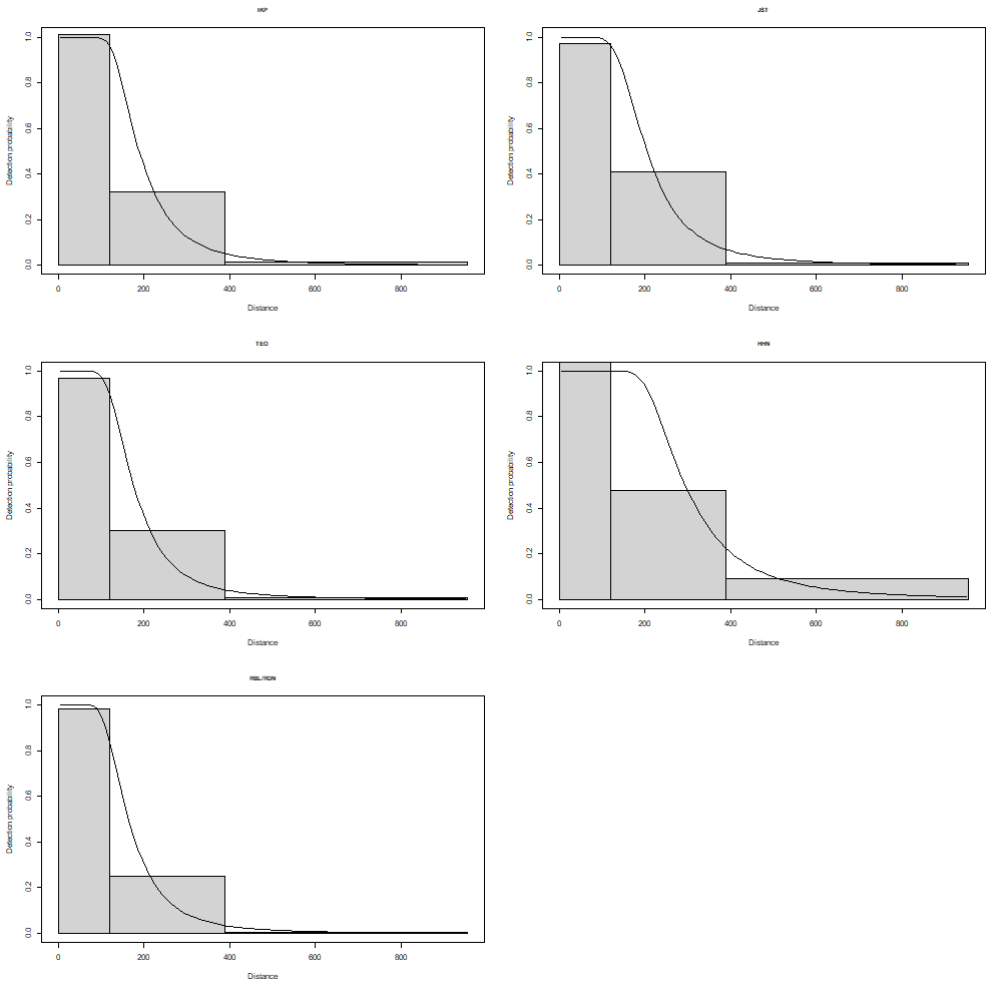

Figure 4.48 The estimated alcid detection function for each individual observer. The histogram represents the distances of the observed sightings.

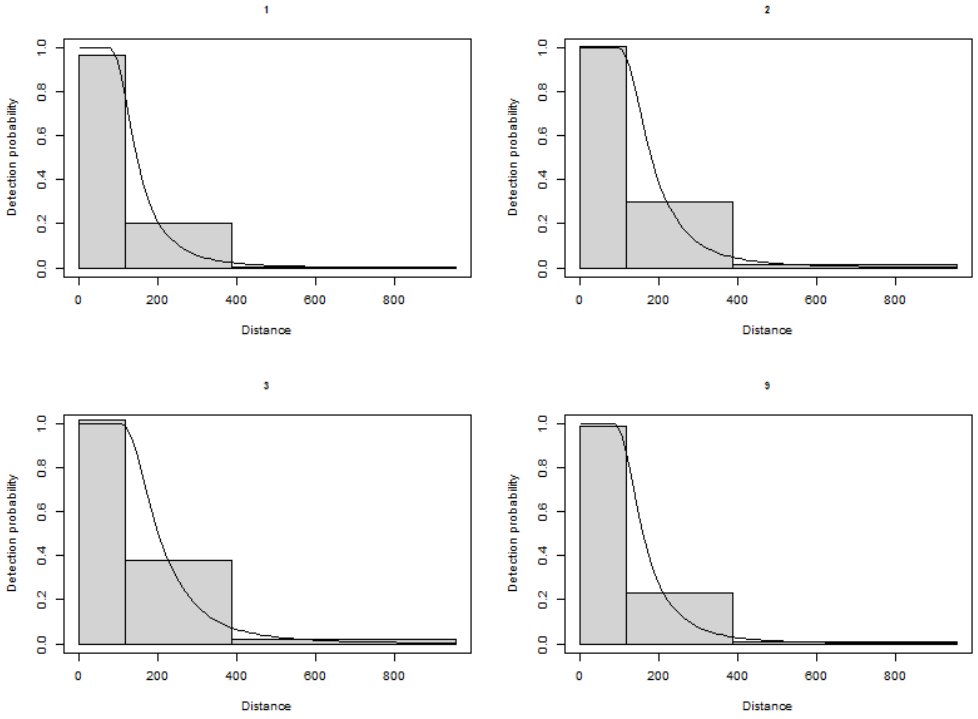

Figure 4.49 The estimated alcid detection function for glare intensity (1 (full sun), 2, 3 (cloudy) and 9 (changeable)). The histogram represents the distances of the observed sightings.

4.1.8.2 Spatial analysis

The spatial analysis data contained 14,453 segments overall, 18.5% of which contained alcid sightings. Figure 4.50 shows the distribution of the distance-corrected counts for each of the two months of surveys.

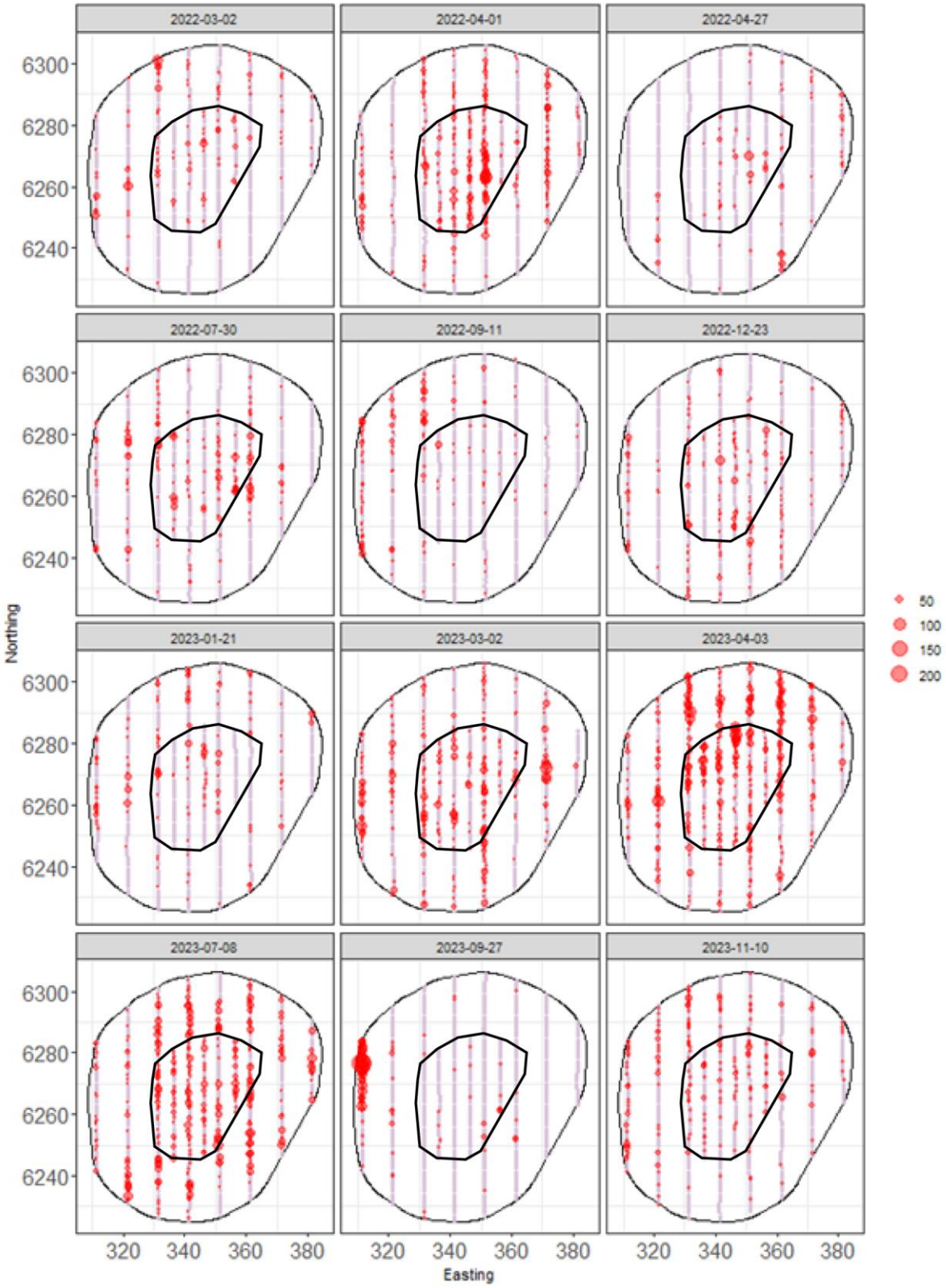

Figure 4.50 Distance-corrected counts for the alcid species group across the 12 surveys. The red circles indicate the distance-corrected counts along the transect lines. The pale purple dots are segments with a count of zero.

4.1.8.3 *Model selection*

For all but two surveys, the models selected included a spatial term (of varying complexity), while the depth covariate (either as a linear or smooth term) was not selected for any surveys. The distance to the coast covariate was selected as a linear term for one model and as a smooth term for one model. This shows there was compelling evidence for non-uniform spatial patterns in almost all surveys, but given these spatial patterns, there was no depth relationship and limited evidence for a distance-to-coast relationship. The spatial surfaces selected ranged from 3 to 11 parameters for the spatial term (Table 4.9).

Table 4.9 Model selection results for alcids for each survey. The model column represents the terms in the model. The distribution column represents the type of distribution model used. The variable 1D column indicate which of the 1D variables has been included in the final model, while variable 2D refers to the spatial smooth. The number of degrees of freedom (df) for each term are given where applicable. "NA" indicates a non-applicable value. The dispersion and Tweedie parameters are as defined in section 3.4.2.1.

Name	Model	Distribution	Variable 1D	Variable 2D	Number of parameters	Dispersion parameter	Tweedie parameter
2 March 2022	Best 1D2D	Tweedie	s(DC, df = 2)	s(x,y, df = 8)	11	12.1	1.24
1 April 2022	2D Only	Tweedie	NA	s(x,y, df = 7)	8	9.1	1.28
27 April 2022	2D Only	Tweedie	NA	s(x,y, df = 5)	6	10.2	1.24
30 July 2022	2D Only	Tweedie	NA	s(x,y, df = 3)	4	14.0	1.28
11 September 2022	2D Only	quasipoisson	NA	s(x,y, df = 11)	12	6.7	NA
23 December 2022	2D Only	Tweedie	NA	s(x,y, df = 9)	10	10.7	1.17
21 January 2023	Intercept only	Tweedie	NA	NA	1	12.3	1.18
2 March 2023	2D Only	Tweedie	NA	s(x,y, df = 5)	6	9.7	1.30
3 April 2023	2D Only	Tweedie	NA	s(x,y, df = 11)	12	10.1	1.28
8 July 2023	2D Only	Tweedie	NA	s(x,y, df = 8)	9	9.5	1.32
27 September 2023	2D Only	Tweedie	NA	s(x,y, df = 4)	5	17.5	1.30
10 November 2023	Distance to coast	quasipoisson	DC, df = 1	NA	2	10.4	NA

The estimated abundances and associated 95-percentile confidence intervals for each survey are given in Table 4.10 and Figure 4.51.

Table 4.10 Estimated survey abundance and density (N/km^2) of alcids. The 95% CI are percentile-based confidence intervals.

Month	Area (km^2)	Estimated count	95% CI count	Estimated density	95% CI density
2 March 2022	4,812	4,637	(3,082, 6,997)	1.0	(0.6, 1.5)
1 April 2022	4,812	14,460	(9,418, 22,460)	3.0	(2, 4.7)
27 April 2022	4,812	2,561	(1,610, 4,032)	0.5	(0.3, 0.8)
30 July 2022	4,812	7,416	(5,035, 10,559)	1.5	(1, 2.2)
11 September 2022	4,812	4,706	(3,248, 7,280)	1.0	(0.7, 1.5)
23 December 2022	4,812	6,029	(3,872, 8,990)	1.3	(0.8, 1.9)

21 January 2023	4,812	5,188	(3,801, 7,294)	1.1	(0.8, 1.5)
2 March 2023	4,812	14,003	(9,041, 21,286)	2.9	(1.9, 4.4)
3 April 2023	4,812	25,028	(18,082, 35,311)	5.2	(3.8, 7.3)
8 July 2023	4,812	27,245	(21,264, 35,912)	5.7	(4.4, 7.5)
27 September 2023	4,812	6,975	(4,839, 10,510)	1.4	(1, 2.2)
10 November 2023	4,812	7,392	(5,553, 9,617)	1.5	(1.2, 2)

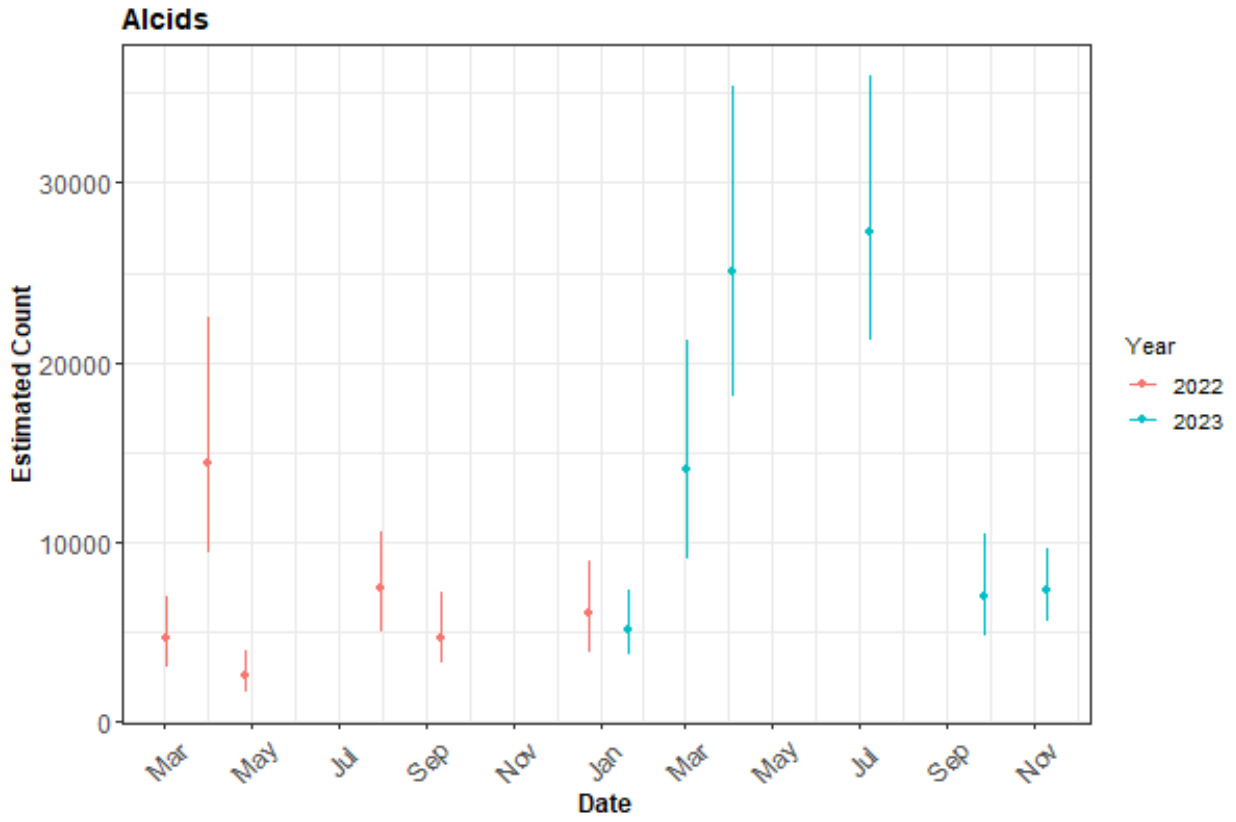

Figure 4.51 The estimated count of alcids for each survey. The 95% CI are percentile-based confidence intervals are from a parametric bootstrap with 500 replicates. The abundances are comparable as each survey's area is the same.

4.1.8.4 Spatial results

Figure 4.52 shows the estimated counts of alcids in each 1 km^2 grid cell for each month. Generally, the estimated abundances fitted well with the raw data, and there were no notable misalignments. In areas where the estimated counts were systematically higher, the abundances were also relatively high, and there were no areas with large, estimated abundances unsupported by the data.

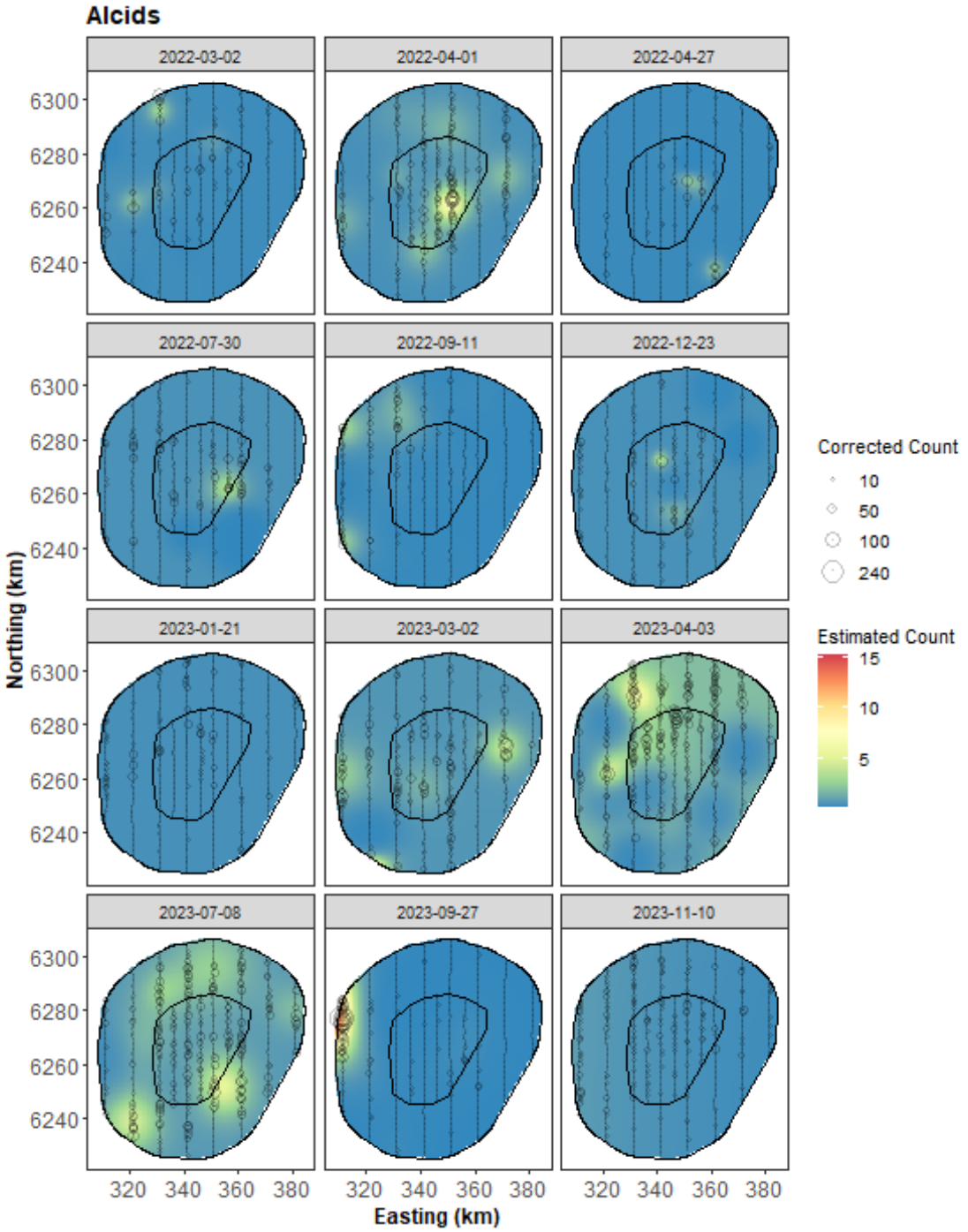

Figure 4.52 The estimated razorbill/common guillemot abundance across the study site for each survey. The estimated counts are per 1 km x 1 km grid cell. The open circles show the observed corrected count. The coloured graphics represent the predicted counts in each location.

4.1.8.5 Uncertainty in spatial predictions

Broadly, the highest CoV scores were associated with 'almost zero' predictions, and it is known that the CoV metric is highly sensitive to any uncertainty for very small predictions. There was one larger value in the southeastern corner of the extended bird survey area, but that was otherwise absent from the data. There was no material overlap between

high values of the CoV metric and the transect lines/locations with non-zero counts, resulting in no concerns in this case (Figure 4.53).

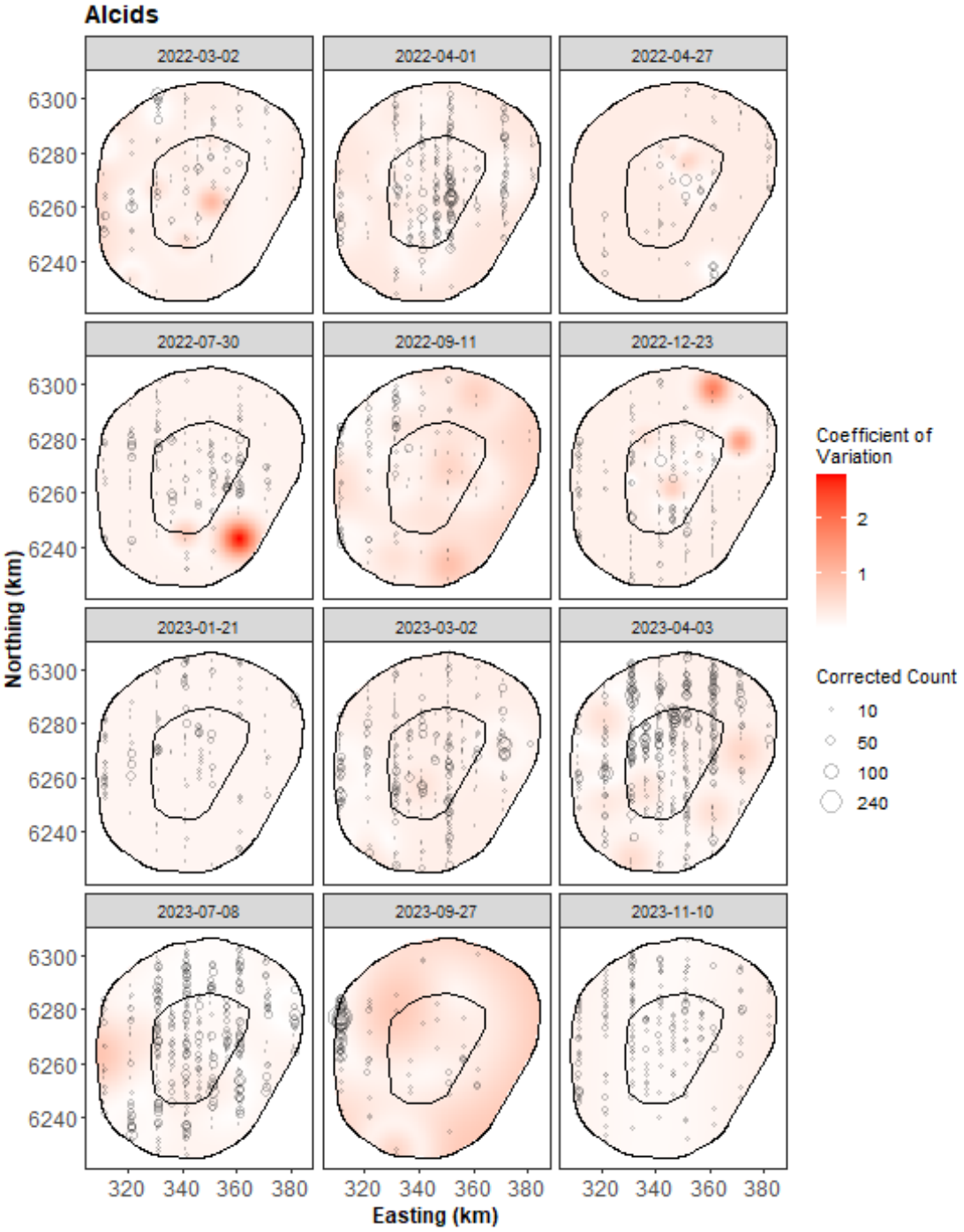

Figure 4.53 The Coefficient of Variation (CoV) across the study region for each survey. The open circles show the distance corrected alcid counts, where applicable, and the polygons represent the area of the extended bird survey area (black line). The presence of dark red CoV scores in areas with virtually zero predictions is an artefact of the very small prediction rather than any notable concern.

4.1.8.6 *Model diagnostics*

A blocking structure was used to account for potential residual non-independence for each model and a robust standard error approach was based on unique transects. In each model, we saw a reassuring decay to zero (indicated

by the red and grey lines in Figure 4.54 implying that an appropriate blocking structure was used. All the plots in Figure 4.54 are examples from the 12 alcid models. A full set for all models is available on request.

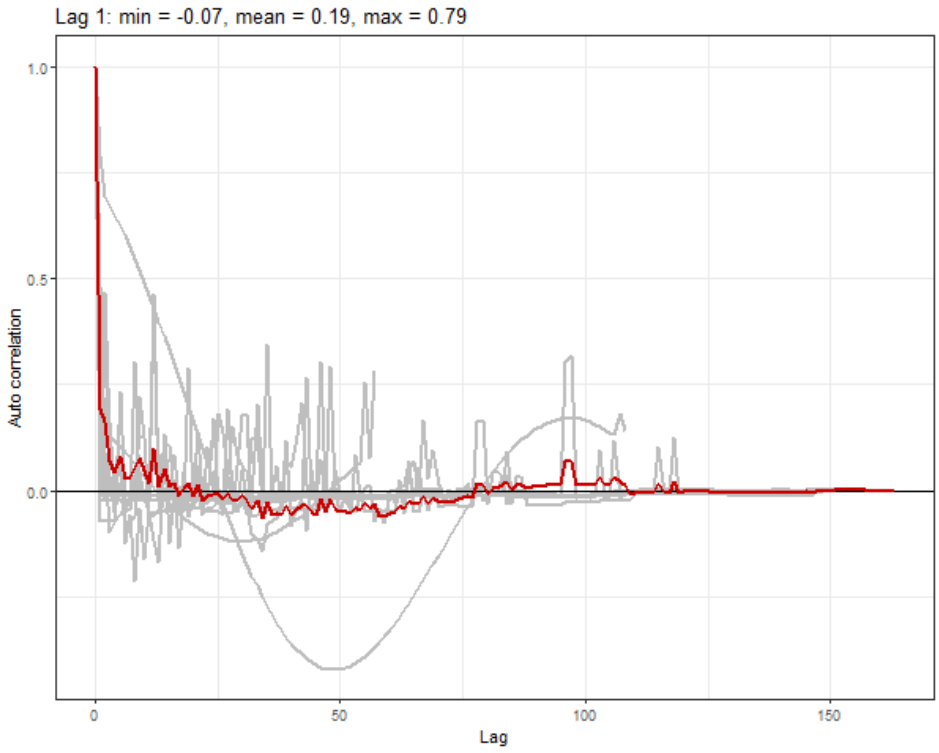

Figure 4.54 Example of alcid Auto Correlation Function (ACF) plot. The grey lines represent the residual correlation observed in each transect, and the red line is the average of these values across transects.

The assumed mean-variance relationship was examined, and agreement was generally shown between the assumed (Quasi-Poisson or Tweedie) lines and the observed values. Figure 4.55 and Figure 4.56 show example relationships for a quasi-Poisson and a Tweedie model. The DHARMa diagnostics, shown for an example alcid model in Figure 4.57, confirmed the nature of the mean-variance relationship was appropriate in all cases. In the example shown, there is no compelling evidence against the null hypothesis of a correct overall residual distribution, as indicated by the p-values for the associated tests, and the residuals were also considered homogeneous.

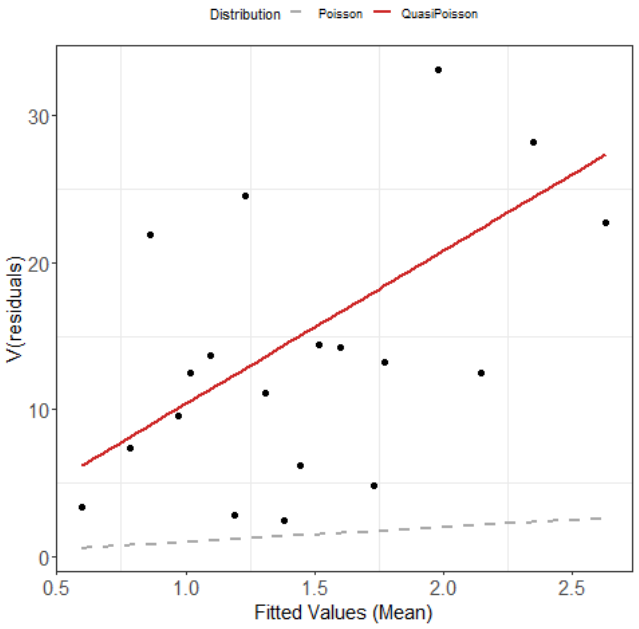

Figure 4.55 Example of quasi-Poisson mean-variance relationship (red line) and actual (black dots) for alcids. The black dots are based on 20 quantiles of the model residuals, and for reference, the grey dashed line shows the 1:1 relationship.

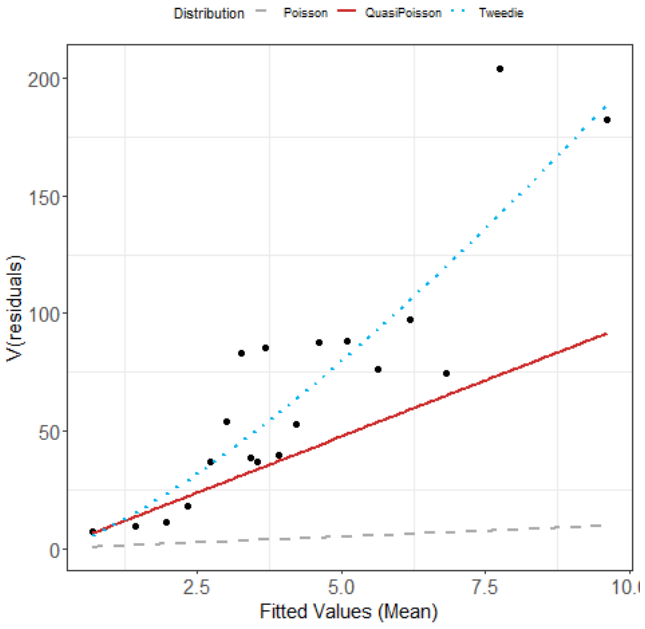

Figure 4.56 Example of estimated Tweedie mean-variance relationship (blue dashed line) for alcids. The red line shows the $V(\mu)=\phi\mu$ relationship, and the grey line shows the 1:1 relationship.

The example DHARMa diagnostic plots (Figure 4.57) show that the distributional assumption for the model is appropriate, and the model is correctly specified.

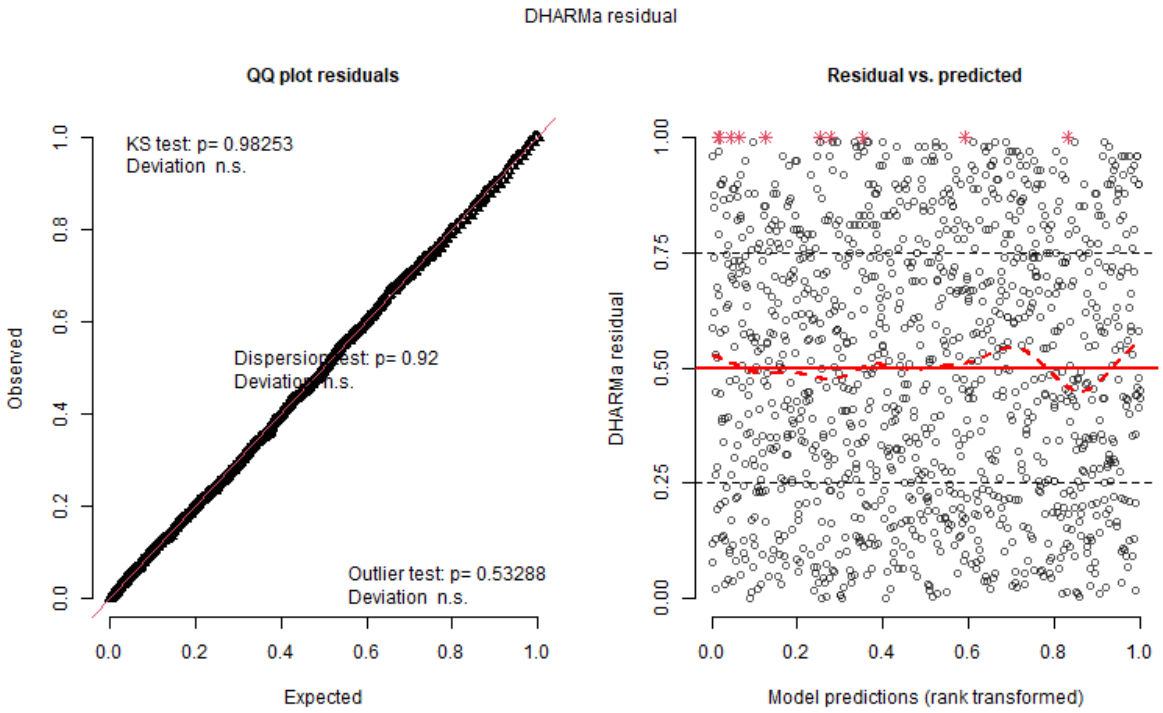

Figure 4.57 Alcid DHARMa diagnostics. Example QQ plot (left) and residuals against predicted values (right). The red stars are outliers, and the red line is a smooth spline around the mean of the residuals.

4.1.8.7 Areas of persistence

There is moderate to low persistence across the 12 surveys (Figure 4.58). The highest persistence (~ 50%) occurs in the western edge of the extended bird survey area. There is also moderate persistence in the central-north and western parts of the survey area.

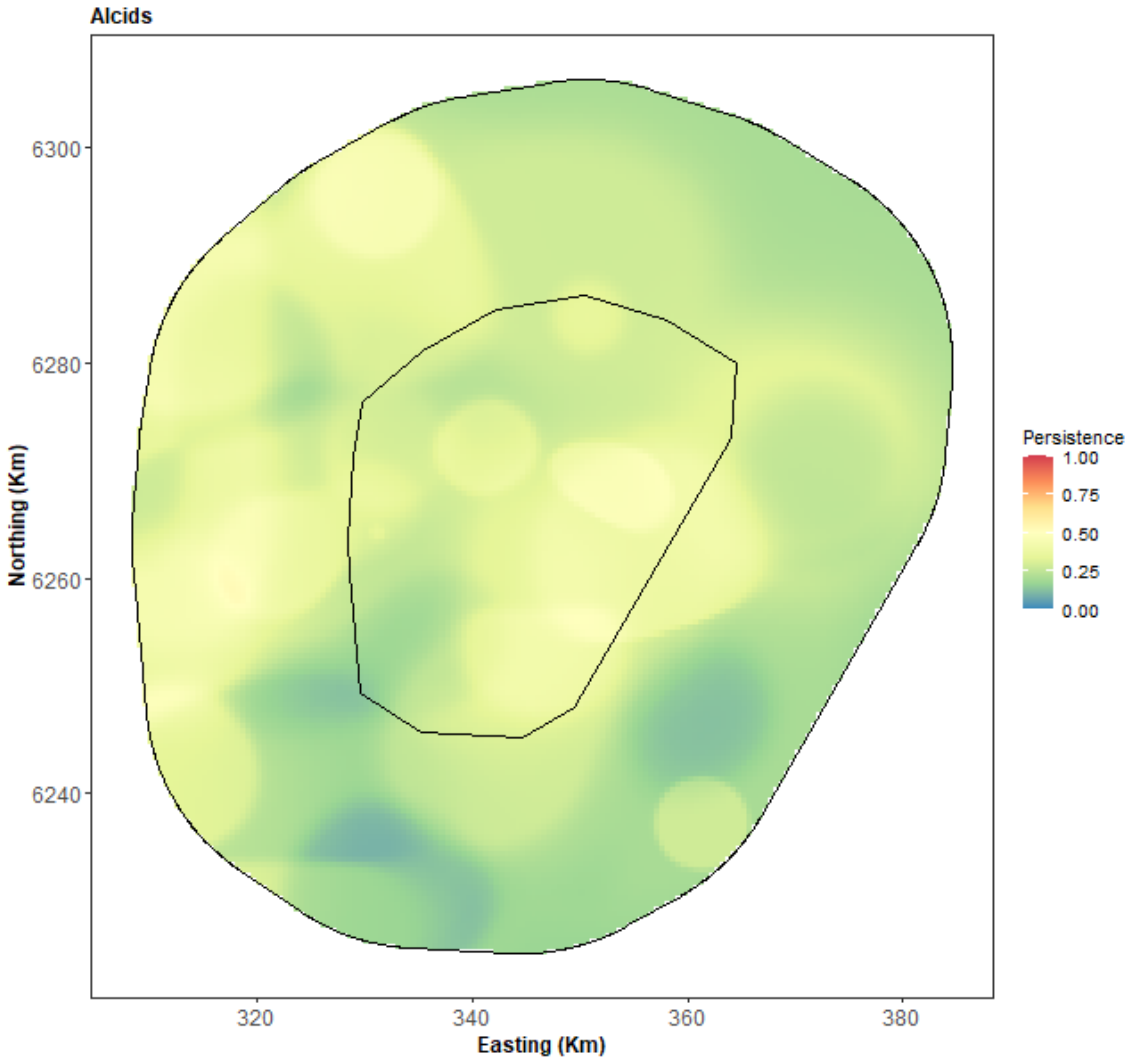

Figure 4.58 Alcid persistence scores across the twelve surveys.

4.2 Aerial survey data from the entire Danish North Sea 2019

To supplement the data presented in the rest of this report, data from aerial surveys of the entire Danish North Sea in April and May 2019 (Petersen, Nielsen, & Clausen, 2019) are here used to model total abundances and spatial distributions of four bird species or species groups, namely northern fulmar, red-throated/black-throated diver, northern gannet, black-legged kittiwake, and razorbill/common guillemot. The surveys were conducted on 19 and 20 April and 14 May 2019.

These data were gathered and analysed the same way as the data gathered and presented in the above chapter 4.1.

4.2.1 Northern fulmar

4.2.1.1 Model specification

The distance analysis and spatial modelling for these data were described in chapter 3.4 with a few exceptions. In addition to bathymetry and distance to coast, sea surface temperature and salinity data were also available and included as covariates.

Ideally, these three surveys would be analysed together for complete geographic coverage. However, owing to the temporal gap to the third survey, for each species, an April-based model and a May-based model were fitted, in addition to a model with the April and May-based data fitted together. This permitted predictions to out-of-set data to be made and a (weighted) cross-validation score to be calculated for each candidate modelling approach and for an objective comparison. Scores for each model (April, May or Combined) are given, and the preferred CV score is highlighted for the reader. Modelling results for the best-performing model are displayed alongside model-based estimates of abundance.

Lastly, persistence was not calculated as there are no repeated surveys of the region.

Model diagnostics for the previous analysis and for brevity are not presented here. In all cases, the diagnostic assessments for the combined model (April and May together) or the separate month models returned no concern.

4.2.1.2 Distance analysis

The average probability of sighting northern fulmars was estimated to be 0.24 (CoV = 0.05). This probability was estimated using a half-normal detection function and group size as a covariate (Figure 4.59). As group size increases, the probability of detection also increases.

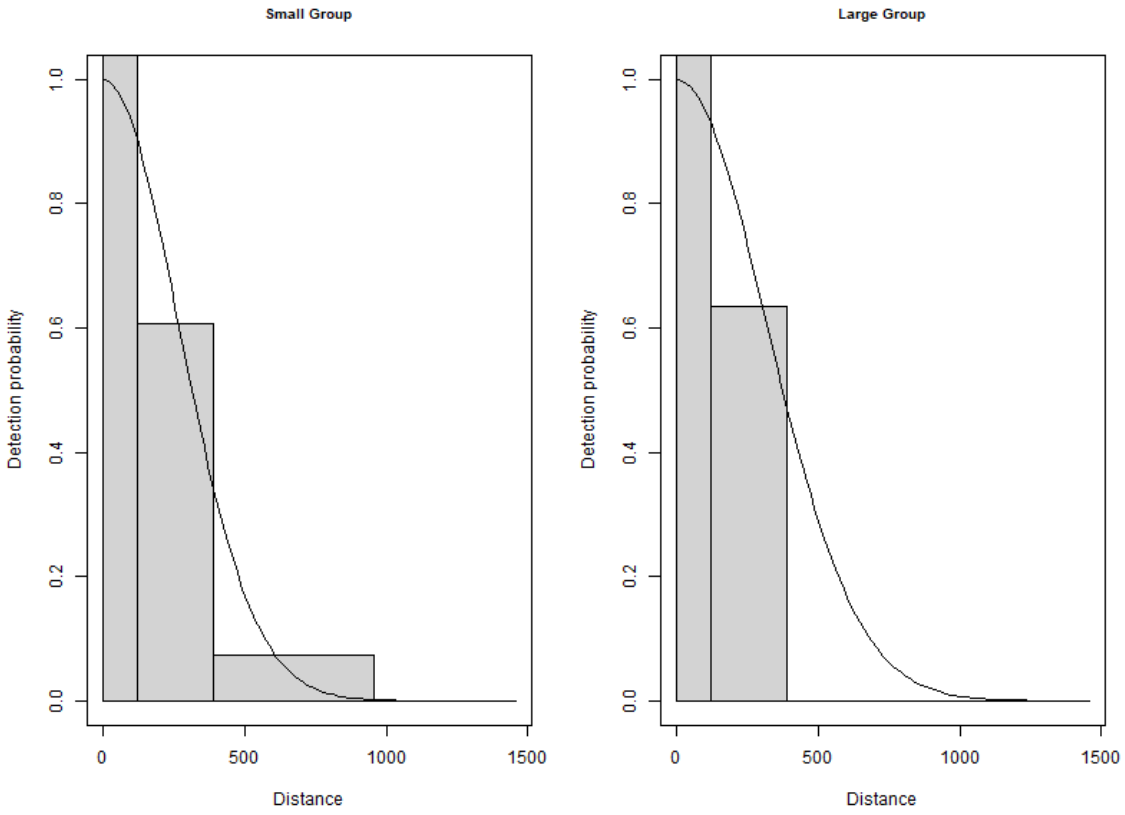

Figure 4.59 The estimated northern fulmar detection function for small and large group sizes for the entire North Sea data set from April and May 2019. The histogram represents the distances of the observed sightings. Large and small are defined by the 10 and 90 quantiles of the distribution of observed group sizes.

4.2.1.3 *Spatial analysis*

The data for the spatial analysis contained 7,988 segments overall, 1.8% of which were segments containing northern fulmar sightings. Data from April had 0.1% of segments with sightings, and May had 13%. Figure 4.60 shows the distribution of the distance corrected counts for each of the two months of surveys.

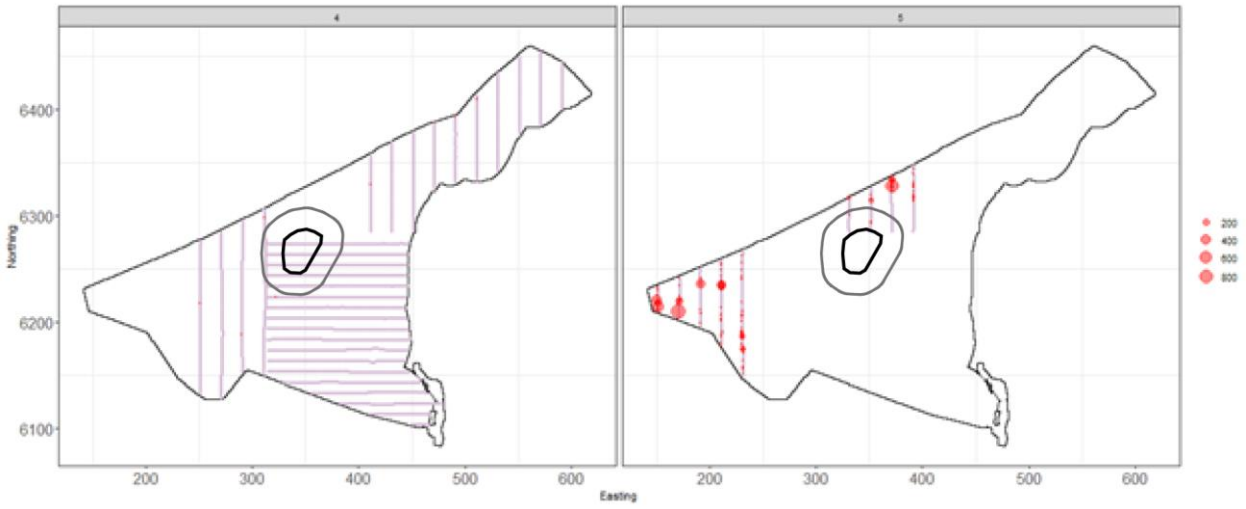

Figure 4.60 Distance-corrected counts for the northern fulmar species across the three surveys for the entire North Sea data set from April and May 2019. The red circles indicate the distance-corrected counts along the transect lines. The pale purple dots are segments with a count of zero.

4.2.1.4 *Model selection*

The best model for northern fulmars was a combined model fitted using data across months collectively (Model (4) and (5) in combination, Table 4.11). Additionally, for the separate month-based models, there was compelling evidence for non-uniform spatial patterns in April (4) out of a 'one-covariate' (non-spatial term) model in May (5). The spatial surface for month 4 was underpinned by just 4 parameters, whilst a 'distance to coast' model based on 5 parameters was deemed suitable for May (5). The combined model (selected here) contained a spatial term with 11 associated parameters and returned an estimated count of 46,437 (34,216, 193,705).

Table 4.11 Model selection results for northern fulmar for each April and May 2019 survey. The model column represents the terms in the model.

Name	Model	Number of parameters	Dispersion parameter	CV score
April (4)	2D Only	4	8.77	0.040
May (5)	Distance to coast	5	75.93	2282.927
Combined	2D Only	11	118.96	288.144
April (4) and May (5) blend	-	9	NA	292.688

The estimated abundances, densities and associated 95% percentile confidence intervals for each month are given in Table 4.12.

Table 4.12 Estimated abundance and density (N/km^2) of northern fulmar for each survey in April and May 2019. The 95% CI are percentile-based confidence intervals.

Model	Month	Area (km^2)	Estimated count	95% CI count	Estimated density	95% CI density
Combined	4	48,338	2,421	(854, 11,539)	0.1	(0, 0.2)
Combined	5	10,647	44,017	(33,362, 182,166)	4.1	(3.1, 17.1)
Combined	45	58,985	46,437	(34,216, 193,705)	0.8	(0.6, 3.3)

4.2.1.5 Spatial results

Figure 4.61 shows the estimated counts of northern fulmar in each 1 km^2 grid cell for each month. Generally, the estimated abundances fit the raw data well, and there were no notable misalignments. In areas where the estimated counts were systematically higher, the abundances were also relatively high, and there were no areas with large, estimated abundances.

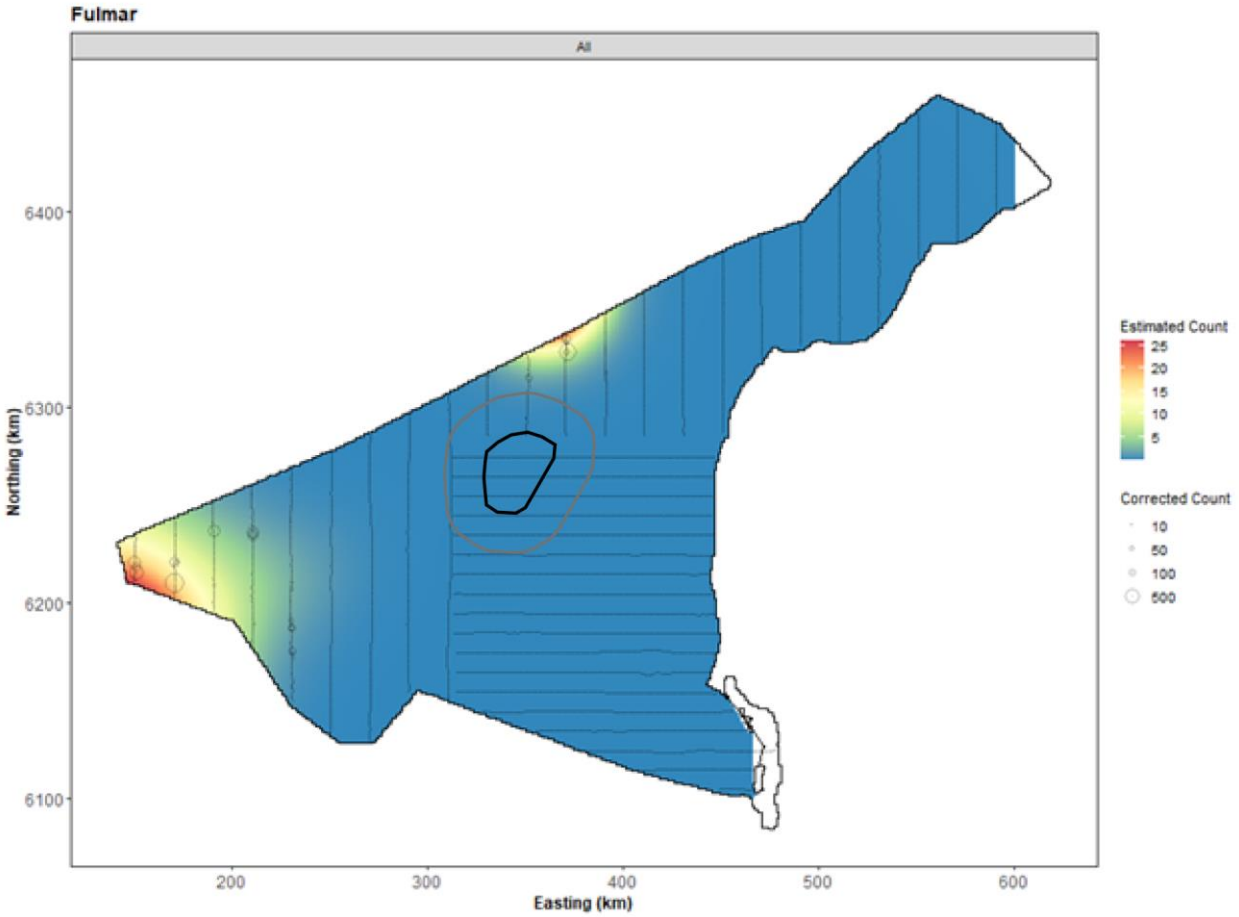

Figure 4.61 The estimated northern fulmar abundance across the study site for each survey for the entire North Sea data set from April and May 2019. The estimated counts are per 1 km x 1 km grid cell. The open circles show the observed corrected count. The coloured graphics represent the predicted counts in each location.

4.2.1.6 Uncertainty in spatial predictions

The highest CoV scores were associated with 'almost zero' predictions, and it is known that the CoV metric is highly sensitive to any uncertainty for very small predictions. There was no material overlap between high values of the CoV metric and the transect lines/locations with non-zero counts, resulting in no concerns in this case (Figure 4.62).

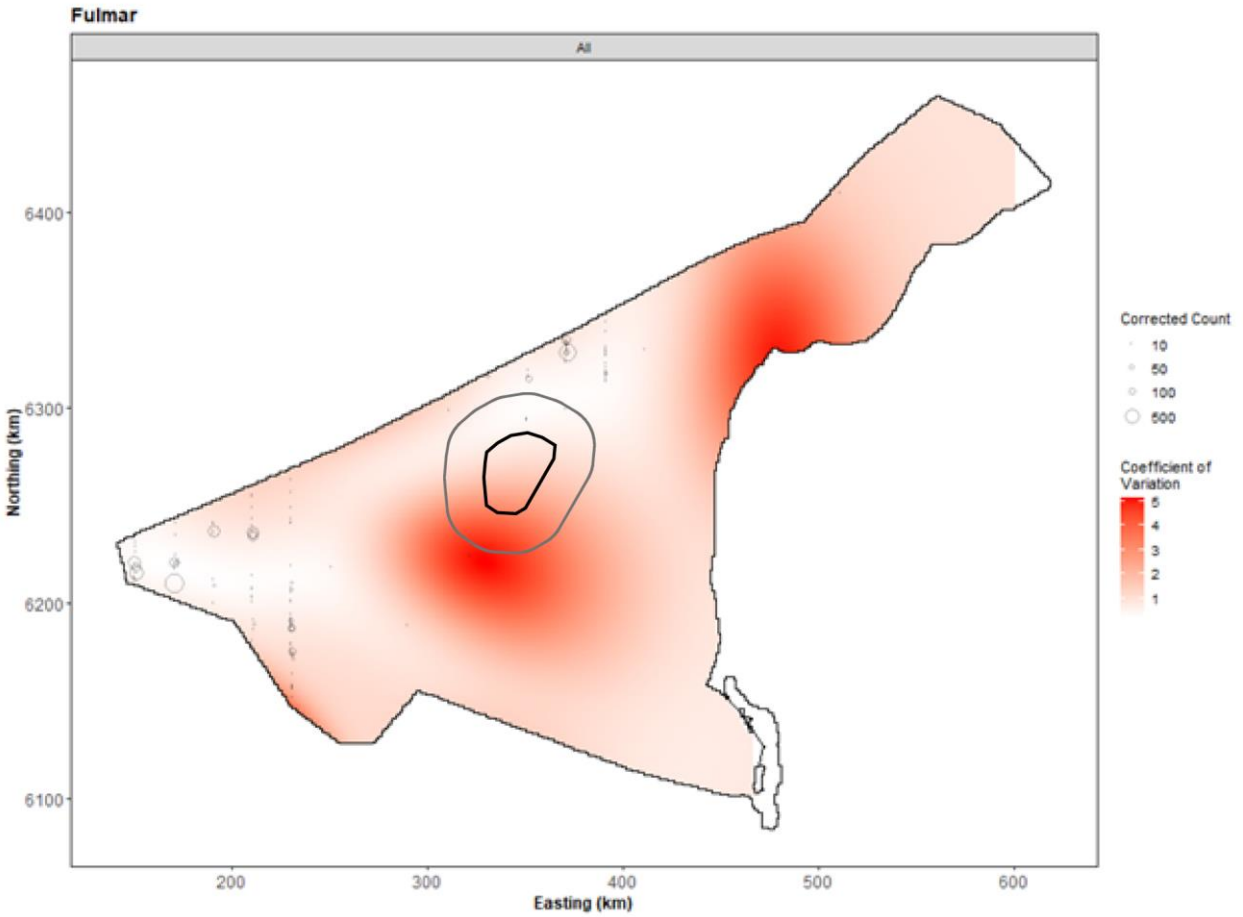

Figure 4.62 The Coefficient of Variation (CoV) across the study region for each survey for the entire North Sea data set from April and May 2019. The open circles show the distance corrected northern fulmar counts, where applicable. The presence of dark red CoV scores in areas with virtually zero predictions is an artefact of the very small prediction rather than of any notable concern.

4.2.1.7 Model diagnostics

A blocking structure was used to account for potential residual non-independence for each model and a robust standard error approach was based on unique transects. In each case, we saw a reassuring decay to zero (indicated by the red and grey lines in Figure 4.63 and Figure 4.64), implying that an appropriate blocking structure was used. The assumed mean-variance relationship was examined, and agreement was generally shown between the assumed and the observed values (Figure 4.65).

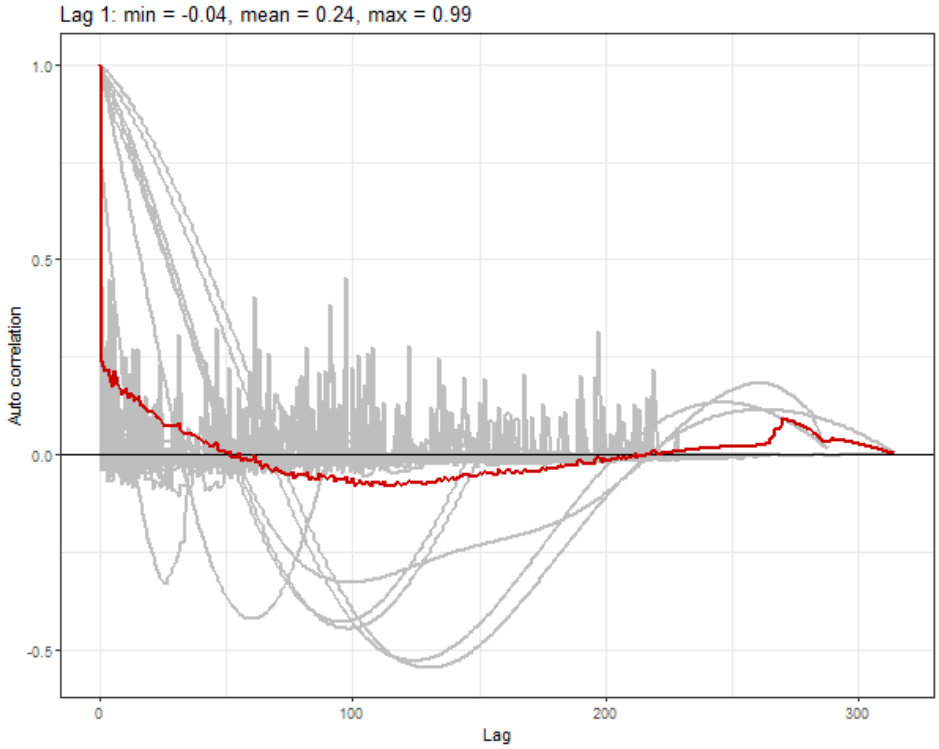

Figure 4.63 Example Auto Correlation Function (ACF) plot for northern fulmar for the 2019 data set. The grey lines represent the residual correlation observed in each transect, and the red line is the average of these values across transects.

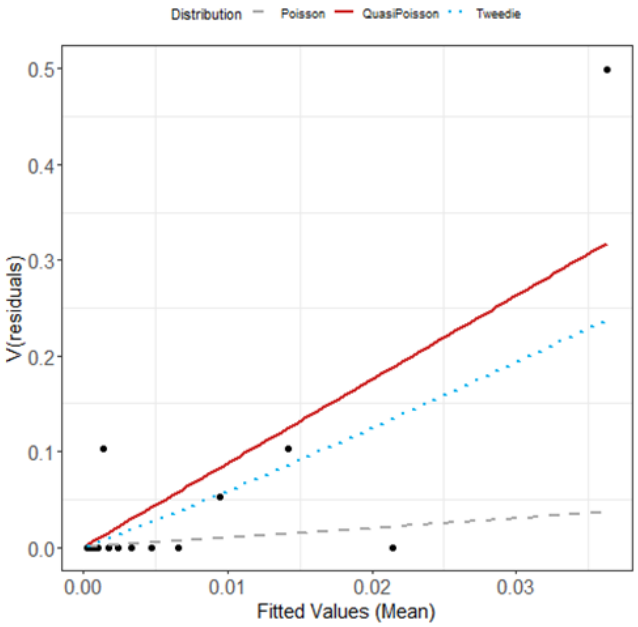

Figure 4.64 Example estimated Tweedie mean-variance relationship (blue dashed line) for northern fulmar for the 2019 data set. The red line shows the $V(\mu)=\phi\mu$ relationship, and the grey line shows the 1:1 relationship.

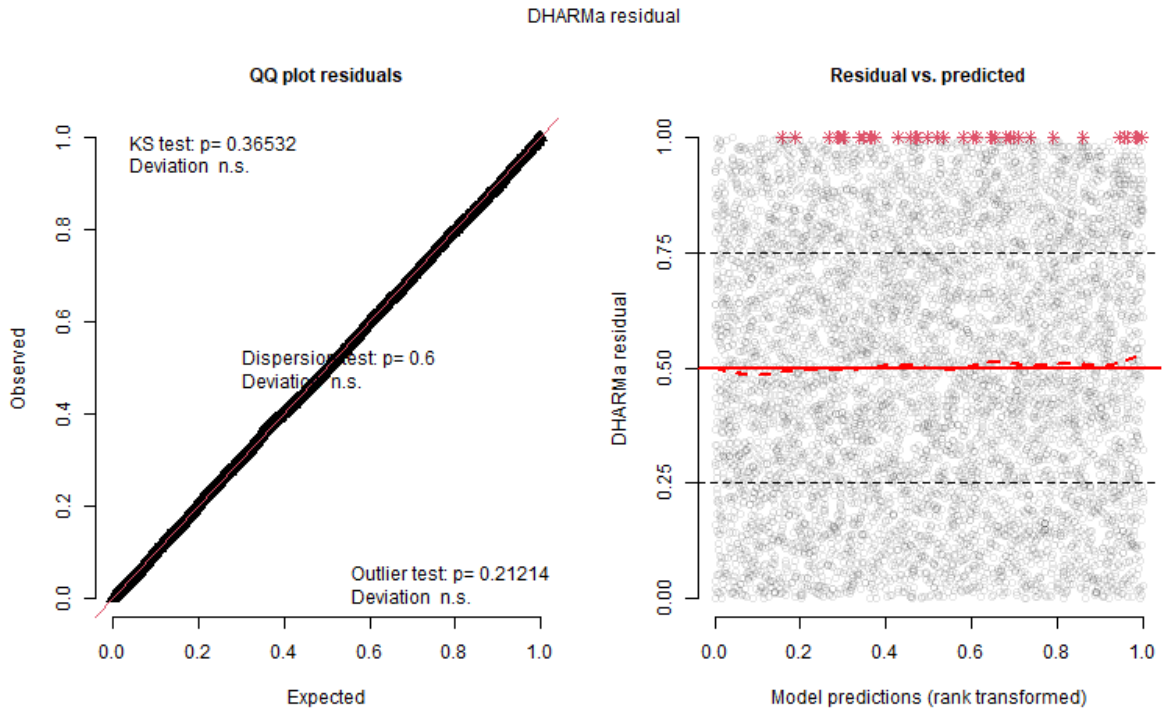

Figure 4.65 DHARMa diagnostics. Example QQ plot (left) and residuals against predicted values (right) for northern fulmar for the 2019 data set. The red stars are outliers, and the red line is a smooth spline around the mean of the residuals.

4.2.2 Red-throated/black-throated diver

4.2.2.1 Distance analysis

The average probability of sighting divers was estimated to be 0.15 (CoV = 0.08). This probability was estimated using a hazard rate detection function, and no covariates were selected (Figure 4.66).

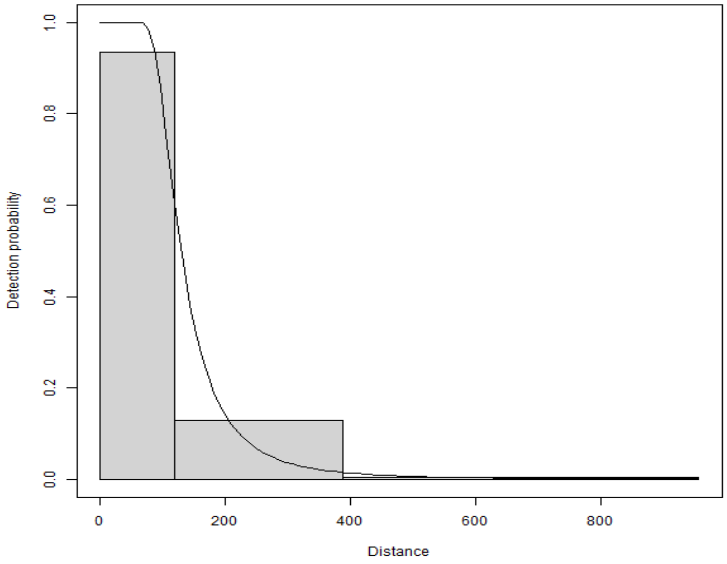

Figure 4.66 The estimated diver detection function. The histogram represents the distances of the observed sightings.

4.2.2.2 *Spatial analysis*

The data for the spatial analysis contained 7,988 segments overall, 2.5% of which were segments containing diver sightings. April (4) had 3% of segments with sightings, and May (5) had <0.1%. Figure 4.67 shows the distribution of the distance corrected counts for each of the two months of surveys.

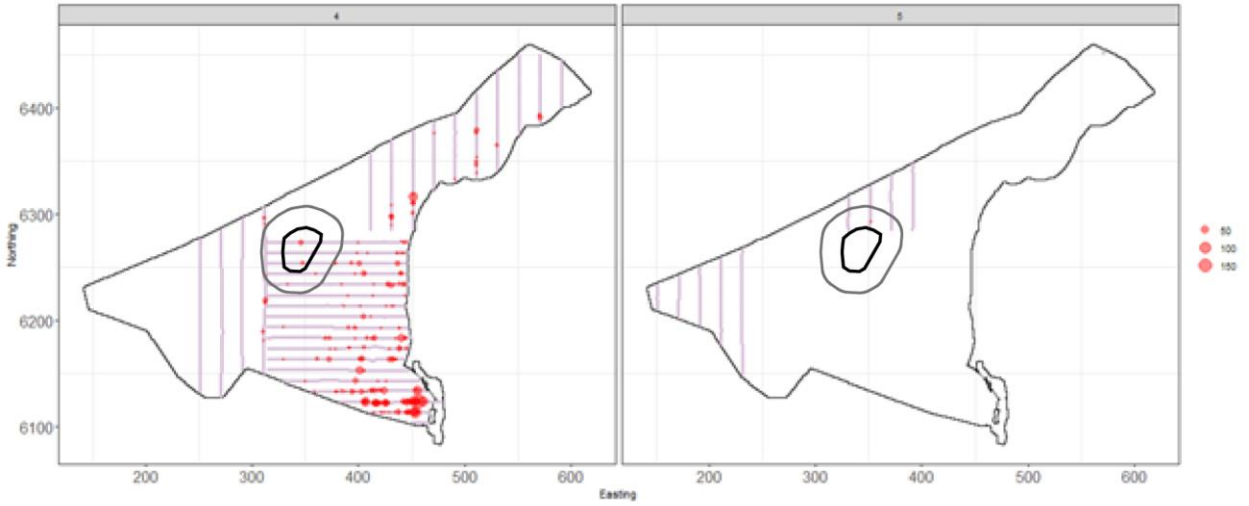

Figure 4.67 Distance-corrected counts for the diver species across the three surveys for the entire North Sea data set from April and May 2019. The red circles indicate the distance-corrected counts along the transect lines. The pale purple dots are segments with a count of zero.

4.2.2.3 *Model selection*

The best model(s) for the diver species were two separate models, one for each month (Table 4.13), and while there was compelling evidence for non-uniform spatial patterns in April (4), the selected model for May (5) did not contain a spatial element and settled on 'distance from coast' as the sole covariate. The spatial surface for April (4) was underpinned by 11 parameters, whilst a one-covariate model (*df* = 3) was deemed sufficient for May (5). Interestingly, the combined model selected salinity as the sole covariate, but this was not chosen when each month was considered separately.

Table 4.13 Model selection results for divers for each April and May 2019 survey. The model column represents the terms in the model.

Name	Model	Number of parameters	Dispersion parameter	CV score
April (4)	2D Only	11	25.95	14.452
May (5)	Distance to coast	3	9.42	0.040
Combined	Salinity	4	29.74	12.869
April (4) and May (5) blend	-	14	NA	12.592

The estimated abundances, densities and associated 95 percentile confidence intervals for each month are given in Table 4.14, where 'Model' represents the model for month 4 and month 5, respectively.

Table 4.14 Estimated abundance and density (N/km^2) of divers for each survey in April and May 2019. The 95% CI are percentile-based confidence intervals.

Model	Month	Area (km^2)	Estimated count	95% CI count	Estimated density	95% CI density

April (4)	4	48,338	22,574	(11,038, 49,870)	0.5	(0.2, 1)
May (5)	5	10,647	74	(10, 646)	0.0	(0, 0.1)

4.2.2.4 Spatial results

Figure 4.68 shows each month's estimated diver counts in each 1 km^2 grid cell. Generally, the estimated abundances fit the raw data well, and there were no notable misalignments. In areas where the estimated counts were systematically higher, the abundances were also relatively high, and there were no areas with large, estimated abundances unsupported by the data.

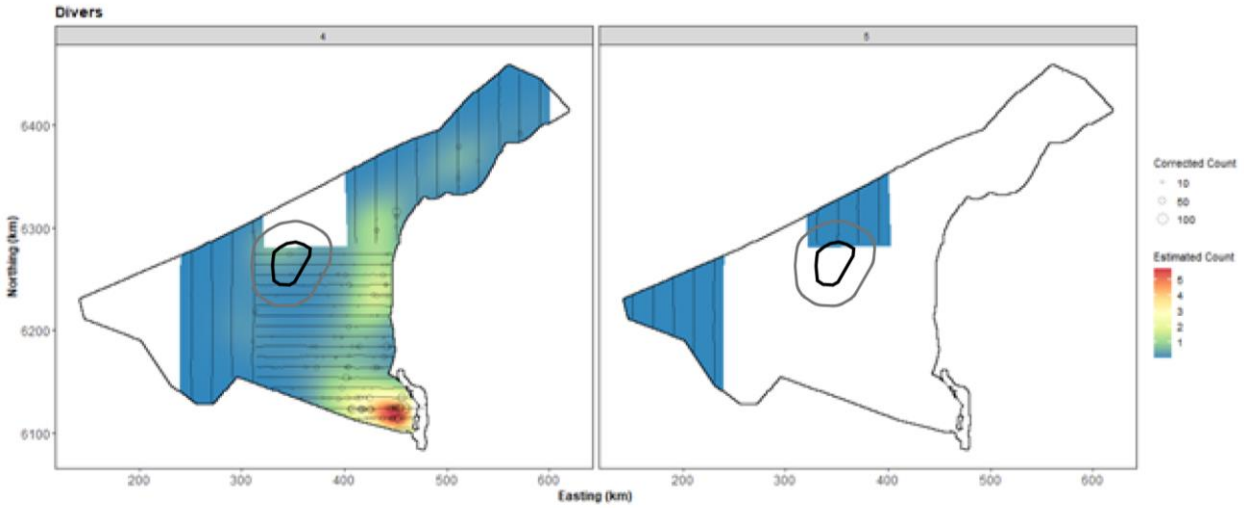

Figure 4.68 The estimated diver abundance across the study site for each survey for the entire North Sea data set from April and May 2019. The estimated counts are per 1 km x 1 km grid cell. The open circles show the observed corrected count. The coloured graphics represent the predicted counts in each location.

4.2.2.5 Uncertainty in spatial predictions

The highest CoV scores were associated with 'almost zero' predictions, and it is known that the CoV metric is highly sensitive to any uncertainty for very small predictions. The only slight exception to this was the central hotspot, where a small number of non-zero values were observed; however, this CoV was still of a reasonable magnitude. Otherwise, there was no material overlap between the high values of the CoV metric and the transect lines/locations with non-zero counts, resulting in no concerns in this case (Figure 4.69).

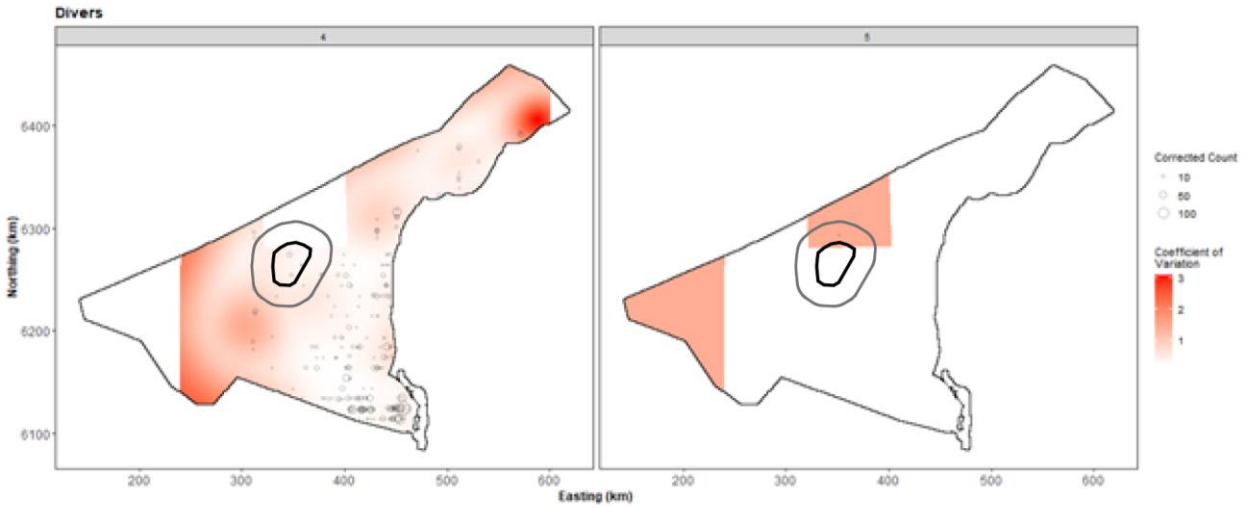

Figure 4.69 The Coefficient of Variation (CoV) across the study region for each month for the entire North Sea data set from April and May 2019. The open circles show the distance corrected diver counts, where applicable, and the polygons represent the extended bird survey area (black line). The presence of dark red CoV scores in areas with virtually zero predictions is an artefact of the very small prediction rather than any notable concern.

4.2.2.6 Model diagnostics

Several diagnostic assessments were made for each model (Figure 4.70 and Figure 4.73), and no concerns were noted in either model. The plots for the month 5 model look peculiar for one value, but this is unsurprising due to a model fitted to very few data points with sightings.

A blocking structure was used to account for potential residual non-independence for each model and a robust standard error approach was based on unique transects. In each case, we saw a reassuring decay to zero (indicated by the red and grey lines in Figure 4.71 and Figure 4.74), implying that an appropriate blocking structure was used.

The assumed mean-variance relationship was examined, and the agreement between the assumed (red) lines and the observed values was generally shown (Figure 4.72 and Figure 4.75).

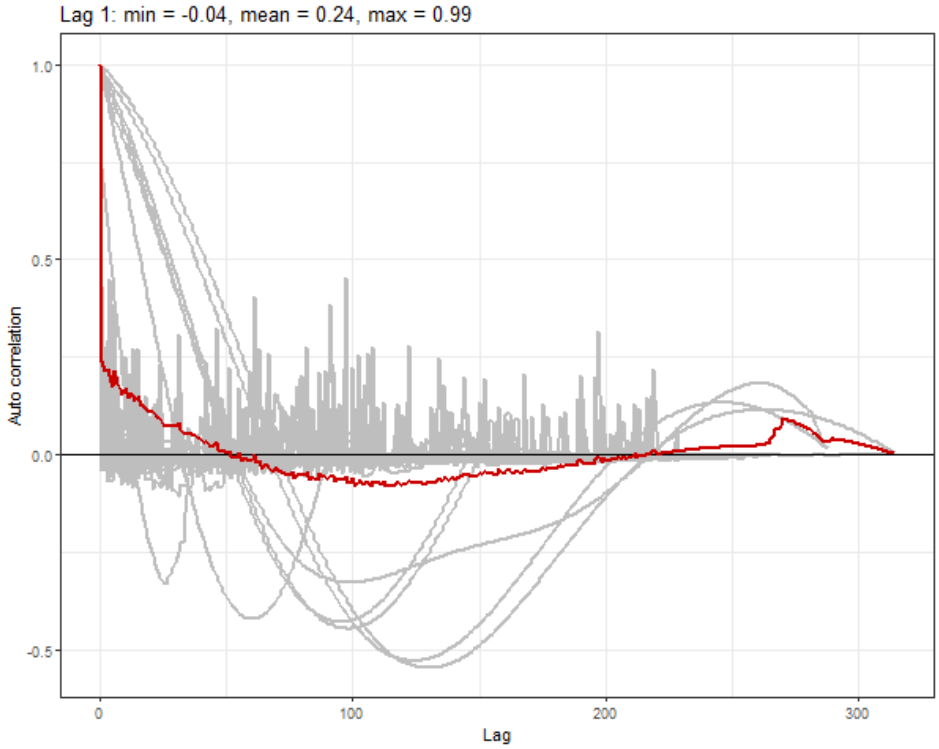

Figure 4.70 Example red-throated/black-throated diver Auto Correlation Function (ACF) plot for the 2019 'Month 4' data set. The grey lines represent the residual correlation observed in each transect, and the red line is the average of these values across transects.

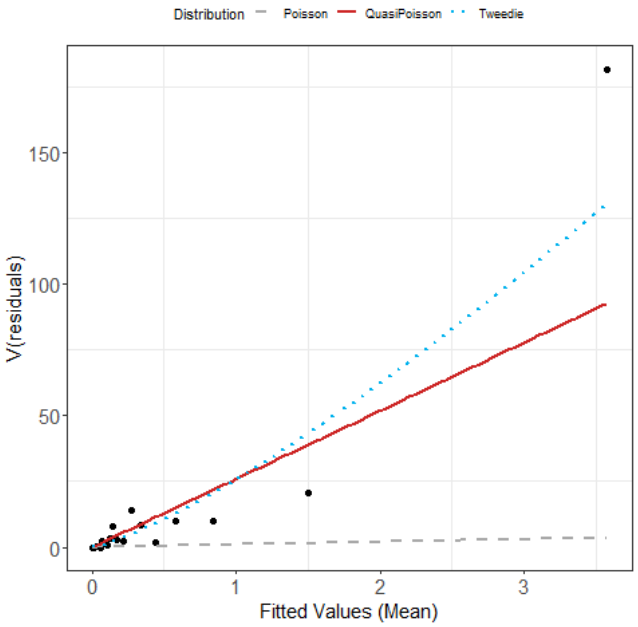

Figure 4.71 Example estimated Tweedie mean-variance relationship (blue dashed line) for red-throated/black-throated diver for the 2019 'Month 4' data set. The red line shows the $V(\mu)=\phi\mu$ relationship, and the grey line shows the 1:1 relationship.

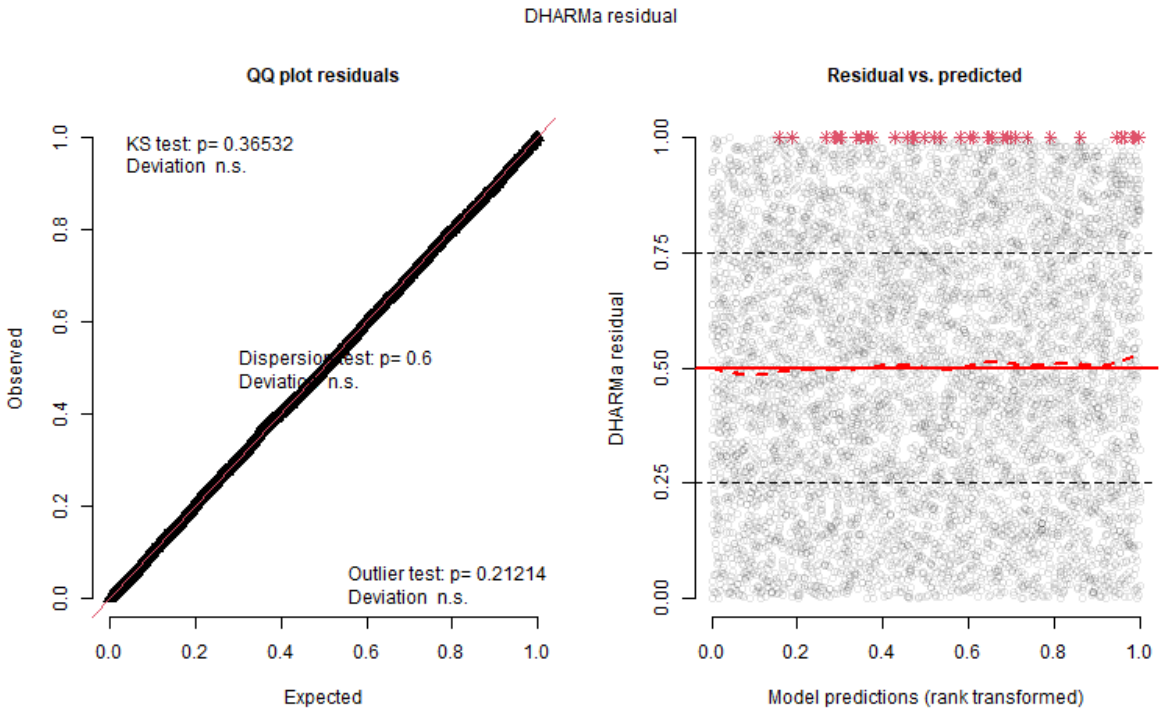

Figure 4.72 DHARMa diagnostics. Example QQ plot (left) and residuals against predicted values (right) for red-throated/black-throated diver of the 2019 'Month 4' data set. The red stars are outliers, and the red line is a smooth spline around the mean of the residuals.

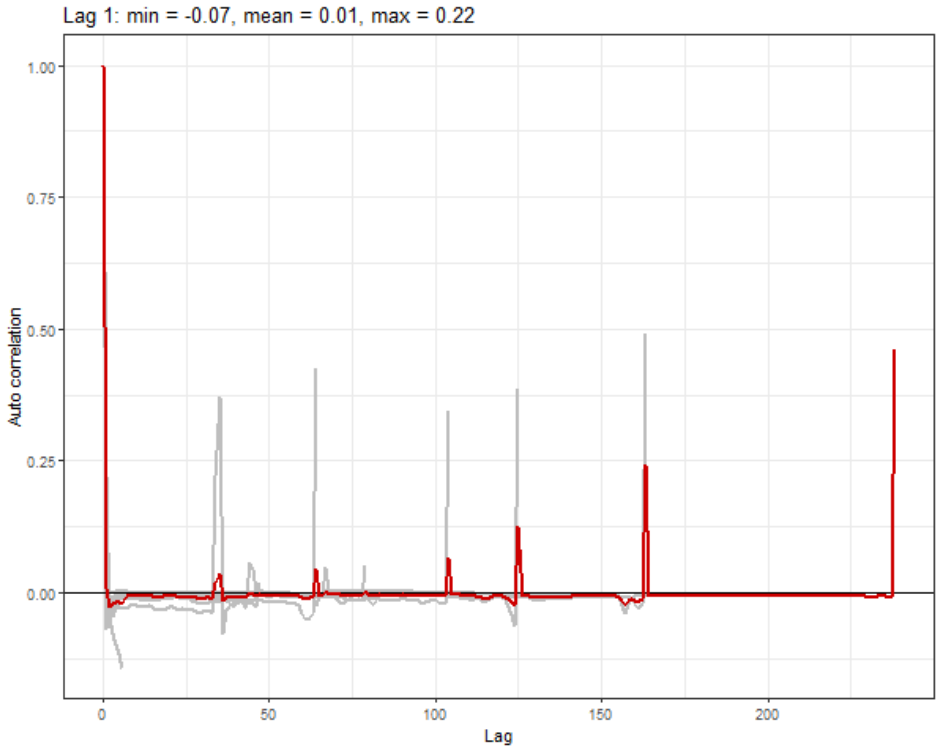

Figure 4.73 Example red-throated /black-throated diver Auto Correlation Function (ACF) plot for the 2019 'Month 5' data set. The grey lines represent the residual correlation observed in each transect, and the red line is the average of these values across transects.

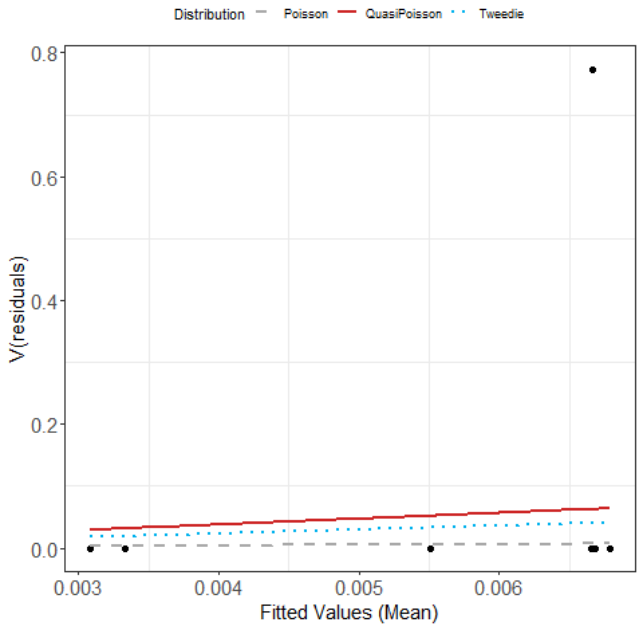

Figure 4.74 Example estimated Tweedie mean-variance relationship (blue dashed line) for red-throated/black-throated diver for the 2019 'Month 5' data set. The red line shows the V(μ)=ϕμ relationship, and the grey line shows the 1:1 relationship.

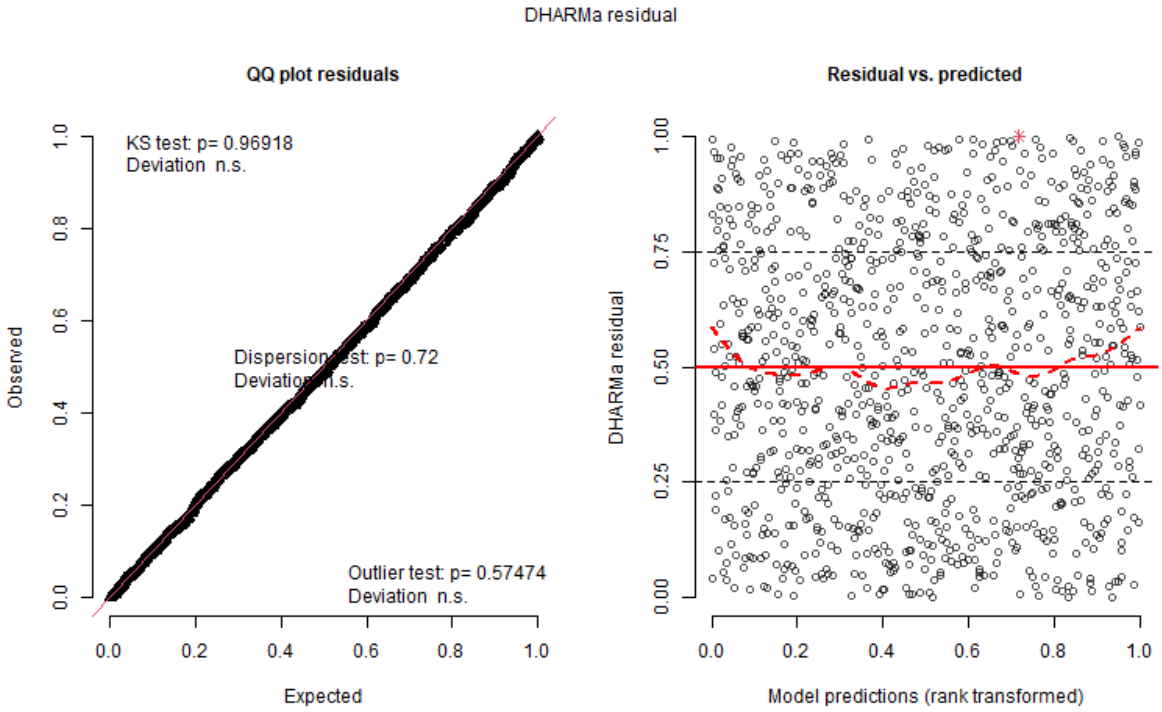

Figure 4.75 DHARMa diagnostics. Example QQ plot (left) and residuals against predicted values (right) for red-throated/black-throated diver of the 2019 'Month 5' data set. The red stars are outliers, and the red line is a smooth spline around the mean of the residuals.

4.2.3 Northern gannet

4.2.3.1 Distance analysis

The average probability of sighting northern gannets was estimated at 0.33 (CoV = 0.03). This probability was estimated using a hazard rate detection function and included observer and group size as covariates (Figure 4.76 and Figure 4.77). Of note is that observer 'JST' was estimated to miss animals on the line (under the model), while observers 'MEN' and 'MN' had rapidly declining detection functions. Additionally (and not surprisingly), the larger the group, the higher the estimated probability of detection.

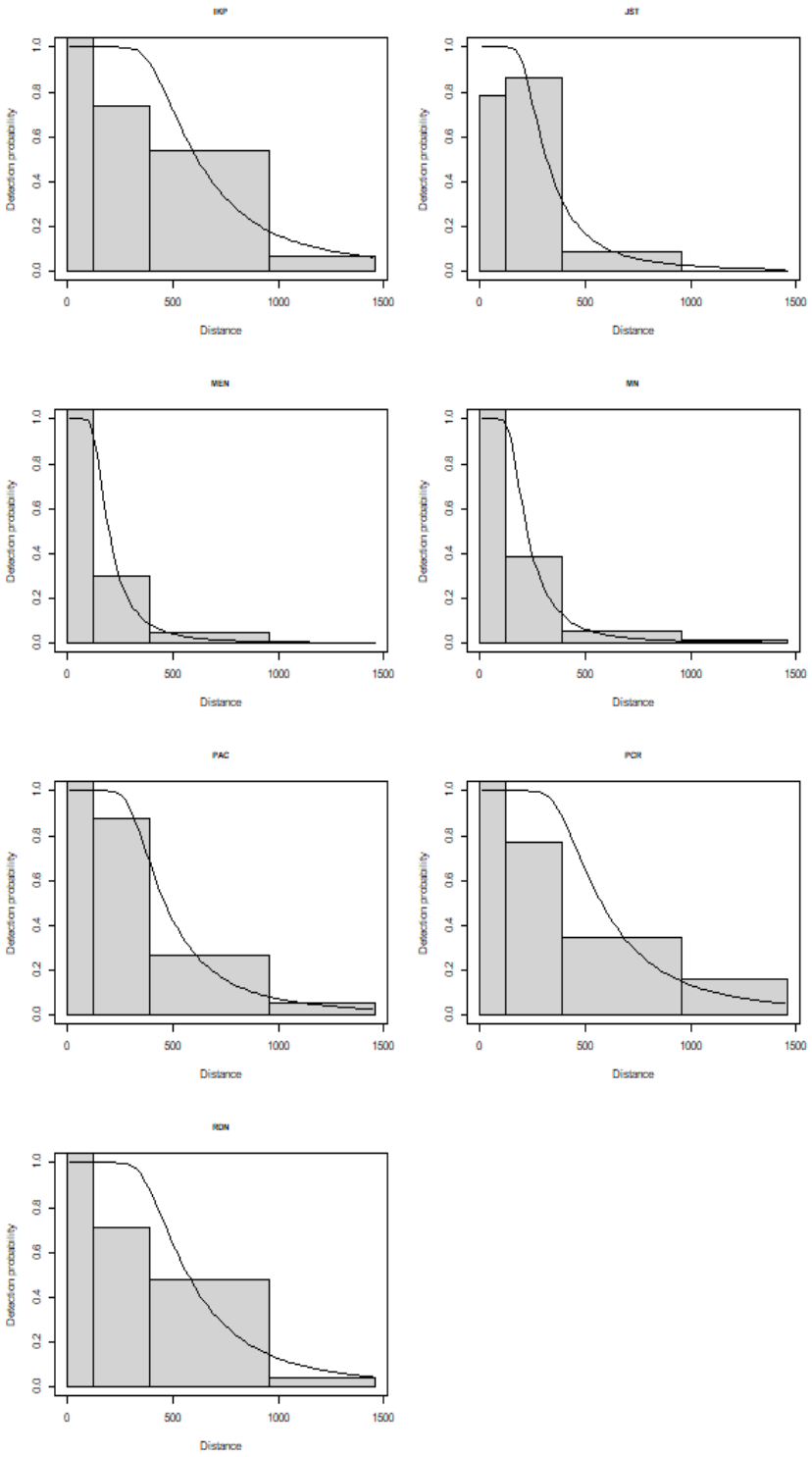

Figure 4.76 The estimated northern gannet detection function for each of the observers. The histograms are the distances of the observed sightings.

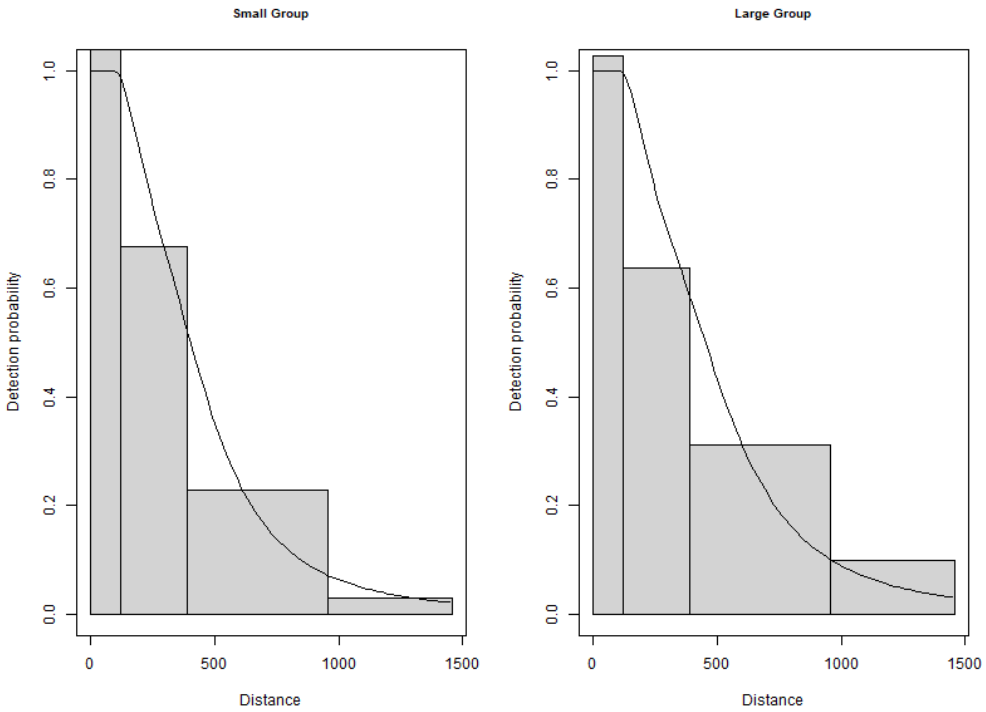

Figure 4.77 The estimated northern gannet detection function for small and large group sizes. The histogram represents the distances of the observed sightings. Large and small are defined by the 10 and 90 quantiles of the distribution of observed group sizes.

4.2.3.2 Spatial analysis

The data for the spatial analysis contained 6,964 segments, 14% of which were segments containing northern gannet sightings. April (4) had 14.6% of segments with sightings, and May (5) had 9.7%. Figure 4.78 shows the distribution of the distance corrected counts for each of the two months of surveys.

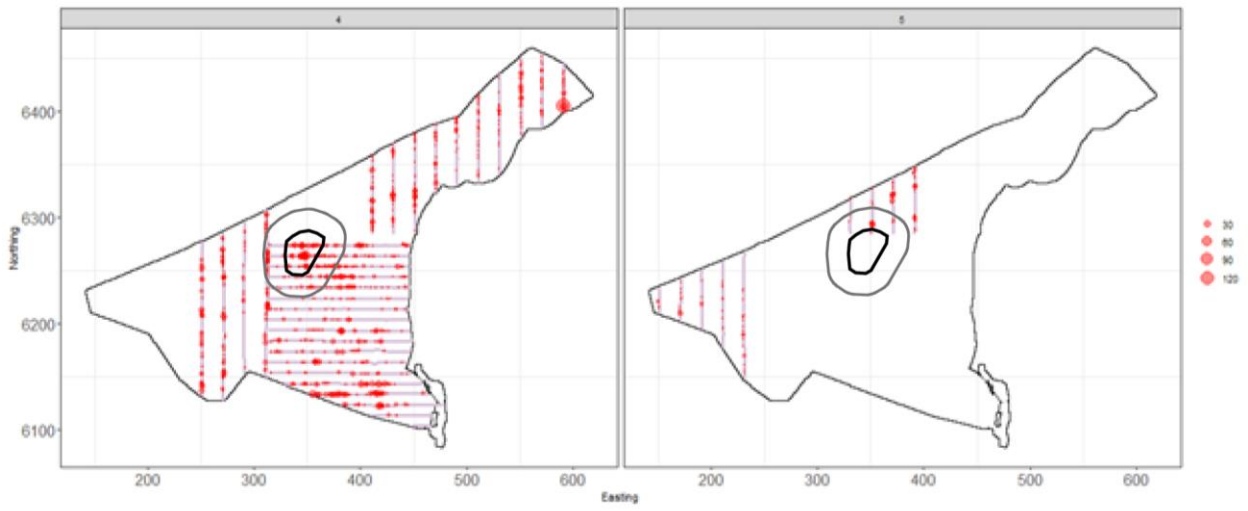

Figure 4.78 Distance-corrected counts for the northern gannet species across the three surveys for the entire North Sea data set from April and May 2019. The red circles indicate the distance-corrected counts along the transect lines. The pale purple dots are segments with a count of zero.

4.2.3.3 Model selection

The best model for northern gannets was a blended model of April and May-based models (Table 4.15; *df* = 13). There was compelling evidence for non-uniform spatial patterns in April (4) (*df* = 9), while the simpler (non-linear salinity only) model was chosen for May (5).

Table 4.15 Model selection results for northern gannets for each April and May 2019 survey. The model column represents the terms in the model.

Name	Model	Number of parameters	Dispersion parameter	CV score
April (4)	Best 1D2D	9	9.45	10.128
May (5)	Salinity	2	15.53	2.768
Combined	Best 1D2D	13	9.10	9.039
April (4) and May (5) blend	-	11	NA	9.184

The estimated abundances, densities and associated 95-percentile confidence intervals for each month are given in Table 4.16.

Table 4.16 Estimated northern gannets' survey abundance and density (N/km2) in April and May 2019. The 95% CI are percentile-based confidence intervals.

Model	Month	Area (km^2)	Estimated count	95% CI count	Estimated density	95% CI density
Combined	4	48,338	26,950	(18,205, 41,345)	0.6	(0.4, 0.9)
Combined	5	10,647	4,773	(3,173, 7,422)	0.4	(0.3, 0.7)
Combined	45	58,985	31,723	(21,378, 48,767)	0.5	(0.4, 0.8)

4.2.3.4 Spatial results

Figure 4.79 shows the estimated counts of northern gannets in each 1 km^2 grid cell for each month. Generally, the estimated abundances fit the raw data well, and there were no notable misalignments. In areas where the estimated counts were systematically higher, the abundances were also relatively high, and there were no areas with large, estimated abundances unsupported by the data.

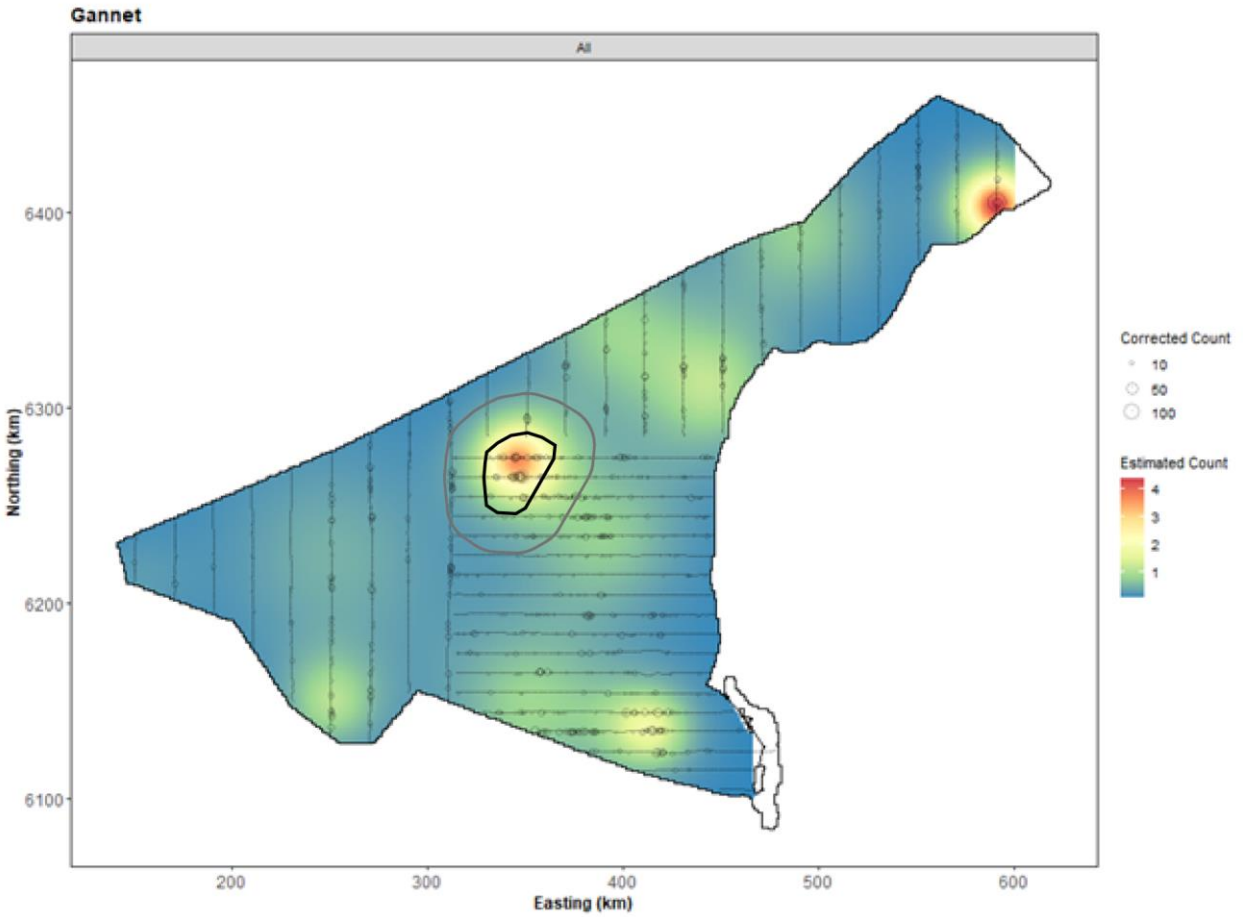

Figure 4.79 The estimated northern gannet abundance across the study site for each survey for the entire North Sea data set from April and May 2019. The estimated counts are per 1 km x 1 km grid cell. The open circles show the observed corrected count. The coloured graphics represent the predicted counts in each location.

4.2.3.5 Uncertainty in spatial predictions

Even the highest CoV scores were very modest (~0.5) and were unproblematically distributed across the surface (Figure 4.80).

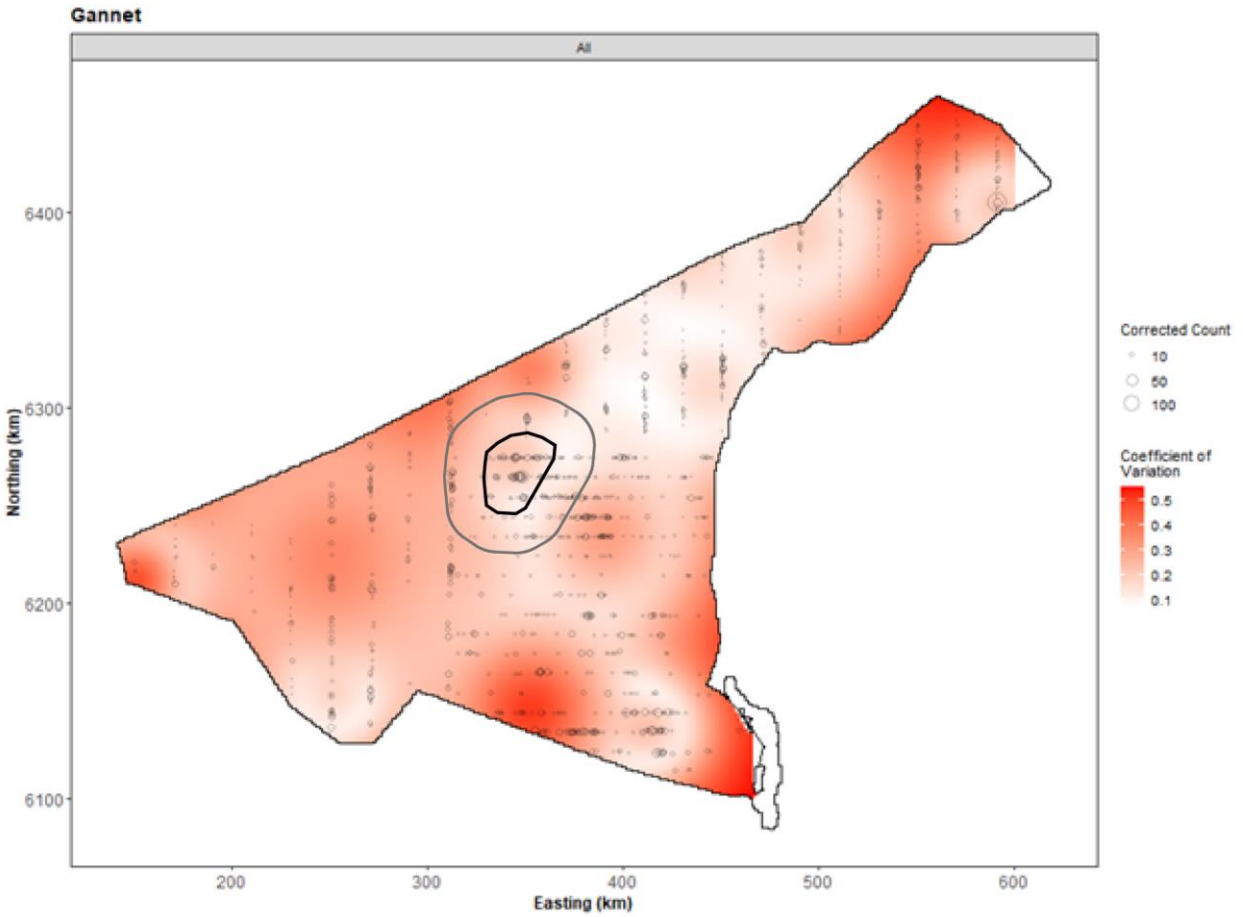

Figure 4.80 The Coefficient of Variation (CoV) across the study region for the entire North Sea data set from April and May 2019. The open circles show the distance corrected northern gannet counts, where applicable, and the polygons represent the area of the extended bird survey area (black line). The presence of dark red CoV scores in areas with virtually zero predictions is an artefact of the very small prediction rather than any notable concern.

4.2.3.6 Model diagnostics

The diagnostic assessments for each model (Figure 4.81) generated no concerns.

A blocking structure was used to account for potential residual non-independence for each model and a robust standard error approach was based on unique transects. In each case, we saw a reassuring decay to zero (indicated by the red and grey lines in Figure 4.82), implying that an appropriate blocking structure was used.

The assumed mean-variance relationship was examined, and there was generally agreement between the assumed (red) lines and the observed values (Figure 4.83).

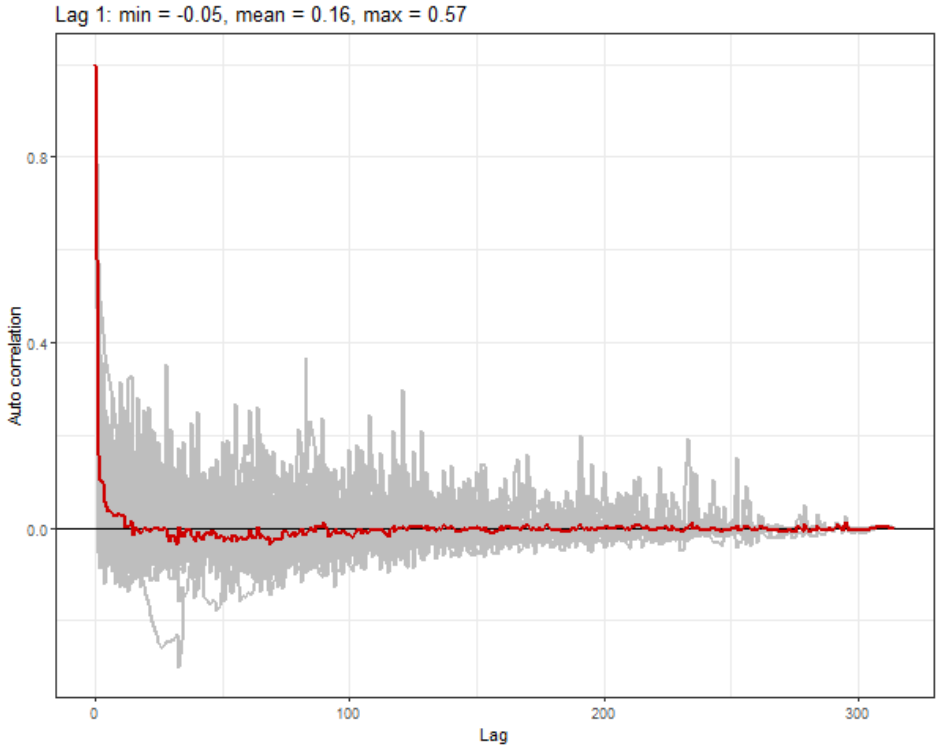

Figure 4.81 Example northern gannet Auto Correlation Function (ACF) plot for the 2019 data set. The grey lines represent the residual correlation observed in each transect, and the red line is the average of these values across transects.

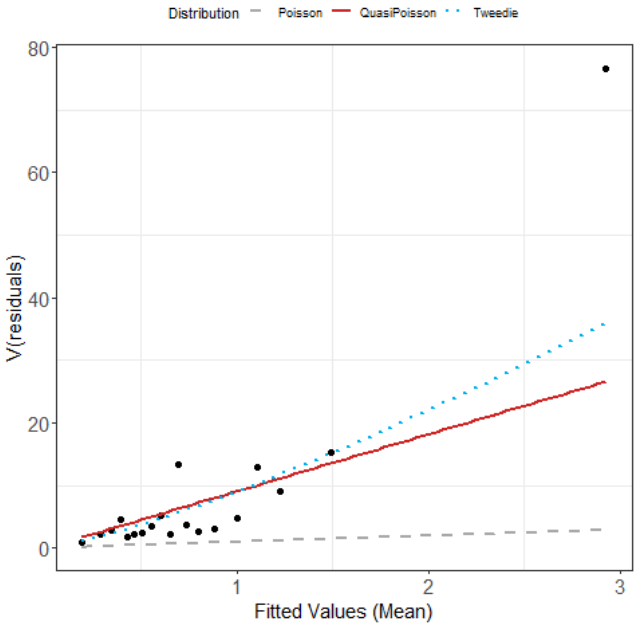

Figure 4.82 Example estimated Tweedie mean-variance relationship (blue dashed line) for northern gannet for the 2019 data set. The red line shows the $V(\mu)=\phi\mu$ relationship, and the grey line shows the 1:1 relationship.

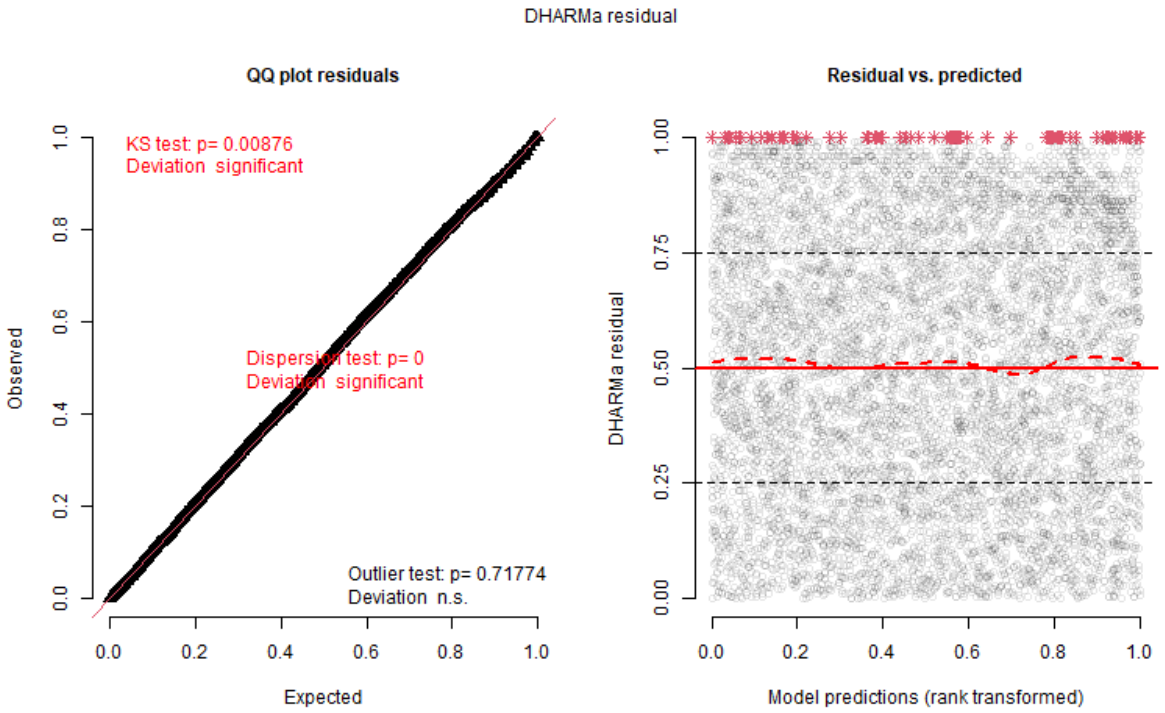

Figure 4.83 DHARMa diagnostics. Example QQ plot (left) and residuals against predicted values (right) for the northern gannet of the 2019 data set. The red stars are outliers, and the red line is a smooth spline around the mean of the residuals.

4.2.4 Black-legged kittiwake

4.2.4.1 Distance analysis

The average probability of sighting black-legged kittiwakes was estimated to be 0.23 (CoV = 0.1). This probability was estimated using a half-normal detection function and no covariates (Figure 4.84).

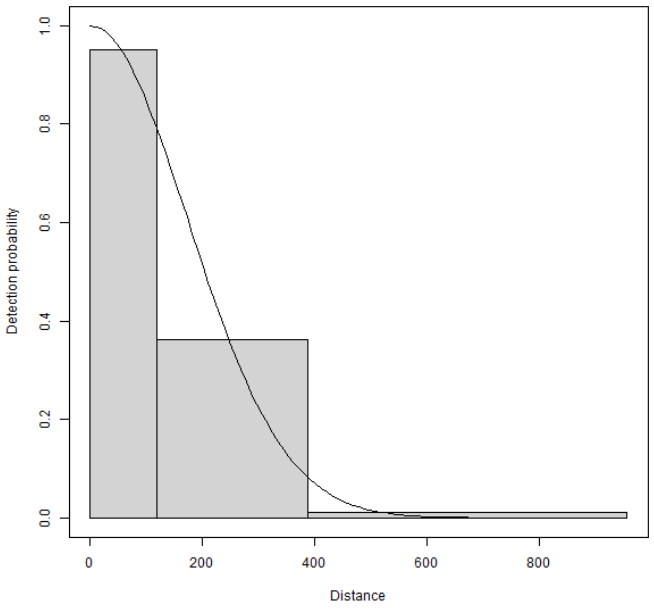

Figure 4.84 The estimated black-legged kittiwake detection function. The histogram represents the distances of the observed sightings.

4.2.4.2 Spatial analysis

The data for the spatial analysis contained 7,988 segments overall, 0.8% of which were segments containing black-legged kittiwake sightings. April (4) had 0.5% of segments with sightings, and May (5) had 2.4%. Figure 4.85 shows the distribution of the distance corrected counts for each of the two months of surveys.

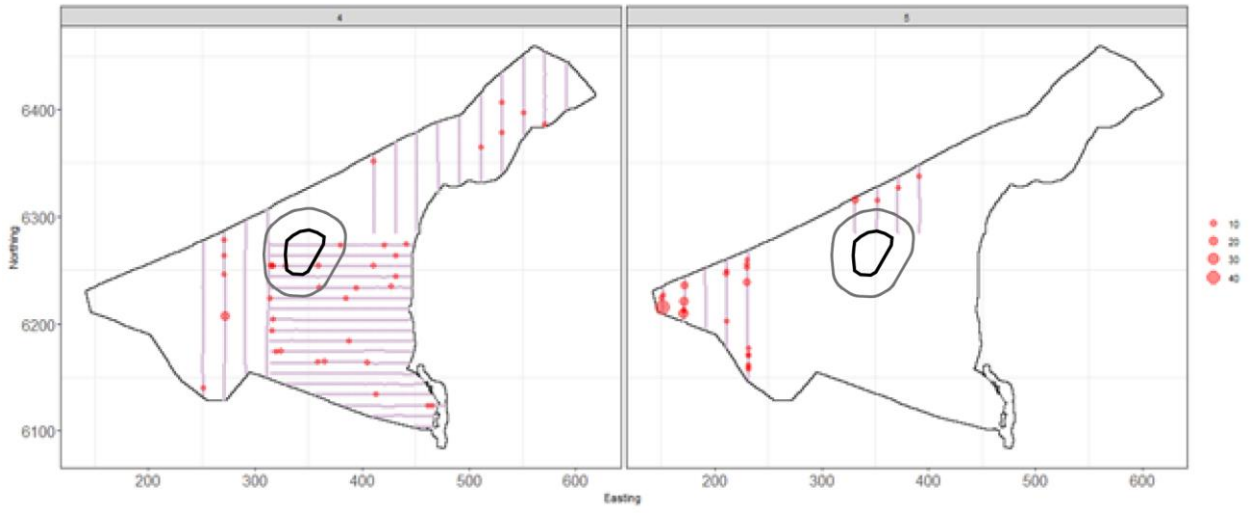

Figure 4.85 Distance-corrected counts for the black-legged kittiwake species across the three surveys for the entire North Sea data set from April and May 2019. The red circles indicate the distance-corrected counts along the transect lines. The pale purple dots are segments with a count of zero.

4.2.4.3 Model selection

The best model(s) for the black-legged kittiwake species were two separate models, one for each month (Table 4.17). There was compelling evidence for non-uniform spatial patterns in May (5) (*df* = 14) but no patterns whatsoever in April (4) (*df* = 1).

Table 4.17 Model selection results for black-legged kittiwake for each April and May 2019 survey. The model column represents the terms in the model.

Name	Model	Number of parameters	Dispersion parameter	CV score
April (4)	Initial Model	1	12.41	0.231
May (5)	Best 1D2D	14	11.79	3.574
Combined	2D Only	9	13.72	0.666
April (4) and May (5) blend	-	15	NA	0.659

The estimated abundances, densities and associated 95-percentile confidence intervals for each month are given in Table 4.18.

Table 4.18 Estimated abundance and density (N/km^2) of black-legged kittiwake for each survey in April and May 2019. The 95% CI are percentile-based confidence intervals.

Model	Month	Area (km^2)	Estimated count	95% CI count	Estimated density	95% CI density
April (4)	April (4)	48,338	2,393	(935, 7,804)	0.0	(0, 0.2)
May (5)	May (5)	10,647	2,079	(1,005, 6,516)	0.2	(0.1, 0.6)

4.2.4.4 Spatial Results

Figure 4.86 shows the estimated counts of black-legged kittiwakes in each 1 km^2 grid cell for each month. Generally, the estimated abundances fit the raw data well, and there were no notable misalignments. In areas where the estimated counts were systematically higher, the abundances were also relatively high, and there were no areas with large, estimated abundances unsupported by the data.

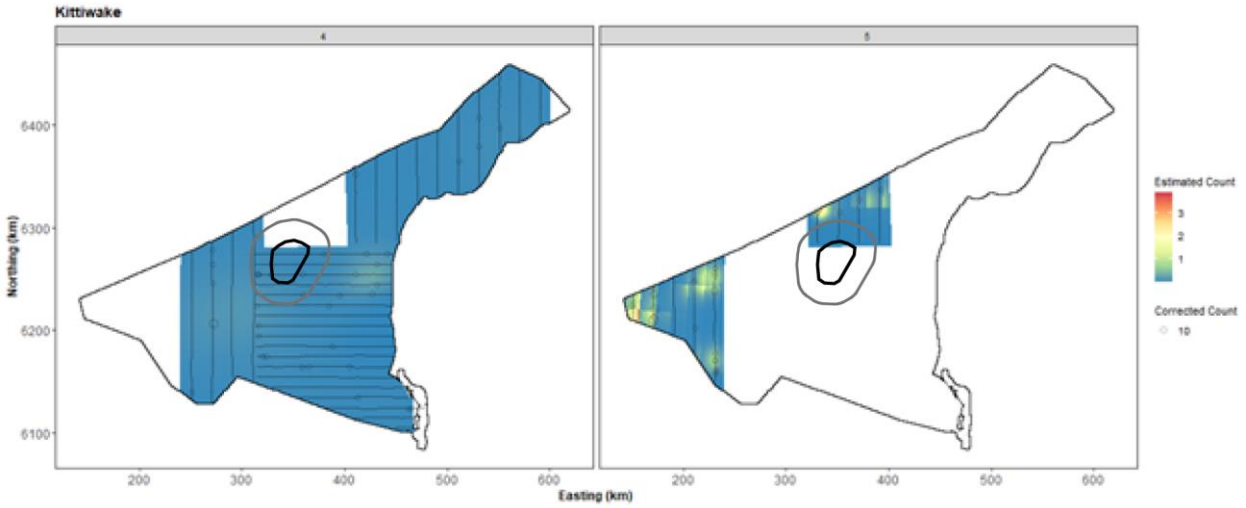

Figure 4.86 The estimated black-legged kittiwake abundance across the study site for each survey for the entire North Sea data set from April and May 2019. The estimated counts are per 1 km x 1 km grid cell. The open circles show the observed corrected count. The coloured graphics represent the predicted counts in each location.

4.2.4.5 Uncertainty in spatial predictions

The highest CoV scores were either associated with 'almost zero' predictions or moderately high values, and it is known that the CoV metric is highly sensitive to any uncertainty for very small predictions. Additionally, the magnitude of these highest values was still moderate (Figure 4.87).

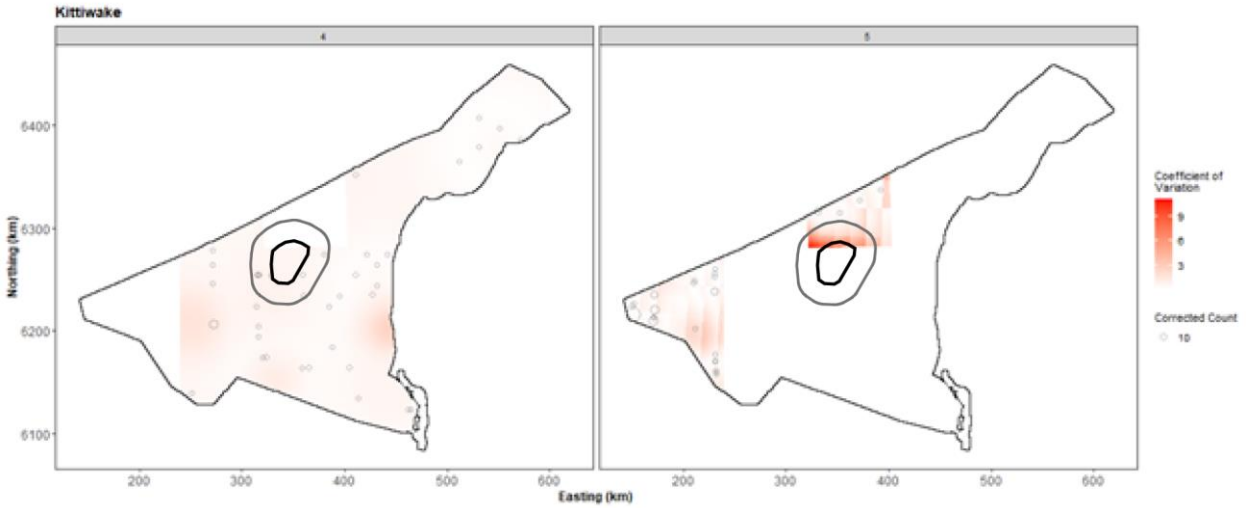

Figure 4.87 The Coefficient of Variation (CoV) across the study region for each month for the entire North Sea data set from April and May 2019. The open circles show the distance corrected black-legged kittiwake counts, where applicable, and the polygons represent the area of the extended bird survey area (black line). The presence of dark red CoV scores in areas with virtually zero predictions is an artefact of the very small prediction rather than any notable concern.

4.2.4.6 *Model diagnostics*

The diagnostic assessments for each model (Figure 4.88 and Figure 4.91) generated no concerns. A blocking structure was used to account for potential residual non-independence for each model and a robust standard error approach was based on unique transects. In each case, we saw a reassuring decay to zero (indicated by the red and grey lines in Figure 4.89 and Figure 4.92), implying an appropriate blocking structure was used. The assumed mean-variance relationship was examined, and the agreement between the assumed (red) lines and the observed values was generally shown (Figure 4.90 and Figure 4.93).

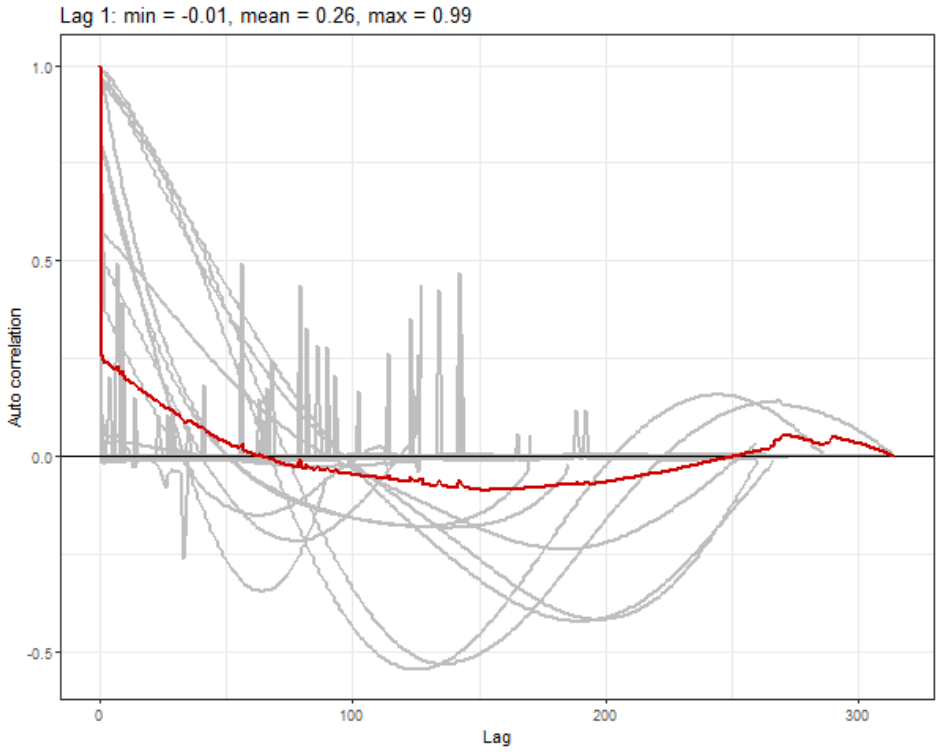

Figure 4.88 Example of black-legged kittiwake Auto Correlation Function (ACF) plot for the 2019 'Month 4' data set. The grey lines represent the residual correlation observed in each transect, and the red line is the average of these values across transects.

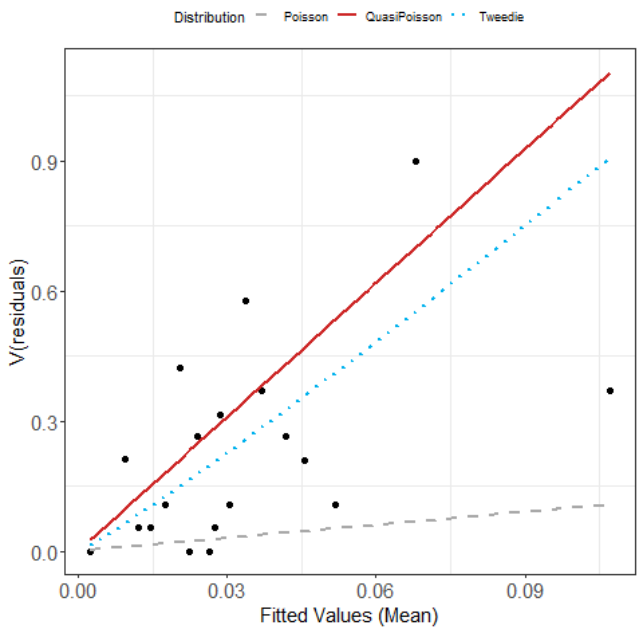

Figure 4.89 Example estimated Tweedie mean-variance relationship (blue dashed line) for black-legged kittiwake for the 2019 'Month 4' data set. The red line shows the V(μ)=ϕμ relationship, and the grey line shows the 1:1 relationship.

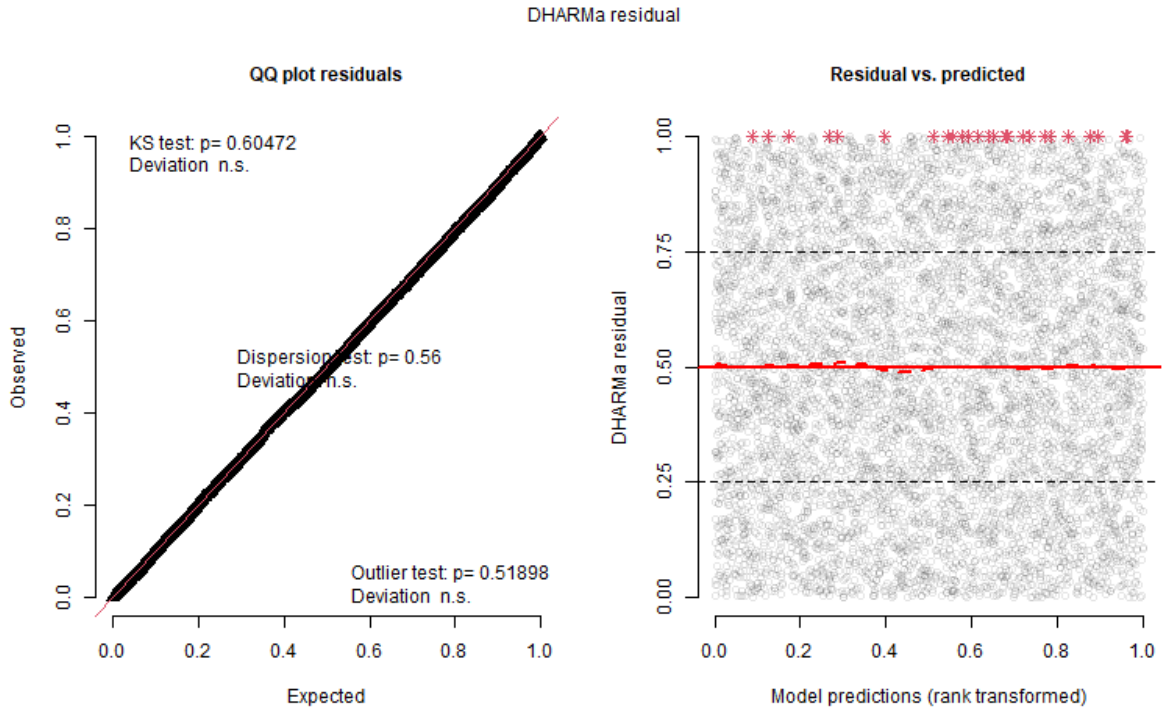

Figure 4.90 DHARMa diagnostics. Example QQ plot (left) and residuals against predicted values (right) for black-legged kittiwake of the 2019 Month 4 data set. The red stars are outliers, and the red line is a smooth spline around the mean of the residuals.

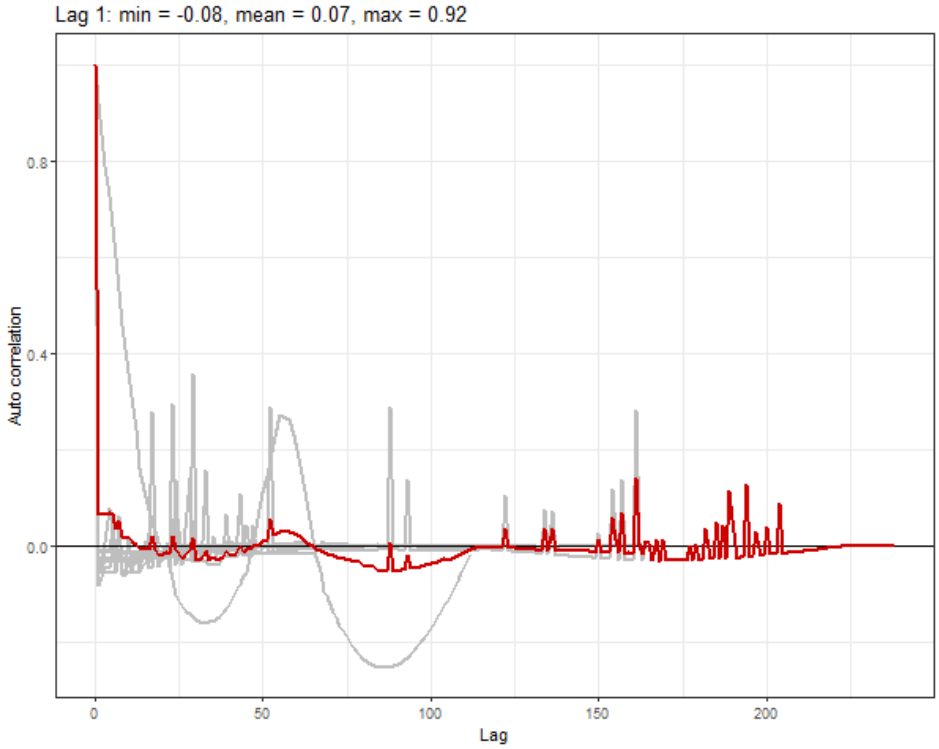

Figure 4.91 Example northern black-legged kittiwake Auto Correlation Function (ACF) plot for the 2019 'Month 5' data set. The grey lines represent the residual correlation ob-served in each transect, and the red line is the average of these values across transects.

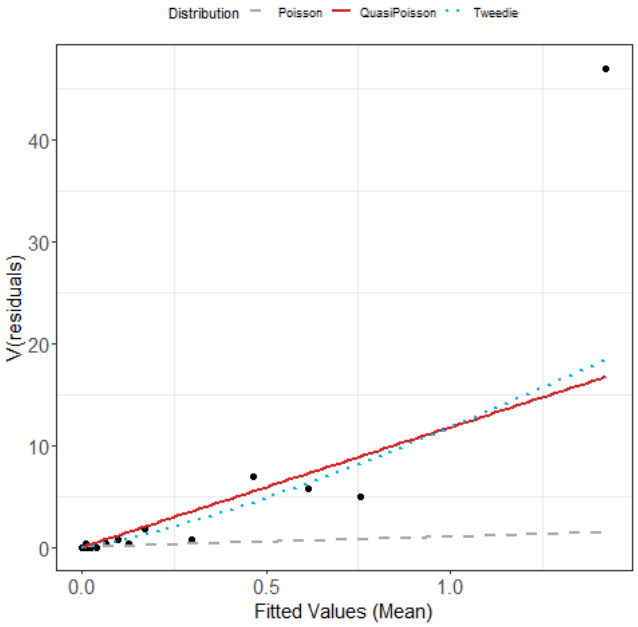

Figure 4.92 Example estimated Tweedie mean-variance relationship (blue dashed line) black-legged kittiwake for the 2019 'Month 5' data set. The red line shows the $V(\mu)=\phi\mu$ relationship, and the grey line shows the 1:1 relationship.

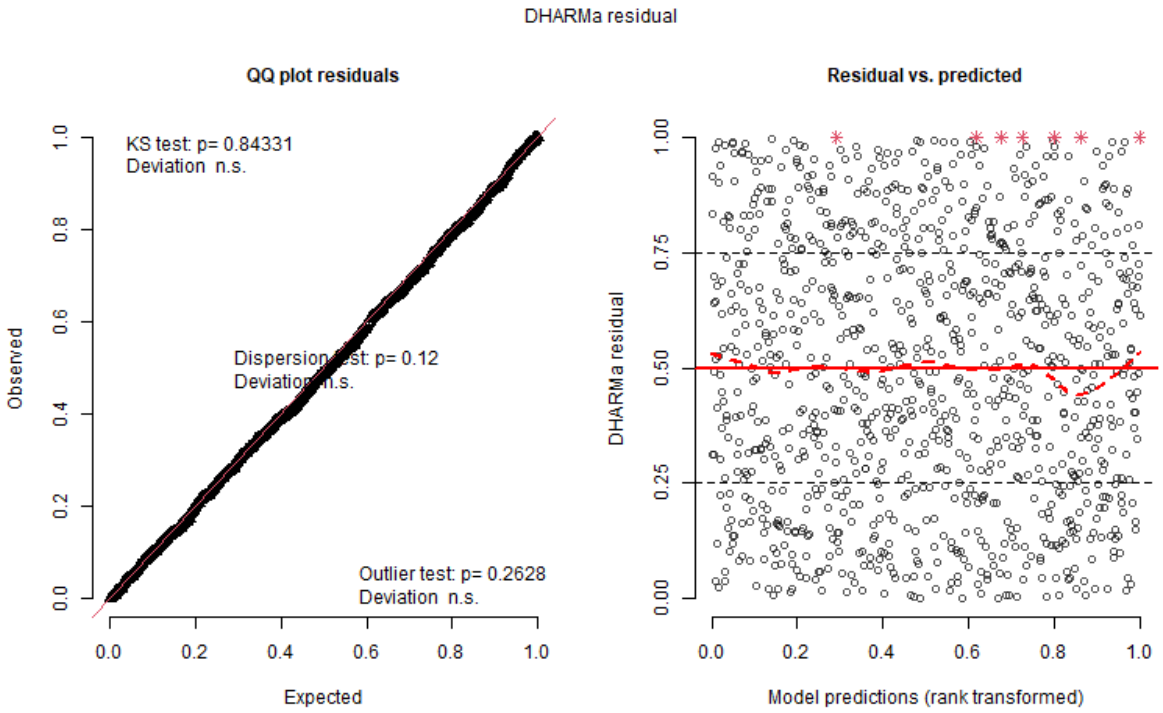

Figure 4.93 DHARMa diagnostics. Example QQ plot (left) and residuals against predicted values (right) for black-legged kittiwake of the 2019 'Month 5' data set. The red stars are outliers, and the red line is a smooth spline around the mean of the residuals.

4.2.5 Razorbill/common guillemot

4.2.5.1 Distance analysis

The average probability of sighting auks was estimated to be 0.16 (CoV = 0.04). This probability was estimated using a half-normal detection function and observer as a covariate (Figure 4.94). Observer MEN was estimated to miss animals on the line, and MEN and MN had rapidly declining detection functions.

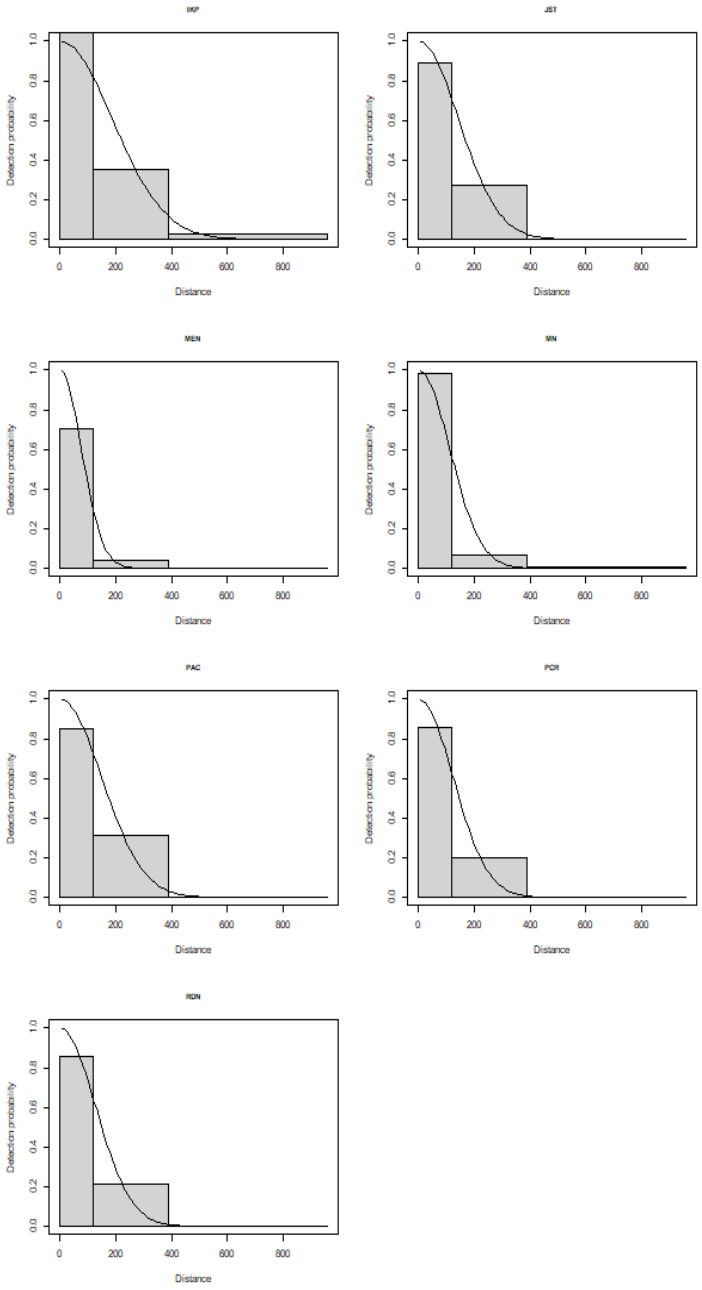

Figure 4.94 The estimated auk detection function for each of the individual observers. The histogram represents the distances of the observed sightings.

4.2.5.2 Spatial analysis

The data for the spatial analysis contained 7,988 segments overall, 9% of which were segments containing auk sightings. April (4) had 10.5% of segments with sightings, and May (5) had 2%. Figure 4.95 shows the distribution of the distance corrected counts for each of the two months of surveys.

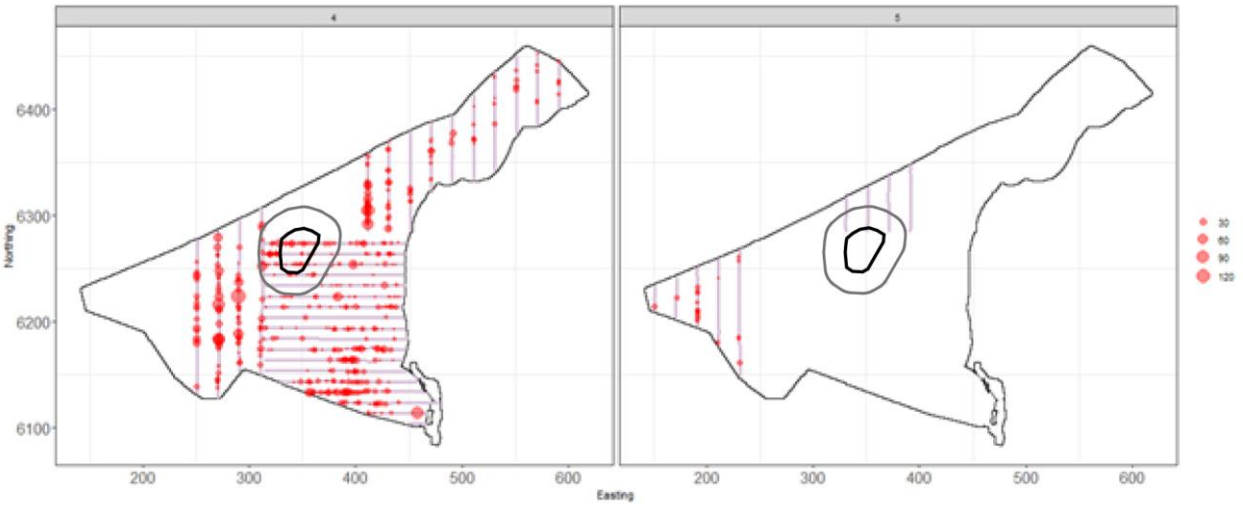

Figure 4.95 Distance-corrected counts for the auk species group across the three surveys for the entire North Sea data set from April and May 2019. The red circles indicate the distance-corrected counts along the transect lines. The pale purple dots are segments with a count of zero.

4.2.5.3 Model Selection

The best model(s) for the auk species were two separate models, one for each month (Table 4.19). There was compelling evidence for non-uniform spatial patterns in April (4), while no significant spatial patterns were estimated to hold in May (5) (however, this area is very small and homogeneous in this case). The spatial surface for April (4) was estimated to need 11 parameters, whilst an intercept-only model was deemed sufficient for May (5), which returns a single (mean) estimate across the area for May (5).

Table 4.19 Model selection results for auks for each April and May 2019 survey. The model column represents the terms in the model.

Name	Model	Number of parameters	Dispersion parameter	CV score
April (4)	2D Only	11	26.78	27.398
May (5)	Initial Model	1	19.69	2.053
Combined	Best 1D2D	8	30.55	24.264
April (4) and May (5) blend	-	12	NA	24.150

The estimated abundances, densities and associated 95-percentile confidence intervals for each month are given in Table 4.20.

Table 4.20 Estimated abundance and density (N/km^2) of auks for each survey in April and May 2019. The 95% CI are percentile-based confidence intervals.

Model	Month	Area (km^2)	Estimated count	95% CI count	Estimated density	95% CI density
April (4)	4	48,338	87,378	(52,044, 151,299)	1.8	(1.1, 3.1)
May (5)	5	10,647	2,303	(683, 8,479)	0.2	(0.1, 0.8)

4.2.5.4 *Spatial results*

Figure 4.96 shows the estimated counts of auks in each 1 km^2 grid cell for each month. Generally, the estimated abundances fitted well with the raw data, and there were no notable misalignments. In areas where the estimated counts were systematically higher, the abundances were also relatively high, and there were no areas with large, estimated abundances unsupported by the data.

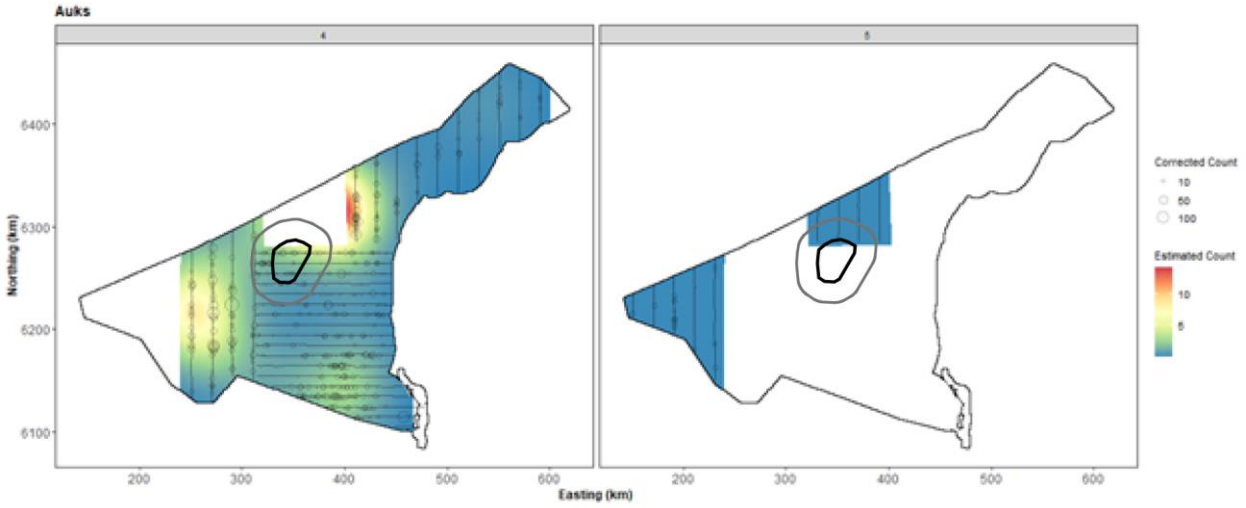

Figure 4.96 The estimated auk abundance across the study site for each survey for the entire North Sea data set from April and May 2019. The estimated counts are per 1 km x 1 km grid cell. The open circles show the observed corrected count. The coloured graphics represent the predicted counts in each location.

4.2.5.5 *Uncertainty in spatial predictions*

Broadly, the highest CoV scores were associated with 'almost zero' predictions, and it is known that the CoV metric is highly sensitive to any uncertainty for very small predictions. There was one larger value in the southeastern corner of the survey area, but that was otherwise absent from the data. There was no material overlap between high values of the CoV metric and the transect lines/locations with non-zero counts; therefore, there were no concerns in this case (Figure 4.97).

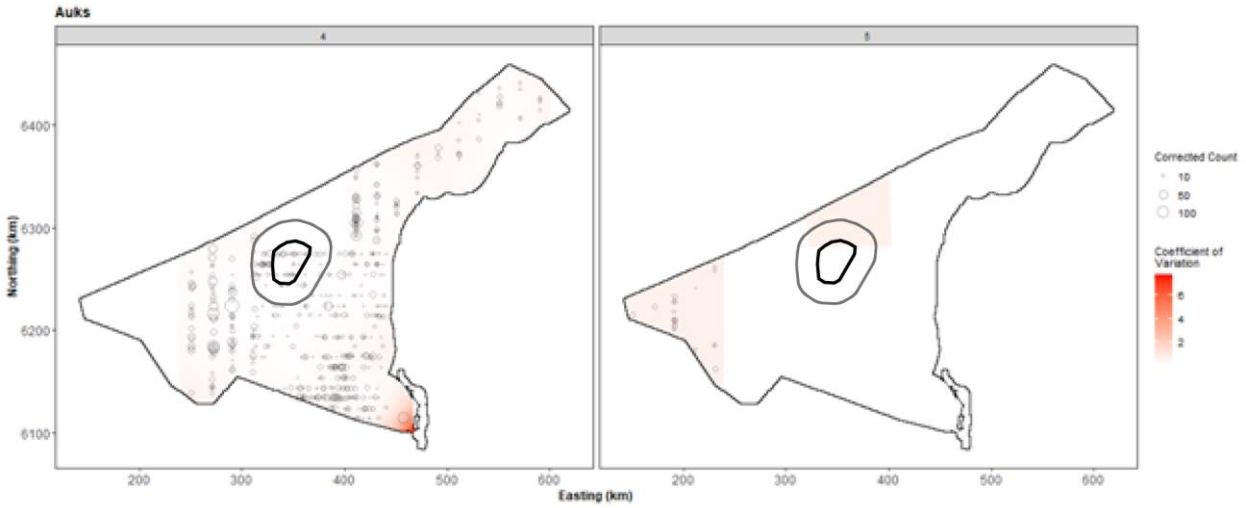

Figure 4.97 The Coefficient of Variation (CoV) across the study region for each month for the entire North Sea data set from April and May 2019. The open circles show the distance corrected auk counts, where applicable, and the polygons represent the area of the extended bird survey area (black line). The presence of dark red CoV scores in areas with virtually zero predictions is an artefact of the very small prediction rather than any notable concern.

4.2.5.6 Model diagnostics

The diagnostic assessments for each model (Figure 4.98 and Figure 4.101) did not present any concerns. While the plots for month 5 were less conclusive, this is unsurprising given there are very few data points with sightings, and consequently, a very simplistic 'mean only' model was selected.

A blocking structure was used to account for potential residual non-independence for each model and a robust standard error approach was based on unique transects. In each case, we saw a reassuring decay to zero (indicated by the red and grey lines in Figure 4.99 and Figure 4.102), implying an appropriate blocking structure was used.

The assumed mean-variance relationship was examined and generally showed agreement between the assumed (red) lines and the observed values (Figure 4.100 and Figure 4.103), which justified using a Tweedie distribution in each case.

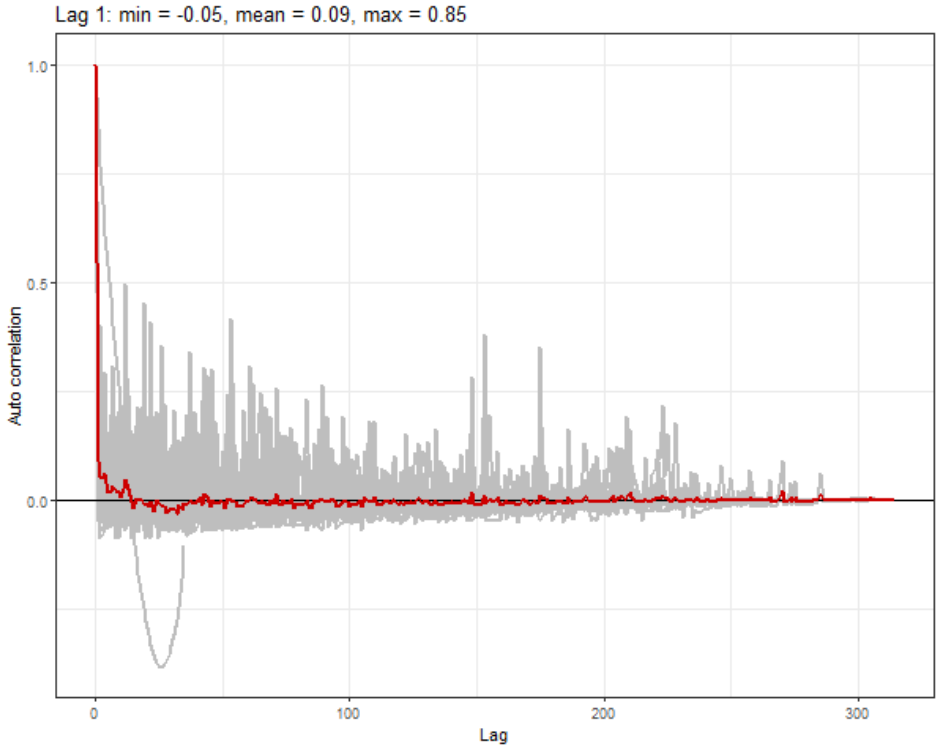

Figure 4.98 Example of Auto Correlation Function (ACF) plot for razorbill/common guillemot for the 2019 'Month 4' data set. The grey lines represent the residual correlation observed in each transect, and the red line is the aver-age of these values across transects.

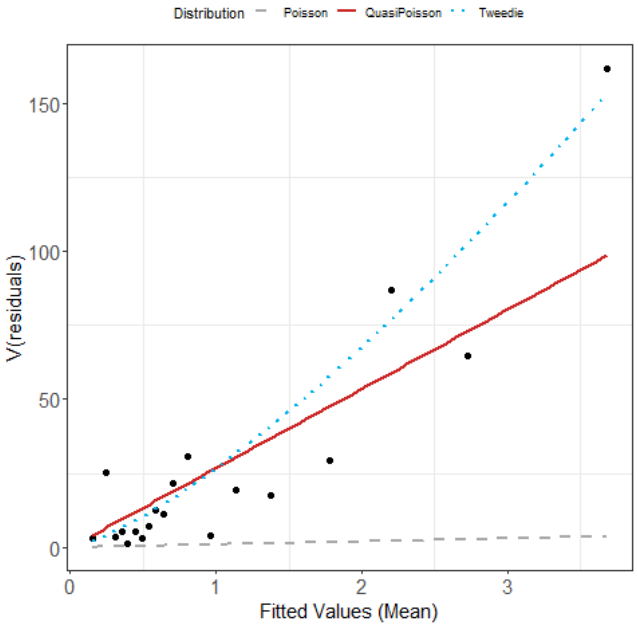

Figure 4.99 Example estimated Tweedie mean-variance relationship (blue dashed line) for razorbill/common guillemot for the 2019 'Month 4' data set. The red line shows the $V(\mu)=\phi\mu$ relationship, and the grey line shows the 1:1 relationship.

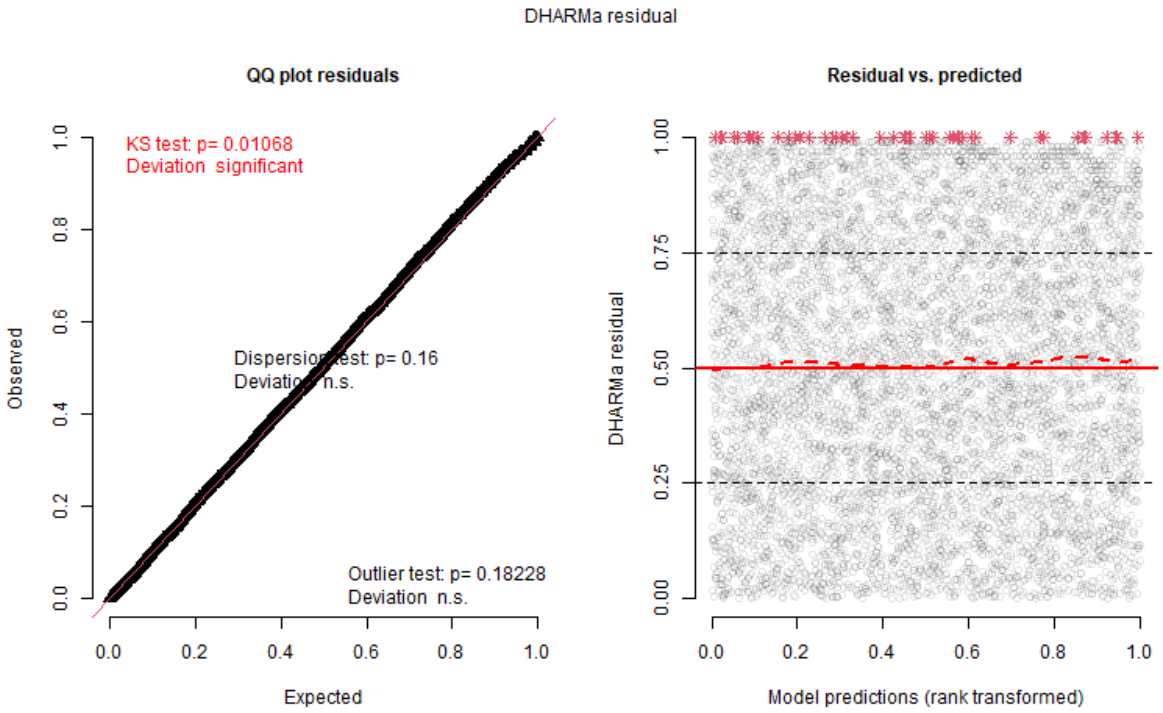

Figure 4.100 DHARMa diagnostics. Example QQ plot (left) and residuals against predicted values (right) for razorbill/common guillemot of the 2019 'Month 4' data set. The red stars are outliers, and the red line is a smooth spline around the mean of the residuals.

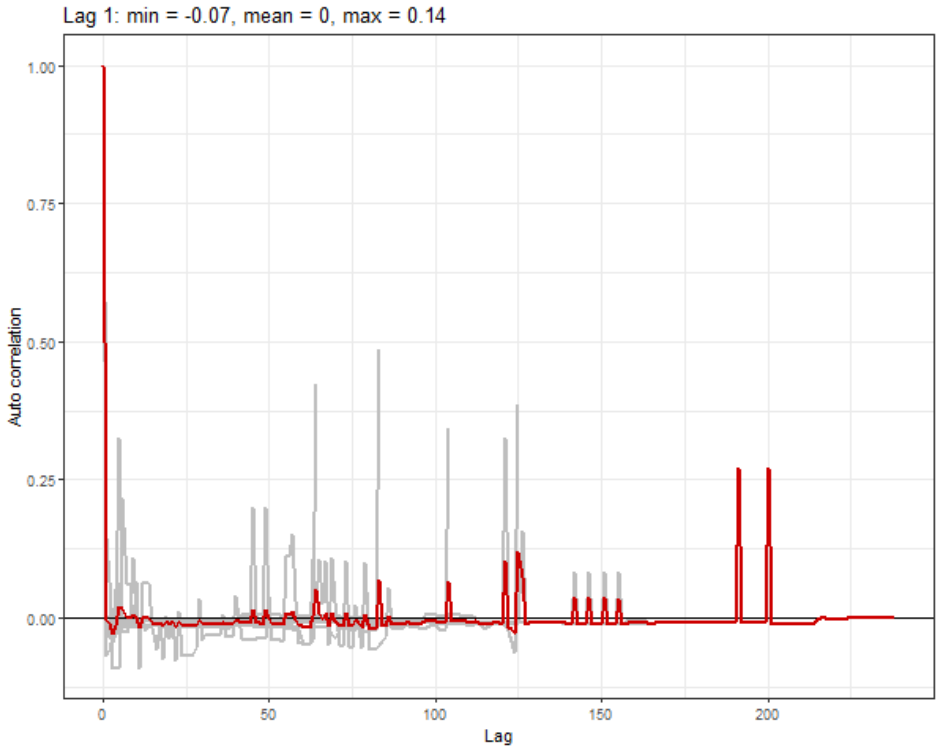

Figure 4.101 Example of Auto Correlation Function (ACF) plot for razorbill/common guillemot for the 2019 'Month 5' data set. The grey lines represent the residual correlation observed in each transect, and the red line is the average of these values across transects.

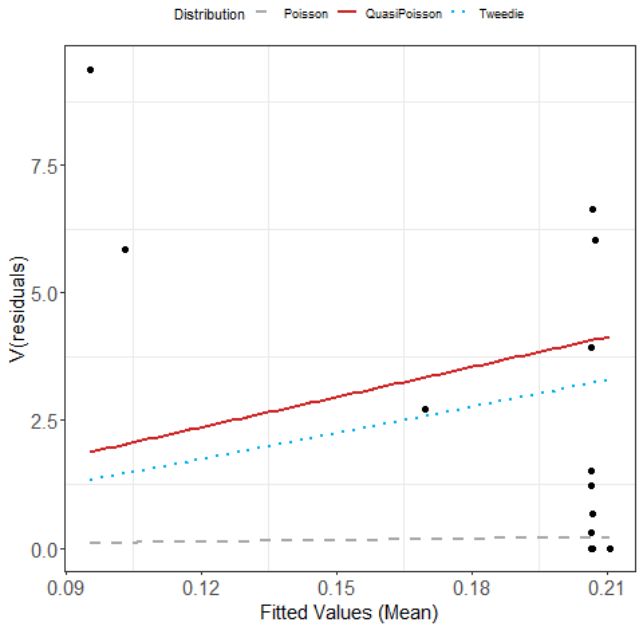

Figure 4.102 Example estimated Tweedie mean-variance relationship (blue dashed line) for razorbill/common guillemot for the 2019 'Month 5' data set. The red line shows the V(μ)=ϕμ relationship, and the grey line shows the 1:1 relationship.

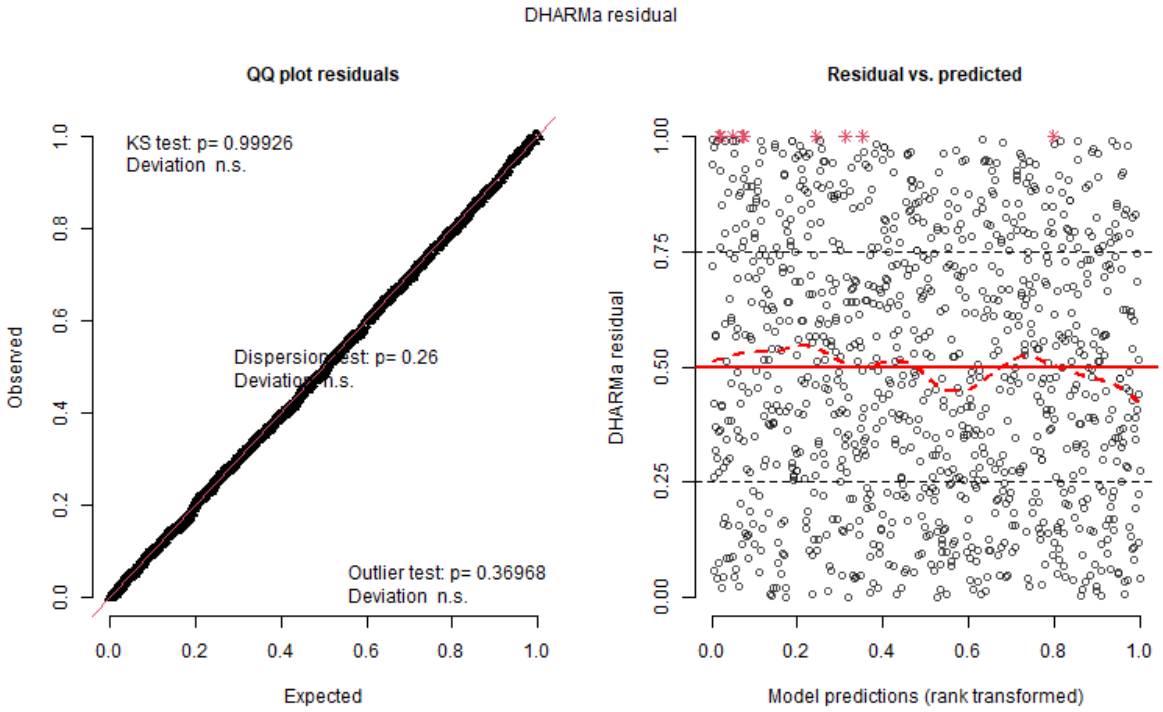

Figure 4.103 DHARMa diagnostics. Example QQ plot (left) and residuals against predicted values (right) for razorbill/common guillemot of the 2019 Month 5 data set. The red stars are outliers, and the red line is a smooth spline around the mean of the residuals.

4.3 Ship-based surveys

This chapter presents the results of the eleven ship-based surveys, focusing on two main topics: bird flight altitudes and the composition of bird species that were difficult to identify during the aerial surveys. During the ship-based survey period from November 2021 to March 2023, 2,551 birds were observed foraging, resting or moving within the survey area, comprising a total of 52 species (Table 4.21).

Table 4.21 The table shows the number of observations (first) and individuals (second) of each bird species observed during the eleven ship-based surveys (N_{obs} = 1,616, N_{ind} = 2,551). Species are listed alphabetically.

Species	Survey ID											Total
	S1	S2	S3	S4	S5	S6	S7	S8	S9	S10	S11	
Arctic skua	0	0	0	0	2/2	3/3	0	0	0	0	0	5/5
Arctic tern	0	0	0	0	1/2	0	1/1	0	0	0	0	2/3
Atlantic puffin	0	0	0	0	0	0	0	0	0	1/1	0	1/1
Black-headed gull	3/3	0	0	0	0	0	0	0	1/1	0	1/2	5/6
Black-legged kittiwake	52/55	27/31	8/9	11/17	12/18	60/88	0	7/8	33/33	37/40	49/60	296/359
Brambling	0	0	0	0	0	0	0	2/3	0	0	0	2/3
Brant goose	0	0	0	0	0	0	1/23	0	0	0	0	1/23
Common blackbird	0	0	0	0	0	0	0	3/12	0	1/1	2/11	6/24
Common chiffchaff	0	0	0	0	0	0	0	0	0	0	1/1	1/1
Common guillemot	10/19	1/1	2/2	4/4	2/2	0	0	3/3	16/23	4/4	13/19	55/77
Common guillemot/razorbill	0	0	2/3	0	0	0	0	0	0	0	0	2/3
Common gull	9/9	0	0	0	3/4	1/1	0	4/4	8/8	4/4	3/4	32/34
Common merganser	0	0	0	0	0	0	0	0	1/2	0	0	1/2
Common ringed plover	0	0	0	0	0	0	1/1	0	0	0	0	1/1
Common scoter	0	0	0	0	1/3	1/3	0	1/2	0	1/1	3/38	7/47
Common snipe	0	0	0	0	0	0	3/9	1/1	0	0	0	4/10
Common starling	2/31	0	0	0	0	0	0	0	4/114	0	0	6/145
Common swift	0	0	0	0	0	0	3/7	0	0	0	0	3/7
Common tern	0	0	0	0	3/13	1/1	1/1	0	0	0	0	5/15
Common wood pigeon	0	1/1	0	0	0	0	0	0	1/1	0	3/20	5/22
Common/artic tern	0	0	0	0	0	0	1/3	0	0	0	0	1/3
Dunlin	0	0	0	0	0	0	5/20	0	0	0	0	5/20
Eurasian curlew	0	0	0	0	0	0	0	0	0	0	1/1	1/1
Eurasian oystercatcher	0	0	0	0	0	0	2/35	0	0	0	0	2/35

Species	Survey ID											Total
	S1	S2	S3	S4	S5	S6	S7	S8	S9	S10	S11	
Eurasian skylark	0	0	0	0	0	0	0	0	0	4/7	0	4/7
Eurasian teal	0	0	0	0	0	0	3/6	0	0	0	0	3/6
Eurasian wigeon	0	0	0	0	0	0	0	0	0	1/2	0	1/2
Eurasian wood-cock	3/3	0	0	0	0	0	0	1/1	0	0	0	4/4
European golden plover	0	0	0	0	0	0	1/14	0	0	0	0	1/14
European her-ring gull	40/41	14/21	0	0	3/4	2/6	0	7/7	139/201	34/38	7/13	246/331
European robin	0	0	0	0	0	0	0	0	0	0	1/1	1/1
Fieldfare	0	0	0	0	0	0	0	3/21	1/1	0	0	4/22
Great black-backed gull	15/15	24/27	2/2	3/3	4/4	1/2	4/7	3/3	19/29	23/23	24/34	122/149
Great skua	0	0	1/1	1/1	0	1/1	0	0	0	0	0	3/3
Lesser black-backed gull	0	0	19/21	5/60	14/37	32/51	17/20	0	0	0	33/68	120/257
Little auk	0	0	0	0	0	0	0	0	1/3	0	0	1/3
Mallard	0	0	0	1/1	0	0	0	0	0	0	0	1/1
Meadow pipit	0	0	0	0	0	0	0	0	0	0	1/1	1/1
Northern fulmar	1/1	8/9	18/18	20/20	51/72	42/93	43/46	8/10	11/11	11/12	26/28	239/320
Northern gannet	23/25	9/9	29/29	69/101	29/48	32/36	68/79	15/17	28/32	7/7	81/106	390/489
Northern wheat-ear	0	0	0	0	1/1	0	0	0	0	0	0	1/1
Razorbill	0	0	1/2	0	0	0	0	0	5/9	2/2	2/2	10/15
Red-breasted merganser	0	0	0	0	0	0	0	0	1/2	0	0	1/2
Red-throated diver	0	1/1	0	1/1	2/2	4/5	0	0	1/1	2/2	0	11/12
Redwing	0	0	0	0	0	0	0	3/48	1/2	0	1/10	5/60
Ruddy turnstone	0	0	0	0	0	0	1/4	0	0	0	0	1/4
Sandwich tern	0	0	0	0	1/4	0	0	0	0	0	0	1/4
Song thrush	0	0	0	0	0	0	0	1/2	0	0	0	1/2
Wader sp.	0	0	0	0	0	0	1/2	0	0	0	0	1/2
Western yellow wagtail	0	0	0	0	0	0	1/1	0	0	0	0	1/1
Wilson's storm petrel	0	0	0	0	0	1/1	0	0	0	0	0	1/1
Yellow-legged gull	0	0	0	0	0	0	0	0	0	1/1	0	1/1

4.3.1 Bird flight altitude

This chapter presents the flight altitude distribution of bird species observed during the ship-based surveys across altitude intervals ranging from 0 to 225 m above sea level. Overall, northern gannet, European herring gull, and northern fulmar were the most frequently observed species during ship-based surveys (Table 4.22). In contrast, the skua, common gull, and sea ducks were among the least frequently observed.

Observed birds showed a pronounced preference for lower flight altitudes, with 75.2% of all birds recorded within the 0-25 m altitude interval (Table 4.22). For example, northern gannets and northern fulmars were all observed flying within the lowest altitude interval. While some species, such as the lesser black-backed gull and terns, displayed a more varied flight altitude distribution, the numbers remained relatively small, especially above 125 meters. Consequently, observations above this altitude accounted for less than 1% of the total. The subsequent subchapters provide a detailed analysis of the flight altitude distribution for the most observed species or species groups.

Table 4.22 Flight altitudes of species/species groups observed during the eleven ship-based surveys. The table shows the number of observed individuals within each 25 m flight altitude interval (N = 2,464).

Species	Altitude interval (m)									Total
	0-25	26-50	51-75	76-100	101-125	126-150	151-175	176-200	201-225	
Red-throated diver	7	3	2	0	0	0	0	0	0	12
Northern fulmar	314	2	0	0	0	0	0	0	0	316
Northern gannet	425	54	9	0	0	0	0	0	0	488
Sea ducks	46	5	0	0	0	0	0	0	0	51
Waders	62	29	23	4	0	0	0	0	0	118
Skuas	7	1	0	0	0	0	0	0	0	8
Common gull	24	8	2	0	0	0	0	0	0	34
Lesser black-backed gull	74	63	32	60	0	0	0	0	0	229
European herring gull	170	85	39	14	9	3	1	3	2	326
Great black-backed gull	76	43	15	5	0	2	0	1	0	142
Black-legged kittiwake	315	33	3	1	0	0	0	0	0	352
Terns	25	0	0	0	0	0	0	0	0	25
Alcids	95	0	0	0	0	0	0	0	0	95
Passerines	214	39	0	15	0	0	0	0	0	268
Total (individuals)	**1,854**	**365**	**125**	**99**	**9**	**5**	**1**	**4**	**2**	**2,464**
Total (proportion %)	**75.2**	**14.8**	**5.1**	**4.0**	**0.4**	**0.2**	**0.0**	**0.2**	**0.1**	

4.3.1.1 Red-throated diver

Flight altitudes of red-throated divers were assessed using 11 altitude records obtained from 11 observations. These observations encompassed a total of 12 birds. Predominantly, red-throated divers were observed flying alone (90.9%), with the largest recorded flock consisting of two birds (9.1%) and an average flock size of 1.1 (± 0.1) birds. Most flights occurred below 50 m (83.3%) (Table 4.23 and Figure 4.104). The highest recorded flight altitude was observed when two individuals flew together at 60 m above sea level.

Table 4.23 Flight altitudes of red-throated divers observed during the eleven ship-based surveys. The table shows the number and proportion of altitude records and observed individuals occurring within each 25 m flight altitude interval (N_{rec} = 11; N_{ind} = 12).

Altitude interval (m)	Altitude records		Individuals	
	Total	Proportion	Total	Proportion
0-25	7	0.64	7	0.58
26-50	3	0.27	3	0.25
51-75	1	0.09	2	0.17
76-100	0	0.00	0	0.00
101-125	0	0.00	0	0.00
126-150	0	0.00	0	0.00
151-175	0	0.00	0	0.00
176-200	0	0.00	0	0.00
201-225	0	0.00	0	0.00

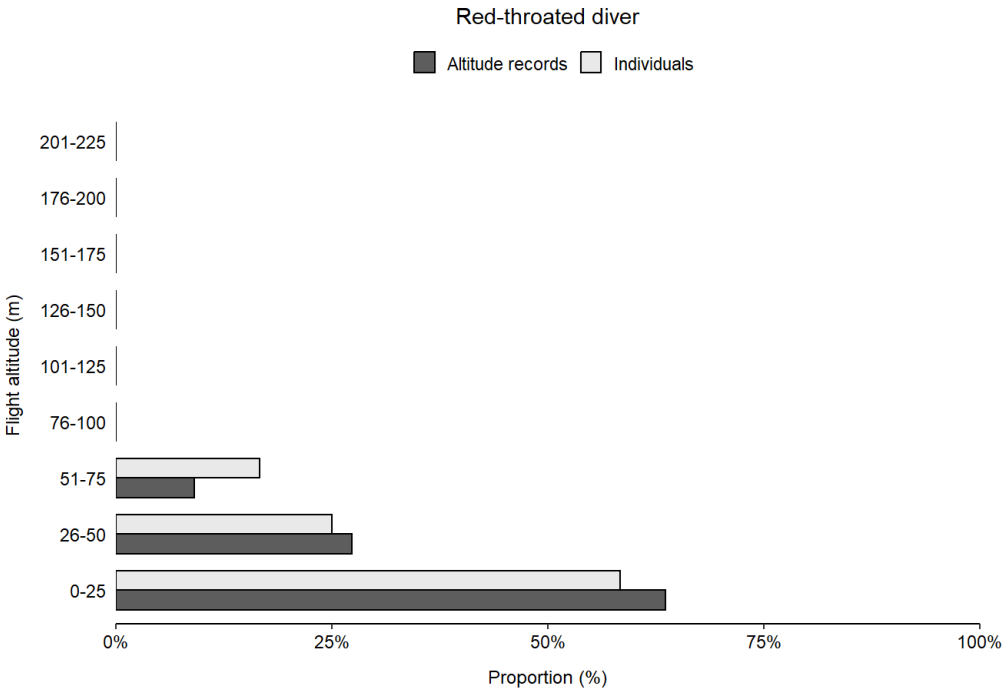

Figure 4.104 Flight altitudes of red-throated divers observed during the eleven ship-based surveys. The figure shows the percentage of altitude records (dark grey) and individuals (light grey) occurring within each 25 m flight altitude interval (N_{rec} = 11; N_{ind} = 12).

4.3.1.2 Northern fulmar

Flight altitudes of northern fulmars were assessed using 300 altitude records obtained from 237 observations. These observations included a total of 316 individuals. Most northern fulmars were observed flying alone (89.9%), with a maximum recorded flock size of 50 birds (0.4%) and an average flock size of 1.3 (± 0.2) birds. Nearly all flights occurred below 25 m (99.4%), with the highest recorded flight altitude being 30 m (Table 4.24 and Figure 4.105).

Table 4.24 Flight altitudes of northern fulmars observed during the eleven ship-based surveys. The table shows the number and proportion of altitude records and observed individuals occurring within each 25 m flight altitude interval (N_{rec} = 300; N_{ind} = 316).

Altitude interval (m)	Altitude records		Individuals	
	Total	Proportion	Total	Proportion
0-25	298	0.99	314	0.99
26-50	2	0.01	2	0.01
51-75	0	0.00	0	0.00
76-100	0	0.00	0	0.00
101-125	0	0.00	0	0.00
126-150	0	0.00	0	0.00
151-175	0	0.00	0	0.00
176-200	0	0.00	0	0.00
201-225	0	0.00	0	0.00

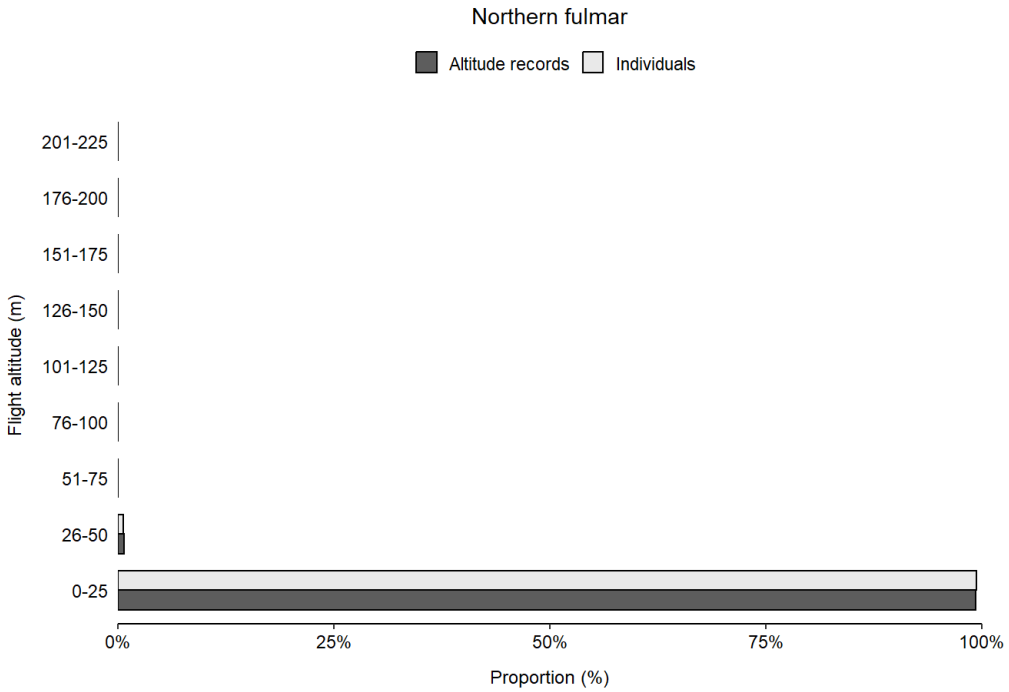

Figure 4.105 Flight altitudes of northern fulmars observed during the eleven ship-based surveys. The figure shows the percentage of altitude records (dark grey) and individuals (light grey) occurring within each 25 m flight altitude interval (N_{rec} = 300; N_{ind} = 316).

4.3.1.3 Northern gannet

Flight altitudes of northern gannets were analysed using 480 altitude records obtained from 387 observations encompassing 488 birds. Northern gannets were predominantly observed flying alone (86.0%), with a maximum recorded flock size of 7 birds (0.3%). The average flock size was 1.2 (± 0.0) birds. Most northern gannets were flying below 25 m (87.1%), while 11.1% were flying at altitudes ranging from 26 to 50 m (Table 4.25 and Figure 4.106). The highest recorded flight altitude for northern gannets was 68 m.

Table 4.25 Flight altitudes of northern gannets observed during the eleven ship-based surveys. The table shows the number and proportion of altitude records and observed individuals occurring within each 25 m flight altitude interval (N_{rec} = 480; N_{ind} = 488).

Altitude interval (m)	Altitude records		Individuals	
	Total	Proportion	Total	Proportion
0-25	413	0.86	425	0.87
26-50	56	0.12	54	0.11
51-75	11	0.02	9	0.02
76-100	0	0.00	0	0.00
101-125	0	0.00	0	0.00
126-150	0	0.00	0	0.00
151-175	0	0.00	0	0.00
176-200	0	0.00	0	0.00
201-225	0	0.00	0	0.00

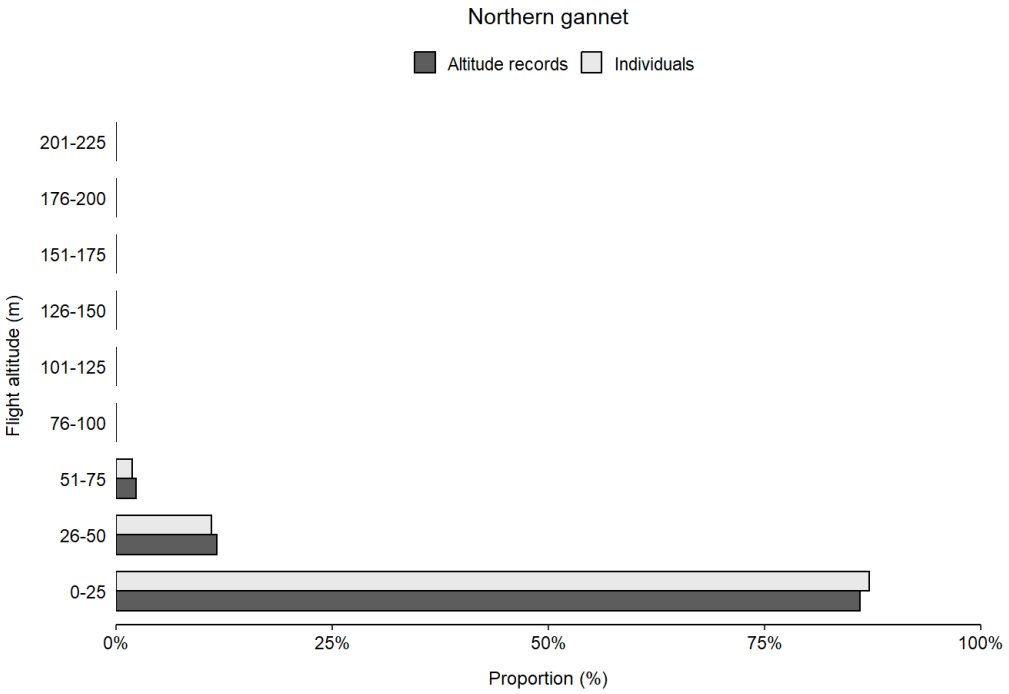

Figure 4.106 Flight altitudes of northern gannets observed during the eleven ship-based surveys. The figure shows the percentage of altitude records (dark grey) and individuals (light grey) occurring within each 25 m flight altitude interval (N_{rec} = 480; N_{ind} = 488).

4.3.1.4 Sea ducks

Flight altitudes of sea ducks were analysed by pooling altitude records obtained from observations of common merganser, red-breasted merganser, and common scoter. Consequently, flight altitudes were analysed using 10 altitude records from 9 observations, encompassing 51 individuals. Sea ducks were predominantly observed flying in pairs (44.4%), with 22.2% flying alone and 22.2% in flocks of three. The mean flock size was 5.7 (± 3.7) birds, increased by a large flock of 35 common scoters. Most sea ducks were observed flying below 25 m (90.2%), with a smaller proportion

(9.8%) flying at altitudes between 26 and 50 m (Table 4.26 and Figure 4.107). The highest flight altitude recorded was 46 m, observed in a pair of common mergansers.

Table 4.26 Flight altitudes of sea ducks observed during the eleven ship-based surveys. The table shows the number and proportion of altitude records and observed individuals occurring within each 25 m flight altitude interval (N_{rec} = 10; N_{ind} = 51).

Altitude interval (m)	Altitude records		Individuals	
	Total	Proportion	Total	Proportion
0-25	8	0.80	46	0.90
26-50	2	0.20	5	0.10
51-75	0	0.00	0	0.00
76-100	0	0.00	0	0.00
101-125	0	0.00	0	0.00
126-150	0	0.00	0	0.00
151-175	0	0.00	0	0.00
176-200	0	0.00	0	0.00
201-225	0	0.00	0	0.00

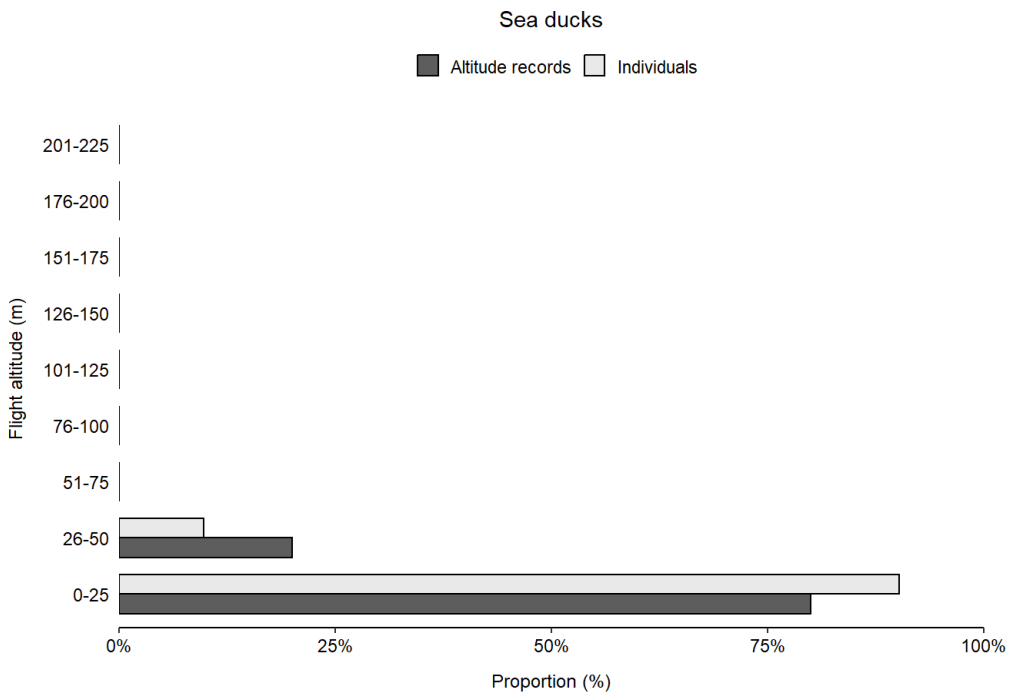

Figure 4.107 Flight altitudes of sea ducks observed during the eleven ship-based surveys. The figure shows the percentage of altitude records (dark grey) and individuals (light grey) occurring within each 25 m flight altitude interval (N_{rec} = 10; N_{ind} = 51).

4.3.1.1 Waders

Flight altitudes of waders were analysed by pooling altitude records obtained from observations of common ringed plover, European golden plover, common snipe, dunlin, Eurasian curlew, Eurasian oystercatcher, Eurasian woodcock, ruddy turnstone, and unspecified wader species (wader sp.). The pooled flight altitude analysis was made utilising 28

altitude records from 20 observations, encompassing 118 birds. Waders were observed flying alone in half of the observations (50%), with 15% observed in pairs. The mean flock size was 4.6 (± 1.4) birds, influenced by a notable flock of 23 Eurasian oystercatchers.

Approximately half of the waders were recorded flying at altitudes below 25 m (52.5%), while 24.6% flew at altitudes between 26 and 50 m, and 22.9% flew at altitudes above 50 m (Table 4.27 and Figure 4.108). However, the highest flight altitude recorded was a common sipe flying 83 m above sea level.

Table 4.27 Flight altitudes of waders observed during the eleven ship-based surveys. The table shows the number and proportion of altitude records and observed individuals occurring within each 25 m flight altitude interval (N_{rec} = 28; N_{ind} = 118).

Altitude interval (m)	Altitude records		Individuals	
	Total	Proportion	Total	Proportion
0-25	21	0.75	62	0.53
26-50	4	0.14	29	0.25
51-75	2	0.07	23	0.20
76-100	1	0.04	4	0.03
101-125	0	0.00	0	0.00
126-150	0	0.00	0	0.00
151-175	0	0.00	0	0.00
176-200	0	0.00	0	0.00
201-225	0	0.00	0	0.00

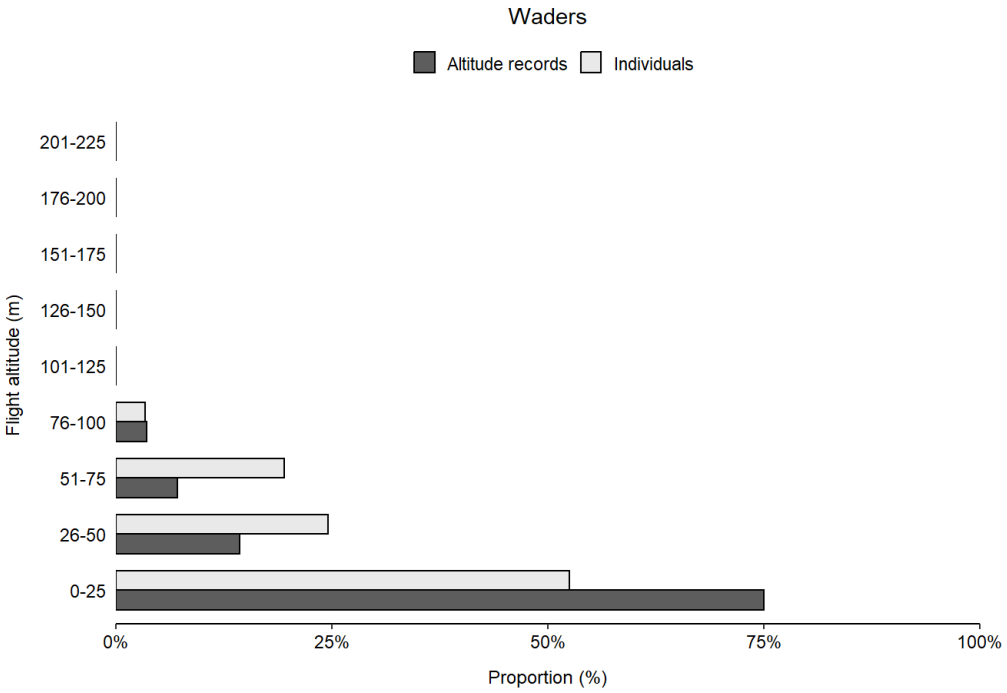

Figure 4.108 Flight altitudes of waders observed during the eleven ship-based surveys. The figure shows the percentage of altitude records (dark grey) and individuals (light grey) occurring within each 25 m flight altitude interval (N_{rec} = 28; N_{ind} = 118).

4.3.1.2 *Skuas*

Flight altitudes of skuas were analysed by pooling altitude records obtained from arctic and great skua observations. Pooled flight altitudes were analysed using 10 altitude records from 8 skua observations, encompassing 8 birds. Skuas were exclusively observed flying alone. The majority of skuas were recorded flying below 25 m (87.5%), with a small portion (12.5%) flying at altitudes between 25 m and 50 m (Table 4.28 and Figure 4.109). The highest flight altitude recorded was 32 m, obtained from an arctic skua.

Table 4.28 Flight altitudes of skuas observed during the eleven ship-based surveys. The table shows the number and proportion of altitude records and observed individuals occurring within each 25 m flight altitude interval (N_{rec} = 10; N_{ind} = 8).

Altitude interval (m)	Altitude records		Individuals	
	Total	Proportion	Total	Proportion
0-25	9	0.90	7	0.88
26-50	1	0.10	1	0.13
51-75	0	0.00	0	0.00
76-100	0	0.00	0	0.00
101-125	0	0.00	0	0.00
126-150	0	0.00	0	0.00
151-175	0	0.00	0	0.00
176-200	0	0.00	0	0.00
201-225	0	0.00	0	0.00

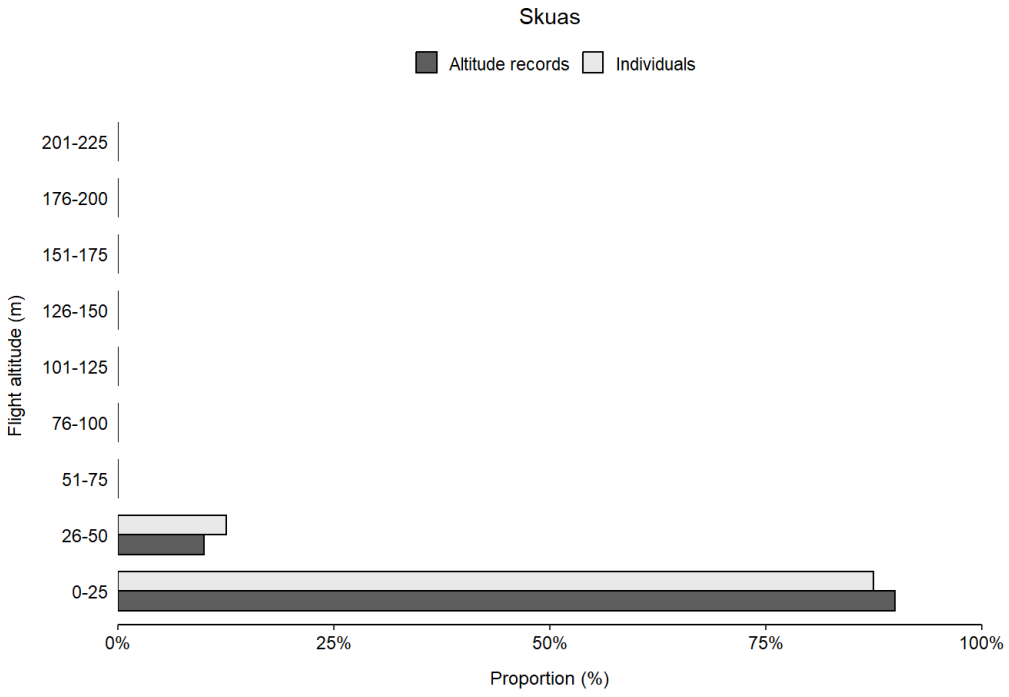

Figure 4.109 Flight altitudes of skuas observed during the eleven ship-based surveys. The figure shows the percentage of altitude records (dark grey) and individuals (light grey) occurring within each 25 m flight altitude interval (N_{rec} = 10; N_{ind} = 8).

4.3.1.3 *Common gull*

Flight altitudes of common gulls were analysed using 35 altitude records obtained from 32 observations, encompassing 34 birds. Common gulls were predominantly observed flying alone (90.6%), with the remaining observed flying in pairs. This resulted in a mean flock size of 1.1 (± 0.0) birds, with the largest flock recorded consisting of 2 birds.

Most common gulls were recorded flying at altitudes below 25 m (70.6%), while 23.5% were observed flying at altitudes between 26 and 50 m (Table 4.29 and Figure 4.110). The highest flight altitude recorded for common gulls was 54 m above sea level.

Table 4.29 Flight altitudes of common gulls observed during the eleven ship-based surveys. The table shows the number and proportion of altitude records and observed individuals occurring within each 25 m flight altitude interval (N_{rec} = 35; N_{ind} = 34).

Altitude interval (m)	Altitude records		Individuals	
	Total	Proportion	Total	Proportion
0-25	26	0.74	24	0.71
26-50	7	0.20	8	0.24
51-75	2	0.06	2	0.06
76-100	0	0.00	0	0.00
101-125	0	0.00	0	0.00
126-150	0	0.00	0	0.00
151-175	0	0.00	0	0.00
176-200	0	0.00	0	0.00
201-225	0	0.00	0	0.00

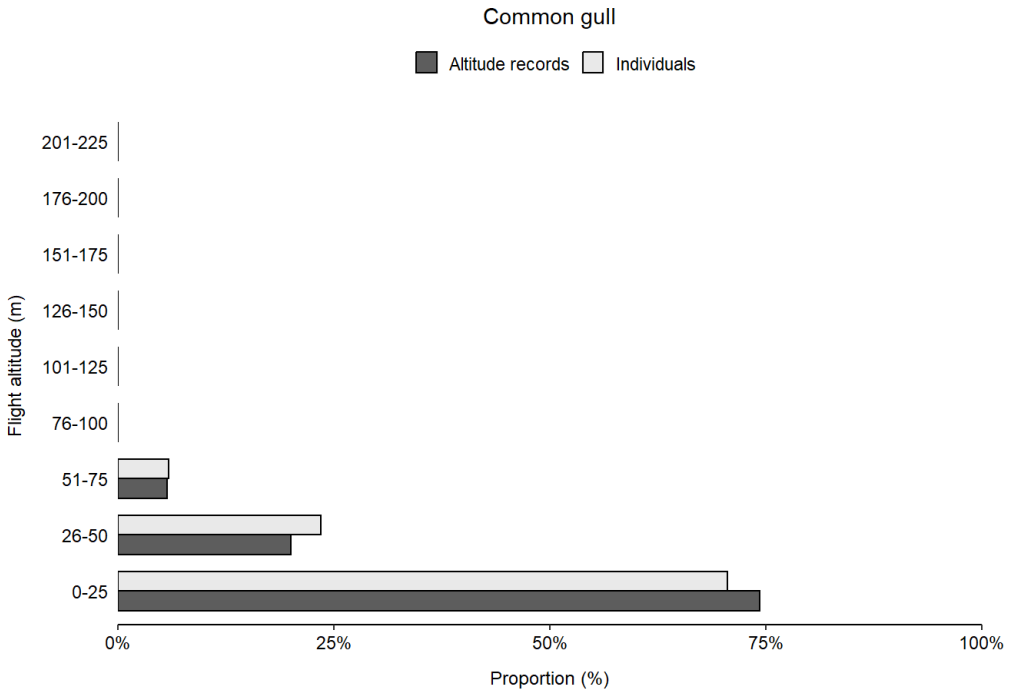

Figure 4.110 Flight altitudes of common gulls observed during the eleven ship-based surveys. The figure shows the percentage of altitude records (dark grey) and individuals (light grey) occurring within each 25 m flight altitude interval (N_{rec} = 35; N_{ind} = 34).

4.3.1.4 *Lesser black-backed gull*

Flight altitudes of lesser black-backed gulls were analysed using 141 altitude records from 118 observations, encompassing 229 birds. These were predominantly observed flying alone (88.1%), with a mean flock size of 1.9 (± 0.5) birds. The largest recorded flock consisted of 55 birds.

Flight altitudes for lesser black-backed gulls ranged from 0 to 100 m, with 27.5% of flights occurring within the 26-50 m interval (Table 4.30 and Figure 4.111). The highest flight altitude recorded was 100 m above sea level.

Table 4.30 Flight altitudes of lesser black-backed gulls observed during the eleven ship-based surveys. The table shows the number and proportion of altitude records and observed individuals occurring within each 25 m flight altitude interval (N_{rec} = 141; N_{ind} = 229).

Altitude interval (m)	Altitude records		Individuals	
	Total	Proportion	Total	Proportion
0-25	58	0.41	74	0.32
26-50	62	0.44	63	0.28
51-75	16	0.11	32	0.14
76-100	5	0.04	60	0.26
101-125	0	0.00	0	0.00
126-150	0	0.00	0	0.00
151-175	0	0.00	0	0.00
176-200	0	0.00	0	0.00
201-225	0	0.00	0	0.00

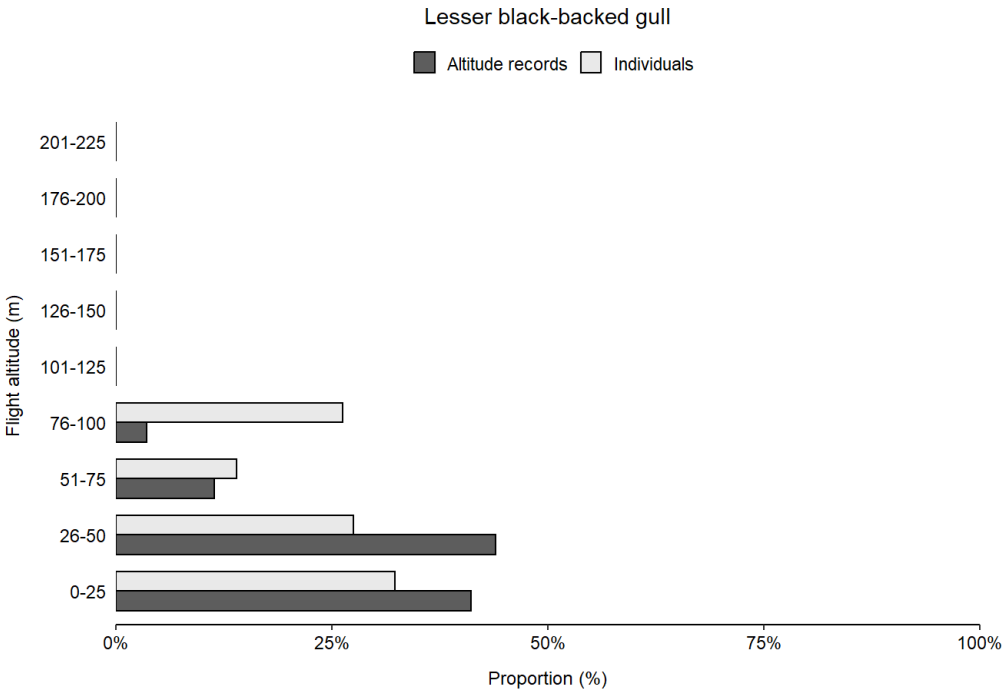

Figure 4.111 Flight altitudes of lesser black-backed gulls observed during the eleven ship-based surveys. The figure shows the percentage of altitude records (dark grey) and individuals (light grey) occurring within each 25 m flight altitude interval (N_{rec} = 141; N_{ind} = 229).

4.3.1.5 European herring gull

Flight altitudes of European herring gulls were analysed using 258 altitude records obtained from 244 observations, encompassing 326 birds. Most European herring gulls were observed flying alone (89.3%), with a mean flock size of 1.3 (± 0.1) birds. However, the largest recorded flock included 20 birds.

European herring gulls exhibited the highest recorded flight altitude among all species observed during eleven ship-based surveys, flying 214 m above sea level. Furthermore, European herring gulls generally flew at higher altitudes than other species (Table 4.31 and Figure 4.112). Despite this, most (78.2%) individuals were recorded flying at altitudes below 50 m.

Table 4.31 Flight altitudes of European herring gulls observed during the eleven ship-based surveys. The table shows the number and proportion of altitude records and observed individuals occurring within each 25 m flight altitude interval (N_{rec} = 258; N_{ind} = 326).

Altitude interval (m)	Altitude records		Individuals	
	Total	Proportion	Total	Proportion
0-25	121	0.47	170	0.52
26-50	74	0.29	85	0.26
51-75	34	0.13	39	0.12
76-100	13	0.05	14	0.04
101-125	8	0.03	9	0.03
126-150	3	0.01	3	0.01
151-175	1	0.00	1	0.00
176-200	2	0.01	3	0.01
201-225	2	0.01	2	0.01

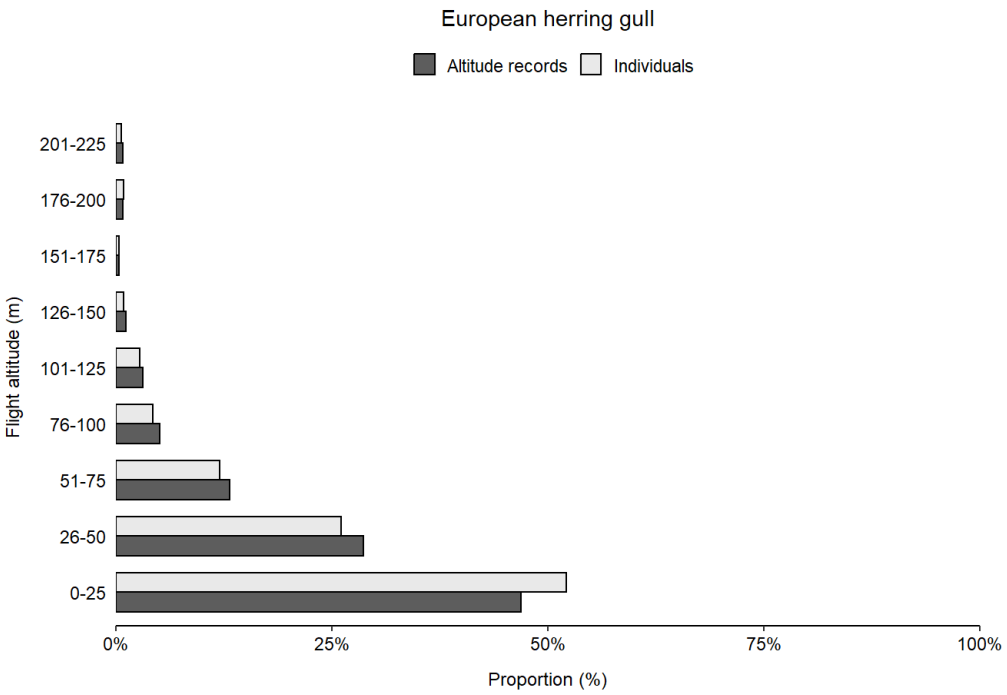

Figure 4.112 Flight altitudes of European herring gulls observed during the eleven ship-based surveys. The figure shows the percentage of altitude records (dark grey) and individuals (light grey) occurring within each 25 m flight altitude interval (N_{rec} = 258; N_{ind} = 326).

4.3.1.6 *Great black-backed gull*

Flight altitudes of great black-backed gulls were analysed using 141 altitude records from 120 observations, encompassing 142 birds. These were predominantly observed flying alone (92.5%), with a mean flock size of 1.2 (± 0.1) birds and a maximum flock size of 5 birds.

Great black-backed gulls were generally recorded flying at higher altitudes than most other observed species, with individuals reaching altitudes as high as 184 m above sea level. However, most flights were recorded within the 0-25 m (53.5%) and 26-50 m (30.3%) altitude intervals (Table 4.32 and Figure 4.113).

Table 4.32 Flight altitudes of great black-backed gulls observed during the eleven ship-based surveys. The table shows the number and proportion of altitude records and observed individuals occurring within each 25 m flight altitude interval (N_{rec} = 141; N_{ind} = 142).

Altitude interval (m)	Altitude records		Individuals	
	Total	Proportion	Total	Proportion
0-25	74	0.53	76	0.54
26-50	43	0.31	43	0.30
51-75	17	0.12	15	0.11
76-100	4	0.03	5	0.04
101-125	0	0.00	0	0.00
126-150	2	0.01	2	0.01
151-175	0	0.00	0	0.00
176-200	1	0.01	1	0.01
201-225	0	0.00	0	0.00

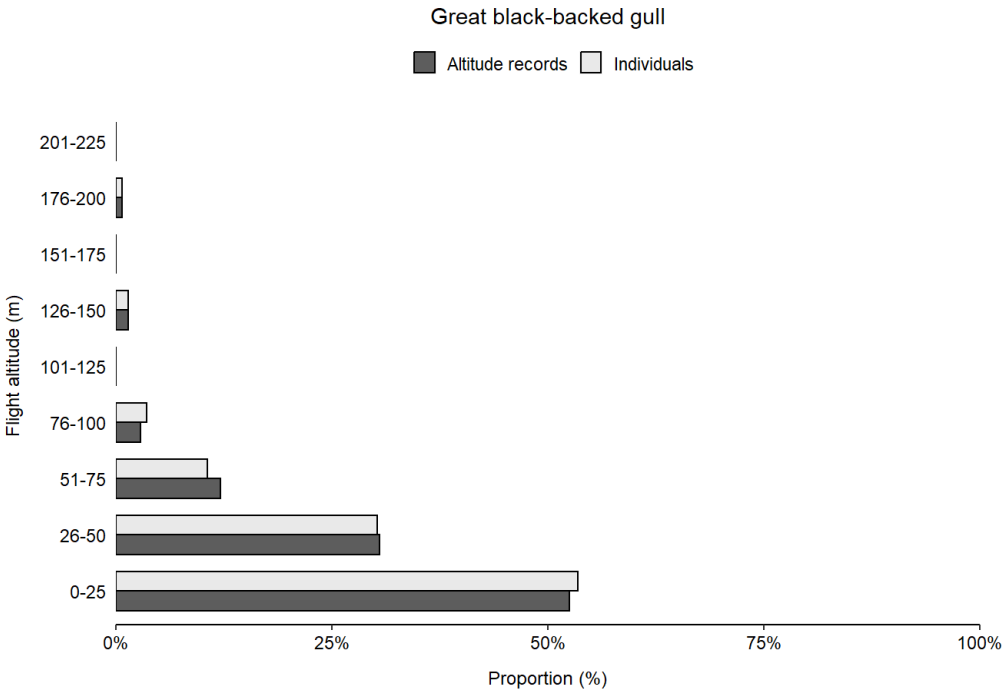

Figure 4.113 Flight altitudes of great black-backed gulls observed during the eleven ship-based surveys. The figure shows the percentage of altitude records (dark grey) and individuals (light grey) occurring within each 25 m flight altitude interval (N_{rec} = 141; N_{ind} = 142).

4.3.1.7 Black-legged kittiwake

Flight altitudes of black-legged kittiwakes were analysed using 324 altitude records from 294 observations, encompassing 352 individual birds. These were predominantly observed flying alone (88.8%) or in pairs (7.5%). Consequently, the mean flock size was 1.2 (± 0.0) birds, with a maximum observed flock size of 10.

Most black-legged kittiwakes were recorded flying at altitudes below 25 m (89.5%). However, fewer flights occurred at altitudes between 26 and 50 m (9.4%), with very few recorded birds flying above this range .(

and Figure 4.114). The highest flight altitude recorded for black-legged kittiwakes was 79 m above sea level.

Table 4.33 Flight altitudes of black-legged kittiwakes observed during the eleven ship-based surveys. The table shows the number and proportion of altitude records and observed individuals occurring within each 25 m flight altitude interval (N_{rec} = 324; N_{ind} = 352).

Altitude interval (m)	Altitude records		Individuals	
	Total	Proportion	Total	Proportion
0-25	288	0.89	315	0.90
26-50	32	0.10	33	0.09
51-75	3	0.01	3	0.01
76-100	1	0.00	1	0.00
101-125	0	0.00	0	0.00
126-150	0	0.00	0	0.00
151-175	0	0.00	0	0.00
176-200	0	0.00	0	0.00
201-225	0	0.00	0	0.00

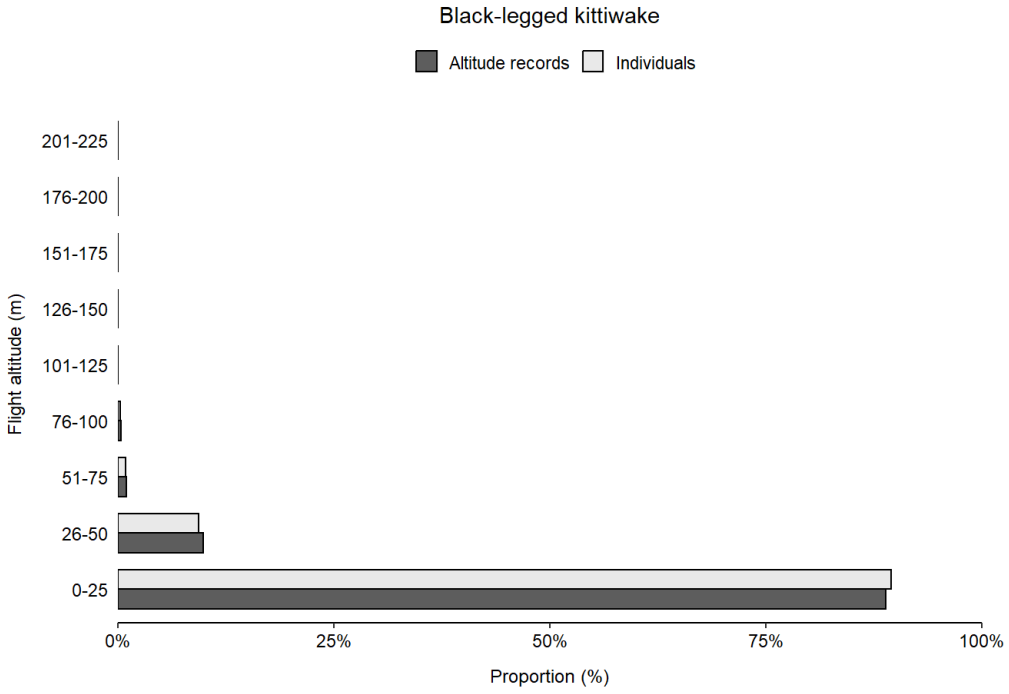

Figure 4.114 Flight altitude of black-legged kittiwakes observed during the eleven ship-based surveys. The figure shows the percentage of altitude records (dark grey) and individuals (light grey) occurring within each 25 m flight altitude interval (N_{rec} = 324; N_{ind} = 352).

4.3.1.8 Terns

Flight altitudes of terns were analysed by pooling altitude records obtained from observations of arctic, common, and sandwich terns. A total of 14 altitude records obtained from 9 observations were analysed, encompassing 25 birds. Terns were primarily observed flying alone (33.3%) or in small flocks, with an average flock size of 2.8 (± 0.7) birds. The largest observed flock consisted of 8 common terns.

Terns were exclusively recorded flying at altitudes below 25 m, with the highest recorded flight altitude being 16 m above sea level, observed in a common tern (Table 4.34 and Figure 4.115).

Table 4.34 Flight altitudes of terns observed during the eleven ship-based surveys. The table shows the number and proportion of altitude records and observed individuals occurring within each 25 m flight altitude interval (N_{rec} = 14; N_{ind} = 25).

Altitude interval (m)	Altitude records		Individuals	
	Total	Proportion	Total	Proportion
0-25	14	1.00	25	1.00
26-50	0	0.00	0	0.00
51-75	0	0.00	0	0.00
76-100	0	0.00	0	0.00
101-125	0	0.00	0	0.00
126-150	0	0.00	0	0.00
151-175	0	0.00	0	0.00
176-200	0	0.00	0	0.00
201-225	0	0.00	0	0.00

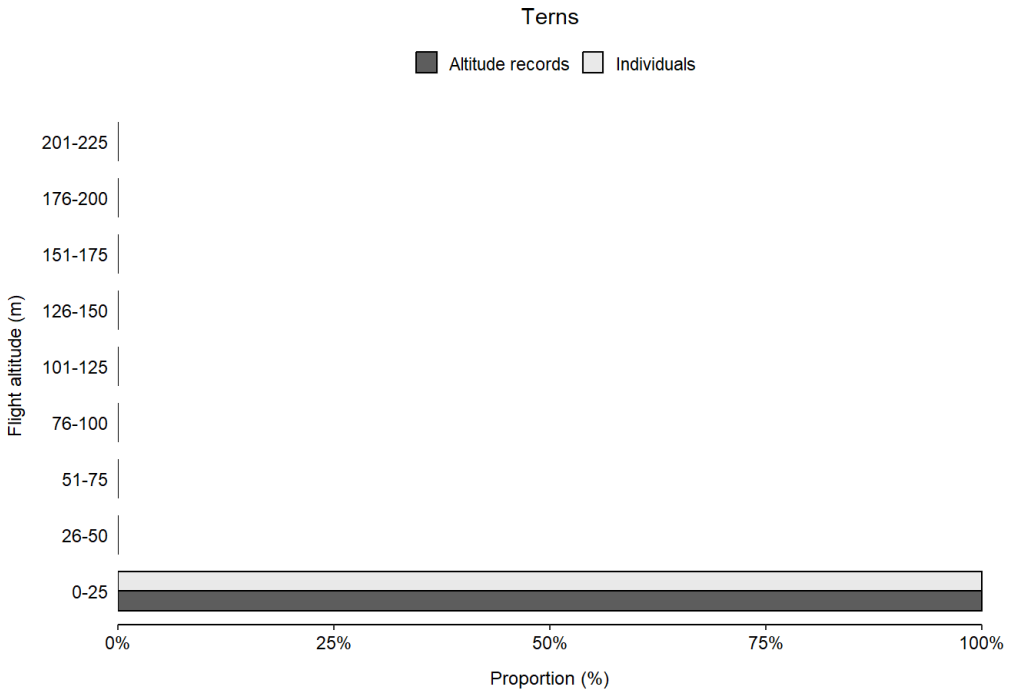

Figure 4.115 Flight altitudes of terns observed during the eleven ship-based surveys. The figure shows the percentage of altitude records (dark grey) and individuals (light grey) occurring within each 25 m flight altitude interval (N_{rec} = 14; N_{ind} = 25).

4.3.1.9 Alcids (razorbill and common guillemot)

Alcid flight altitudes were assessed by pooling altitude records obtained from common guillemots and razorbills observations. A total of 69 altitude records obtained from 67 separate observations, encompassing 95 birds, were analysed. Alcids were predominantly observed flying alone (82.1%) or in pairs (10.4%), resulting in an average flock size of 1.4 (± 0.2) birds. The largest observed flock, which was common guillemots, consisted of 8 individuals.

Alcids were exclusively recorded flying at altitudes below 25 m, with the highest flight altitude recorded being 13 m above sea level, observed in common guillemot (Table 4.35 and Figure 4.116).

Table 4.35 Flight altitudes of alcids observed during the eleven ship-based surveys. The table shows the number and proportion of altitude records and observed individuals occurring within each 25 m flight altitude interval (N_{rec} = 69; N_{ind} = 95).

Altitude interval (m)	Altitude records		Individuals	
	Total	Proportion	Total	Proportion
0-25	69	1.00	95	1.00
26-50	0	0.00	0	0.00
51-75	0	0.00	0	0.00
76-100	0	0.00	0	0.00
101-125	0	0.00	0	0.00
126-150	0	0.00	0	0.00
151-175	0	0.00	0	0.00
176-200	0	0.00	0	0.00
201-225	0	0.00	0	0.00

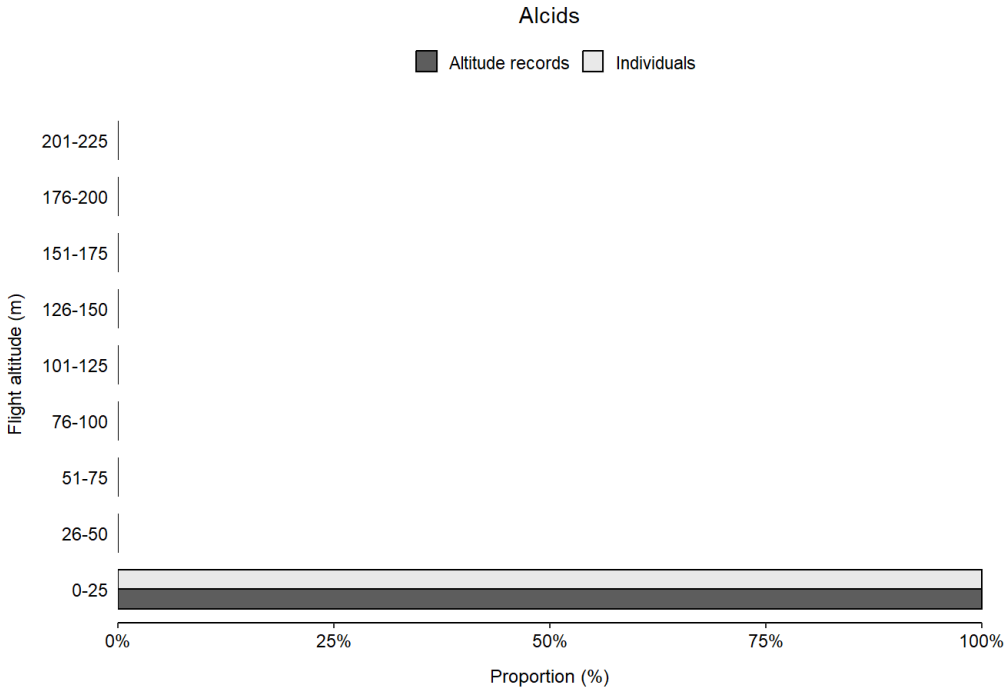

Figure 4.116 Flight altitudes of alcids observed during the eleven ship-based surveys. The figure shows the percentage of altitude records (dark grey) and individuals (light grey) occurring within each 25 m flight altitude interval (N_{rec} = 69; N_{ind} = 95).

4.3.1.10 Passerines

Passerines were the largest species group analysed for flight altitudes in this study. The flight altitudes of passerines were determined by combining altitude records obtained from observations of several species: brambling, common blackbird, common chiffchaff, common starling, Eurasian skylark, European robin, fieldfare, meadow pipit, northern wheatear, redwing, song thrush, and western yellow wagtail. A total of 33 altitude records obtained from different observations, encompassing 268 individual birds, were pooled for this analysis.

Passerines were often observed flying in flocks, with only 39.4% flying alone. On average, these flocks consisted of 8.1 birds (± 2.5), although one notable flock of common starlings numbered 80. Most passerines flew at altitudes below 25 meters, accounting for 79.9% of the birds (Table 4.36 and Figure 4.117). However, the highest recorded flight altitude among passerines was a common starling flying at 100 m above sea level.

Table 4.36 Flight altitudes of passerines observed during the eleven ship-based surveys. The table shows the number and proportion of altitude records and observed individuals occurring within each 25 m flight altitude interval (N_{rec} = 33; N_{ind} = 268).

Altitude interval (m)	Altitude records		Individuals	
	Total	Proportion	Total	Proportion
0-25	28	0.85	214	0.80
26-50	4	0.12	39	0.15
51-75	0	0.00	0	0.00
76-100	1	0.03	15	0.06
101-125	0	0.00	0	0.00
126-150	0	0.00	0	0.00
151-175	0	0.00	0	0.00
176-200	0	0.00	0	0.00
201-225	0	0.00	0	0.00

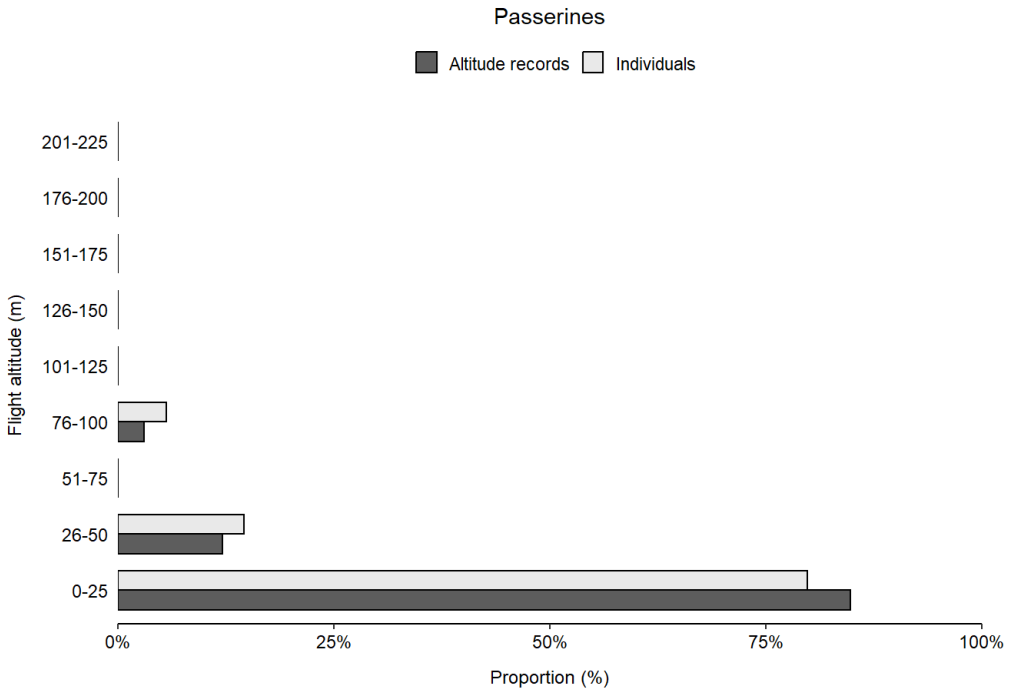

Figure 4.117 Flight altitude of passerines observed during the eleven ship-based surveys. The figure shows the percentage of altitude records (dark grey) and individuals (light grey) occurring within each 25 m flight altitude interval (N_{rec} = 33; N_{ind} = 268).

4.3.2 Species composition

Some species groups proved difficult to identify to species during the aerial surveys. That is especially true for species of divers, gulls, terns, and alcids. However, ship-based surveys offer better prospects for species identification within

these groups. Consequently, the species composition within divers, gulls (excluding black-headed gulls and black-legged kittiwakes), terns and alcids were determined based on the eleven ship-based surveys.

4.3.2.1 Divers

Divers were observed during ship-based surveys S2 (14-15 February 2022), S4 (22-25 April 2022), S5 (30 April -2 May 2022), S6 (20-21 May 2022), S9 (13-14 November 2022) and S10 (14-16 February 2023). In total, 12 individual divers were identified during the ship-based surveys, all of which were red-throated divers.

4.3.2.2 Gulls

In total, 772 individual gulls were identified during the ship-based surveys (Table 4.37). European herring gull was the most abundantly recorded gull species and comprised 42.9% of all recorded individuals. Of the remaining identified individual gulls, 33.3% were lesser black-backed gulls, 19.3% were great black-backed gulls, 4.4% were common gulls, and 1% were yellow-legged gulls.

Table 4.37 Gull species observed during the eleven ship-based surveys. The table shows the number and proportion of observations and individuals of each species observed during the ship-based surveys (N_{obs} = 521; N_{ind} = 772).

Species	Observations		Individuals	
	Total	Proportion	Total	Proportion
Common gull	32	0.061	34	0.044
European herring gull	246	0.472	331	0.429
Great black-backed gull	122	0.234	149	0.193
Lesser black-backed gull	120	0.230	257	0.333
Yellow-legged gull	1	0.002	1	0.001

Gulls were observed during all ship-based surveys. However, the proportion of common, European herring, great black-backed, lesser black-backed, and yellow-legged gulls varied greatly depending on the survey (Figure 4.118; Table 4.21). For example, lesser black-backed gulls were completely absent from surveys S1 (15-16 November 2021), S2 (14-15 February 2022), S8 (22 October 2022), S9 (13-14 November 2022) and S10 (14-16 February 2023), where European herring gull was the most observed species. In contrast, the great black-backed gull was observed during all surveys. Yellow-legged gulls were only observed during survey S10 (14-16 February 2023), comprising 1.5% of the gulls observed.

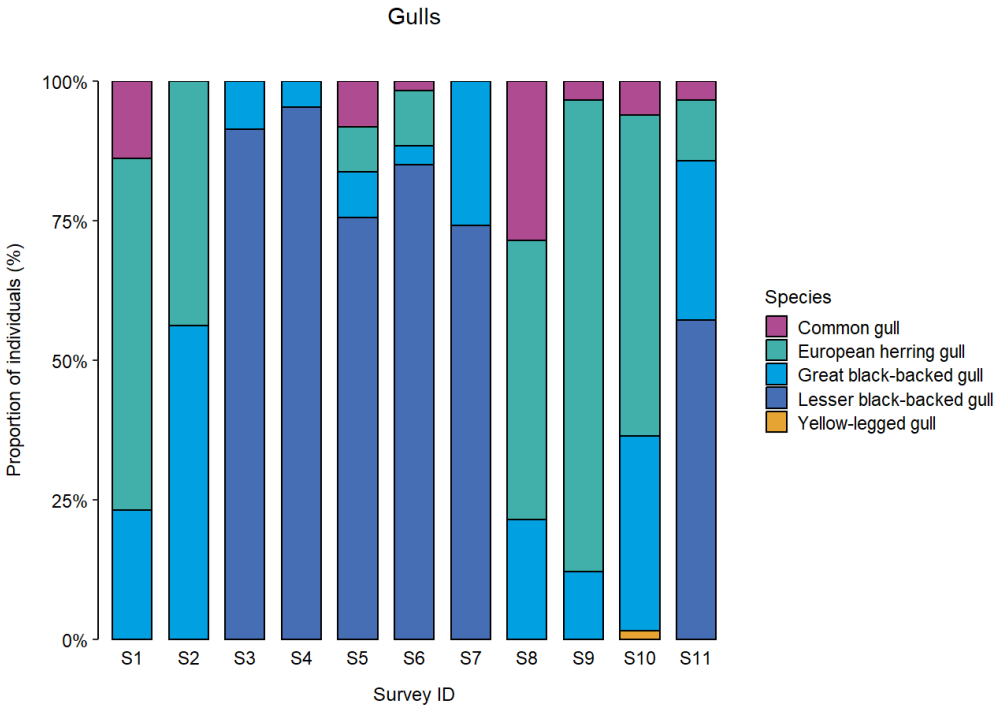

Figure 4.118 Gull species observed during the eleven ship-based surveys. The figure shows the proportion of individuals of each species observed during each ship-based survey (N_{obs} = 521; N_{ind} = 772).

4.3.2.3 Terns

In total, 22 individual terns were identified during the ship-based surveys (Table 4.38). Of these, 13.6% were arctic terns, 68.2% were common terns, and 18.2% were sandwich terns.

Table 4.38 Tern species observed during the eleven ship-based surveys. The table shows the number and proportion of observations and individuals of each species observed during the ship-based surveys (N_{obs} = 8; N_{ind} = 22).

Species	Observations		Individuals	
	Total	Proportion	Total	Proportion
Arctic tern	2	0.250	3	0.136
Common tern	5	0.625	15	0.682
Sandwich tern	1	0.125	4	0.182

Terns were only observed during ship-based surveys S5 (30 April – 2 May 2022), S6 (20-21 May 2022) and S7 (24-26 August 2022). However, the proportion of arctic, common and sandwich terns varied greatly depending on the survey (Figure 4.119; Table 4.21). Whereas all terns observed during survey S6 were identified as common terns, common terns comprised 68.4% and 50% of the terns observed during surveys S5 and S6, respectively. Arctic terns comprised 10.5% and 50% of the terns observed during surveys S5 and S6, respectively. Sandwich terns were only observed during ship-based survey S5 but comprised 21.1% of the terns observed.

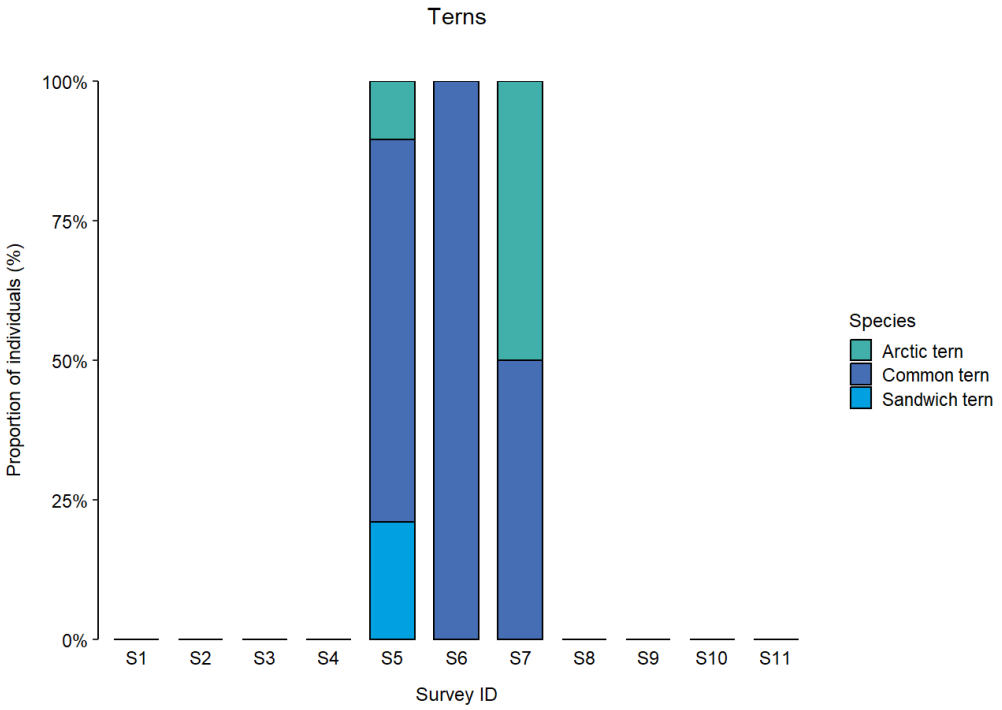

Figure 4.119 Tern species observed during the eleven ship-based surveys. The figure shows the proportion of individuals of each species observed during each ship-based survey (N_{obs} = 8; N_{ind} = 22).

4.3.2.4 Alcids

In total, 92 individual alcids were identified during the ship-based surveys. Of these, 83.7% were common guillemots, while 16.3% were razorbills (Table 4.39).

Table 4.39 Alcid species observed during the eleven ship-based surveys. The table shows the number and proportion of observations and individuals of each species observed during the ship-based surveys (N_{obs} = 65; N_{ind} = 92).

Species	Observations		Individuals	
	Total	Proportion	Total	Proportion
Common guillemot	55	0.846	77	0.837
Razorbill	10	0.154	15	0.163

The proportion of common guillemots relative to razorbills varied greatly depending on the ship-based survey (Figure 4.120; Table 4.21). For example, all alcids observed during surveys S1 (15-16 November 2021), S2 (14-15 February 2022), S4 (22-25 April 2022), S5 (30 April – 2 May 2022) and S8 (22 October 2022) were identified as common guillemots. In contrast, razorbills comprised 50%, 28.1%, 33.3% and 9.5% of alcids observed during surveys S3 (12 April 2022), S9 (13-14 November 2022), S10 (14-16 February 2023) and S11 (28-30 March 2023), respectively. No alcids were observed during surveys S6 (20-21 May 2022) and S7 (24-26 August 2022).

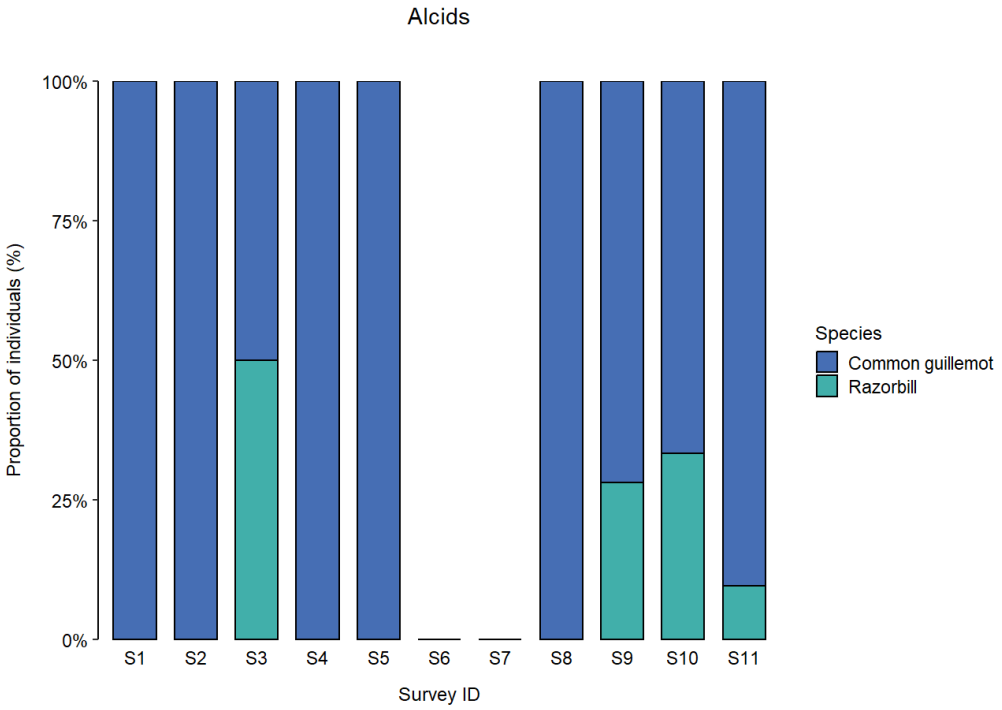

Figure 4.120 Alcid species observed during the eleven ship-based surveys. The figure shows the proportion of individuals of each species observed during each ship-based survey (N_{obs} = 65; N_{ind} = 92).

4.4 The proportion of birds flying

To assist in estimating the flight volume of birds in the extended bird survey area, we assessed the ratio between birds flying and sitting on the water using the combined set of observations from the aerial surveys. This was done by the number of observations (clusters, i.e. in flocks) and the number of individuals weighed by cluster size.

While most divers, razorbills and common guillemots were recorded as sitting on the water, most gulls and terns were recorded flying. Northern gannets and northern fulmars were intermediate to the previous groups (Figure 4.121).

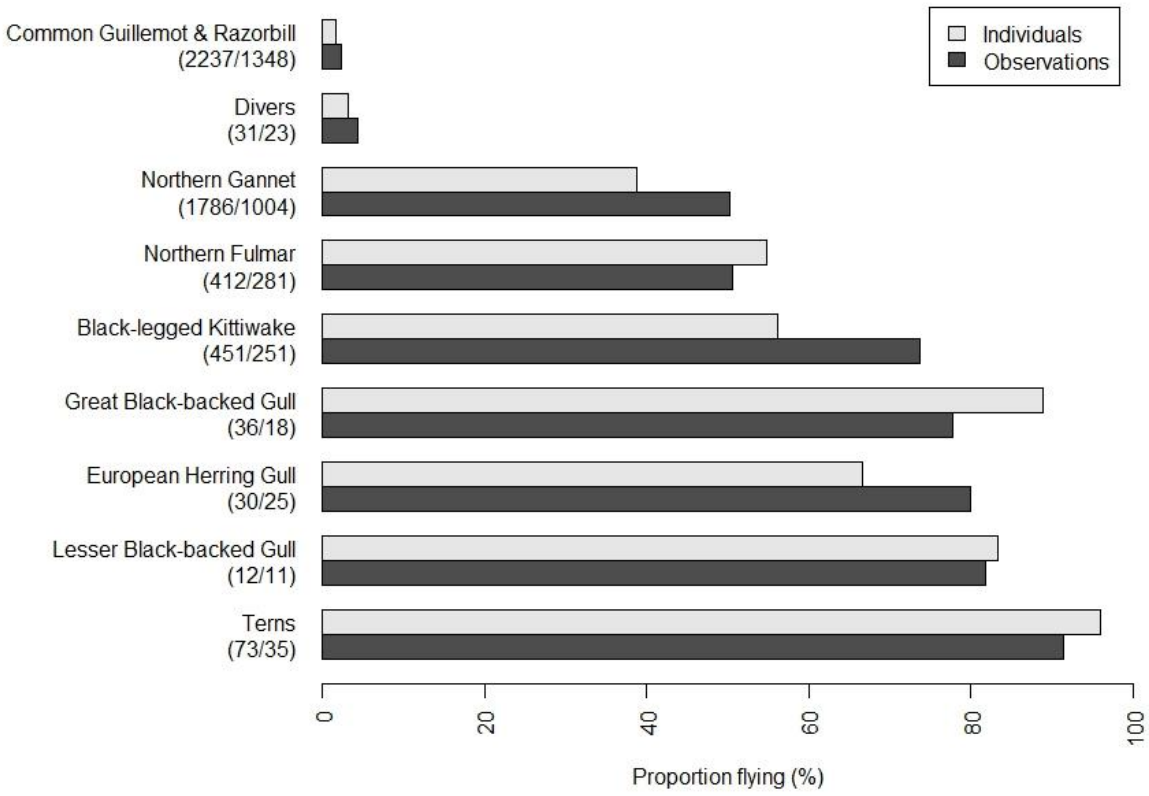

Figure 4.121 Proportion of birds flying (instead of sitting on the water) observed during aerial surveys. The proportion is shown separately for observations (dark grey) and individuals (light grey). Only those species/species groups with a minimum of 10 observations are included. The number of observed individuals and observations are given in brackets under species names.

5. Discussion

The data set generated from twelve aerial surveys and eleven ship-based surveys of birds in the North Sea Energy Island survey area 2022-2023 forms the basis for this baseline report. The aerial surveys were successful in delivering information on the estimated abundance and modelled distribution of relevant bird species in the area, confirming very low levels of abundance of most species observed there, with only four typically offshore avian species (for instance, northern fulmar, northern gannet, black-legged kittiwake and razorbill/common guillemot) dominating those observations. The methods were highly successful in generating precision-based estimates of each species concerned, seasonal density distribution maps across the extended bird survey area and persistence mapping for each species for future comparisons. The ship-based surveys were highly successful in providing general data on local bird movements and relative flight frequencies and enabling the relative frequency of species-specific flight heights to allow for incorporation of these parameters into future collision risk modelling. The ship surveys also provided important insight to correct the species composition data from aerial surveys for species that are difficult to identify from the air.

For the species for which spatial models were conducted, there was a pronounced variation in distribution between individual surveys, but - evaluated over more surveys - the area utilisation, modelled as persistency, was rather even over the extended bird survey area. The depth profile of the survey area is very uniform, and the area is away from

hydrographical structures that create stable variation across space and time. The bird species in the extended bird survey area depend on prey items (fish and/or zooplankton) that are also highly variable in their distribution across the survey area. We assume this is the reason for the clumped bird distributions for single surveys and the rather even distribution observed when modelling over many surveys.

These surveys demonstrated the presence of high numbers, especially razorbills/common guillemots. The numbers were highest in April to July, and higher numbers were recorded in 2023 than in 2022. The highest density of razorbill/common guillemot in 2022 was 3.0 birds/km^2 on 1 April 2022, while in 2023, densities of 5.2 birds/km^2 and 5.7 birds/km^2 were recorded on 3 April and 8 July 2023, respectively. The corresponding results from the data for the entire Danish North Sea from April 2019 showed an overall razorbill/common guillemot density of 1.8 birds/km^2 across the majority of the area, while a survey from the North Sea in May 2019 showed very low densities of this species group, and a contracting difference between densities of the same area between the two surveys (Figure 4.96).

Regarding recognising macro-environmental features that might affect the data gathered in the summer of 2022, it is important to record that the northeast Atlantic gannet population was severely adversely affected by a major avian influenza outbreak at several of their North Atlantic colonies. This has been estimated to have caused a 25 % decline in the breeding population of the United Kingdom between 2021 and 2023 (Tremlett et al. 2024). There is no doubt that this level of mortality will have influenced the abundance of northern gannets recorded in the extended bird survey area during the summer period. In contrast, in September 2022, after the outbreak, almost 3,000 northern gannets were estimated to be present in the extended bird survey area. We interpret this to reflect the fact that the non-breeding elements of the population potentially escaped infection and remained unaffected by the outbreak. The presence of such birds in this area could explain the relatively high abundance of the species in the extended bird survey area in September.

We should be prudent in concluding too much from the data collected relating to bird flight altitude, as we could only undertake such observations during daylight. Previous experience suggests avian flight heights and behaviour differ during daylight and nighttime when birds have been observed to fly higher, so our observations only describe diurnal patterns of flight activity. As a result, it is recommended that information on nocturnal flight intensity and altitudes be supplemented for future environmental assessments of offshore wind farm projects in the area. Likewise, data collection was generally conducted under good weather conditions, which prevents us from describing flight activity under harsher weather conditions, such as poor visibility, heavy precipitation, and strong winds.

We should also caution that our observation base (the vessel) represents a potentially significant bias to some species, especially those known to be ship followers or avoid ships. This is particularly the case for species which perceive the vessel as a potential foraging site or place to roost, such as some gull and seabird species (e.g. European herring gull, black-legged kittiwake, northern fulmar and northern gannet) and land birds searching for a dry safe landing. Gulls were often observed changing their flight altitude when approaching the vessel; high-flying individuals typically descend, and low-flying birds ascend near the boat. Low-flying migrant species may also increase altitude when passing by the vessel. For this reason, under the present data collection protocol, we derived flight altitudes as far away from the vessel as possible to reduce or eliminate such bias.

The proportion of birds flying (relative to those resting/feeding on the water) was obtained from observations from the aerial surveys. It should be kept in mind that some birds can flush as a response to the approaching aircraft, and thus, the calculation of the proportion of flying birds can potentially be overestimated. This may be particularly true for some duck species, such as the common scoter. This is not believed to be a major source of bias for the species in our extended bird survey area.

There was from the onset of this project scheduled for recording of bird flight information from a radar system on a platform west of the phase 1 area. This proved to be impractical, and the ship-based platform was chosen for the purpose.

The ship-based surveys recorded rare bird species that use the area for resting and foraging, such as sooty shearwater, Wilson's storm petrel, long-tailed skua, little auk, and Atlantic puffin. The observation of Wilson's storm petrel was the first individual ever recorded in Denmark.

6. Conclusion

This report presents the results of bird studies in and around the NSEI survey area. The data was collected during twelve aerial surveys from March 2022 to December 2023 and eleven ship-based surveys between November 2021 and March 2023.

The area's avifauna was dominated by offshore bird species, with northern fulmar, northern gannet, black-legged kittiwake, razorbill and common guillemot being the most numerous. Other gull species than black-legged kittiwake, such as European herring gull, lesser black-backed gull and great black-backed gull were also frequently recorded in the area.

Terns were recorded in low numbers in the extended bird survey area. Arctic tern was most abundant, while common tern occurred in lower numbers. Terns are migratory species and not present in Danish waters over the winter.

The extended bird survey area's most abundant bird species group was razorbill and common guillemot, dominated by common guillemot observations. Estimates of total abundance revealed between 27,245 birds on 8 July 2023 and 4,637 on 2 March 2022. The abundance of northern fulmars was estimated to be between 64 (3 April 2023) and 2,364 individuals (27 September 2023) in the extended bird survey area. Northern gannets were present in the extended bird survey area all year, with an estimated abundance of 16 birds in December and 3,797 on 1 April 2022. The abundance of black-legged kittiwakes in the extended bird survey area fluctuated greatly. During surveys in July and September 2022 and July 2023, no black-legged kittiwakes were recorded. The estimated abundance for the remaining surveys revealed numbers between 219 (1 April 2022) and 2,822 (2 March 2023). In April, the North Sea Energy Island survey has high razorbill/common guillemot densities. Densities of up to 5.2 birds/km^2 were estimated for the North Sea Energy Island in April 2023. Corresponding data from April 2019 showed a lower density of razorbills/common guillemots for the general area, namely 1.8 birds/km^2. The April 2019 data within the North Sea Energy Island area had an average razorbill/common guillemot density very similar to the average density, namely 1.9 birds/km^2.

For the four species or species groups mentioned above, persistence analyses were carried out, and the results showed generally low levels of persistence between the distributions and abundances for the twelve aerial surveys.

Existing data on bird abundances and distributions from aerial surveys conducted in April/May 2019 and covering the entire Danish North Sea indicated the presence of an estimated number of 22,648 red-throated divers/black-throated divers, 46,437 northern fulmars, 31,723 northern gannets, 4,472 black-legged kittiwakes and 89,681 razorbills/common guillemots in the Danish North Sea at that time.

The flight altitude of birds was investigated from ship-based surveys. These results represent daylight observations only and might differ from nocturnal flight patterns, which we could not measure. Most species or species groups flew very low over the sea surface. For example, northern fulmars, terns, and alcids almost exclusively flew at altitudes below 25 m. Similarly, over 80% of northern gannets, red-throated divers, skuas, common gulls, black-legged kittiwakes,

passerines and sea ducks (100%) were predominantly recorded flying at altitudes below 50 m. In contrast, waders, lesser black-backed gulls, European herring gulls, and great black-backed gulls were generally recorded flying at higher altitudes than most other species observed, with over 50% of individuals flying above 25 m and as high as 184 m above sea level.

7. References

AEWA. (2022). Agreement on the conservation of African-Eurasian Migratory Waterbirds (AEWA). *Agreement text and annexes as amended at the 8th session of the meeting of the parties to AEWA 26-30 September 2022*. Budapest, Hungary.

Ainley, D. G., Nettleship, D. N., & Storey, A. E. (2021). Common Murre (Uria aalge). In S. M. Billerman, P. G. Rodewald, & B. K. Keeney (Eds.), *Birds of the world*. Ithaca, NY: Cornell Lab of Ornithology.

BirdLife International. (2018). *The IUCN Red List of Threatened Species 2018: Fulmarus glacialis*. Hentet 05. 07 2014 fra https://dx.doi.org/10.2305/IUCN.UK.2018-2.RLTS.T22697866A132609419.en

BirdLife International. (2021a). *European Red List of Birds*. Publications Office of the European Union.

BirdLife International. (2021b). *The IUCN Red List of Threatened Species 2021*. Hentet 05. 07 2024 fra https://www.iucnredlist.org/en

BirdLife International. (2024). *IUCN Red List of Birds*. Hentet 04. 07 2024 fra https://datazone.birdlife.org

Buckland, S. T., Anderson, D. R., Burnham, K. P., Laake, J. L., Borchers, D. L., & and Thomas, L. (2001). *Introduction to Distance Sampling*. Oxford: Oxford University Press.

Buckland, S., Rexstad, E., Marques, T., & Oedekoven, C. (2015). *Distance sampling: methods and applications*. Switzerland: Springer International Publishing.

Danish Energy Agency. (2022). *Energiø Nordsøen - Rammerne for det kommende planforslag til brug for miljøvurdering*. Center for Energy Islands.

Garthe, S., Peschko, V., Fifield, D. A., Borkenhagen, K., Nyegaard, T., & Dierschke, J. (2024). Migratory pathways and winter destinations of Northern Gannets breeding at Helgoland (North Sea): known patterns and increasing importance of the Baltic Sea. *Journal of Ornithology*, https://doi.org/10.1007/s10336-024-02192-x.

Hatch, S. A., Robertson, G. J., & Baird, P. H. (2020). Black-legged Kittiwake (Rissa tridactyla). I S. M. Billerman (Red.), *Birds of the world*. Ithaca, NY: Cornell Lab of Ornithology.

Laursen, K., Pihl, S., Durinck, J., Hansen, M., Skov, H., Frikke, J., & Danielsen, F. (1997). Numbers and distribution of waterbirds in Denmark 1987-1989. *Danish Review of Game Biology, 14*(1), 1-184.

Lavers, J., Hipfner, J. M., & Chapdelaine, G. (2020). Razorbill (Alca torda). I S. M. Billerman (Red.), *Birds of the world*. Ithaca, NY: Cornell Lab of Ornithology.

Leys, C., Ley, C., Klein, O., Bernard, P., & Licata, L. (2013). Detecting outliers: do not use standard deviation around the mean, use absolute deviation around the median. *Journal of Experimental Social Psychology, 49*(4), 764-766.

Lyngs, P., & Kampp, K. (1996). Ringing recoveries of Razorbills Alca torda and Guillemots Uria aalge in Danish waters. *Dansk Ornitologisk Forenings Tidsskrift, 90*, 119-132.

Mallory, M. L., Hatch, S. A., & Nettleship, D. N. (2020). Northern Fulmar (Fulmarus glacialis). In S. M. Billerman (Ed.), *Birds of the world*. Ithaca, NY: Cornell Lab of Ornithology.

Marques, F. F., & Buckland, S. T. (2004). Covariate models for the detection function. I *Advanced Distance Sampling* (s. 31-47). Oxford: Oxford University Press.

Marques, T. A., Thomas, L., Fancy, S. G., & Buckland, S. T. (2007). Improving estimates of bird densities using multiple covariate distance sampling. *The Auk*, 1229-1243.

Mowbray, T. B. (2020). Northern Gannet (Morus bassanus). In S. M. Billerman (Ed.), *Birds of the world*. Ithaca, NY: Cornell Lab of Ornithology.

Nielsen, R., & Petersen, I. (2014). *Abundance and distribution of birds and marine mammals in Jammerbugten in 2012 and 2013. Report commissioned by the Environmental Group under the Danish Environmental Monitoring*

Programme through contract with Vattenfall. DCE - Danish Centre for Environment and Energy. Aarhus University.

NIRAS. (2015). *Vesterhav Nord Offshore Windfarm. EIA background report commissioned by Eenrginet.dk.* . NIRAS.

NIRAS. (2015). *Vesterhav Syd Offshore Windfarm. EIA background report commissioned by Eenrginet.dk.* NIRAS.

Petersen, I. K., Nielsen, R. D., & Mackenzie, M. L. (2014). *Post-construction evaluation of bird abundances and distributions in the Horns Rev 2 offshore wind farm area, 2011 and 2012. Report commissioned by DONG Energy.* DCE - Danish Centre for Environment and Energy. Aarhus University.

Petersen, I., & Sterup, J. (2019). *Number and distribution of birds in and around two potential offshore wind farm areas in the Danish North Sea and Kattegat. Scientific report no. 327.* DCE - Danish Centre for Environment and Energy. Aarhus University.

Petersen, I., Nielsen, R., & Clausen, P. (2016). *Vurdering af IBA'er (Important Bird Areas) i relation til fuglebeskyttelsesområder - med særligt henblik på marine arter og områder. Tenisk rapport nr. 202.* DCE - Nationalt Center for Miljø og Energi. Aarhus Universitet.

Petersen, I., Nielsen, R., & Clausen, P. (2019). *Opdateret vurdering af IBA udpegninger i relation til otte specifikke marine områder. Teknisk rapport nr. 203.* DCE - Nationalt Center for Miljø og Energi. Aarhus Universitet.

Scott-Hayward, L. A., Mackenzie, M. L., & Walker, C. G. (2023). MRSea R package (V1.5.0): spatially adaptive uni and bi-variate regression splines using SALSA.

Scott-Hayward, L. A., Mackenzie, M. L., Donovan, C. R., Walker, C. G., & Ashe, E. (2014). Complex Region Spatial Smoother (CReSS). *Journal of Computational and Graphical Statistics, 23*(2), 340-360.

Skov, H., Durinck, J., Leopold, M. F., & Tasker, M. L. (1995). *Important bird areas in the North Sea, including the Channel and the Kattegat.* Cambridge: BirdLife International.

Stokke, B. G., Dale, S., Jacobsen, K.-O., Lislevand, T., Solvang, R., & & Strøm, H. (2021). *Artsdatabanken. Norsk rødliste for arter 2021: Fugler Aves*. Hentet 05. 07 2024 fra https://artsdatabanken.no/rodlisteforarter2021/Artsgruppene/fugler

Stone, C., Webb, A., Barton, C., Ratcliffe, N., Reed, T., Tasker, M., . . . Pienkowski, M. (1995). *An atlas of seabird distribution in north-west European waters.* Peterborough: Joint Nature Conservation Committee.

Tasker, M., Webb, A., Hall, A., Pienkowski, M., & Langslow, D. (1987). *Seabirds in the North Sea.* Nature Conservancy Council.

Tremlett, C., Morley, N., & Wilson, L. (2024). *UK seabird colony counts in 2023 following the 2021-22 outbreak of Highly Pathogenic Avian Influenza. RSPB research report 76.* Sandy, Bedfordshire: RSPB Centre for Conservation Science.

Walker, C., Mackenzie, M., Donovan, C., & O'Sullivan, M. (2010). SALSA - a Spatially Adaptive Local Smoothing Algorithm. *Journal of Statistical Computation and Simulation, 81*(2), 179-191.

Wetlands International. (2022). *Waterbird population estimates. CSR 8 estimates*. Hentet 05. 07 2024 fra http://wpe.wetlands.org

Appendix 1

Modelling methods

Detailed description of data analyses for abundance estimates

The data collected are animal counts in the North Sea area of Denmark. All survey data were collected using visual aerial methods, so correction for declining detectability with increasing distance from the plane was accounted for. The resulting distance-corrected counts tend to show that the variation in the number of birds increases as the average number of birds increases (i.e., there is a mean-variance relationship), so a Tweedie-based count model was used for spatial analysis.

As each survey was analysed separately, only spatial explanatory variables were considered. Since bird numbers are often thought to be related to environmental characteristics, such as the depth of the water and distance to the coastline, these variables were considered part of each analysis. A flexible approach was taken to ensure these relationships were suitably informed by the data and the shape of these relationships was evidence-based. For example, a species could prefer a particular depth range (i.e. the shape of the relationship between bird numbers and depth could rise and fall), or it could be simpler (e.g. numbers could systematically increase/decrease with depth).

The model selection approach used in the following analyses selects the details of these relationships informed by the data while ensuring that the resulting relationships are not 'overfitted' (i.e., more complex than necessary) to the data available. The underlying relationships in each case were sought, rather than a 'fine-tuned' version of these relationships, which would fit perfectly to the data set collected for each species in each survey but not represent any other set of observations from this survey or area (even if they were collected at a similar time from the same area).

While including environmental relationships in models can be relatively simple to understand, it is important to note that if these terms are included in a model (in this way), they are assumed to be true everywhere across the survey region. If bird numbers are assumed to be highest at some depth, this is assumed to be true for all areas of the study region with that depth. This is often unrealistic in practice since there are many (other) influences in addition to the variable(s) under consideration which act together to make locations attractive/unattractive to birds (some of which might be changing daily). Additionally, all the variables giving rise to bird numbers in particular locations are unlikely to be known or available for consideration/selection in the model, and thus, localised spatial patterns often remain. For this reason, a spatial surface was also considered for each model to account for localised surface patterns. These terms were also permitted to be flexible (and informed by the data) but were chosen to not be 'overfitted' to any survey - instead, they represent the underlying spatial patterns likely to be observed at a similar time in the same survey area. To achieve this balance between fit to the survey data and to avoid 'fine-tuning' each model to represent the exact observations sampled for each survey, a '5-fold cross-validation' procedure was used. This divides the data up into buckets (folds) with (relatively) equal numbers of observations (whilst maintaining transects) and uses 4 of these folds to choose a model and the remaining fold (which is left out of model fitting and selection) to 'test' the model. This prevents overfitting since a finely tuned model would fit almost perfectly to the 4 folds but look very different from the 'left-out' fold since it was not included in the model fitting and choice, even though it was collected as part of each survey.

The additional feature of these analyses is that how the data were collected was acknowledged and respected when reporting the level of uncertainty in model results. These data were collected along transects over time, and data collected this way tends to result in data points close together (in space or time) that are more similar than data points collected randomly from potentially very different parts of the survey area within some time window. This is akin to measuring the body weight of 10 human subjects monthly for 10 consecutive months (N = 100) compared with measuring the body weight of 100 different human subjects once throughout 10 months (also N = 100). Traditional ways of reporting the uncertainty about model estimates (e.g., bird counts in any given location) often assume the modelled data are either randomly sampled in some way or the variables included in the model fully explain these patterns of

similarity in these observations collected along transects resulting in uncorrelated residuals (differences between observed and predicted values). This is far from guaranteed, and the approach used here was to measure the extent of similarity observed in model residuals (within transects – the correlated panels/blocks) and use this value to increase the uncertainty about model estimates so that the results can be interpreted in the usual way.